PREPARATION OF POLYURETHANE AND POLYISOCYANURATE FOAMS CATALYZED BY METAL ACETATE-AMMONIA COMPLEXES

Miss Benjatham Sukkaneewat

จุฬาลงกรณ์มหาวิทยาลัย
CHULALONGKORN UNIVERSITY

A Dissertation Submitted in Partial Fulfillment of the Requirements
for the Degree of Doctor of Philosophy in Petrochemistry and Polymer
Science
Field of Study of Petrochemistry and Polymer Science
Faculty of Science
Chulalongkorn University
Academic Year 2018
Copyright of Chulalongkorn University

การเตรียมโฟมพอลิยูรีเทนและพอลิไอโซไซยานูเรตเร่งปฏิกิริยาด้วยสารประกอบเชิงซ้อนโลหะแอ
ซีเทต-แอมโมเนีย

น.ส.เบญจธรรม สุขณีวัฒน์

จุฬาลงกรณ์มหาวิทยาลัย
CHULALONGKORN UNIVERSITY

วิทยานิพนธ์นี้เป็นส่วนหนึ่งของการศึกษาตามหลักสูตรปริญญาวิทยาศาสตรดุษฎีบัณฑิต
สาขาวิชาปิโตรเคมีและวิทยาศาสตร์พอลิเมอร์ สาขาวิชาปิโตรเคมีและวิทยาศาสตร์พอลิเมอร์
คณะวิทยาศาสตร์ จุฬาลงกรณ์มหาวิทยาลัย
ปีการศึกษา 2561
ลิขสิทธิ์ของจุฬาลงกรณ์มหาวิทยาลัย

Thesis Title	PREPARATION OF POLYURETHANE AND POLYISOCYANURATE FOAMS CATALYZED BY METAL ACETATE-AMMONIA COMPLEXES
By	Miss Benjatham Sukkaneewat
Field of Study	Petrochemistry and Polymer Science
Thesis Advisor	Associate Professor Nuanphun Chantarasiri, Ph.D.

Accepted by the Faculty of Science, Chulalongkorn University in Partial Fulfillment of the Requirement for the Doctor of Philosophy

.... Dean of the Faculty of Science
(Professor POLKIT SANGVANICH, Ph.D.)

DISSERTATION COMMITTEE

.... Chairman
(Associate Professor NAPIDA HINCHIRANAN, Ph.D.)
.... Thesis Advisor
(Associate Professor Nuanphun Chantarasiri, Ph.D.)
.... Examiner
(Professor VITHAYA RUANGPORNVISUTI, Dr.rer.nat.)
.... Examiner
(Associate Professor SIRILUX POOMPRADUB, Ph.D.)
.... External Examiner
(Assistant Professor Duangruthai Sridaeng, Ph.D.)

จุฬาลงกรณ์มหาวิทยาลัย
CHULALONGKORN UNIVERSITY

เบญจธรรม สุขณีวัฒน์ :
การเตรียมโฟมพอลิยูรีเทนและพอลิไอโซไซยานูเรตเร่งปฏิกิริยาด้วยสารประกอบเชิงซ้อนโลหะแอซีเทต-แอมโมเนีย. (PREPARATION OF POLYURETHANE AND POLYISOCYANURATE FOAMS CATALYZED BY METAL ACETATE-AMMONIA COMPLEXES) อ.ที่ปรึกษาหลัก : รศ. ดร.นวลพรรณ จันทรศิริ

สารประกอบเชิงซ้อนโลหะแอซีเทต-แอมโมเนีย คือ $Cu(Amm)$ และ $Zn(Amm)$ (เมื่อ $Amm = ammonia$) ถูกสังเคราะห์ และพิสูจน์เอกลักษณ์ด้วยเทคนิคยูวี-วิสิเบิลสเปกโทรสโกปี และมาลดิ-ทอฟ แมสสเปกโทรเมตรี จากนั้นถูกนำไปใช้เร่งปฏิกิริยาการเกิดเจล (ปฏิกิริยาพอลิเมอไรเซชัน) และปฏิกิริยาการฟู (ปฏิกิริยาการเกิดก๊าซคาร์บอนไดออกไซด์) ของโฟมพอลิยูรีเทนแบบแข็งและโฟมพอลิไอโซไซยานูเรต การเตรียมโฟมพอลิไอโซไซยานูเรตจะผสมสารละลายโพแทสเซียม ออกโทเอต ในไดเอทิลีน ไกลคอล ซึ่งเป็นตัวเร่งปฏิกิริยาไตรเมอไรเซชันกับ $Cu(Amm)$ หรือ $Zn(Amm)$ เพื่อให้ได้ตัวเร่งปฏิกิริยาผสมที่สามารถเร่งได้ทั้งปฏิกิริยาการเกิดเจล ปฏิกิริยาการฟู และปฏิกิริยาไตรเมอไรเซชัน จากนั้นเปรียบเทียบประสิทธิภาพในการเร่งปฏิกิริยาของ $Cu(Amm)$ และ $Zn(Amm)$ กับตัวเร่งปฏิกิริยาที่ใช้ในอุตสาหกรรม คือ เอ็น,เอ็น-ไดเมทิลไซโคลเฮกซิลแอมีน $(DMCHA)$ และศึกษาสมบัติการเร่งปฏิกิริยาโดยใช้เคมีคำนวณด้วยวิธีทฤษฎีเดนซิตีฟังก์ชัน (วีธีดีเอฟที) ซึ่งพิสูจน์ให้เห็นว่า $Cu(Amm)$ และ $Zn(Amm)$ เป็นตัวเร่งปฏิกิริยาประเภทกรดลิวอิส ที่สามารถลดพลังงานกระตุ้น และเพิ่มค่าคงที่อัตราการเกิดปฏิกิริยาการเกิดเจล และปฏิกิริยาการฟูได้ โดยเมื่อเปรียบเทียบกับตัวเร่งปฏิกิริยา $DMCHA$ พบว่า $Cu(Amm)$ มีประสิทธิภาพ ในการเร่งปฏิกิริยาสูงกว่า แต่ $Zn(Amm)$ มีประสิทธิภาพในการเร่งปฏิกิริยาด้อยกว่า โดยโฟมพอลิยูรีเทน แบบแข็งที่เร่งปฏิกิริยาด้วย $Cu(Amm)$ มีความหนาแน่น เปอร์เซ็นต์การเกิดปฏิกิริยาของสารประกอบ ไอโซไซยาเนต และความต้านทานต่อแรงกดอัดที่ใกล้เคียงกับโฟมพอลิยูรีเทนแบบแข็งที่เร่งปฏิกิริยาด้วย $DMCHA$ โฟมพอลิไอโซไซยานูเรตที่เตรียมโดยใช้ค่าดัชนีไอโซไซยาเนตเท่ากับ 200 จะมีความต้านทาน ต่อแรงกดอัด สมบัติการหน่วงไฟ และความเสถียรต่อความร้อน ที่สูงกว่าโฟมพอลิยูรีเทนแบบแข็ง โดยโฟมพอลิไอโซไซยานูเรตที่เตรียมจากตัวเร่งปฏิกิริยาผสมของสารละลายโพแทสเซียม ออกโทเอต กับ $Cu(Amm)$ หรือ $Zn(Amm)$ จะไม่เปราะและไม่แตกหักเมื่อทดสอบความต้านทานต่อแรงกดอัด เหมือนโฟมที่เตรียมจากตัวเร่งปฏิกิริยาผสมของสารละลายโพแทสเซียม ออกโทเอตกับ $DMCHA$

สาขาวิชา	ปิโตรเคมีและวิทยาศาสตร์พอลิเมอร์	ลายมือชื่อนิสิต	....
ปีการศึกษา	2561	ลายมือชื่อ อ.ที่ปรึกษาหลัก	....

5972863323 : MAJOR PETROCHEMISTRY AND POLYMER SCIENCE
KEYWOR   METAL ACETATE-AMMONIA COMPLEXES,
D: POLYURETHANE FOAM, POLYISOCYANURATE FOAM,
         CATALYST, DFT METHOD

Benjatham Sukkaneewat : PREPARATION OF POLYURETHANE AND POLYISOCYANURATE FOAMS CATALYZED BY METAL ACETATE-AMMONIA COMPLEXES. Advisor: Assoc. Prof. Nuanphun Chantarasiri, Ph.D.

Metal acetate-ammonia complex solutions, namely Cu(Amm) and Zn(Amm), were synthesized and characterized by UV-visible spectroscopy and MALDI-TOF mass spectrometry. Cu(Amm) and Zn(Amm) were used as homogeneous catalysts for accelerating gelling (urethane formation) and blowing reactions (CO_2 generation) of rigid polyurethane (RPUR) and polyisocyanurate (PIR) foams. Potassium octoate solution in diethylene glycol, which was used as a trimerization catalyst, was mixed with Cu(Amm) or Zn(Amm) to give a catalyst mixture which can catalyze gelling, blowing and trimerization reactions for the preparation of PIR foams. The catalytic activity of Cu(Amm) and Zn(Amm) in gelling and blowing reactions was compared to that of *N,N*-dimethylcyclohexylamine (DMCHA), which is an industrial catalyst, and studied by density functional theory (DFT) method, which revealed that Cu(Amm) and Zn(Amm) were Lewis acid catalysts and could decrease the activation energy, but increase the rate constant of gelling and blowing reactions. Cu(Amm) had higher catalytic activity, while Zn(Amm) had lower catalytic activity than DMCHA. Cu(Amm) gave rigid PUR foams with comparable density, % isocyanate conversion and compression strength to those of DMCHA. PIR foams prepared from the mixtures of potassium octoate solution with Cu(Amm) or Zn(Amm) at isocyanate index of 200 had better compression strength, fire-retarded properties and thermal stability than their relating rigid PUR foams. These PIR foams were the ductile materials which had higher compression strength and did not rupture during the compressing test in comparison to the PIR foam prepared from the mixture of potassium octoate solution with DMCHA.

Field of Study:	Petrochemistry and Polymer Science	Student's Signature	....
Academic Year:	2018	Advisor's Signature	....

ACKNOWLEDGEMENTS

Benjatham Sukkaneewat

TABLE OF CONTENTS

Page

จุฬาลงกรณ์มหาวิทยาลัย

CHULALONGKORN UNIVERSITY

LIST OF TABLES

จุฬาลงกรณ์มหาวิทยาลัย

CHULALONGKORN UNIVERSITY

LIST OF FIGURES

LIST OF SCHEMES

LIST OF ABBREVIATIONS

%	Percentage
ε	Molar absorptivity
Ψ	Wave function
Å	Angstrom
ATR-IR	Attenuated Total Reflectance-Infrared
Amm	Ammonia
B3LYP	Becke 3-Parameter, Lee, Yang and Parr
cm	Centimeter
cm^{-1}	Unit of wavenumber
°C	Degree Celsius (centrigrade)
Cu(Amm)	Copper-ammonia complex
DBTDL	Dibutyltin dilaurate
DFT	Density functional theory
DMCHA	*N,N*-Dimethylcyclohexylamine
E	Energy
e	Electron
$\Delta E^{\ddagger}$	Activation energy
E_g	Energy gab
eV	Electron volt
FMO	Frontier molecular orbital
FTIR	Fourier Transform Infrared Spectrophotometer
G	Gibbs free energy
ΔG^{o}_{298}	Change of standard Gibbs free energy
g	Gram
H	Enthalpy
$\hat{H}$	Hamiltonian
ΔH^{o}_{298}	Change of standard enthalpy
h	Hour
h	Plank's constant

HF	Hartree–Fock
HOMO	Highest occupied molecular orbital
INT	Intermediate
IRC	Intrinsic reaction coordinate
K	Equilibrium constant
κ	Kappa
k_B	Boltzman's constant
$k(T)$	Rate constant
KOH	Potassium hydroxide
KOct	Potassium octoate
Kg	Kilogram
kV	Kilovolt
LUMO	Lowest unoccupied molecular orbital
M	Metal
M(OAc)$_2$	Metal acetate
m^3	Cubic meter
MDI	4,4'-Methane diphenyl diisocyanate
mg	Milligram
min	Minute
mL	Milliliter
mm	Millimeter
mmol	Millimole
N	Newton unit
NBO	Natural bond orbital
NCO	Isocyanate
NCO	Isocyanate index
OAc	Acetate
OHV	Hydroxyl value
pbw	Part by weight
PIR	Polyisocyanurate
PMDI	Polymeric 4,4'-methane diphenyl diisocyanate
PUR	Polyurethane

PS	Polystyrene
QM	Quantum mechanics
Q_{PCT}	Partial charge transfer
Q_R	Partition functions for reactant
QST2	Quadratic synchronous transit
Q_{TS}	Partition functions for transition state
R	Gas constant
rpm	Round per minute
RPUR	Rigid polyurethane
RT	Room temperature
ref	Reference
s	Second
SCF	Self–consistent–field
SEM	Scanning Electron Microscope
T	Absolute temperature
t	Time
TEDA	Triethylenediamine
TDI	Toluene diisocyanate
TGA	Thermogravimetric Analysis
T_{max}	Temperatures at maximum rate of weight loss
TS	Transition state
UV	Ultraviolet
Zn(Amm)	Zinc-ammonia complex
ZPVE	Zero point vibrational energy

CHAPTER 1

INTRODUCTION

Polyisocyanurate-polyurethane (PIR) and rigid polyurethane (PUR) foams have been extensively utilized as thermal insulation materials for constructions and buildings owing to their low thermo-conductivity, light weight, good dimensional stability and small water absorption (1-3). The repeating units of rigid PUR and PIR foams are urethane and isocyanurate-urethane linkages, respectively. The contained isocyanurate structures of PIR foam provide the inherent thermal stability and fire-retarded properties to the foams (4-6). Therefore, PIR foams have been required for the applications which need more thermal stability and fire-retarded properties in comparison to the conventional rigid polyurethane foams. The included urethane structures are necessary for reducing the brittleness of PIR foam due to the fact that unmodified PIR foams with too many isocyanurate structures are extremely fragile and unable to use in practical applications (4, 7). The two main reactions of PUR foam are gelling (polymerization) and blowing reactions which are the reactions between equivalent amount of isocyanate compound with alcohol and water, respectively. The products of gelling and blowing reactions are polyurethane and carbon dioxide gas, respectively. The carbon dioxide is the blowing gas for generating the foaming process and leading to the cellular structures of the foam. For the processing of PIR foam, the excess amount of isocyanate compound is used. Therefore, the three main reactions which lead to PIR foams compose gelling, blowing and trimerization reactions. Trimerization reaction is the cyclization reaction between three isocyanate groups to give isocyanurate structures (8).

Catalysts are important for all main reactions of rigid PUR and PIR foams. The general isocyanurate catalysts for accelerating the rate of trimer formation are quaternary ammonium salts and alkali metal carboxylates, such as potassium octoate (KOct) and potassium acetate (KOAc). Gelling and blowing catalysts are also needed for accelerating and balancing the rate of gelling and blowing reactions, respectively, during the foam formation. Two types of industrial catalysts, which are widely used for the production of rigid PUR and PIR foams, are tertiary amines and organotin

compounds due to their good catalytic activity in gelling and blowing reactions. Organotin compounds, such as dibutyltin dilaurate (DBTDL), dibutyltindilaurylmercaptide and stannous octoate, are the Lewis acid catalysts and show the effective catalytic activity in gelling reaction. Tertiary amines, such as *N,N*-dimethylcyclohexylamine (DMCHA), triethylamine (TEA) and triethylenediamine (TEDA), are the Lewis base catalysts and can accelerate both gelling and blowing reactions (8-10). The catalyst system for PIR foam are the mixtures of tertiary amines or organotin compounds with the isocyanurate catalysts (1, 11, 12) in order to obtain the optimum reaction rate among gelling, blowing and trimerization reactions. However, the solubility of DMCHA and potassium octoate solution the diethylene glycol in the presence of water is limited (13). In addition, Organotin compounds and tertiary amine catalysts are concerned about their toxicity and strong odor problems, respectively (10, 14-17).

From the above drawbacks, metal compounds, metal complexes and organocatalysts have been investigated as alternative catalysts for gelling and blowing reactions in various polyurethane applications. For instance, waterborne polyurethanes were prepared by use of bismuth carboxylate and zinc acetylacetonate as catalysts (18, 19). Manganese acetylacetonate/triethylenediamine catalyst system (20) was a good catalyst for polymerization of isophorone diisocyanate-diethylene glycol. A mixture of neodymium chloride Schiff base and triethylenediamine was used to accelerate semi-rigid PUR foams (21). Iron acetylacetonate was a catalyst in the preparation of composite scaffold between polyurethane foam and nanohydroxyapatite (22). Examples for organocatalysts are basic and organic compounds derived from guanidine, amidine and phosphonic acid (17, 23). There have been development of catalysts with desirable catalytic properties for rigid PUR foam in our research group. These catalysts are copper acetate-amine (24), copper acetate-ethanolamine and zinc acetate-ethanolamine complexes (25).

Copper acetate- and zinc acetate-ammonia complexes, namely Cu(Amm) and Zn(Amm), are of interest as the catalysts for gelling and blowing reactions of rigid PUR and PIR foams. Cu(Amm) have been applied for several works such as the Schweizer's reagent for dissolving cellulose in rayon processing (26) and the metal precursors for synthesis of copper oxide in the applications of lithium-ion battery (27) and the heterogeneous catalysts (28, 29). Zn(Amm) have also been utilized as the

metal precursors for synthesis of zinc oxide in the applications of solar cell (30) and thin film transistors (31). However, both Cu(Amm) and Zn(Amm) have never been reported as the catalysts for rigid PUR and PIR foams, especially in the aqueous solution form. Therefore, the investigation of catalytic activity of Cu(Amm) and Zn(Amm) in gelling and blowing reactions has been performed in this work. The complex formation of copper or zinc acetate with ammonia can occur using water as the solvent to obtain the aqueous solutions of Cu(Amm) and Zn(Amm), respectively. These aqueous catalyst solutions are expected to improve the solubility with all starting materials of rigid PUR and PIR foams and can be used for the foam processing without the purifying step. Water in catalyst solutions can serve as a chemical blowing agent for both foams.

Objectives of the research

The objectives of this work are as follow:

- To synthesize and characterize metal-ammonia complex aqueous solutions, namely Cu(Amm) and Zn(Amm)

- To use these catalyst solutions as the homogeneous catalysts for accelerating gelling and blowing reactions of rigid PUR and PIR foams

- To experimentally and theoretically study their catalytic activity in gelling and blowing reactions

- To compare their catalytic activity to the industrial catalyst system (DMCHA catalyst) and

- To investigate the obtained properties of rigid PUR and PIR foams catalyzed by Cu(Amm) and Zn(Amm).

Scope of the research

The scope of research investigation is summarized in Figure 1.1, which covers four parts of experimental and theoretical studies and corresponds to the research objectives listed above. The details of each part are as follows:

- In the first part, Cu(Amm) and Zn(Amm) have been synthesized in water from the coordination reaction of copper or zinc acetates with ammonia using the

molar ratio of metal acetate:ammonia of 1:6 and characterized by UV-visible spectrophotometry, FT-IR spectroscopy and MALDI-TOF mass spectrometry.

- The second and the third parts have been conducted in order to evaluate the catalytic activity of Cu(Amm) and Zn(Amm) in gelling and blowing reactions of rigid PUR and PIR foams using experimental investigation. The reaction time of the foams, which indicate the catalytic reactivity of the catalysts, has been measured. The important parameters have been varied. For example, in rigid PUR foam processing, the catalysts have been varied their contents of 0.5, 1.0 and 1.5 pbw to confirm their characteristic of gelling and blowing catalysts and to study the effect of catalyst contents on the foam properties. NCO indices have been varied of 160, 200 and 250 to investigate their effect on PIR/PUR proportions of the foams. The obtained properties of rigid PUR and PIR foams, which are affected by the catalytic activity of Cu(Amm) and Zn(Amm), including physical properties, PIR/PUR proportions, % isocyanate conversion, fire-retarded properties, thermal properties and mechanical properties have been investigated. These foam properties have been compared to those obtained from DMCHA catalyst (for the rigid PUR foam) and the catalyst mixture of DMCHA with potassium octoate solution (for the PIR foam).

- The last part of this research is computational study. The reaction pathways with involved configurations and the thermodynamic properties of catalyzed gelling and blowing reactions have been studied. The catalytic mechanism with electron transfer process and the HOMO-LUMO orbital distributions with energy gab between catalyzed compounds have been investigated. All calculations have been carried out with the GAUSSIAN 09 program using DFT method at CAM–B3LYP/6–31G(d)] level of theory.

PREPARATION OF POLYURETHANE AND POLYISOCYANURATE FOAMS CATALYZED BY METAL ACETATE-AMMONIA COMPLEXES

Part I: Synthesis and characterization of Cu(Amm) and Zn(Amm) aqueous solutions

UV-Visible spectroscopy

FT-IR spectroscopy

MALDI-TOF mass spectrometry

Part II: Preparation of rigid PUR foams using Cu(Amm) and Zn(Amm) as gelling and blowing catalysts

Part III: Preparation of PIR foams catalyzed by Cu(Amm) and Zn(Amm) as the gelling and blowing catalysts and potassium octoate as the trimerization catalyst

Physical properties:
- density
- foam appearance
- morphology

Catalytic efficiency:
- reaction time
- NCO conversion
- PIR/PUR proportion

Fire-retarded properties:
- burning test
- % limiting oxygen index

Thermal properties:
thermogravimetric analysis (TGA)

Mechanical properties:
compression test

Comparison of catalytic activity and foam properties to those of DMCHA for rigid PUR foams and the mixture of DMCHA and potassium octoate solution for PIR foams

Part IV: Study catalytic properties of Cu(Amm) and Zn(Amm) in gelling and blowing reactions using computational study [CAM–B3LYP/6–31G(d)]

Reaction pathways with involved configurations

Catalytic mechanism with electron transfer (Natural bond orbital analysis)

HOMO-LUMO orbital distributions with energy gab (Frontier molecular orbital analysis)

Thermodynamic and kinetic investigation of catalyzed gelling and blowing reactions

Figure 1.1 Experimental diagram.

CHAPTER 2

THEORY AND LITERATURE REVIEWS

2.1 General background

Polyurethane (PUR) materials utilized for industries were originated by Otto-Bayer and his co-workers in the late 1930s. The potential applications of PUR at that initial time were the fiber, the adhesive, the coating and the foam. However, the development of these polymer materials has been conducted over the past thirty years. Some examples of important development of PUR are listed in Table 2.1. Until now, PUR materials play the vital role in several industries. The number of PUR applications has been increased from furnitures to footwears and constructions to cars. This makes PUR to be one of the most versatile polymer materials. The wide range of grades and product types (Figure 2.1), whose density varies in the range of 6-1,220 kg/m^3 from the elastomer to the hard plastic including our rigid PUR foam, can be obtained with various PUR formulations (8, 32). Polyisocyanurate-polyurethane (PIR) materials are obtained by trimerization reaction of isocyanate groups accompanying with the polymerization between isocyanate with hydroxyl groups. This makes these materials to have both isocyanate and urethane linkages in the structures. The first patent reporting about isocyanurate-urethane linkages of PIR foam appeared in 1961 (4) and the aim of this work was to increase the crosslink density of conventional PUR foam. However, the thermal properties of this polymer were first reported via the TGA results by Nicholas and Gmitter in 1965 (33). Unlike the urethane linkages of the conventional PUR materials, the isocyanurate linkages in PIR materials do not have labile hydrogen which can be dissociated at low temperature. This leads PIR materials to have better thermal properties than the conventional PUR materials (4).

Rigid PUR foams are the PUR materials having the cellular structures. They are mostly utilized for the constructions, such as the boardstock, sandwich panels, refrigeration and technical insulation, due to the long-term thermal insulating performance together with the dimensional stable and light weight. Rigid PUR foams can be produced in the wide range of density of 10-1,000 kg/m^3, however, most are

used in the range of 28-50 kg/m^3 (8). The density is the important property for determining the applications of rigid PUR foam. The major developments of rigid PUR foam have purposed to increase the use of environmentally friendly starting materials, especially the blowing agent of the foams, and improve the fire performance. For PIR foams, their applications are similar to those of rigid PIR foams and emphasize for the fire-saver constructions such as petrochemical tanks and pipelines (4, 8).
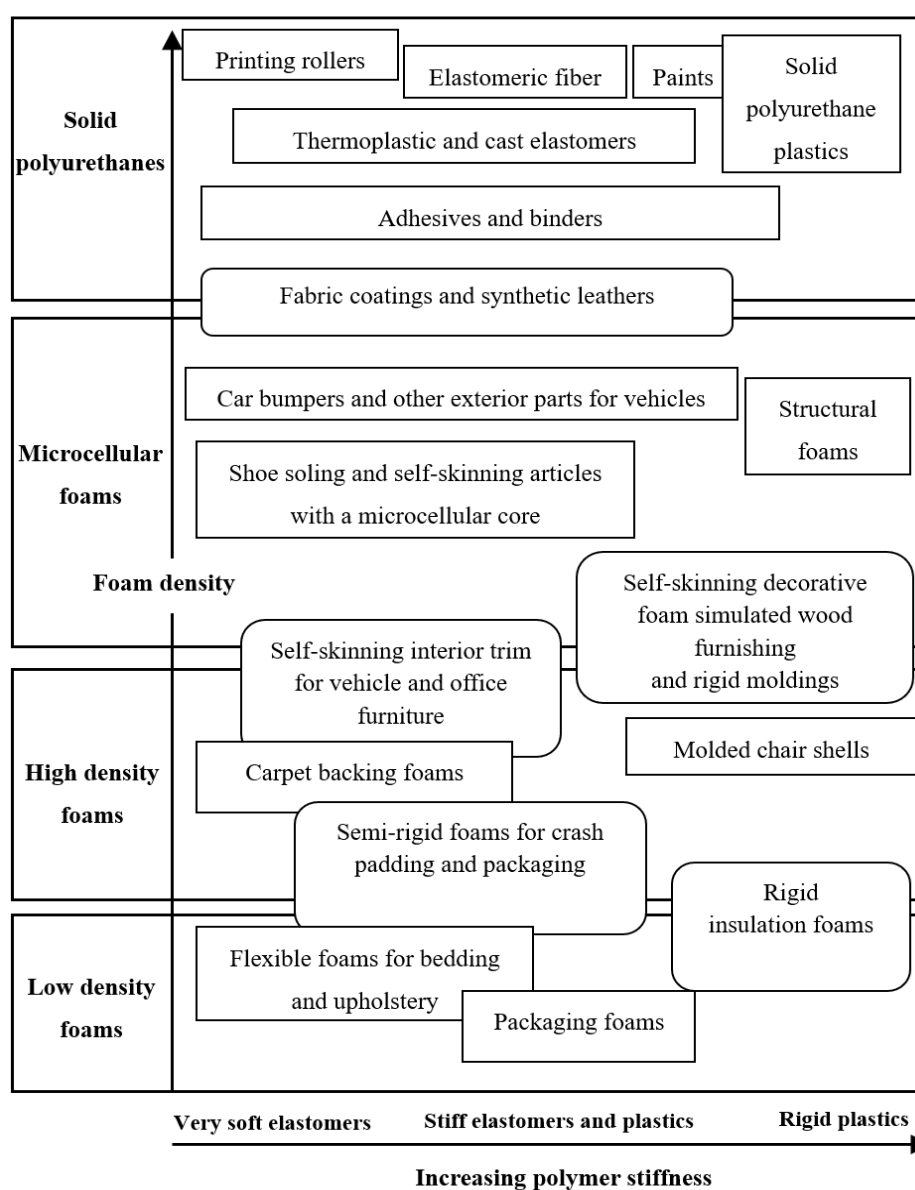
Figure 2.1 The wide range of grades and product types of polyurethane (8).

Table 2.1 Important development of polyurethanes (32).

Periods	Developments
1937-40	Otto Bayer and co-worker made polymer by polyaddition processes from various diisocyanates with glycols and/or diamines.
1940-45	Development of millable polyurethane elastomers and adhesives in Germany (I.G. Farben), U.K. (ICI) and the U.S.A. (Du Pont). Polyurethane coatings for barrage balloon (ICI), synthetic polyurethane bristles (I.G. Farben).
1945-47	Manufacture of millable polyurethane elastomers, coatings and adhesives
1950	Cast elastomers from polyester diols, diisocyanate prepolymers and chain-extenders
1953	First flexible polyurethane foam manufacture with a Bayer system using a high pressure machine, a polyester polyol and TDI.
1956	First manufacture of polyether-based flexible polyurethane foam in the U.S.A. using a two stage or 'pre-polymer' process.
1957	ICI introduces the first commercially available polymeric MDI composition for rigid polyurethane foam manufacture.
1959	ICI introduces the first rigid foam system based on polymeric MDI and a polyether polyol.
1959	'One-shot' system for flexible polyether-based foam introduced in U.S.A.
1960	ICI introduces the first polymeric MDI-based semi-rigid energy absorbing foam for vehicles.
1960-65	Rigid foam blowing by chlorofluoromethanes.
1962	First production line molded 'deep seat' flexible polyurethane car cushions at Austin-Morris (U.K.).
1963	ICI demonstrates production line manufacture of refrigerators using MDI-based polyurethane foam.
1963	First cold-store built entirely from metal-faced polyurethane rigid foam laminate mad continuously (Australia).
1964	ICI inverse- and floating- platen systems for the continuous manufacture for rigid polyurethane foam-cored build boards in production.
1965	First commercial production of self-skinning flexible foam (Soc. Quillery, France).
1968	ICI introduces isocyanurate rigid foams.
1968	General Motors make the first polyurethane microcellular bumper for the Pontiac G.T.O.
1973	MDI based 'soft-face' bumpers made by RIM system for Chevrolet taxis.
1979	ICI introduces wholly-MDI-based systems for flexible foam molding.
1983	ICI introduces system to make dual-hardness, molded seating from MDI-based, flexible foam.

The chemistry, starting materials and manufacturing processes of rigid PUR and PIR foams are similar, except that the different isocyanate index and the specific catalyst system are used for each foam type as described in the following sections.

2.2 Chemistry

Rigid PUR and PIR foams are obtained by several exothermic reactions of isocyanate compound. PUR structures are formed by the reaction between di- or polyfunctional isocyanate compounds with di- or polyfunctional hydroxyl compounds, while PIR structures are formed by trimerization of isocyanate groups (4, 8, 32, 34). For simplicity, the reactions which lead to the formation of urethane, isocyanurate and the other linkages in rigid PUR and PIR foams are described using monofunctional compounds as follows:

2.2.1 Primary reactions of isocyanate

Isocyanates can react with active hydrogens to form urethane, amine, and substituted urea linkages. All primary reactions of isocyanate are exothermic reactions, whose heat release gives the energy to cure PUR or PIR chains, to drive the foaming process and to increase the other secondary reactions. Several catalysts are employed to enhance and balance the rate among virous reactions. The details of primary reaction are as follows:

2.2.1.1 Reaction of isocyanate with polyol (gelling reaction or polymerization)

Gelling reaction (Scheme 2.1) is the polymerization reaction between isocyanate compound with polyol (alcohol). The product of the reaction is a carbamate (urethane) linkage, which can be called "polyurethane" for the higher molecular weight polymer. The rate of reaction depends on the structures of polyol and isocyanate. Aliphatic polyol having the terminated primary hydroxyl group is the most reactive and can react with isocyanate compound around ten times faster than the polyol having second hydroxyl group. Steric hindrance of isocyanate structure

also influences the rate of gelling reaction. Gelling catalysts are necessary for accelerating this reaction rate (8, 32, 34).

$$R-NCO \quad + \quad R'-OH \quad \longrightarrow \quad R-\overset{H}{N}-\overset{\overset{\displaystyle O}{\|}}{C}-OR'$$

Isocyanate   Hydroxyl   Urethane
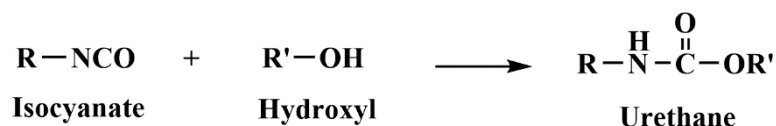
Scheme 2.1 Reaction of isocyanate with polyol (8).

2.2.1.2 Reaction of isocyanate with water (blowing reaction)

Blowing reaction (Scheme 2.2) is the reaction between isocyanate with water for producing carbamic acid intermediate which further decomposes to be carbon dioxide (CO_2) gas and primary amine. CO_2 acts as the blowing gas and inflates the foams to form the cellular structure. Water is called "a chemical blowing agent". This reaction is as important as the gelling reaction due to the fact that the density of the foams relates with the amount of CO_2 generated from the blowing reaction. Blowing catalysts are needed for this reaction (8, 9, 32, 34).

$$R-NCO \quad + \quad H_2O \quad \longrightarrow \quad \left[R-\overset{H}{N}-\overset{\overset{\displaystyle O}{\|}}{C}-OH \right]$$

Isocyanate   Water   Carbamic acid

$$R-NH_2 \quad + \quad CO_2 \uparrow$$

Amine   Carbon dioxide
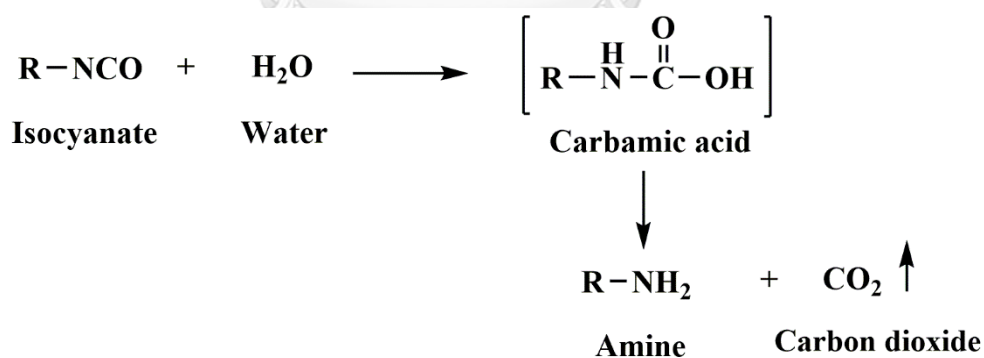
Scheme 2.2 Reaction of isocyanate with water (8).

2.2.1.3 Reaction of isocyanate with amines

The amine product from blowing reaction can further react with isocyanate to give substituted urea (Scheme 2.3), which can be a chain extender to

increase primary and secondary hydrogen bonding yielding in higher crosslink density of the foam. The reaction of aliphatic isocyanate with primary amine occurs about 100-1000 times faster than the reaction of isocyanate with alcohol. The reactivity of amine depends on its basicity and structure. The aliphatic amine with higher basicity shows more reactivity to react with isocyanate than aromatic amine. The electron withdrawing group along with steric hindrance of the carbon atom next to nitrogen atom can reduce the reactivity of amine (8, 32).

$$R-NCO \quad + \quad R'-NH_2 \quad \longrightarrow \quad R-\overset{H}{N}-\overset{\overset{O}{\parallel}}{C}-\overset{H}{N}-R'$$

Isocyanate   **Amine**   **Substituted urea**
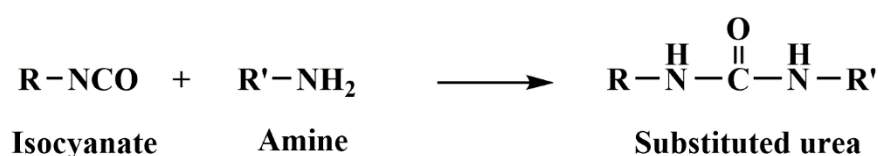
Scheme 2.3 Reaction of isocyanate with amine (8).

2.2.2 Secondary reactions of isocyanate

Isocyanate can undergo the secondary reactions with the active hydrogens of urethane and urea, which are the products of the primary reactions. These reactions can give the products which can affect both physical and mechanical properties of the foam by increasing the crosslink and branch density. All secondary reactions of isocyanate are listed as follows (4, 8, 32):

2.2.2.1 Reaction of isocyanate with urethane

Isocyanate can react with the active hydrogen of urethane to form allophanate linkage (Scheme 2.4).

$$R-NCO \quad + \quad R'-\overset{H}{N}-\overset{\overset{O}{\parallel}}{C}-OR'' \quad \longrightarrow \quad R'-\overset{H}{N}-\overset{\overset{O}{\parallel}}{C}-\underset{\underset{COOR''}{|}}{NR''}$$

Isocyanate   **Urethane**   **Allophanate**
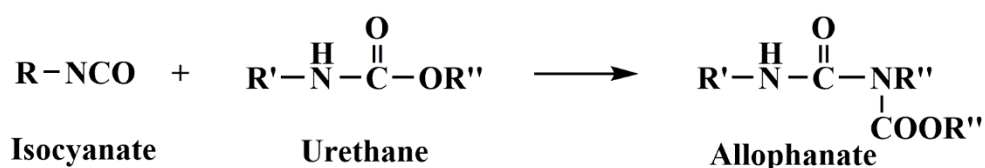
Scheme 2.4 Reaction of isocyanate with urethane (8).

2.2.2.2 Reaction of isocyanate with urea

Likewise, the reaction between isocyanate with active hydrogen of urea gives the biuret linkage (Scheme 2.5).

Scheme 2.5 Reaction of isocyanate with urea (8).

2.2.2.3 Trimerization reaction

Three isocyanates from the excess amount of isocyanate compound (isocyanate index > 100) can undergo a cyclization reaction through C=N bonds resulting in a six-membered ring called a trimer or isocyanurate (Scheme 2.6), which can be "polyisocyanurate" for the higher molecular weight polymer (4, 8, 32). Polyisocyanurate are thermally stable and can improve both fire-retarded properties and thermal stability of PIR foam. The foams with adequate PIR proportion have self-extinguishing properties and can be increased decomposition temperature to 250-300 °C (35).

Scheme 2.6 Trimarization reaction of isocyanate (8).

Among secondary reactions of isocyanate, the reaction with urea is the fastest and can occur at the lower temperature than the trimerization and the reaction with urethane. All these secondary reactions are the crosslinking and branching reactions. The number of products of each reaction can be controlled using the specific functionality of reactant, reaction temperature and catalyst types.

2.3 Starting materials

Isocyanate and polyol compounds are the major starting materials of rigid PUR and PIR foams. In order to modify the properties of the foams to reach the commercial and industrial requirements, other additives, namely catalyst, blowing agent, flame retardant, surfactant, filler, chain extender and viscosity reducer are used in the formulations of the foam. The details of these starting materials are given as follows (8, 32, 36):

2.3.1 Isocyanate compounds

Various types of aromatic and aliphatic isocyanate compounds can be found in the production of rigid PUR and PIR foams. However, more than 95% of all foams are prepared from toluene diisocyanate (TDI) and methane diphenyl diisocyanate (MDI).

2.3.1.1 Toluene diisocyanate (TDI)

Toluene diisocyanate is the viscous liquid with the boiling point of 120 ℃. it can be synthesized via the direct nitration of toluene obtaining the product ratio of 2,4:2,6- dinitrotoluenes of 80:20. These dinitrotoluenes are further hydrogenated, phosgenated and distilled to obtain TDI liquid, which composes of 2,4:2,6-TDI isomer of 80:20. Chemical structures of 2,4 and 2,6-TDI are presented in Figure 2.2. TDI mixture can cause a serious toxic hazard and have a marked effect on the respiratory system and the skin. On the other hand, the diisocyanate of MDI based on diaminodiphenylmethane is safer to use and has much lower volatile component than that of TDI.
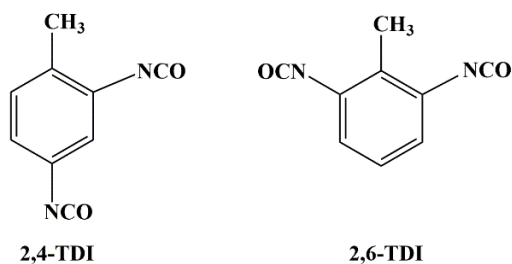
Figure 2.2 Chemical structures of 2,4 and 2,6-TDI (8).

2.3.1.2 4,4'- Methane diphenyl diisocyanate (MDI)

4,4′-Methane diphenyl diisocyanate is the crystalline solid at room temperature. The melting and boiling points of this chemical are 38 and 195 °C, respectively. Therefore, it can be slightly heated to become the viscous liquid when used. MDI composes of two main types, namely monomeric MDI and polymeric MDI (PMDI). PMDI contains 55% of 4,4'- and 2,4'- diisocyanate isomers, 25% of triisocyanate and small amount of the 2,2′-diisocyanate isomer. Pure MDI, which is obtained from the distillation of PMDI, mostly contains 4,4′- diisocyanate isomer. The chemical structures of PMDI and monomeric MDI are shown in Figure 2.3.
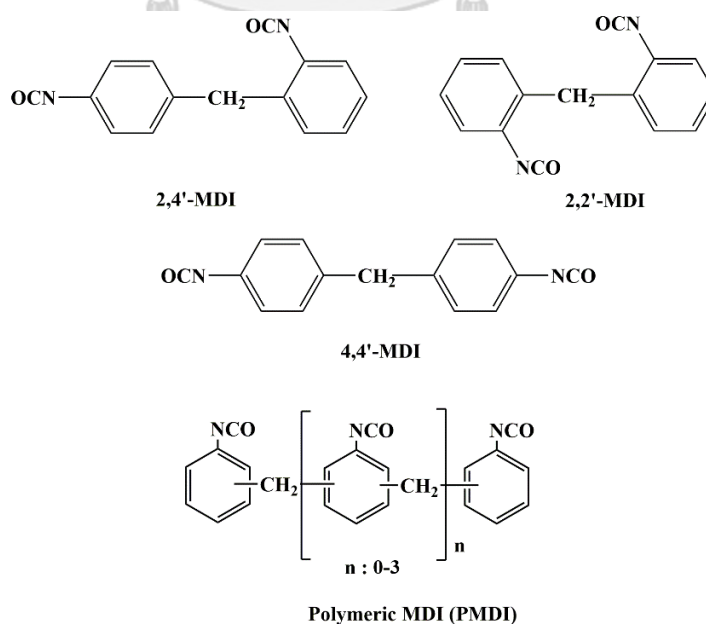
Figure 2.3 The chemical structure of MDI and PMDI (8, 32).

MDI can be manufactured to have the wide range of functionality, structures and composition for several applications of polyurethane as shown in Table 2.2.

Table 2.2 Several MDI starting material for different applications (32).

Isocyanate compounds	Average functionality	Material types
Pure MDI	2.0	High performance PUR elastomer
Modified pure MDI liquid	2.01-2.1	High performance PUR elastomer and microcellular PUR elastomer.
Low functionality polyisocyanate liquid	2.1-2.3	Flexible, semi-rigid and rigid (structural) PUR foams.
Low viscosity polyisocyanate liquid	2.5	High density flexible PUR foam
Low viscosity polymeric MDI	2.7	Low density rigid PUR foam, PIR foam and particle binders
High functionality polymeric MDI	2.8-3.1	Rigid PUR and PIR foams.

2.3.2 Polyols

The two main types of polyol for the production of rigid PUR and PIR foams are hydroxyl-terminated polyether and polyester polyols. These polyols are prepolymers whose different structures, functionality and molecular weight affect the final properties of the foam. The polyols with low functionality and high molecular weight are mostly employed for the preparation of flexible polyurethane foam. In contrast, the high functionality and low molecular weight polyols are used to processed rigid PUR and PIR foams due to the reason that they can provide the high crosslink density, which enhances the mechanical properties of the foams. Moreover, the distance between chain segment of polyol is another factor affecting the rigidity of the foams. The polyol with shorter chain segment can give the foams with more rigidity and tighter networks. In general, polyols for rigid PUR and PIR foams have

molecular weight, functionality and hydroxyl value in the range of 150-1000 g/mol, 2.5-8.0 and 250-1000 mgKOH/g, respectively (36, 37).

2.3.2.1 Polyether polyols

Polyether polyols are the long chain-polyols which range from viscous liquid to waxy solid based on their structures and molecular weight. These polyols are synthesized from ring opening reactions of ethylene or propylene oxide using the polyfunctional initiators. Polyether polyols have been widely used for the processing of rigid PUR and PIR foams owing to their low cost and viscosity. Furthermore, the foams processed from polyether polyols show better resilience and hydrolysis resistance than the foams processed from polyester polyols. The chemical structure of polyether polyol is presented in Figure 2.4.

2.3.2.2 Polyester polyols

Polyester polyols are synthesized from the condensation reactions of diols (and triol) with dicarboxylic acid, such as adipic acid, sebacic acid and *m*-phthalic acid. When compared to polyether polyols, polyester polyols seem more reactive and give the foams with better mechanical properties and organic solvent resistance. However, polyester polyols are more expensive and have higher viscosity than polyether polyols. Thus, they are used only for the applications that require superior properties. The chemical structure of polyester polyol is presented in Figure 2.4.

$$H \left[O - R - O - R \right]_n O - R - OH$$

Polyether polyol

$$H \left[O - R' - \overset{\overset{\displaystyle O}{\|}}{C} - O - R - \overset{\overset{\displaystyle O}{\|}}{C} \right]_n O - R' - OH$$
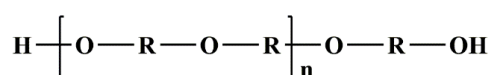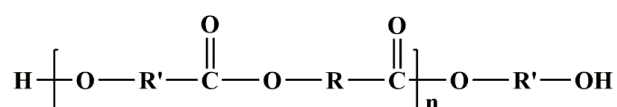
Polyester polyol

Figure 2.4 Basic chemical structures of polyether and polyester polyols (37).

2.3.3 Catalysts

The generally used catalysts for rigid PUR and PIR foams can be divided into three categories as blowing, gelling and trimerization catalysts which are based on the main reactions they promote as shown in Table 2.3. These include a wide range of chemical structures, such as tertiary amines, organotin compounds, quaternary alkali metal carboxylates and ammonium salts. The different structures and properties of catalyst lead to the several catalytic mechanisms in the formation of rigid PUR and PIR foams (8, 10, 36).

Table 2.3 The typical catalysts and their catalytic activity used in the processing of rigid PUR and PIR foams (36).

Catalyst	Code	Catalytic activity
Tertiary amines		
Pentamethyldiethylene triamine	PMDETA	Blowing catalyst
Triethylenediamine	TEDA	Gelling catalyst
N,N-Dimethylcyclohexylamine	DMCHA	Blowing/ gelling catalysts
Quaternary ammonium salts		
2-Hydroxyl propyl trimethyl ammonium salt	TMR-2	Delayed action/ trimerization catalysts
Alkali metal carboxylates		
Potassium acetate	KOAc	Gelling/ trimerization catalysts
Potassium octoate	KOct	Gelling/ trimerization catalysts
Organotin compounds		
Stannous octate	SnOct	Gelling catalyst
Dibutyltin dilaurate	DBTCL	Gelling catalyst

In the production of rigid PUR foams, catalysts are needed to balance between gelling and blowing reactions. The catalytic activity affects not only the reaction rate but also the ultimate properties of the final polymer. With suitable

catalysts, the desired properties of rigid PUR foam can be obtained. The catalyst activity of gelling and blowing catalysts depends on the basicity and the steric hindrance around the active site of the catalyst. The selection of catalyst for foam processing is based on the catalytic reactivity, odor, toxicity, solubility and cost of the catalyst. The effect of catalytic activity in gelling and blowing reactions on the foam properties is shown in Figure 2.5. In general, the strong gelling catalysts give the foams with high adhesive strength and good dimensional stability, but the reaction mixture has poor flowability in mold. On the other hand, strong blowing catalysts give the low density of foams and better flowability. However, the foams have poor adhesive strength (9).
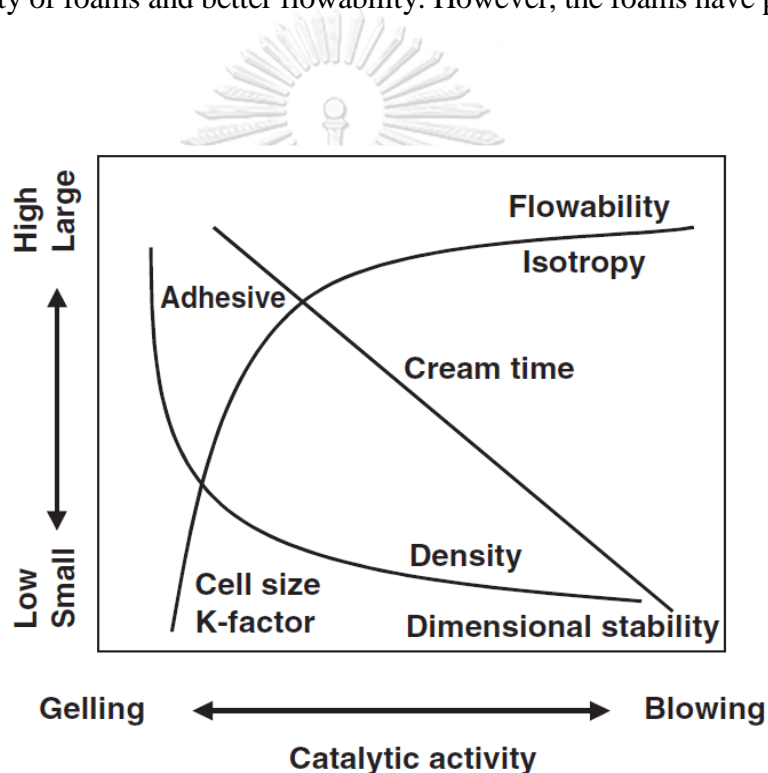
Figure 2.5 The effect of catalytic activity on the foam properties (9).

PIR foams contain both polyurethane and polyisocyanurate structures. The optimum proportion between PUR and PIR in the foam structures is required due to the fact that the foams containing too few PIR structures do not give the fire-retarded properties, while the foams containing too many PIR structures are brittle (38). Thus, in order to obtain the suitable composition of PIR foams, the catalyst mixtures composing of gelling, blowing and trimerization catalysts are commonly used for the

catalytic systems of PIR foam. The details of all catalysts of rigid PUR and PIR foams are described as follows:

2.3.3.1 Tertiary amine catalysts

Tertiary amines can accelerate both isocyanate–polyol (gelling) and isocyanate–water (blowing) reactions. However, their catalytic activity in blowing reaction appears to be better than that in gelling reaction. The most relevant parameters which affect their reactivity are basicity and steric hindrance around the amino nitrogen atom. Catalytic activity normally increases with increasing the basicity and decreasing the steric hindrance in the structures. The ability to form hydrogen bonds and the spatial separation between active sites also affect the catalytic selectivity. Some of the most commonly used tertiary amine catalysts are *N,N*-dimethylcyclohexylamine, triethylenediamine and dimethylaminoethoxyethanol (9). Two catalytic mechanisms of tertiary amine have been proposed. The first is nucleophilic catalysis given by Baker (Scheme 2.7), the mechanism starts by the tertiary nitrogen of amine coordinating with the carbonyl carbon of the isocyanate group, then complex intermediate is formed. This intermediate further reacts with the hydrogen from polyol or water to produce urethane linkage or carbamic acid, respectively.

Scheme 2.7 Catalytic mechanism of tertiary amine given by Baker (8).

The second mechanism is general base catalysis given by Farka (Scheme 2.8), the activation starts by the tertiary nitrogen of amine interacting with the proton of polyol or water to form a complex intermediate and then reacts with the isocyanate to give urethane linkage or carbamic acid, respectively (8, 9).

$$R'{-}OH \ + \ R''_3N \longrightarrow \ R''_3N{\cdots}H{\cdot\cdot}O{-}R' \ + \ R{-}N{=}C{=}O$$

$$R{-}N{=\!=}C{=\!=}O$$

$$R''_3N{\cdots}H{\cdot\cdot}O{-}R'$$

$$R''_3N \ + \ R{-}\overset{H}{N}{-}C\overset{O}{\underset{O-R'}{}}$$
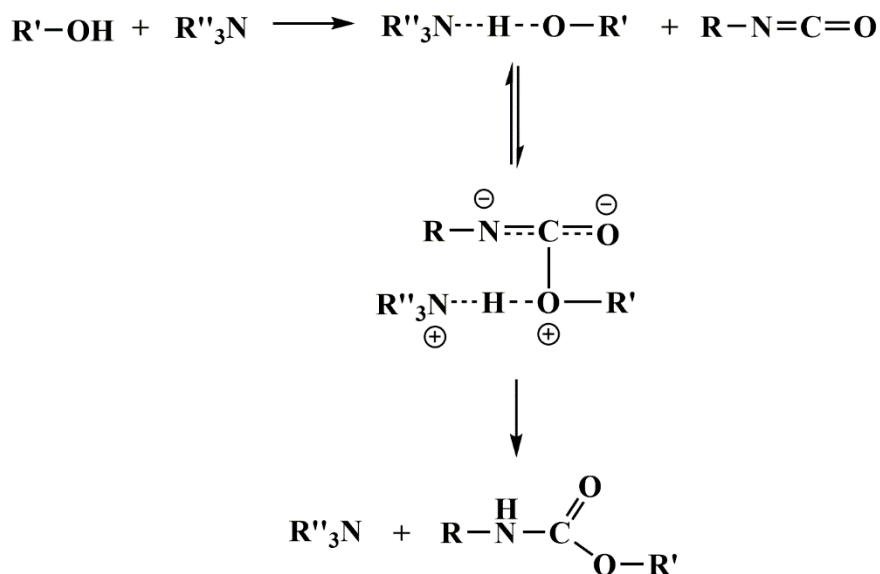
Scheme 2.8 Catalytic mechanism of tertiary amine given by Farka (8).

2.3.3.2 Organometallic catalysts

Organometallic compounds are classified to be predominantly gelling catalysts even though they can slightly increase the rate of blowing reaction. Organotin compounds are the most widely used, while organomercury and organolead catalysts are also used in other applications, namely PUR elastomers and rigid spray PUR foams, respectively. However, both mercury and lead catalysts have unfavorable hazard properties, and therefore, alternatives are always being sought. Among organotin catalysts, the diorganotin (IV) ester compounds show remarkably high catalytic activity toward urethane forming. Examples are dibutyltin dilaurate (DBTDL), dibutyltin *bis*(2-ethylhexanoate) and dibutyltindilaurylmercaptide. The proposed catalytic mechanism of tin (IV) catalysts (Scheme 2.9) is the reaction of tin with polyol to form tin alkoxide, which further reacts with isocyanate to obtain a

complex. Transferring of the alkoxide anion to the coordinated isocyanate affords an *N*-stannylurethane, which then undergoes alcoholysis to obtain the urethane linkage and the original tin alkoxide (8, 10).
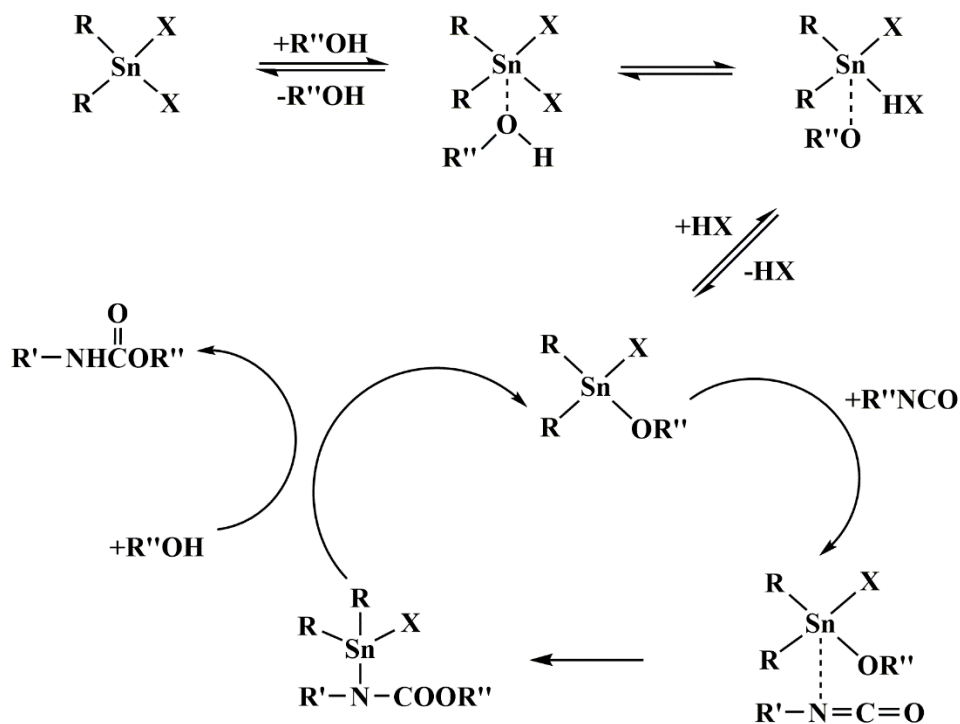
Scheme 2.9 Catalytic mechanism of tin (IV) salt catalyst (8).

Tin (II) 2-ethylhexanoate or stannous octoate has also been used as the catalyst for the foams. The catalytic mechanism of this tin (II) salts is shown in Scheme 2.10. Tin coordinates with isocyanate and polyol to form the ternary complex, which further converts to urethane. Two possible pathways of coordination of stannous octoate have been reported. Tin may first coordinate with polyol and then reacts with isocyanate. In the second one, tin may coordinate with oxygen of isocyanate and then reacts with the polyol (8).

The catalyst mixtures between tertiary amine and tin compound are often used with the purpose of achieving a balance between blowing and gelling reactions. When using the catalyst combination, synergetic effect between amine and tin in the catalytic process of urethane formation is found (8, 39-41). The synergetic mechanism is proposed as shown in Scheme 2.11.

R−NCO + R'−OH + SnX$_2$ ⟶ $\left[\begin{array}{c} \text{structure} \end{array}\right]$

R−N=C=O−SnR$_2$'''X$_2$ + R''$_3$N···H···O−R'

$$R-N\overset{\ominus}{=}C\overset{\ominus}{=}O-SnR_2'''X_2$$

R''$_3$N···H···O−R'
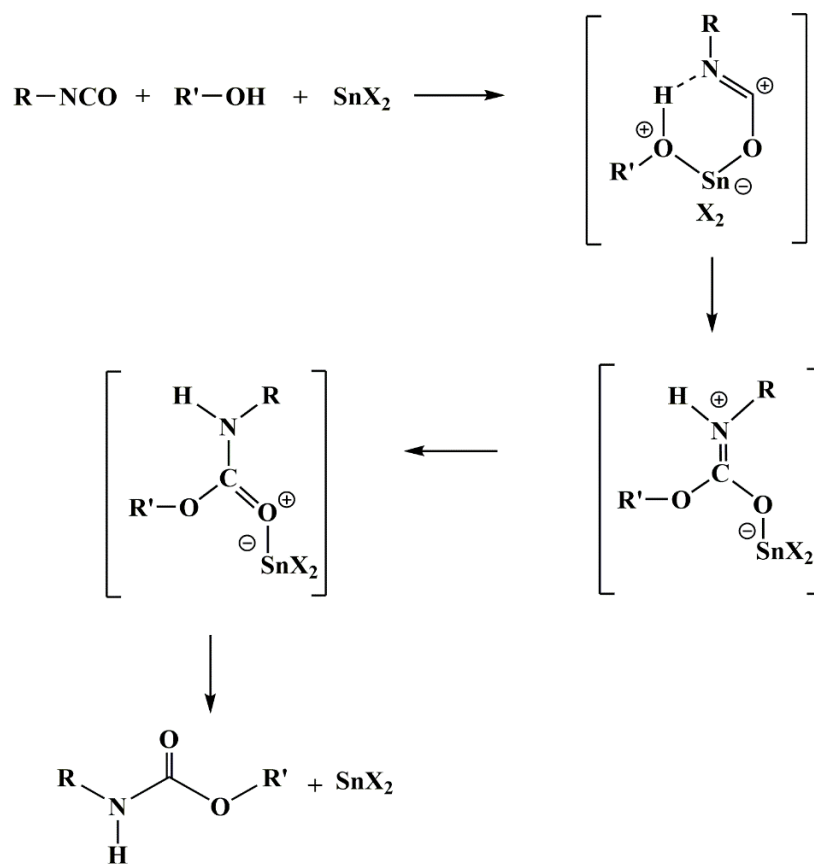
Scheme 2.10 Catalytic mechanism of tin (II) salt catalyst (8).

urethane + R''$_3$N + R$_2$'''SnX$_2$
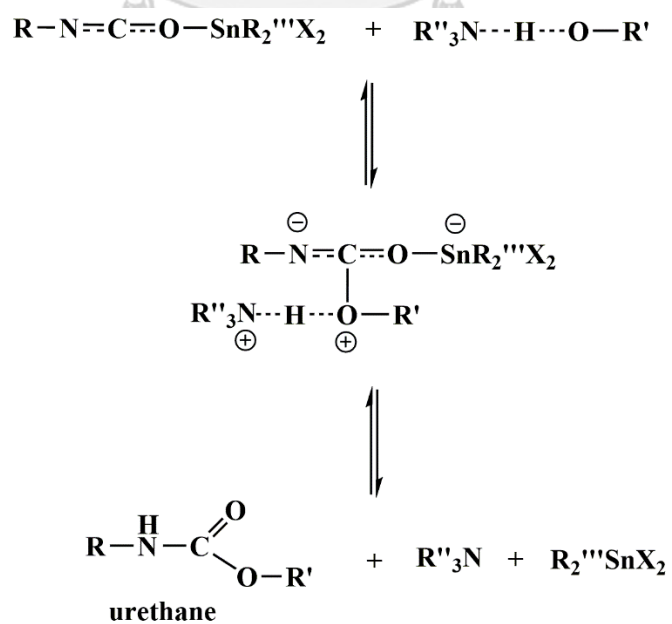
Scheme 2.11 Catalytic mechanism of tin-amine synergism (8).

2.3.3.3 Trimerization catalysts (isocyanurate catalysts)

Typical isocyanurate catalysts for PIR foams are quaternary ammonium salts of tetraalkylmonoamine (e.g., methyltriethylammonium octanoate), some tertiary amines [e.g., tris(*N,N*-dimethylaminopropyl)hexahydrotriazine and *N*-methylimidazole] and alkali metal carboxylates (e.g., potassium acetate and potassium 2-ethylhexanoate). A comparative study between tetraalkylammonium carboxylates and tertiary amines has shown their potential to accelerate trimerization reaction. This result is explained by the fact that oxyanionic bases are more nucleophilic and therefore more catalytically active than tertiary amines with similar basicity. The proposed catalytic trimerization mechanism is shown in Scheme 2.12. Anionic nitrogen is the reactive species which induce the cyclization of isocyanates (8, 10).
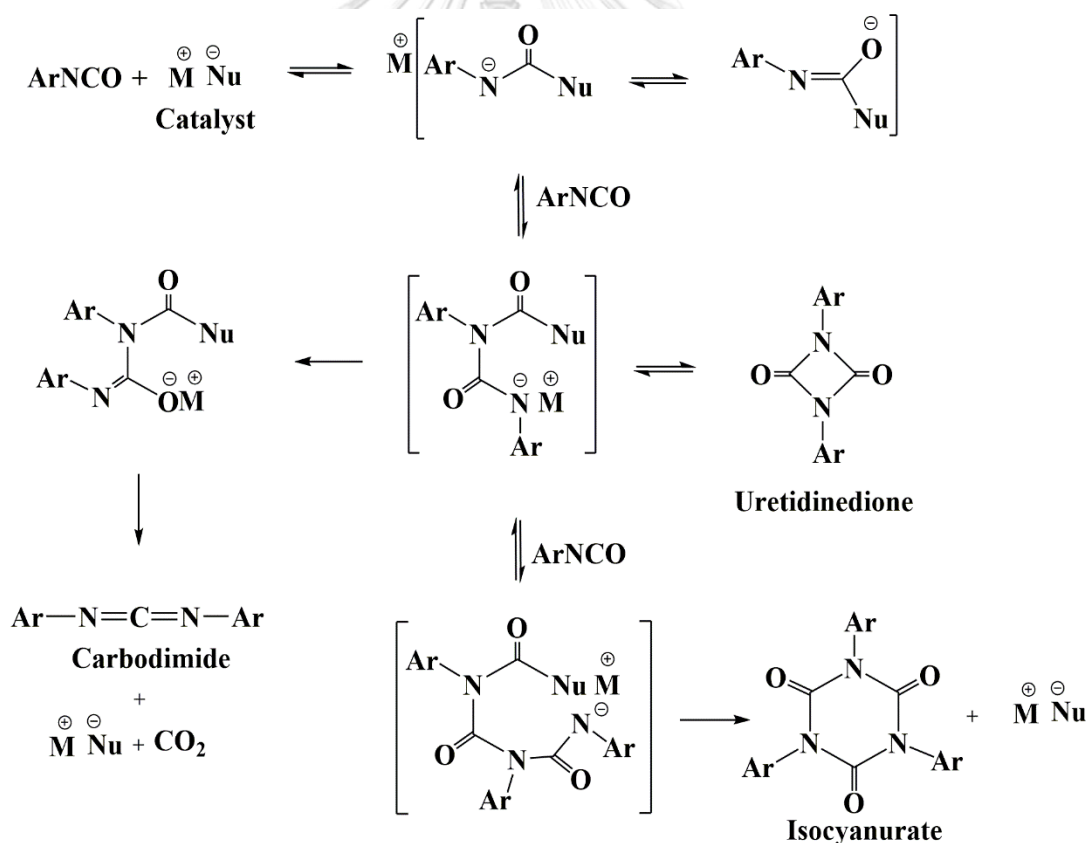
Scheme 2.12 Catalytic mechanism of isocyanurate catalyst (8).

2.3.4 Blowing agents

Both rigid PUR and PIR foams are prepared using blowing agents to generate gas bubbles which increase their volume along with the time and inflate the foams to have the cellular structure. Blowing agents can be classified in two types as physical and chemical blowing agents. The properties of the foam depend on both the types and the blowing agent content. Water is the chemical blowing agent, which reacts with isocyanate to obtain CO_2 gas bubbles as previous discussed. This blowing reaction not only gives polyurea crosslink but also releases the exothermic heat needed for completing the other reactions. Physical blowing agents, such as pentane, monofluorotrichloromethane and difluorodichloromethane, create the cellular structure of the foam by evaporation process and do not give the reaction for increasing the crosslink density of the foam. However, they can give the foams with lower density than those prepared from the chemical blowing agent (42).

The use of monofluorotrichloromethane and difluorodichloromethane increases the depletion of ozone layer. Therefore, the development of environmentally friendly blowing agents has become an important and urgent issue for the industry of rigid PUR and PIR foams. The use of pentane increases flammability of the foam. Therefore, higher amount of flame retardant is needed for the foams blown with this blowing agent (43).

2.3.5 Surfactants

A surface-active chemicals or surfactants are necessary for the processing of the foam since they help to reduce the surface tension of CO_2 gas during the foaming process and enhance the foam rising. Moreover, the surfactants can also stabilize the gas bubbles generated at the nucleation process (44). Polydimethyl siloxane-polyether copolymer called silicon surfactant has been widely utilized as the surface-active chemical for rigid PUR and PIR foams. It has substituted the organic and nonionic surfactants since the late 1950s.

The chemical structure of silicone surfactant is presented in Figure 2.6, where x and y are the average number of dimethylsiloxy and methylpolyethersiloxy groups, respectively, per molecule. Likewise, m and n are the average number of units

of polyethylene oxide and polypropylene oxide, respectively. R corresponds to polyether group. the normal amount of silicone surfactant used in the formulations of rigid PUR and PIR foams is 0.4–2.0 pbw of polyol. The chemical structure of silicone surfactant can be modified for the other applications of PUR, which may need more specific and complex processing, by varying the number of units and lengths of polydimethylsiloxane main chain and polyether pendant. One molecule of typical silicone surfactant for rigid PUR and PIR foams contains 10-50 silicon units with the average molecular weight of polyether chain of 400-1500 g/mol. Ethylene oxide content is different in the range of 50-100%. Polysiloxane:polyether proportion is 3:1-10:1. The total molecular weight of the silicone surfactant is in the range of 1,500-15,000 g/mol.
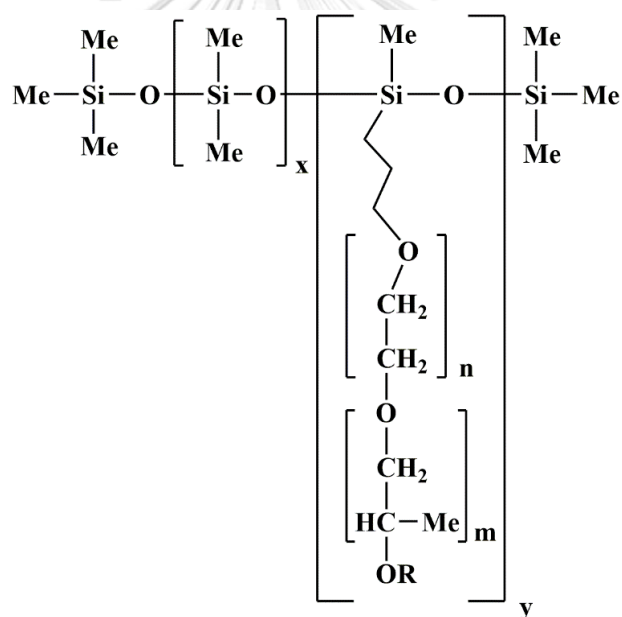
Figure 2.6 Chemical structure of silicone surfactant (8).

2.3.6. Flame retardants

Several Flame retardants are needed for rigid PUR foams since these foams are highly flammable. In the case of PIR foam, PIR structure can provide the inherently fire-retarded properties to the foams. However, the flame retardants are still used for PIR foams in some specific applications, which are strictly concerned about

fire safety. The flame retardants can be classified to additive and reactive flame retardants. The additive flame retardants are incorporated with the foams by physical mixing, which leads to the poor compatibility, easy leaching and decrease of mechanical properties of the foam. Examples of additive flame retardants are halogenated paraffins, inorganic oxides, organic phosphates (alkyl-, aryl- and ammonium-phosphates), phosphonates and bromine-containing compounds (5, 45). The chemical structures of some additive flame retardants are shown in Figures 2.7 and 2.8
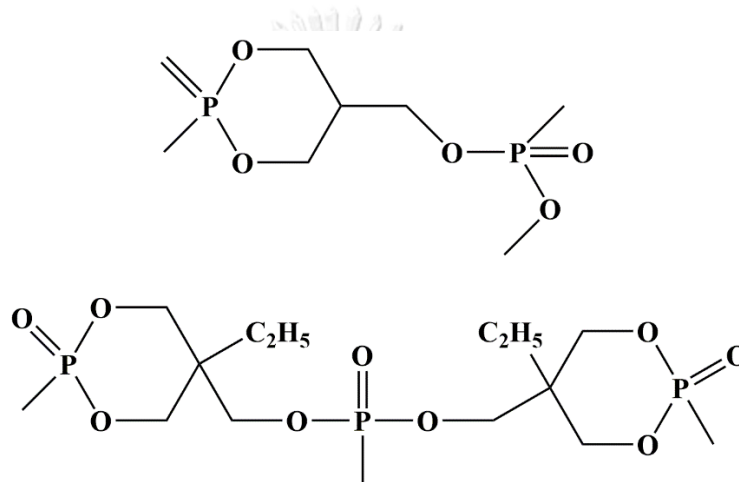
Figure 2.7 Chemical structures of alkyl phosphate and diphosphonate ester (5).
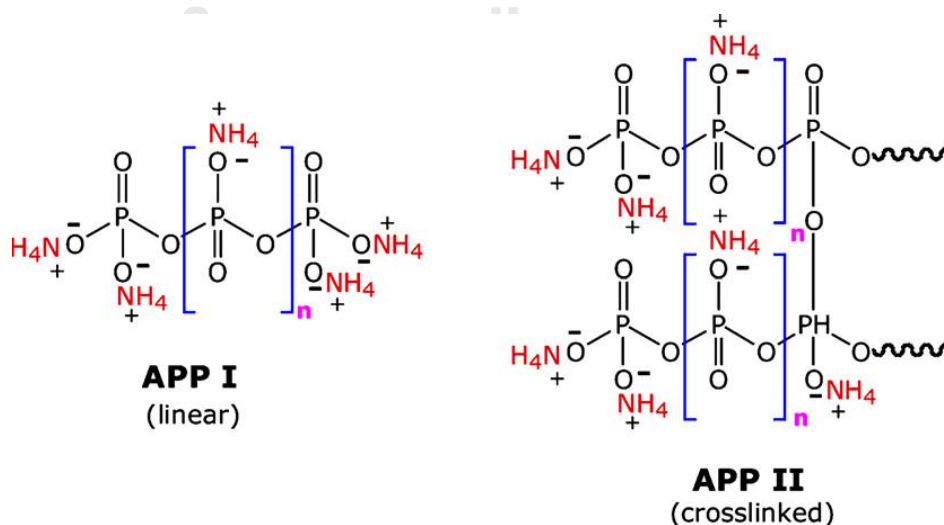
Figure 2.8 Chemical structures of ammonium polyphosphates (5).

The reactive flame retardants are the organic compounds with the active functional groups, which can form the covalent bond with the polyol, isocyanate or the other suitable functional groups of starting materials of the foam. This can improve the compatibility between polymer and the flame retardants and reduce the leaching problem of additive flame retardant. Examples of reactive flame retardants are organophosphorus compounds containing hydroxyl or amine groups, organoboron and organosilicon compounds (5, 45). The chemical structures of some reactive flame retardants are shown in Figures 2.9.

Bis(3-hydroxyphenyl) phenyl phosphate

Trimethallyl borate

Tris[3-(trimethoxysilyl)propyl]isocyanurate
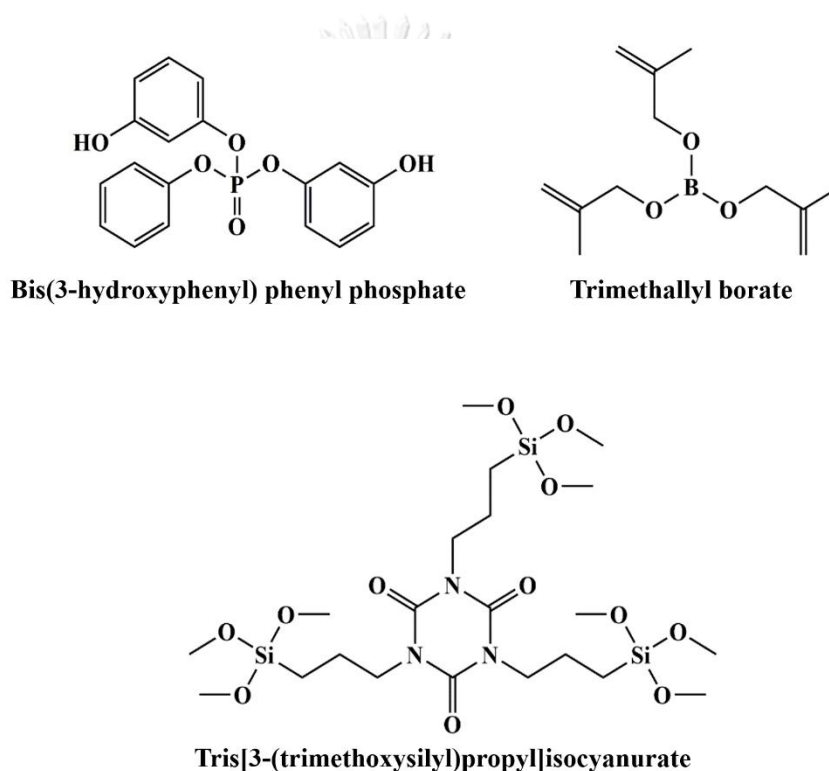
Figure 2.9 Chemical structures of reactive flame retardant (5).

2.3.7 Fillers

The objectives of use of filler are to reduce cost, improve the mechanical properties and enhance the thermal stability. Specific fillers can be employed to improve the water resistance of the foam. Particle and fiber are typical forms of filler, which are selected to use based on the applications of the foam. Particle filler is used in the flexible PUR foams for reducing flammability and increasing foam stiffness.

However, it can improve the thermal stability of rigid PUR foams. Mineral filler is sometimes utilized for reducing cost and increasing the compressive strength of rigid PUR foams (8, 46).

2.3.8 Viscosity reducers

The demand of viscosity reducer for the area of rigid PUR and PIR foams has increased due to the reason that the trend of these foam systems moves to decrease the use of physical blowing agent by replacing with water. This leads to higher viscosity of foam system because more crosslinks can occur by the secondary reactions of isocyanate with urea or amine. However, the viscosity of foam system can be decreased by using the viscosity reducer. This additive can also aid the processing of the foam. Examples of viscosity reducers are glycol ether, dimethyl ester and propylene carbonate (8).

2.3.9 Chain extenders

Difunctional chemicals with low molecular weight, such as glycols, diamines or hydroxyl amines can be chain extenders for rigid PUR and PIR foams. These additives can react with isocyanate to obtain polyurethane or polyurea short segments, which can increase the intermolecular interaction and crosslink between the polymer chains (46).

2.4 Formulations

Amount of isocyanate required for the reactions with polyol and other reactive chemicals is calculated in order to obtain the theoretical amount of isocyanate, which shows the stoichiometric equivalent. The theoretical amount of isocyanate can increase or decrease depending on several parameters, such as amount of reactive chemicals in the formulation, properties of the foam, ambient conditions and production scales. The varied amount of isocyanate used in the actual processing compared to the theoretical amount of isocyanate is called the "isocyanate index", which can be obtained by the following equation (8, 34, 46):

$$\text{Isocyanate index} = \frac{\text{actual amount of isocyanate}}{\text{theoretical amount of isocyanate}} \times 100 \qquad (2.1)$$

The typical method to calculate the quantity of the reactive starting materials used for the preparation of rigid PUR and PIR foams requires the technical values, namely isocyanate, hydroxyl and acid values as well as equivalent weight of polyol, water and other reactive chemicals defined as follows (8, 34, 46):

Isocyanate value (% NCO group) is the weight percentage of reactive isocyanate groups:

$$\text{Isocyanate value} = \% \text{ NCO group} = \frac{42 \times \text{functionality}}{\text{molar mass}} \times 100$$

$$= \frac{4200}{\text{equivalent weight}} \qquad (2.2)$$

Hydroxyl value is sometime called the hydroxyl number of the polyol. It shows the concentration of reactive hydroxyl groups per unit weight of the polyol, which can react with isocyanate. The unit of hydroxyl value is mg KOH/g of polyol (milligram of KOH equivalent to the active hydroxyl content of 1 gram of polyol).

$$\text{Hydroxyl value} = \frac{56.1 \times \text{functionality}}{\text{molar mass}} \times 1000$$

$$= \frac{56.1}{\text{equivalent weight}} \times 1000 \qquad (2.3)$$

Acid value is expressed as mg KOH/g of polyol and numerically equal to hydroxyl value in isocyanate use.

Equivalent weight of polyol, water and other reactive chemicals is calculated using the molar mass and functionality of reactive chemicals, which can react with isocyanate. For example, water has two functional groups to react with two isocyanate

groups. Therefore, the equivalent weight of water can be calculated by the following equation:

$$\text{Equivalent weight} = \frac{\text{molar mass}}{\text{functionality}} = \frac{18}{2} \qquad (2.4)$$

2.5 Mechanical properties

Compression properties are the most important mechanical properties of rigid PUR and PIR foams sine these materials are mainly applied as the insulations inside many constructions. The compression properties of rigid PUR and PIR foams are obviously different from those of flexible PUR foams. The compression stress-strain curves as well as the strength obtained from the compression testing can be used to characterize and classify the different types of foam. Compression load deflection is given to deform the foam samples in order to measure the load-enduring properties of the foams (46). The testing procedures are rather close to those of noncellular polymer materials, which can be performed according to ASTM D 1621-16. A universal testing machine (UTM) with the compression cages and two parallel flat plates is applied for the compression test of the foam as shown in Figure 2.10.
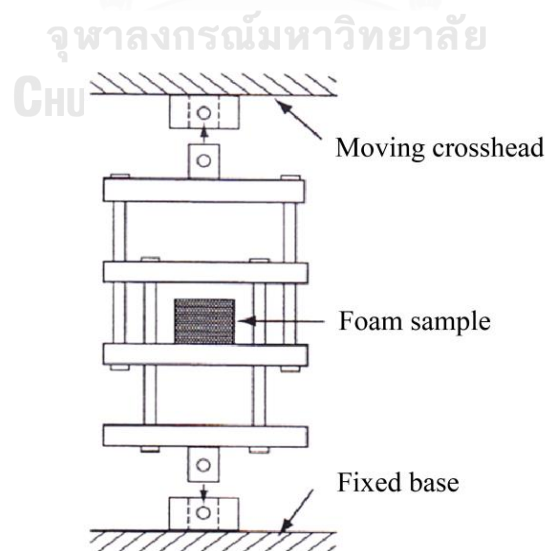
Figure 2.10 The instrument for compression test of the foam (46).

Characteristics of compression energy absorption and deformation of the different foams strongly depend on the density and cell morphology. For instance, the flexible PUR foams having open-cell feature as shown in Figure 2.11 can respond with the compression load by bending and stretching their cell walls and recovering their cell structures after the release of load.
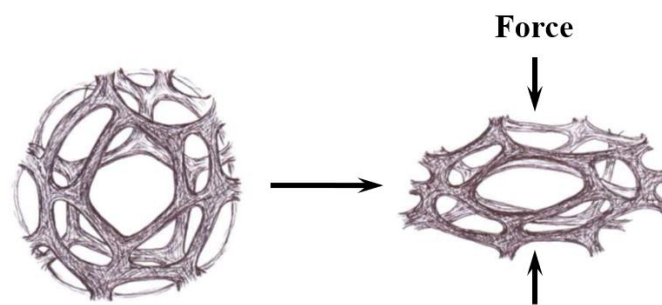
Figure 2.11 Appearance of open-cell flexible foam during compression test (46).

In the case of rigid PUR and PIR foams having closed-cell feature as shown in Figure 2.12, their cells become more compacted during compression test. The entrapped gas inside the cells difficultly escapes and compresses the cell walls. This leads the foams to resist to the deformation. However, when the compression load exceeds the limit of the foam resistance, the foam cells will rupture resulting in the permanent deformation of the rigid foam.
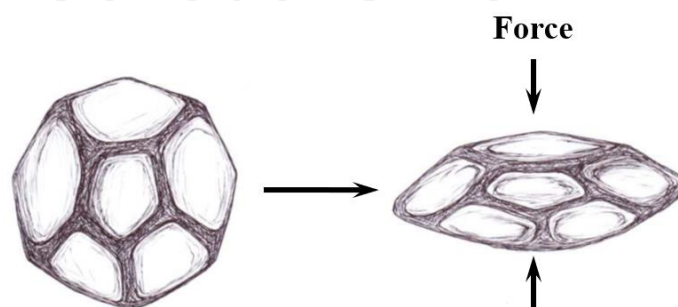
Figure 2.12 Appearance of closed-cell rigid foam during compression test (46).

Closed cell rigid foams (rigid PUR and PIR foams) show very limited to no yielding behavior. The energy absorption characteristic of foam can be presented in the term of compression stress-strain curve (Figure 2.13). The compression strength of rigid foams is usually collected at 10% deformation.
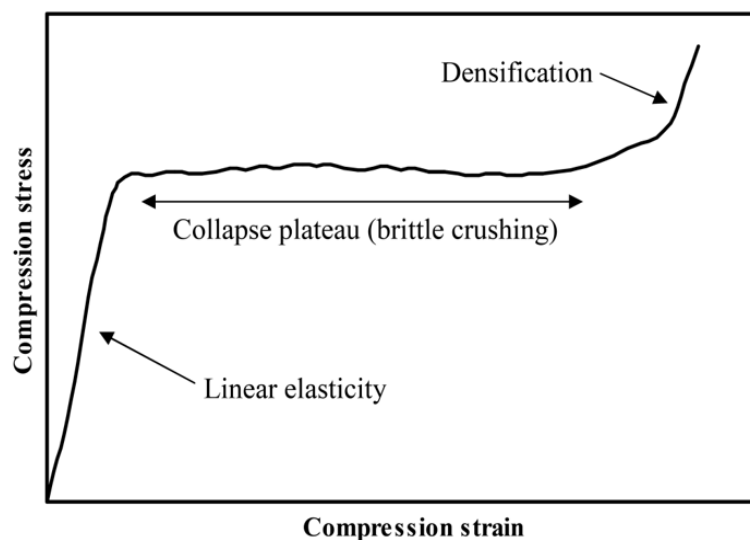
Figure 2.13 Typical compression stress-strain curve of rigid foams (47).

2.6 Theoretical methods

Quantum mechanics (QM) method in quantum chemistry can be utilized in all fields of chemistry for studying the chemical structures, molecular interaction, thermodynamic properties of reaction and etc. QM method is the mathematical explanation for electron behaviors and can be used to predict the molecular or atomic properties. The equations including in QM method have been correctly solved for the one-electron system. An assembly of method has been modified for applying with the multi-electron system. The assumption of basic concept of QM method is the presence function of coordinating so–called wave function (ψ), which composes all probable data about the systems. QM method is classified to ab initio, density functional theory (DFT) and semi–empirical methods. The details of ab initio and DFT methods, which are related with this work, are given in the following section (48).

2.6.1 Ab initio method

Ab initio method is the basic QM principle, which solves the Schrödinger equation with ignoring of fitting to the experiment according to the following equation:

$$\hat{H}\Psi = E\Psi \tag{2.5}$$

where $\hat{H}$ is Hamiltonian. E is the electron energy in orbital. Ψ is electronic wavefunction. This method can be used for only one-electron system. Hartree–Fock (HF) method is the simplest means of ab initio method. HF method starts with the approximation of Ψ of one-electron system recognized as the orbital. In order to obtain Ψ for multi-electron system, linear combination of atomic orbitals (LCAO) is carried out giving polyelectronic wavefunction (Ψ_0) known as Hartee product as:

$$\Psi_0 = \psi_0(1)\psi_0(2)\psi_0(3)........\psi_0(n) \tag{2.6}$$

Ψ_0 depends on the coordinates of all electrons in the atom, $\psi_0(1)$, $\psi_0(2)$, $\psi_0(3)$ and $\psi_0(4)$ are the functions of the first, second, third and fourth electrons, respectively. $\psi_0(n)$ is a initial guess that is expanded by the basis set.

Because of the approximation of HF non-linearity, this equation is further resolved using iteration known as self–consistent–field (SCF) approximation. Ψ_0 is resolved in Schrödinger equation. The SCF approximation is calculated for k cycles until self–consistency is found. After the calculation, spin orbitals together with configuration state functions is created using HF equation.

2.6.2 Density functional theory (DFT) method

DFT method is originated by theorem of Hohenburg and Kohn. The molecular energy is computed from the electron density function. $\rho(x, y, z)\ dxdydz$

is the probability to meet electrons in a volume element, $dxdydz$. According to the relationship of $\rho(x,y,z)$ and one-electron spatial wavefunctions (Ψ_i), the Ψ of HF is obtained as:

$$\rho_0 = \rho_r = \sum_{i=1}^{n} \left|\psi_i^2\right| \tag{2.7}$$

2.6.2.1 Kohn–Sham (KS) Energy

In the calculation of KS energy, non–interacting electrons moving in an effective potential is assumed. The first idea is expression of the molecular energy as a sum of small terms. The second idea is the use of initial guess of the electron density in the KS equations to calculate an initial guess of KS orbitals, which are then refined. The last KS orbitals are employed to compute the electron density and the KS energy, subsequently.

The energy of ground state electron is summed from the kinetic energy, $\langle T[\rho_0]\rangle$, the attraction of the nucleus and electron, $\langle V_{ne}[\rho_0]\rangle$, and the repulsion of electron with each other, $\langle V_{ee}[\rho_0]\rangle$, according to the equation shown below:

$$E_0 = \langle T[\rho_0]\rangle + \langle V_{ne}[\rho_0]\rangle + \langle V_{ee}[\rho_0]\rangle \tag{2.8}$$

The nucleus–electron potential energy can be obtained as:

$$\langle V_{ne}\rangle = \sum_{i=1}^{2n} \sum_{nucleiA} -\frac{Z_A}{r_{iA}} = \sum_{i=1}^{2n} v(r_i) \tag{2.9}$$

where, $v(r_i)$ is the external potential for the attraction of electron i and nucleus. The density function ρ can be introduce into $\langle V_{ne}\rangle$ due to the relation that

$$\int \Psi \sum_{i=1}^{2n} f(r_i)\Psi dt = \int \rho(r)f(r)dr \tag{2.10}$$

where $f(r_i)$ is a function of the coordinate of the *2n* electrons of a system and Ψ is the total wavefunction. $\langle V_{ne} \rangle$ can be obtained as:

$$\langle V_{ne} \rangle = \int \rho_0(r) v(r_i) dr \tag{2.11}$$

The deviation of the real kinetic energy from that of the reference system is:

$$\Delta\langle T[\rho_0] \rangle \equiv \langle T[\rho_0] \rangle - \langle T_r[\rho_0] \rangle \tag{2.12}$$

The $\Delta\langle V_{ee} \rangle$ is the deviation of the real electron–electron repulsion energy from classical charged–cloud coulomb repulsion energy and can be obtained by the summation of repulsion energy for pairs of infinitesimal volume elements $\rho(r_1) dr_1$ and $\rho(r_2) dr_2$ separated by distance r_{12}, as:

$$\Delta\langle V_{ee}[\rho_0] \rangle = \langle V_{ee}[\rho_0] \rangle - \frac{1}{2} \iint \frac{\rho_0(r_1)\rho_0(r_2)}{r_{12}} dr_1 dr_2 \tag{2.13}$$

Therefore, the energy of ground state electron (E_0) is written as:

$$E_0 = \int \rho_0(r) v(r) dr + \langle T_r[\rho_0] \rangle + \frac{1}{2} \iint \frac{\rho_0(r_1)\rho_0(r_2)}{r_{12}} + \Delta\langle T[\rho_0] \rangle + \Delta\langle V_{ee}[\rho_0] \rangle \tag{2.14}$$

The summation of last two terms is called exchange–correlation energy (*Exc*), which can be written as:

$$E_{xc}[\rho_0] \equiv \Delta\langle T_r[\rho_0] \rangle + \Delta\langle V_{ee}[\rho_0] \rangle \tag{2.15}$$

where $\Delta\langle T_r \rangle$ is the kinetic correlation energy of the electron, $\Delta\langle V_{ee} \rangle$ are the potential correlation and the exchange energies.

2.6.2.2 Kohn–Sham (KS) equation

KS equation is used by variation principle because electron density of the reference system is as same as that of real system, so

$$\rho_0 = \rho_r = \sum_{i=1}^{2n} \left| \Psi_i^{KS}(1) \right|^2 \tag{2.16}$$

where Ψ_i^{KS} is the KS spatial orbital. Varying E_0 according to the Ψ_i^{KS} subjects to the constraint that these remain orthonormal lead to the KS equation as:

$$\left[-\frac{1}{2}\nabla_i^2 - \sum_{nucleiA} \frac{Z_A}{r_{iA}} + \int \frac{\rho(r_2)}{r_{12}} dr_2 + v_{xc}(1) \right] \Psi_i^{KS}(1) = \varepsilon_i^{KS} \Psi_i^{KS}(1) \tag{2.17}$$

where ε_i^{KS} are KS energy levels. $v_{xc}(1)$ is the exchange correlation potential. The functional derivative of $E_{xc}[\rho(r)]$ with respect to $\rho(r)$ represents as exchange–correlation potential according to the equation shown below:

$$v_{xc}(r) = \frac{\delta E_{xc}[\rho(r)]}{\delta\rho(r)} \tag{2.18}$$

The Kohn-Sham equations can be written as:

$$\hat{h}^{KS}(1)\Psi_i^{KS}(1) = E_i^{KS}(1)\Psi_i^{KS}(1) \tag{2.19}$$

2.6.2.3 DFT exchange and correlations

The exchange–correlation energy functional (E_{xc}) can be obtained by the summation of the exchange–energy (E_x) and the correlation–energy (E_c) functionals as following equation:

$$E_{xc} = E_x + E_c \tag{2.20}$$

E_x is obtained by the similar method applied for that of HF, However, the KS orbital is used instead of HF orbital. Therefore, E_x can be written as:

$$E_x = -\frac{1}{4}\sum_{i=1}^{n}\sum_{j=1}^{n}\left\langle \theta_i^{KS}(1)\theta_j^{KS}(2)\left|1/r_{12}\right|\theta_j^{KS}(1)\theta_i^{KS}(2)\right\rangle \tag{2.21}$$

where θ_i^{KS} and θ_j^{KS} are the spatial parts of spin–orbital locating at x_1, y_1, z_1 and x_2, y_2, z_2, respectively. r_{12} is the length between x_1, y_1, z_1 and x_2, y_2, z_2. E_c is calculated from E_{xc} by the following equation:

$$E_c \equiv E_{xc} + E_x \tag{2.22}$$

2.7 Literature reviews

The literatures relating to the development of alternative catalysts for rigid PUR and PIR foams, the theory and applications of metal-ammonia complex and the computational investigation of urethane formation reaction have been reviewed as follows:

2.7.1 Catalysts for rigid PUR foam

Because the use of tertiary amine and organotin catalysts have odor and toxicity problems, respectively, development of alternative catalysts for gelling and blowing reactions of rigid PUR foams and the other PUR materials have been reported as follows: Schellekens *et al.* (49) studied the catalytic activity of several metal-based catalysts in urethane formation (gelling reaction) of thermoplastic polyurethane and compared to that of dibutyltin dilaurate (DBTDL) catalyst. Thermal stability and ability of catalysts to accelerate the gelling reaction at low catalyst

concentrations were also investigated. The results indicated that metal-based catalysts act as Lewis acid in the catalytic processes. Fe(III)-based compounds showed remarkable and comparable catalytic activity to DBTDL catalyst. Fe(acac)$_3$ and Fe(tmhd)$_3$ (where acac = acetylacetonate and tmhd = 2,2,6,6-tetramethyl-3,5-heptanedionate) still highly active at very low concentrations resulting in high urethane conversion. FeCl$_3$ was thermally stable and gave PUR with high molecular weight. Inoue *et al.* (20) studied possibility of metal acetylacetonate [M(acac)$_n$]-amine complexes as an efficient catalyst for the model gelling reaction of hexamethylene diisocyanate (HDI) with diethylene glycol (DEG). The mixtures of M(acac)$_n$ (where M = Mn, Fe, Co, Ni and Cu) and triethylenediamine (TEDA) were used as the catalysts. They found that Mn(acac)$_n$-TEDA complex had better catalytic activity than the other complexes and showed comparable catalytic activity to DBTDL catalyst. The reaction rate along with catalytic constant investigated at 30 °C using the concentration of catalyst of 0.00036 mol/l are reported in this literature as shown in Table 2.4.

Table 2.4 Reaction rate and catalytic constant of urethane formation between HDI and DEG using various catalysts (20).

Catalyst	Reaction rate (k/l mol^{-1}h^{-1})	Catalytic constant (K_c) ($K_c \times 10^4$/l^{2}eq^{-1} mol^{-1}h^{-1})
None	0.2	-
DBTDL	139.6	3.8
Mn(acac)$_2$	52.3	1.4
Mn(acac)$_2$-TEDA	102.2	2.8

Sardon *et al.* (50) prepared PUR materials by solution polymerization of hexamethylene diisocyanate with poly(ethylene glycol). Different types of organic acids such as acetic acid, *p*-toluenesulfonic acid and methanesulfonic acid were used to catalyze the reactions. They found that *p*-toluenesulfonic acid was the most effective catalyst for urethane formation exhibiting 97% of PUR conversion after 6 h,

which was higher than that of DBTDL catalyst (82% of the conversion). Moreover, density functional theory (DFT) was conducted to support a dual hydrogen-bonding mechanism of the acid catalysts in PUR catalysis. The mechanism involves electrophilic activation of isocyanate via the isocyanate nitrogen, with simultaneous nucleophilic activation of alcohol. Blank *et al.*(18) investigated the catalytic activity of metal salts and their chelates in the acceleration of gelling and blowing reactions of polyurethane coating in order to use as the alternative of DBTDL. They found that zirconium acetylacetonate chelate or Zr(acac)$_4$ showed more selective catalytic activity toward gelling reaction in comparison to DBTDL. In addition, blowing reaction hardly occurred with using this chelate. Therefore, this catalyst had the potential to develop for PUR coating application. Alsarraf *et al.* (51) studied possibility of cyclic guanidines to be the catalysts for urethane formation. The aim of this work is to find the alternative catalysts for replacement of DBTDL catalyst. Under bulk polymerization, cyclic guanidines effectively catalyzed reaction of diols with diisocyanates leading to PUR with a high molecular weight (M$_w$= 74000 g/mol). The catalytic mechanism of cyclic guanidines was proposed. The cyclic guanidines could act as dual activator which had two different catalytic pathways as shown in Figure 2.14.
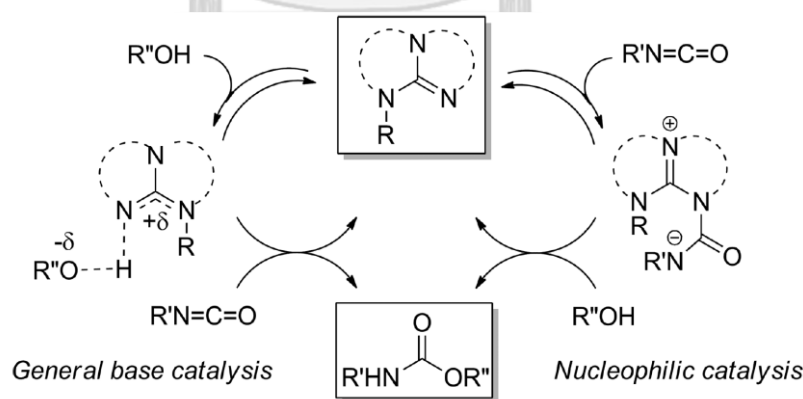
Figure 2.14 Two catalytic mechanisms of cyclic guanidine (51).

Strachota *et al.* (40) compared environmentally friendly catalysts for gelling and blowing reactions of rigid PUR foam to each other. Selected commercially available amines, including *N*-substituted morpholines, were evaluated

as the single catalyst and the catalyst mixture with organotin compound for preparation of rigid PUR foams. They found that the catalyst mixture, which composed of both metal and amine in the system, showed better catalytic activity than the single catalyst. Liao *et al.* (21) synthesized neodymium chloride ($NdCl_3$) Schiff base complex for using as the catalyst mixture with triethylenediamine in the acceleration of gelling and blowing reactions of semi-rigid PUR foams. The results indicated that the ratio of $NdCl_3$ Schiff base complex:triethylenediamine affected its catalytic activity. The reaction time, namely cream time and gelation time decreased with increasing the proportion of triethylenediamine. The most suitable proportion of $NdCl_3$ Schiff base complex:triethylenediamine, which gave the shortest reaction time and comparable catalytic activity to stannous octoate catalyst was 1:2.

Our research group developed metal-amine complexes as alternative catalysts for water-blown rigid PUR foams. For example, Pengjam *et al.* (24) and Sridaeng *et al.* (25) synthesized metal-amine complexes, namely $[Cu(en)_2](OAc)_2$, $[Cu(trien)](OAc)_2$, $[Cu(EA)(OAc)_2]$ and $[Zn(EA)(OAc)_2]$; where, en, trien and EA are ethylenediamine, triethylenetetramine and ethanolamine, respectively. These metal complexes were employed as catalysts for the processing of rigid PUR foams. It was found that $[Cu(en)_2](OAc)_2$ and $[Cu(trien)](OAc)_2$ showed comparable catalytic activity to DMCHA, while $[Cu(EA)(OAc)_2]$ and $[Zn(EA)(OAc)_2]$ had lower catalytic activity than DMCHA.

2.7.2 Catalysts for PIR foam

Catalyst mixtures of trimerization catalyst, industrial gelling and blowing catalysts were used in order to obtain the optimum properties of PIR foams. For example, Xu *et al.* (52) studied effect of different trimerizaton catalysts, namely quaternary ammonium, potassium octoate and potassium acetate, on the thermal properties of PIR foams. Each trimerization catalyst was mixed with gelling and blowing catalysts, namely *N,N*-dimethylcyclohexylamine and pentamethyldiethylenetriamine for using as the catalyst mixture. The highest PIR amount was obtained with using potassium acetate catalyst at 5.0 parts by weight (pbw). PIR foams showed superior thermal stability than reference rigid PUR foams. Moreover, PIR foams had lower

heat release rate and smoke producing rate than rigid PUR foams during burning. Modesti *et al.* (38) used the catalyst mixture between potassium octoate (DABCO® K15) and pentamethyldiethylenetriamine for the processing of PIR foams. The purpose of this research is to develop simply efficient method for evaluating isocyanate conversion and isocyanurate formation using FTIR analysis. The effect of isocyanate indices on isocyanate conversion, isocyanurate formation, physical and mechanical properties of PIR foams was investigated. The increase of isocyanurate formatiom resulted from the increase of isocyanate index and consequently improved both physical and mechanical properties of PIR foam. At optimum amount of catalyst, sufficient isocyanate conversion would be obtained. Okuzono *et al.* (3) studied new catalyst mixtures for PIR foams which exhibited high reactivity at low temperature. The combination of trimerization catalysts with several tertiary amine catalysts was used. The results showed that the catalyst mixtures could improve the flowability, however, the flammability of the foam would be a hazard because the isocyanurate reaction did not fully progressed.

2.7.3 Metal-ammonia complexes

It is well-known that both copper (II) and zinc(II) ions can coordinate with ammonia to form copper- and zinc-ammonia complexes. Hathaway *et al.* (53) prepared copper-ammonia complex and studied the electronic properties of the complex. In addition, Bjerrum *et al.* (54) synthesized zinc-ammonia complex. They reported that addition of ammonia solution to an aqueous solution of the copper(II) and zinc(II) ions gave the successive replacement of coordinated water in $Cu(H_2O)_6^{2+}$ and $Zn(H_2O)_6^{2+}$ by NH_3 to obtain copper-ammonia complex $[Cu(NH_3)_n(H_2O)_{6-n}]^{2+}$ and zinc-ammonia complex $[Zn(NH_3)_n(H_2O)_{6-n}]^{2+}$, respectively, according to the reaction shown in Scheme 2.13.

$$M(H_2O)_6^{2+} + n\,NH_3 \rightleftharpoons M(NH_3)_n(H_2O)_{6-n}^{2+} + n\,H_2O$$

$$M = Cu \text{ and } Zn$$

Scheme 2.13 Coordination of metal-ammonia complexes (53).

The consecutive complexity constants for the reaction of $Cu(H_2O)_6^{2+}$ with NH_3 to give $[Cu(NH_3)_n(H_2O)_{6-n}]^{2+}$, namely $\log k_1$, $\log k_2$, $\log k_3$, $\log k_4$ and $\log k_5$, were 4.15, 3.50, 2.89, 2.13 and -0.52, respectively. For $[Zn(NH_3)_n(H_2O)_{6-n}]^{2+}$, the consecutive complexity constants for the reaction of $Zn(H_2O)_6^{2+}$ with NH_3, namely $\log k_1$, $\log k_2$, $\log k_3$ and $\log k_4$, were 2.37, 2.44, 2.50 and 2.15, respectively (53, 54). Vazquez-Arenas *et al*. (55) studied species distribution in aqueous solution of copper(I)- and copper(II)-ammonia complexes. They found that the composition of the complex depended on NH_4^+:Cu^{2+} ratio and pH of the aqueous solution as presented in Figure 2.15. When using the pH in the range of 8.5 to 10.5, $[Cu(NH_3)_4(H_2O)_2]^{2+}$ was found as the predominant species.
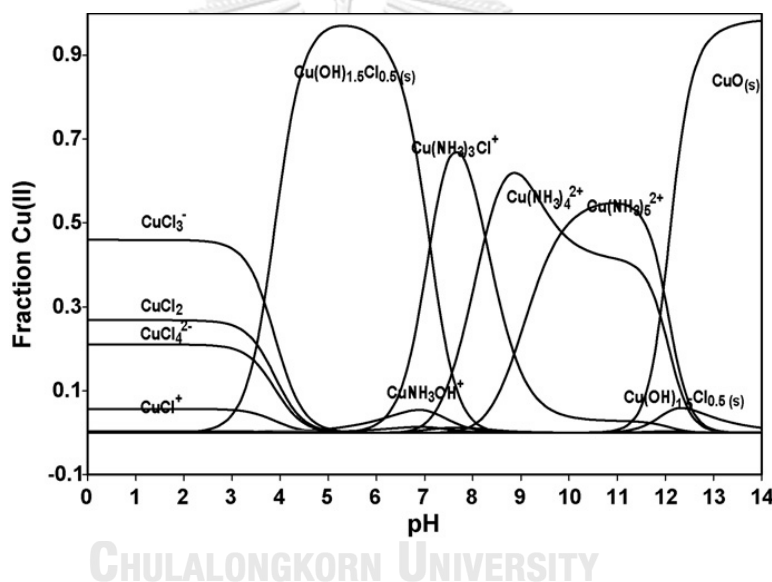
Figure 2.15 Species distribution for copper(II)-ammonia complexes in aqueous solution (55).

For the applications of copper- and zinc-ammonia complexes, a well-known Schweizer's reagent, $[Cu(NH_3)_4(H_2O)_2](OH)_2$, has been utilized to dissolve cellulose in the preparation of rayon fiber (26). The major applications of copper- and zinc-ammonia complexes in many researches tend to be the precursors for transforming into the other forms of copper and zinc compounds. For instance, Chen *et al*.(27) prepared hollow transition-metal oxides (Co_3O_4, NiO, CuO-Cu_2O and ZnO)/nitrogen-doped graphene hybrids using copper- and zinc-ammonia complexes

as the metal precursors. The metal oxides obtained from metal-ammonia complex precursors can be deposited on the graphene sheets. These synthesized materials showed the potential to apply in lithium-ion batteries. Fan *et al.* (56) synthesized copper nanoparticles encapsulated within hexagonal boron nitride (Cu@h-BN), which were obtained by annealing $Cu(NH_3)_4Cl_2$ and KBH_4 under N_2 atmosphere at 900 °C. The Cu@h-BN appeared the low-cost, thermal conductive and high-temperature antioxidation materials. Zhang *et al.* (30) utilized the aqueous solution of zinc-ammonia precursor to synthesize the inverted organic solar cells with Al-doped-ZnO electron transport layer. Metallic Al was soaked into the aqueous solution of zinc-ammonia complex. Armbruster *et al.* (28) prepared the $[Cu(NH_3)_x]^{2+}$-form of heulandite by alternating the Na-form of natural heulandite with the copper-ammonia complex solution. It was found that the structure of copper-ammonia complexes in heulandite was the square planar $[Cu(NH_3)_4]^{2+}$, which coordinated with two axial H_2O molecules having the elongated octahedron complex.

2.7.4 Computational study on the catalytic mechanism of gelling and blowing reactions

Although computational studies on the mechanism of urethane formation (gelling reaction) without using catalyst could be found in several works (57-61), the computational study on the mechanism of CO_2 generation (blowing reaction) has never been reported. Moreover, very few computational studies on the catalytic mechanism of industrial catalysts, namely organotin compounds and tertiary amines, in urethane formation have been found as follows: Devendra *et al.* (62, 63) used dimethyltin diacetate (DMTDA) as the model compound of dibutyltin dilaurate (DBTDL) industrial catalyst to investigate the catalytic mechanism in the urethane formations, which were the model reactions between methanol with methyl or phenyl isocyanate. This computational study was performed using DFT/B3LYP/LANL2DZ/6-31G** (62) and DFT/B3LYP/LANL2DZ/ 6-31G* (63) levels of theory with CPCM solvent model, whose water and toluene were selected to used as the mediums of the reaction in order to investigate the effect of polar and non-polar mediums, respectively, on the urethane formation. They concluded that the tin

model catalyst (DMTDA) showed more catalytic reactivity in the water than that in toluene. The catalytic mechanism started with the formation of tin alkoxide, which was actually reactive form of DMTDA and could catalyze the urethane formation by using tin (Sn) to coordinate with oxygen of aliphatic and aromatic isocyanates. In the case of tertiary amine catalyst, Hatanaka (64) studied the model reaction of methanol with methyl isocyanate using triethylenediamine (TEDA) as the catalyst. The computational study was conducted using the DFT method with B3LYP functional and 3-21G basic set. The computational results revealed that the catalytic mechanism of TEDA involved the protonation of catalyst and the nucleophilic attack from hydroxyl oxygen of alcohol to carbon of isocyanate. Moreover, the activation energy of urethane formation decreased from 11.4 kcal/mol to 5.6 kcal/mol with using TEDA catalyst.

According to the above literature reviews together with the best of our knowledge, copper- and zinc-ammonia complexes have never been experimentally and computationally investigated as the gelling and blowing catalysts for both urethane formation and CO_2 generation. Therefore, the catalytic activity of these metal complexes as well as the obtained properties of rigid PUR and PIR foams have been studied in this work.

CHAPTER 3

EXPERIMENTAL AND COMPUTATIONAL DETAILS

3.1 Chemicals

3.1.1 Chemicals for metal-ammonia complexes synthesis

Copper(II) acetate monohydrate [$Cu(OAc)_2.H_2O$, Sigma-Aldrich, St. Louis, MO, USA], Zinc(II) acetate dihydrate [$Zn(OAc)_2.2H_2O$, Nacalai Tesque, Kyoto, Japan] and ammonia (NH_3) solution with 30 wt% of concentration (Carlo Erba, Val de Reuil, France).

3.1.2 Chemicals for the foam preparation

Polyether polyol (Polimaxx®4221) and polymeric 4,4´-methane diphenyl diisocyanate (PMDI, B9001®, %NCO = 31.0 wt%, average functionality = 2.7). Polysiloxane surfactant (Tegostab®B8461), potassium octoate with 70 wt% of concentration in diethylene glycol (Dabco®K-15) and *N,N*-dimethylcyclohexylamine (DMCHA), the reference industrial catalyst, were obtained from IRPC Public Company Ltd. Distillated water (H_2O) is chemical blowing agent.

3.2 Catalyst preparation

$Cu(OAc)_2$ and $Zn(OAc)_2$ underwent the complex formation in H_2O to obtain the low-viscous catalyst solutions of Cu(Amm) and Zn(Amm), respectively, for the processing of rigid PUR and PIR foams. The method of catalyst synthesis was adapted from that reported in the previous work (65). After synthesis, these catalyst solutions were ready to use for the foam processing without purifying step. H_2O in catalyst solutions could blow the foams and did not interfere the catalytic activity of Cu(Amm) and Zn(Amm).

3.2.1 Synthesis of Cu(Amm) in water

The synthesis of 25 wt% aqueous solution of Cu(Amm) was carried out as follows: an NH_3 solution (1.27 ml, 19.91 mmol) was added into distilled water (3.21 ml). This solution was constantly stirred at room temperature for 10 min. After that, $Cu(OAc)_2.H_2O$ (0.662 g, 3.32 mmol) was added and the Cu(Amm) complex solution was continually stirred at room temperature for 3 h. The complex formation between $Cu(OAc)_2$ with NH_3 took place according to the reaction in Scheme 3.1. Cu(Amm) solution was found as a clear blue solution with weak odor and low viscosity.

UV-visible (MeOH): λ_{max} = 240 and 620 nm and molar absorptivity (ε) = 3,808 and 49, respectively. IR (ATR-IR): ν = 3327 [w; ν(N-H) and ν(O-H)], 1549 [s; ν_{as}(C=O)], 1411 [s; ν_s(C=O)] and 1267 [m; ν(N-H deformation)]. MS (MALDI-TOF, m/z): calcd for $\{[Cu(NH_3)_4(H_2O)_2](OAc)_2+H_2O+NH_3+H\}^+$ = 321.13; found 321.93, $\{[Cu(NH_3)_4(H_2O)_2](OAc)_2+2NH_3+H\}^+$ = 320.14; found 319.93 and $\{[Cu(H_2O)_6](OAc)\}^+$ = 230.03; found 230.12.
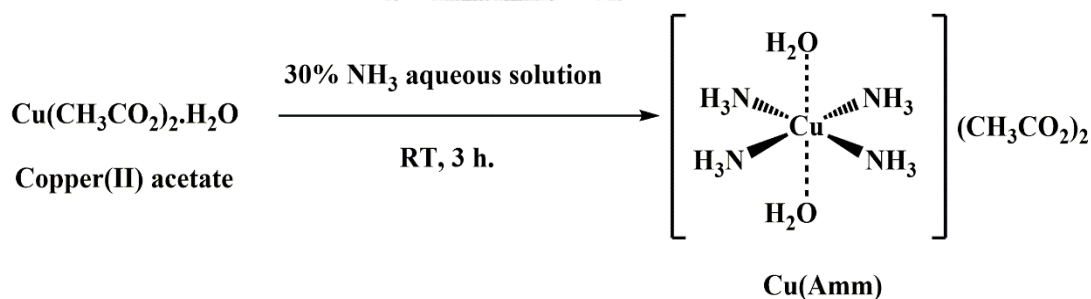
Scheme 3.1 Synthesis of Cu(Amm) solution.

3.2.2 Synthesis of Zn(Amm) in water

The synthesis of 25 wt% aqueous solution of Zn(Amm) was carried out as follows: an NH_3 solution (1.19 ml, 18.66 mmol) was added into distilled water (3.26 ml). This solution was constantly stirred at room temperature for 10 min. After that, $Zn(OAc)_2.2H_2O$ (0.682 g, 3.11 mmol) was added and the Zn(Amm) complex solution was continually stirred at room temperature for 3 h. The complex formation between

Zn(OAc)$_2$ with NH$_3$ took place according to the reaction in Scheme 3.2. Zn(Amm) solution was found as a clear colorless solution with weak odor and low viscosity.

IR (ATR-IR): ν = 3326 [w; ν(N-H) and ν(O-H)], 1549 [s; ν$_{as}$(C=O)], 1411 [s; ν$_s$(C=O)] and 1270 [m; ν(N-H deformation)]. MS (MALDI-TOF, m/z): calcd for

$\{[Zn(NH_3)_2(H_2O)_4](OAc)_2+3H_2O+H\}^+$ = 343.13; found 342.95,

$\{[Zn(NH_3)_4(H_2O)_2](OAc)_2+3H_2O+H\}^+$ = 341.12; found 340.95,

$\{[Zn(NH_3)_4(H_2O)_2](OAc)_2+H_2O+2NH_3+H\}^+$ = 339.15; found 338.95,

$\{[Zn(NH_3)_2(H_2O)_4](OAc)_2+2H_2O+H\}^+$ = 325.08; found 325.92,

$\{[Zn(NH_3)_4(H_2O)_2](OAc)_2+2H_2O+H\}^+$ = 323.11; found 323.92,

$\{[Zn(NH_3)_4(H_2O)_2](OAc)_2+2NH_3+H\}^+$ = 321.14; found 321.93 and

$\{[Zn(NH_3)(H_2O)_5](OAc)\}^+$ = 230.05, found 230.12.
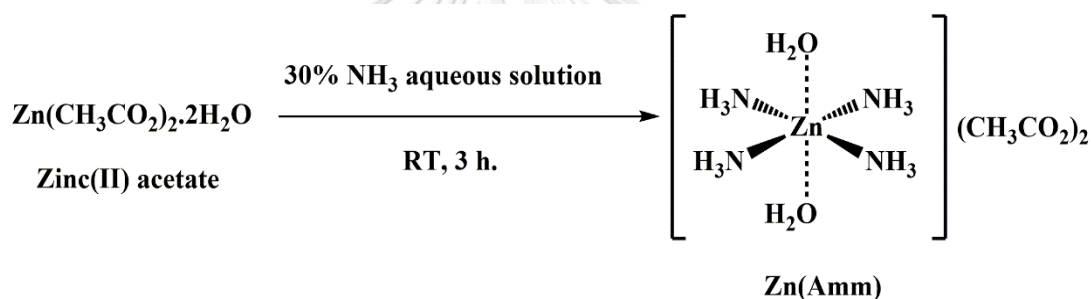
Scheme 3.2 Synthesis of Zn(Amm) solution.

In order to study effect of catalyst and blowing agent contents on the properties of rigid PUR foam, the synthesized catalyst solutions were prepared with several catalysts (metal-ammonia complexes) or blowing agent (water) contents by varying the content of metal compounds, NH$_3$ and H$_2$O in catalyst solutions as summarized in Tables 3.1 and 3.2. When studying the effect of catalyst amount on foam properties, the metal-ammonia complex contents in catalyst solution were varied from 0.5 to 2.0 g while the water amount is constant at 3.0 g (Table 3.1). Likewise, when studying the effect of water contents on foam properties, the water contents in catalyst solution were varied from 3.0 to 5.0 g while the metal-ammonia complex amount is constant at 1.0 g (Table 3.2).

Table 3.1 Chemical amount for synthesis of catalyst solutions (study of catalyst effect).

Catalysts	Total content of catalyst or water		Chemical amount used for preparing catalyst solution					
	Metal complex	Water	Copper acetate		Zinc acetate		Ammonia solution		Water
	(g)	(g)	(g)	(mmol)	(g)	(mmol)	(ml)	(mmol)	(ml)
	0.5	3.0	0.331	1.66	-	-	0.64	10.03	2.60
Cu(Amm)	1.0	3.0	0.662	3.32	-	-	1.27	19.91	2.21
	2.0	3.0	1.323	6.63	-	-	2.54	39.82	1.42
	0.5	3.0	-	-	0.341	1.55	0.60	9.41	2.63
Zn(Amm)	1.0	3.0	-	-	0.682	3.11	1.19	18.66	2.26
	2.0	3.0	-	-	1.365	6.22	2.38	37.31	1.52

Table 3.2 Chemical amount for synthesis of catalyst solutions (study of blowing agent effect).

Catalysts	Total content of catalyst or water		Chemical amount used for preparing catalyst solution					
	Metal complex	Water	Copper acetate		Zinc acetate		Ammonia solution		Water
	(g)	(g)	(g)	(mmol)	(g)	(mmol)	(ml)	(mmol)	(ml)
	1.0	3.0	0.662	3.32	-	-	1.27	19.91	2.21
Cu(Amm)	1.0	4.0	0.662	3.32	-	-	1.27	19.91	3.21
	1.0	5.0	0.662	3.32	-	-	1.27	19.91	4.21
	1.0	3.0	-	-	0.682	3.11	1.19	18.66	2.26
Zn(Amm)	1.0	4.0	-	-	0.682	3.11	1.19	18.66	3.26
	1.0	5.0	-	-	0.682	3.11	1.19	18.66	4.26

3.3 Preparation and of rigid PUR and PIR foams

Both cup test method, which was modified from ASTM D 7487-13, and molded method were used to process rigid PUR and PIR foams. For processing of rigid PUR foams, the constant isocyanate index of 100 was used and metal-ammonia complexes ([Cu(Amm) and Zn(Amm)] were employed as the gelling and blowing catalysts. For processing of PIR foams, the isocyanate indices were varied from 160 to 250 and the catalyst mixtures between potassium octoate (isocyanurate catalyst) with metal-ammonia complexes (gelling and blowing catalysts) were employed as the catalyst systems. Catalytic activity of metal-ammonia complexes on the reactions and the obtained properties of rigid PUR foam were investigated and compared to those accelerated by the industrial catalyst (DMCHA). In the case of PIR foams, the catalytic activity of the mixtures of potassium octoate with metal-ammonia complexes together with the obtained properties of PIR foam were compared to those accelerated by the industrial catalyst system (the mixture of potassium octoate with DMCHA).

3.3.1 Preparation of rigid PUR and PIR foams using cup test method

Two steps of mixing were used to process rigid PUR and PIR foams for cup test method. All foam formulations for rigid PUR and PIR foams are given in Table 3.3. All chemicals in Table 3.3 are showed in parts by weight (pbw) unit, which indicates the weight of each chemical (in gram) per 100 g of polyol.

For rigid PUR foam processing (Figure 3.1), polyol was manually blended with gelling and blowing catalysts (metal-ammonia complex solutions or DMCHA), surfactant and blowing agent (water) in 0.7 l of a paper cup to obtain homogeneously blended polyol in the first mixing step. The addition of H_2O is only required for the foam processed using DMCHA catalyst. In the case of the foams processed using Cu(Amm) and Zn(Amm) solutions, the H_2O is already included as the solvent in the catalyst solutions. In the second mixing step, PMDI with the isocyanate index of 100 was added to the blended polyol, and then, the reaction mixture was mechanically stirred at 2000 rpm for 20 s. The foams were allowed to freely rise. The measurement of reaction time and other properties of the foam was carried out after the foams were kept at room temperature for 48 h to complete the reactions.

The processing method for PIR foams (Figure 3.2) was the same as that of rigid PUR foams. However, the addition of potassium octoate catalyst solution into the polyol was performed in the first mixing step. The PMDI with the higher isocyanate indices of 160, 200 and 250 was employed.

The isocyanate index is the proportion between excess amount of the isocyanate compound, which is used in the real foam processing, per the theoretical equivalent amount of the isocyanate compound required to react with all hydroxyl compounds. The isocyanate index can be calculated according to the following equation (66):

$$\text{Isocyanate index} = \frac{\text{Actual amount of isocyanate used}}{\text{Theoretical amount of isocyanate}} \times 100 \qquad (3.1)$$

The isocyanate index of 100 means that the actual amount of isocyanate used equals the theoretical equivalent amount of isocyanate. While the isocyanate indices of 160, 200 and 250 mean that the actual amount of isocyanate used is higher than the theoretical equivalent amount of isocyanate by 1.6, 2.0 and 2.5 times, respectively. The examples of isocyanate index calculation are shown in Appendix A.

Table 3.3 Foam formulations for processing of rigid PUR and PIR foams.

Chemicals (pbw)	Rigid PUR foam	PIR foams		
Isocyanate index	100	160	200	250
PMDI (B9001®)	166.0	270.0	337.5	421.9
Polyether polyol (Polimaxx® 4221)	100.0	100.0	100.0	100.0
Gelling and blowing catalysts [Cu(Amm), Zn(Amm) or DMCHA]	1.0	0.5	0.5	0.5
Trimerization catalyst (potassium octoate)	-	3.0	3.0	3.0
Surfactant (Tegostab® B8461)	2.5	2.5	2.5	2.5
Blowing agent (water)	4.0	4.0	4.0	4.0
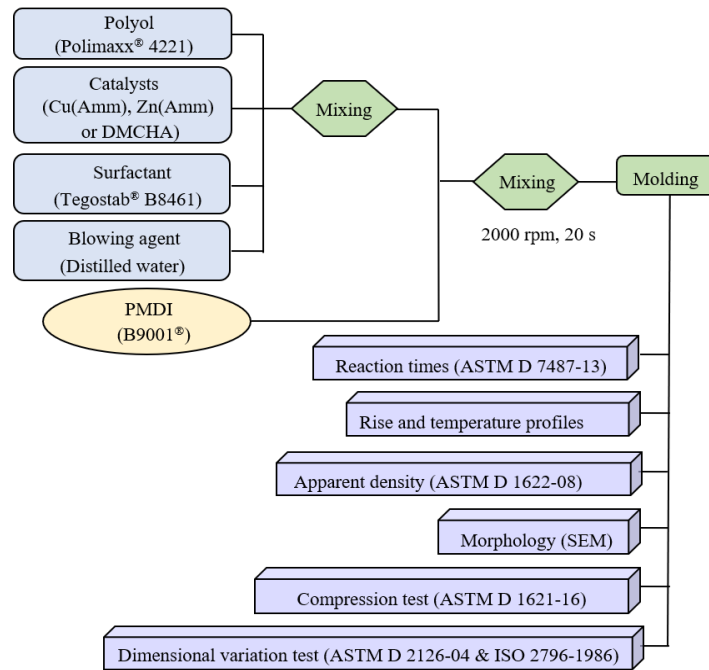
Figure 3.1 Processing steps and characterizations of rigid PUR foam.
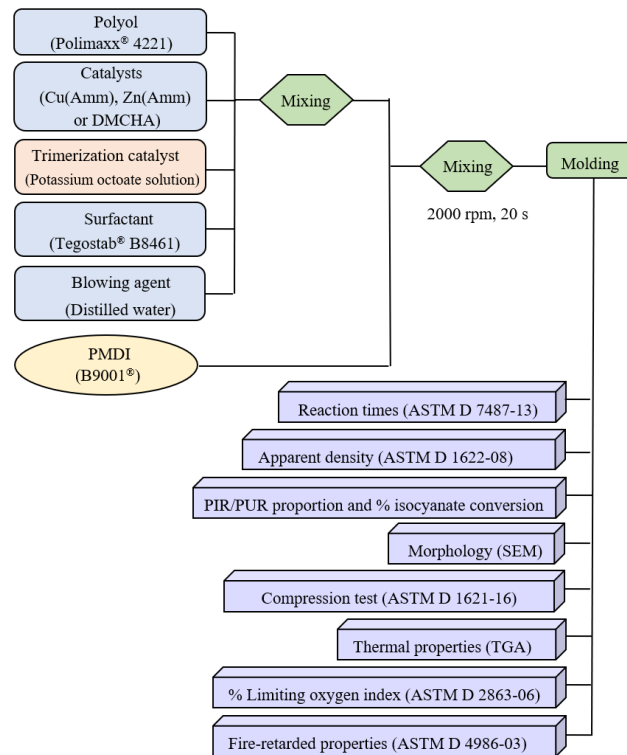
Figure 3.2 Processing steps and characterizations of PIR foam.

3.3.2 Preparation of rigid PUR and PIR foams in the mold

The processing of the molded foams was carried out using the same mixing steps as those of cup test method. However, after all reactants were mechanically stirred at 2000 rpm for 20 s in the second mixing step, the liquid mixture was poured into a 1000 cm^3 plastic mold. The processability of the foams in larger mold was observed. After molded rigid PUR and PIR foams were kept for 48 h, they were investigated the properties as shown in the Figures 3.1 and 3.2, respectively.

3.4 Structural analysis of metal-ammonia complexes

3.4.1 Ultraviolet-visible spectroscopy

The complex formation between metal acetate and NH_3 could be observed by the shifted ultraviolet-visible (UV-visible) spectra of metal-ammonia complexes in comparison to their metal salts. The UV-visible spectra were recorded on UV-vis spectrophotometer (Varian Cary 50, Palo Alto, CA, USA) in the range of 200-900 nm using a medium speed scan. Methanol with the spectrophotometric grade was use as a solvent in this analysis. Molar absorptivity (ε) of the particular wavelength was calculated as the following equation:

$$\varepsilon = A/bc \tag{3.2}$$

where A is measured absorbance, b is cell-path length (cm) and c is concentration of analyte (mol/l)

3.4.2 Fourier transform infrared spectroscopy

The fourier transform infrared (FTIR) spectra of metal-ammonia complexes were recorded on FTIR spectrometer (Perkin Elmer model Spectrum Two, Waltham, MA, USA) between the mid-IR range from 4000 to 500 cm^{-1} at a resolution of 4 cm^{-1}.

3.4.3 Mass spectrometry

The analysis of matrix-associated laser desorption ionization time of flight (MALDI-TOF) mass spectra was performed on a Bruker Daltonics mass spectrometer (USA) using water as a solvent. This analysis is based on the theory that each compound shows its individual fragmentation pattern on its mass spectrum. For analysis, the metal-ammonia complexes were ionized. Their ions were splitted following their different mass and relative abundance. The mass-to-charge ratio (m/z) obtained from MALDI-TOF mass spectra can be used to study the complex formation of synthesized metal-ammonia complexes as it relates with the mass of molecular ions of the complexes.

3.4.4 pH measurement

An Ohaus starter 2100 pH meter was used to measure the pH values of Cu(Amm) and Zn(Amm) solutions prepared with different mole ratio of metal acetate:NH_3 = 1:4 and 1:6 .

3.5 Investigation of rigid PUR and PIR foam properties

3.5.1 Reaction time

The measurement of reaction time of the foam, namely cream time, gel time, tack free time and rise time, by a digital stopwatch was conducted following ASTM D 7487-13 in order to investigate the effect of catalytic activity of catalysts on the reaction time of the foam. Cream time was measured when the foam height reached approximately 5% of total height. Gel time was measured when the stable shape of the foam mixture was observed. Rise time was measured when the rising process of the foams terminated. Tack free time was measured when the foams totally became dry solid.

3.5.2 Density

Apparent density of the foam was measured according to ASTM D 1622-08. The foam samples were cut into a cubic shape, which had the dimensions of 3.0 cm × 3.0 cm × 3.0 cm (length × width × thickness), and then, each sample was weighed with precision. The density was calculated from the mass to volume ratio. The average density of at least ten samples was reported.

3.5.3 Foam height and rise profiles

Foam height processed using cup test method were measured after the blowing reaction was completed. The values were reported in % foam height, which was calculated using the relation to the highest foam. For example, among rigid PUR foams processed using different catalysts, the foam processed using Zn(Amm) was highest (16.6 cm) in comparison to those obtained from DMCHA and Cu(Amm). Therefore, the % foam height of the foam processed using Zn(Amm) was determined as 100%. Whereas the height of foams processed using Cu(Amm) was 14.5 cm. Therefore, % foam height of the foam processed using Cu(Amm) was 87.4%. Rise profiles of the foam were plotted using the data of % foam height as the function of reaction time. The rise profiles relate with the ability of catalyst to accelerate the blowing reaction. The catalysts with suitable catalytic activity in blowing reaction should give the smooth and continual rise profiles without the interrupted pattern.

3.5.4 Foaming temperature and temperature profiles

The temperature change during foaming reaction was detected every 10 s using Digicon DP-71 thermocouple, whose sensor was placed inside the foams. The data were reported as the temperature profiles, which were plotted between foaming temperature versus reaction time. The highest and constant temperature of each temperature profile was reported as the maximum core temperature of the foam.

3.5.5 PIR/PUR proportion and % isocyanate conversion

PIR/PUR proportion and % isocyanate conversion of the foam were calculated from attenuated total reflection infrared (ATR-IR) spectra, which were recorded on a Nicolet 6700 FTIR spectrometer between 4000 to 500 cm^{-1} at a resolution of 4 cm^{-1} and 16 scans. For the calculation, the data were collected via the mode of transmittance and would be converted into the mode of absorbance, which is directly related to the concentration of the functional group by Lambert-Beer's law (35). Frequency assignments for the typical functional groups of rigid PUR and PIR foams are shown in Table 3.4 (35, 67-69). PIR/PUR proportion was obtained from the ratio of normalized absorption peak of isocyanurate functional group at 1415 cm^{-1} per normalized absorption peak of urethane functional group at 1220 cm^{-1}. The percentage of isocyanate conversion was calculated from the normalized absorption peak of remaining isocyanate group at 2277 cm^{-1} after the foams were kept for 48 h.

Table 3.4 Typical functional groups of rigid PUR and PIR foams in ATR-IR spectra (35, 67-69).

Functional groups	Wavenumber (cm^{-1})	Chemical bonds
Isocyanurate	1415	C=O
Isocyanate	2277	N=C=O
Phenyl	1595	Ar-H
Urethane	1220	C-O
Urethane	1710	C=O
Urethane	1307	C-N
Urethane	1510	N-H (bend)
Urethane	3317	N-H (stretch)

3.5.6 Morphology

The morphology and average cell size of the foams in the same (side view) and the opposite (top view) to foam-rising direction were studied with JEOL JSM-6480 LV scanning electron microscope (SEM). The foam samples were sliced with a

sharp blade to have about 0.1 cm of thickness and were coated with gold before scanning to provide an electrically conductive surface of the foam. The cell size of the foam was measured using SEMAFORE program. The average cell size was reported.

3.5.7 Dimensional stability

The dimensional variation of the foam was studied according to ASTM D 2126-04 and ISO 2796-1986. For sample preparation, the foams were cut into a cubic shape with dimensions of 10.0 cm × 10.0 cm × 5.0 cm (length × width × thickness). Then, the sample surface was finished with NO. 0 sandpaper to eliminate the crack on foam surface. The foam dust was blown off using a dryer. Each side (length, width and thickness) of prepared sample was marked at three positions to obtain a precision measurement as shown in Figure 3.3. For dimensional stability test, the foam samples were placed at 70 °C in an oven and at -25 °C in a refrigerator for 1, 7 and 14 days. After the testing period, the foams were removed from the testing conditions and placed at the room temperature for 1 h before they were measured the dimensional change. The dimensional variation of three samples was calculated as the following equation and reported as the average values.

$$\text{Dimensional change (\%)} = [(M_f - M_I)/M_I] \times 100 \qquad (3.3)$$

Where M_f is the final dimension measurement and M_I is the initial dimension measurement.
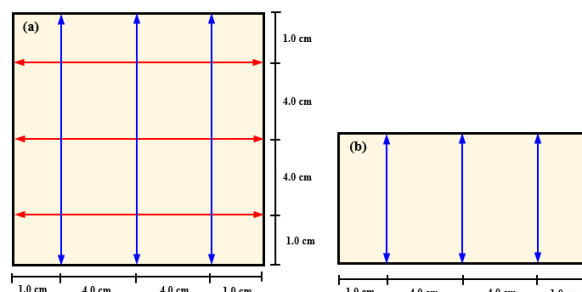
Figure 3.3 Marked positions on the foam surface for (a) the length and the width sides and (b) the thickness side using in the dimensional stability test.

3.5.8 Compression properties

The compression properties of the foam were investigated in the same and the opposite to foam-rising direction (Figure 3.4) according to ASTM D 1621-16 using universal testing machine (Hounsfield H 10 KM). The foam samples were cut into a cubic shape with the dimensions of 5.0 cm × 5.0 cm × 5.0 cm (length × width × thickness). Compression force (0.100 N) moved at 2.54 mm/min to deform the foam samples. Compression strength was noted at 10% strain.
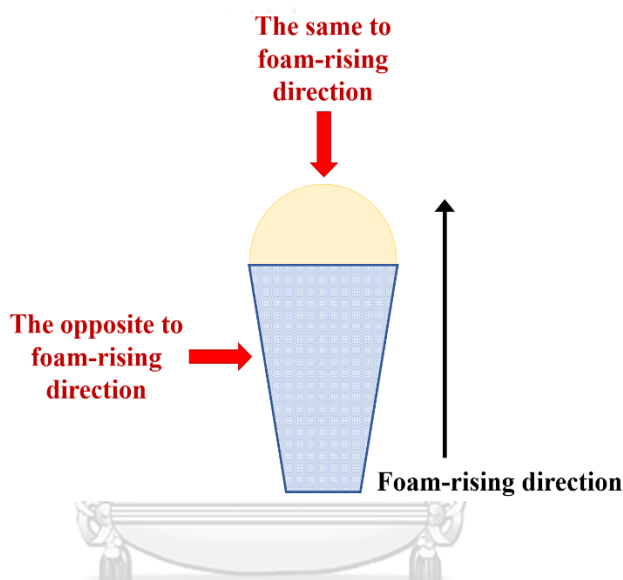
Figure 3.4 The directions of compression test for rigid PUR and PIR foams.

3.5.9 Fire-retarded properties

The fire-retarded properties of the foam were studied through the UL-94 horizontally-oriented burning test and %limiting oxygen index (LOI) measurement. The UL-94 horizontally-oriented burning test was carried out according to ASTM D 4986-03. The foam samples with the dimensions of 15.0 cm × 5.0 cm × 1.3 cm (length × width × thickness) were marked the position at 2.5, 6.0 and 12.5 cm. Then, each sample was horizontally placed over the holder and ignited with fire source. Burning length, burning rate and afterglow time were reported for all foam samples.

%LOI measurement was performed following ASTM D 2863-06. The foam sample with the dimensions of 12.5 cm × 1.0 cm × 1.0 cm (length × width ×

thickness) was vertically placed in the glass column flowed with the mixture of O_2 and N_2. Then, the fire source was applied to the top of foam sample and the combustion behavior of the foam sample was observed. The minimum O_2 concentration in % volume which could maintain the combustion of the foam was recorded.

3.5.10 Thermal properties

Thermogravimetric analysis (TGA) was conducted with Perkin–Elmer Pyris Diamond TG/DTA analyzer to evaluate the thermal properties of the foam. The foam samples were heated under N_2 from 35 to 800 °C by 10 °C /min. The results of thermal properties, namely the temperature at 5 wt% loss ($T_{5\%}$), %weight loss, the maximum degradation temperature (T_{max}), the activation energy for thermal degradation (E_a) and % char residue were reported.

3.6 Computational details

The catalytic mechanism of metal-ammonia complexes in gelling reaction (urethane formation) and blowing reaction (carbon dioxide generation) could be disclosed by computational study. The model compounds of reactant, namely phenyl isocyanate and methanol, were used as the models of polyol and PMDI reactants, respectively. The model compound of product obtained from gelling reaction was methyl phenyl carbamate (urethane), while, the model compounds of product obtained from blowing reaction were carbon dioxide (CO_2) and phenyl amine (aniline). The suitable chemical structures of Cu(Amm) and Zn(Amm) used in this computational study were $[Cu(NH_3)_4]^{2+}$ and $[Zn(NH_3)_4]^{2+}$, respectively.

3.6.1 Structural optimization of model compounds

Full structural optimizations of phenyl isocyanate, methanol, water, urethane, carbon dioxide, phenyl amine, $[Cu(NH_3)_4]^{2+}$ and $[Zn(NH_3)_4]^{2+}$ were carried out using density functional theory (DFT) calculations with the GAUSSIAN 09 program (70). CAM-B3LYP or hybrid density functional B3LYP (the Becke's three–

parameter exchange functional (71) with the Lee–Yang–Parr correlation functional (72) combined with Coulomb-Attenuating Method (73) (the long-range correction version) was employed for all calculations with 6–31G(d) basis set (74). CAM-B3LYP is suggested as the enhanced version of B3LYP that gives better estimation for charge transfer effect on the excitation energy (75).

Considering the structures occurred during the reaction pathways, the intermediate (INT) structures were optimized by CAM-B3LYP/6–31G(d) level of theory. The transition-state (TS) structures for the conversion of phenyl isocyanate/methanol to urethane and the conversion of phenyl isocyanate/water to CO_2 were optimized by the same level of theory using quadratic synchronous transit (QST2) calculating option, which can find the TS structures through the user-given specified structures of the reactant and the product. The single negative imaginary frequency along with the intrinsic reaction coordinate (IRC) calculation (76) were used to verify the obtained TS structures. All electronic properties of optimized structures referred in this work were obtained using the B3LYP/6–31G(d) calculations.

3.6.2 Catalytic reactivity of metal-ammonia complex

Frontier molecular orbital (FMO) analysis was conducted to calculate the highest occupied molecular orbital (HOMO) and the lowest unoccupied molecular orbital (LUMO) energies of reactants when they were activated by $[Cu(NH_3)_4]^{2+}$ and $[Zn(NH_3)_4]^{2+}$. The catalyst reactivity could be investigated from the HOMO−LUMO energy gab (E_g), which is the energy difference between the LUMO of electron acceptor (activated phenyl isocyanate) and the HOMO of electron donor (methanol or water). E_g can be calculated using the following equation:

$$E_g = E_{LUMO\ of\ activated\ phenyl\ isocyanate} - E_{HOMO\ of\ methanol\ or\ water} \qquad (3.4)$$

The catalysts having reactivity should give narrower E_g in comparison to that of noncatalytic reaction. The charge population at transition state was calculated by natural bond orbital (NBO) analysis (77, 78) in GAUSSIAN 09 program for

investigating the intermolecular interaction and partial electron transfer between metal-ammonia complex catalysts and their accelerated components.

3.6.3 Thermodynamic and kinetic investigation

The change of standard enthalpy (ΔH^o_{298}) as well as Gibbs free energy (ΔG^o_{298}) for gelling and blowing reactions has been derived from the zero-point vibrational energy (79) calculated at CAM-B3LYP/6–31G(d) level of theory. The activation energy ($\Delta E^{\ddagger}$) for each reaction step is obtained from the different value between the energy of TS structure and that of reactant structure. The reaction rate constant ($k(T)$) is calculated using $\Delta E^{\ddagger}$ according to the following equation (79, 80):

$$k(T) = \kappa \frac{k_B T}{h} \frac{Q_{TS}}{Q_R} exp\left(\frac{-\Delta E^{\ddagger}}{RT}\right) \qquad (3.5)$$

where k_B, h, R and T are the Boltzmann's constant, the Plank's constant, the gas constant and the absolute temperature, respectively. Q_R and Q_{TS} are the partition functions for the reactant and the transition state whose values are consisted of translational, rotational and vibrational partition functions. The equilibrium constant (K) can be calculated using the following equation:

$$\Delta G^o_{298} = -RTlnK \qquad (3.6)$$

CHAPTER 4

SYNTHESIS OF METAL-AMMONIA COMPLEXES AND PREPARATION OF RIGID POLYURETHANE AND POLYISOCYANURATE FOAMS USING METAL-AMMONIA COMPLEXES AS CATALYSTS

4.1 Preparation and characterization of metal-ammonia complexes

In the first section, the synthesis of metal-ammonia complexes [Cu(Amm) and Zn(Amm)] was carried out using water as solvent in order to obtain the aqueous solution of complexes, which could enhance the solubility between these synthesized catalysts and other liquid raw materials of rigid PUR and PIR foams (65). $Cu(OAc)_2$ and $Zn(OAc)_2$ (where $OAc = CH_3CO_2^-$) were coordinated with NH_3 ligands to obtain Cu(Amm) and Zn(Amm), respectively, as presented in Scheme 4.1. It was found that pH values of Cu(Amm) and Zn(Amm) solutions were 8.63 and 9.03, respectively, when using mole ratio of metal acetate:NH_3 = 1:4. The slight precipitation of $Cu(OAc)_2$ and $Zn(OAc)_2$ was still observed in the solution (Figure 4.1). These solutions of metal-ammonia complex might be not suitable for employing as homogeneous catalysts for the foam processing. However, when increasing the mole ratio of metal acetate:NH_3 to 1:6, pH values of Cu(Amm) and Zn(Amm) solutions increased to 10.63 and 10.38, respectively, and both synthesized metal-ammonia complexes were completely dissolved in H_2O due to the assistance of polar nature between ammonia and water (81). At this mole ratio along with the obtained pH value, the structure of copper-ammonia complex was reported to be $[Cu(NH_3)_4(H_2O)_2](OAc)_2]$ (29, 82).
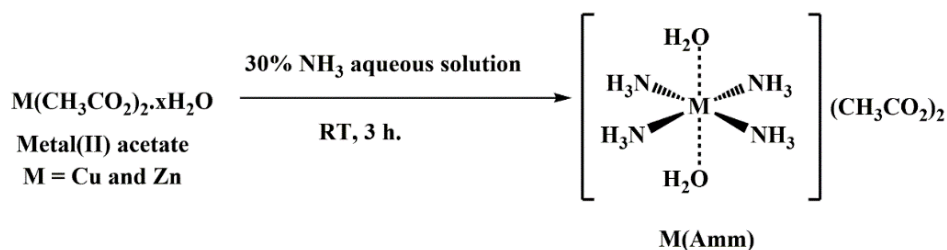
Scheme 4.1 Synthesis of metal-ammonia complexes.

Both metal-ammonia complex solutions were low-viscous liquids and had less odor in comparison to DMCHA industrial catalyst. The metal-ammonia complex solutions with no precipitation were characterized and used for the foam processing.
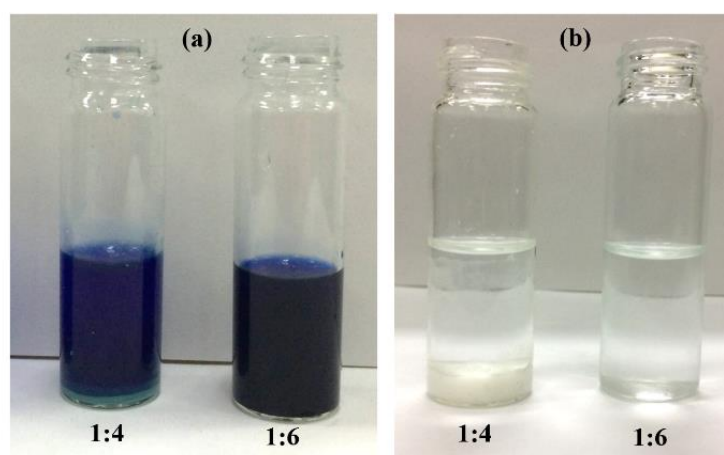
Figure 4.1 Solutions of (a) Cu(Amm) and (b) Zn(Amm) synthesized at different mole ratios of metal acetate:NH$_3$.

4.1.1 Structural analysis of metal-ammonia complexes using MALDI-TOF mass spectrometry

Figure 4.2 and Table 4.1 show mass spectra and the data of molecular ion peaks corresponding with m/z, respectively, of Cu(Amm) and Zn(Amm). The molecular ion peaks of [Cu(NH$_3$)$_4$(H$_2$O)$_2$](OAc)$_2$ [Figure 4.2 (a)] were found at m/z = 321.93 and 319.93, whilst those of [Zn(NH$_3$)$_4$(H$_2$O)$_2$](OAc)$_2$ [Figure 4.2 (b)] were found at m/z = 340.95, 338.96, 323.92 and 321.93. These results indicated that the structures of Cu(Amm) and Zn(Amm) are [Cu(NH$_3$)$_4$(H$_2$O)$_2$](OAc)$_2$ and [Zn(NH$_3$)$_4$(H$_2$O)$_2$](OAc)$_2$, respectively. Each metal center (Cu^{2+} or Zn^{2+}) of the metal-ammonia complex coordinates with four NH$_3$ and two H$_2$O, which bind to metal ions as the monodentate ligands. Two OAc$^-$ groups act as the counter ions. In the case of Zn(Amm), two NH$_3$ ligands could continue to exchange with two H$_2$O molecules resulting in the structure of [Zn(NH$_3$)$_2$(H$_2$O)$_4$](OAc)$_2$, which showed molecular ion peaks at m/z = 342.95 and 325.93. This could be attributed to exchangeable of

ligands, which generally occurs for the synthesis of metal-ammonia complex in the presence of H_2O. As reported in the literatures, Hathaway et al. prepared copper(II)-ammonia complexes and studied their electronic properties (53), while Bjerrum synthesized Zinc(II)-ammonia complexes (54). They suggested that several possible structures of the metal-ammonia complex could be found since the complex formation between metal ions and NH_3 in aqueous solution was equilibrium reaction as illustrated in Scheme 4.2.

$$M(H_2O)_6{}^{2+} + nNH_3 \rightleftharpoons M(NH_3)_n(H_2O)_{6-n}{}^{2+} + nH_2O$$

$$(M = Cu \text{ or } Zn)$$
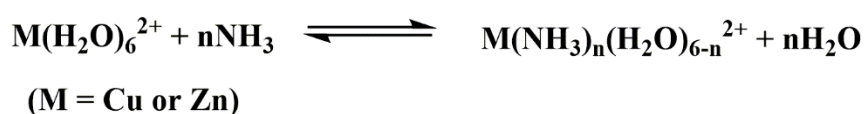
Scheme 4.2 Equilibrium complex formation of metal ions, NH_3 and H_2O.
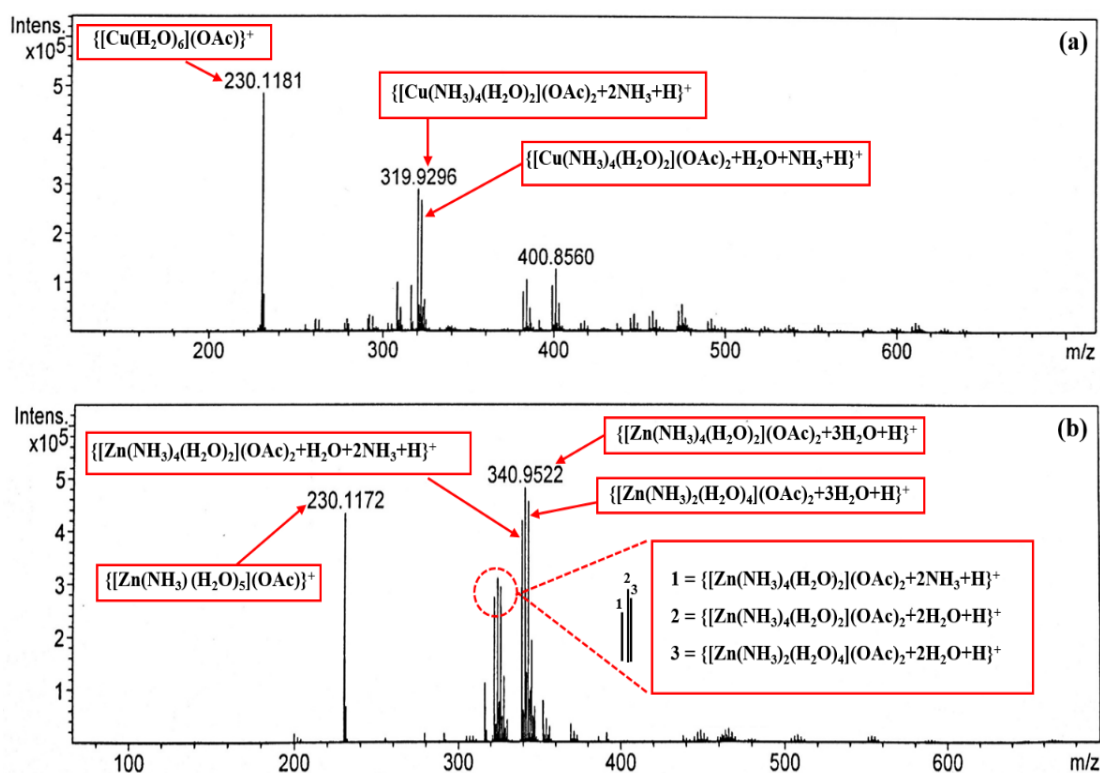
Figure 4.2 MALDI-TOF mass spectra of (a) Cu(Amm) and (b) Zn(Amm) aqueous solutions.

Table 4.1 Molecular ion peaks corresponding with m/z of metal-ammonia complexes.

molecular ion peaks	m/z (Calculated)	m/z (Found)
$\{[Cu(NH_3)_4(H_2O)_2](OAc)_2+H_2O+NH_3+H\}^+$	321.13	321.93
$\{[Cu(NH_3)_4(H_2O)_2](OAc)_2+2NH_3+H\}^+$	320.14	319.93
$\{[Cu(H_2O)_6](OAc)\}^+$	230.03	230.12
$\{[Zn(NH_3)_2(H_2O)_4](OAc)_2+3H_2O+H\}^+$	343.13	342.95
$\{[Zn(NH_3)_4(H_2O)_2](OAc)_2+3H_2O+H\}^+$	341.13	340.95
$\{[Zn(NH_3)_4(H_2O)_2](OAc)_2+H_2O+2NH_3+H\}^+$	339.15	338.96
$\{[Zn(NH_3)_2(H_2O)_4](OAc)_2+2H_2O+H\}^+$	325.08	325.93
$\{[Zn(NH_3)_4(H_2O)_2](OAc)_2+2H_2O+H\}^+$	323.11	323.92
$\{[Zn(NH_3)_4(H_2O)_2](OAc)_2+2NH_3+H\}^+$	321.14	321.93
$\{[Zn(NH_3)(H_2O)_5](OAc)\}^+$	230.05	230.12

4.1.2 Structural optimization of metal-ammonia complexes by density functional theory (DFT) calculations

In order to investigate stability of metal-ammonia complexes in water and to support the characterized structures obtained from mass spectrometric analysis, the structures of $[M(NH_3)_4(H_2O)_2]^{2+}$ (where M = Cu or Zn) were optimized using B3LYP/6-311+g(d,p) level of theory and compared to the other possible structures, namely $[M(NH_3)_6]^{2+}$ and $[M(NH_3)_4]^{2+}$. The optimized structures of copper- and zinc-ammonia complex are shown in Figures 4.3 and 4.4, respectively. It was found that the metal-ammonia complexes with 6 coordination numbers, namely $[Cu(NH_3)_4(H_2O)_2]^{2+}$, $[Zn(NH_3)_4(H_2O)_2]^{2+}$, $[Cu(NH_3)_6]^{2+}$ and $[Zn(NH_3)_6]^{2+}$, had distorted octahedral structures. Whereas the complexes with 4 coordination numbers, namely $[Cu(NH_3)_4]^{2+}$ and $[Zn(NH_3)_4]^{2+}$, showed a square planar structure and a distorted tetrahedral structure, respectively.
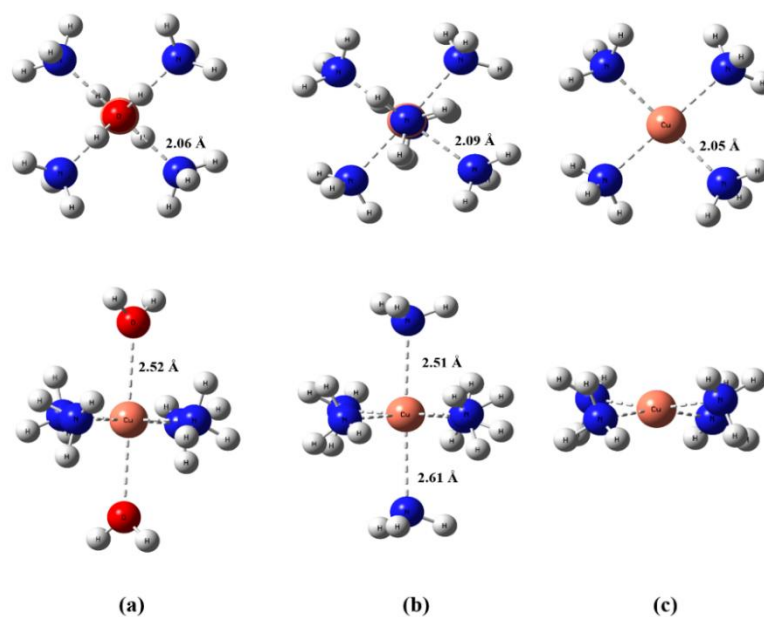
Figure 4.3 B3LYP/6-311+g(d,p) optimized structures of (a) $[Cu(NH_3)_4(H_2O)_2]^{2+}$, (b) $[Cu(NH_3)_6]^{2+}$ and (c) $[Cu(NH_3)_4]^{2+}$ in water. The optimized structures in top and bottom rows are top and side views, respectively.
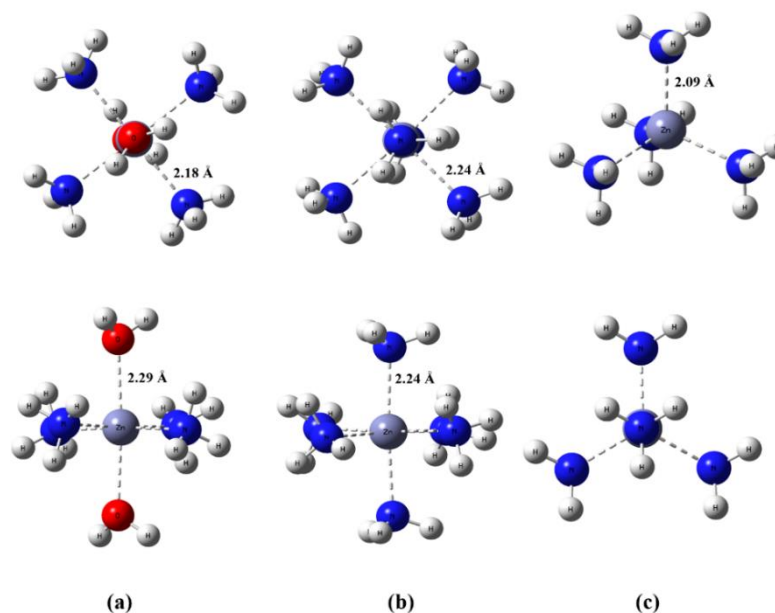
Figure 4.4 B3LYP/6-311+g(d,p) optimized structures of (a) $[Zn(NH_3)_4(H_2O)_2]^{2+}$, (b) $[Zn(NH_3)_6]^{2+}$ and (c) $[Zn(NH_3)_4]^{2+}$ in water. The optimized structures in top and bottom rows are top and side views, respectively.

Total energy of optimized complex structure, which can indicate the stability of the complexes in water, was obtained from frequency analysis (Figure 4.5). The complex with the lowest total energy is the most stable structure. The total energy of both copper- and zinc-ammonia complexes followed the order: $[M(NH_3)_4]^{2+}$ > $[M(NH_3)_6]^{2+}$ > $[M(NH_3)_4(H_2O)_2]^{2+}$. This result pointed out that $[Cu(NH_3)_4(H_2O)_2]^{2+}$ and $[Zn(NH_3)_4(H_2O)_2]^{2+}$ were the most stable structures for copper- and zinc-ammonia complexes, respectively, in water because they possessed the lowest total energy in analogy to the other species in their own groups. This result agrees with the data analyzed from mass spectra as discussed in previous section.

Coordinated bond lengths between metal and ligands, whose positions are determined in Figure 4.6, are reported in Table 4.2. It was found that, for $[Cu(NH_3)_4]^{2+}$ and $[Zn(NH_3)_4]^{2+}$, the four bond lengths between metal and NH_3 of each complex (M---Lig1 to M---Lig4) were equal of 2.05 and 2.09 Å, respectively. For $[Cu(NH_3)_4(H_2O)_2]^{2+}$, $[Zn(NH_3)_4(H_2O)_2]^{2+}$, $[Cu(NH_3)_6]^{2+}$ and $[Zn(NH_3)_6]^{2+}$, the bond lengths between metal and NH_3 in planar position of each complex (M---Lig1 to M---Lig4) were equal and shorter than the bond lengths between metal and H_2O (or NH_3) in axial position (M---Lig5 and M---Lig6). For example, Cu---NH_3 bond of $[Cu(NH_3)_4(H_2O)_2]^{2+}$ in the planar position was 2.06 Å, which was shorter than Cu---H_2O bond (2.52 Å) in the axial position. This similar observation was also found for the other complexes having 6 coordination numbers. This result indicated that the coordination bonds in the planar position of the complexes (M---Lig1 to M---Lig4) were stronger than those in the axial position (M---Lig5 and M---Lig6) (83, 84). For this reason, $[Cu(NH_3)_4(H_2O)_2]^{2+}$ and $[Zn(NH_3)_4(H_2O)_2]^{2+}$ could readily liberate their two H_2O ligands to have the square planar structures (85). These structures show the potential to accelerate gelling and blowing reactions of rigid PUR and PIR foams due to the fact that they contain the vacant sites for interacting with the foam reactants in foam formulation.
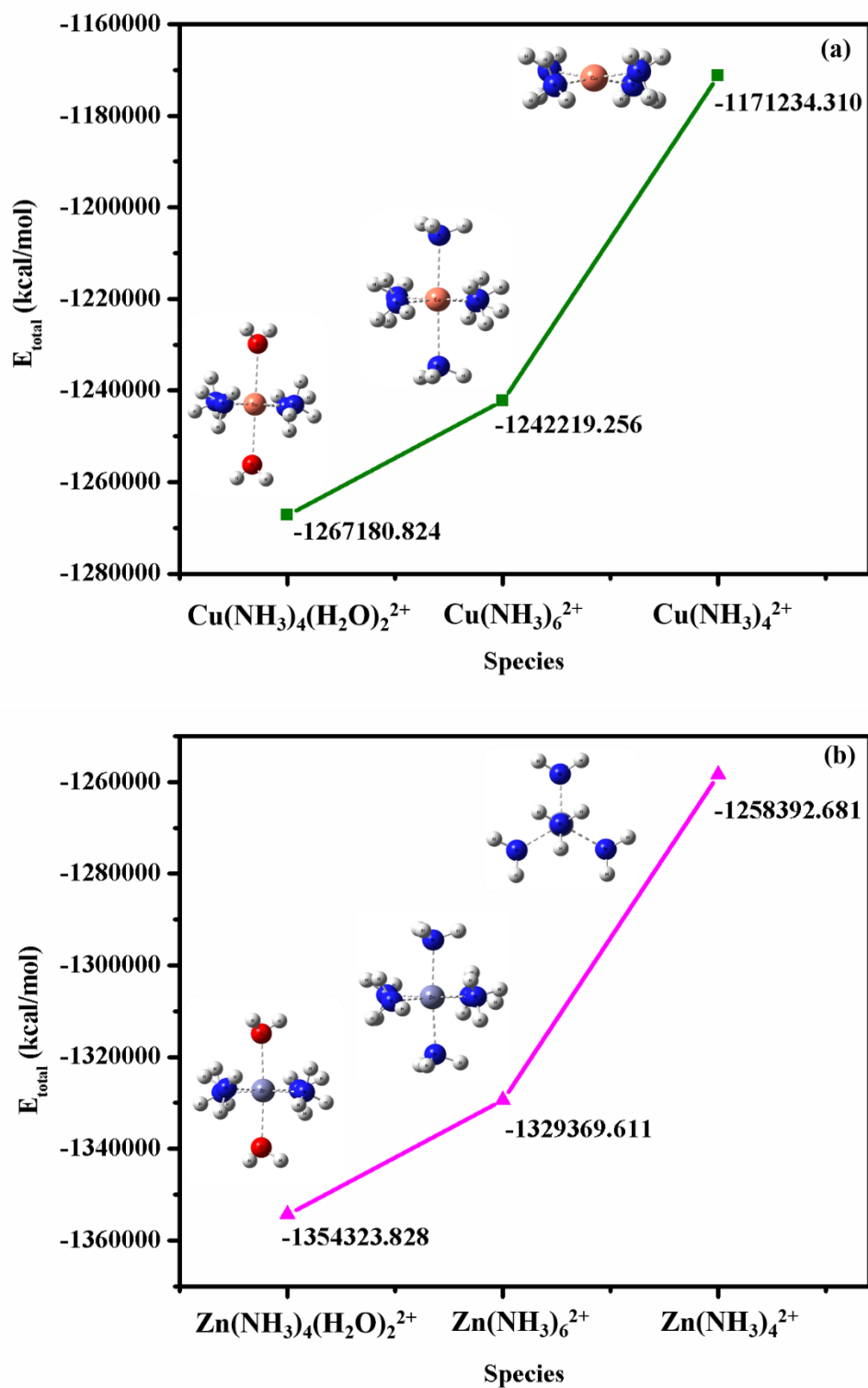
Figure 4.5 Total energy of each optimized structure of (a) copper-ammonia complexes and (b) zinc-ammonia complexes in water.
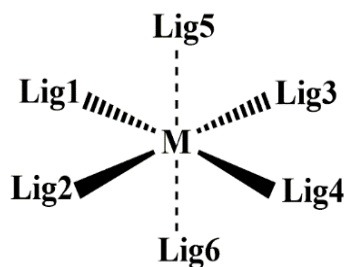
Figure 4.6 Ligand positions in metal-ammonia complexes.

Table 4.2 Metal-ligand bond lengths for each species of metal-ammonia complexes.

Species	Coordination number	Metal-ligand bond length (Å)					
		M⋯Lig1	M⋯Lig2	M⋯Lig3	M⋯Lig4	M⋯Lig5	M⋯Lig6
$[Cu(NH_3)_4(H_2O)_2]^{2+}$	6	2.06	2.06	2.06	2.06	2.52	2.52
$[Cu(NH_3)_6]^{2+}$	6	2.09	2.09	2.09	2.09	2.51	2.61
$[Cu(NH_3)_4]^{2+}$	4	2.05	2.05	2.05	2.05	-	-
$[Zn(NH_3)_4(H_2O)_2]^{2+}$	6	2.18	2.18	2.18	2.18	2.29	2.29
$[Zn(NH_3)_6]^{2+}$	6	2.24	2.24	2.24	2.24	2.24	2.24
$[Zn(NH_3)_4]^{2+}$	4	2.09	2.09	2.09	2.09	-	-

4.1.3 Structural analysis of metal-ammonia complexes using UV-visible spectrophotometry

Most of metal-ammonia complex solutions have colors which are different from those of their metal acetate solutions. Therefore, UV-visible spectrophotometry is a possible method to indicate the complex formation. For Cu(Amm) and Cu(OAc)$_2$, their UV-visible spectra compared to each other are showed in Figure 4.7. The maximum absorbance of Cu(Amm) emerged at 240 nm, which shifted from that of Cu(OAc)$_2$ at 245 nm. Moreover, UV-visible spectrum of Cu(Amm) gave three new peaks at 287, 334 and 620 nm, which were the different patterns from that of Cu(OAc)$_2$. This result is consistent with the UV-visible spectrum of copper-ammonia complex having four coordinated NH$_3$ reported in the literature (55). Unfortunately, the Zn(Amm) and Zn(OAc)$_2$ solutions do not have the color since 3d orbitals of Zn^{2+}

are completely filled with electron. Therefore, UV-visible spectra of Zn(Amm) and Zn(OAc)$_2$ could not be obtained.
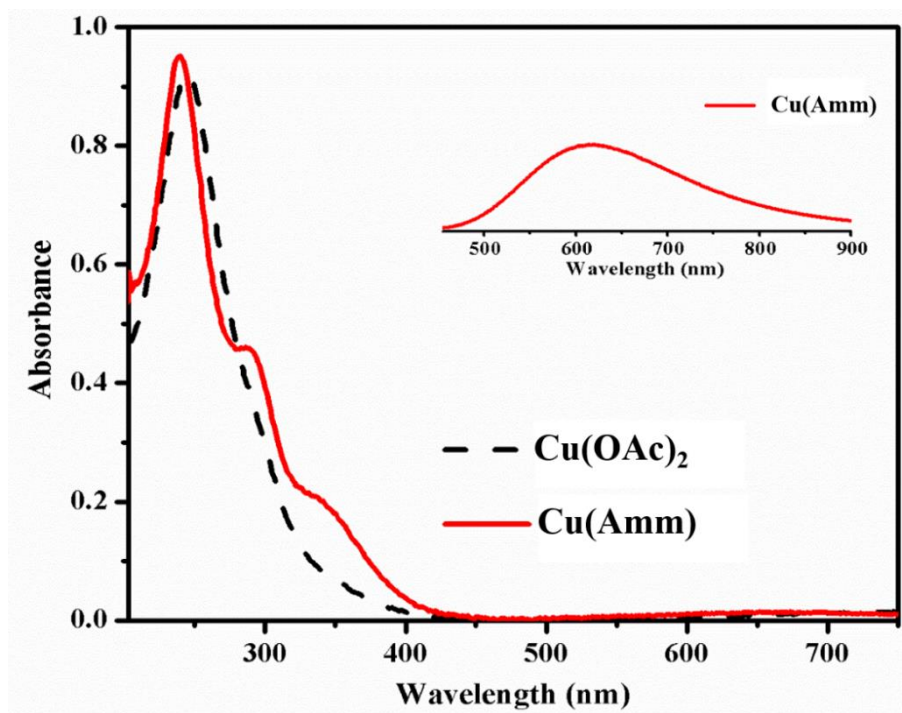
Figure 4.7 UV-visible spectra of Cu(Amm) and Cu(OAc)$_2$.

4.1.4 Structural analysis of metal-ammonia complexes using FTIR spectroscopy

Figure 4.8 presents IR spectra of metal-ammonia complex aqueous solution in comparison to their reactants, namely metal acetate (solid) and NH$_3$ solution. IR spectrum of Cu(Amm) in Figure 4.8(a) demonstrates symmetric and asymmetric C=O stretching of acetate group at 1411 and 1549 cm^{-1}, respectively. It was found that these peaks were different and shifted from the typical symmetric and asymmetric C=O stretching of acetate group of Cu(OAc)$_2$, which appeared at 1418 and 1596 cm^{-1}, respectively (25). In the case of Zn(Amm) in Figure 4.8(b), the symmetric C=O stretching of acetate group of Zn(Amm) shifted to 1411 cm^{-1} in comparison to that of Zn(OAc)$_2$, which appeared at 1435 cm^{-1} (25). Furthermore, Hathaway et al. reported about N-H symmetric deformation of NH$_3$ in copper-ammonia complexes, which

arose in the range of 1272-1087 cm^{-1} (53). This result is in agreement with N-H symmetric deformation of Cu(Amm) and Zn(Amm) in this work which were found at 1267 cm^{-1} at 1270 cm^{-1}, respectively.
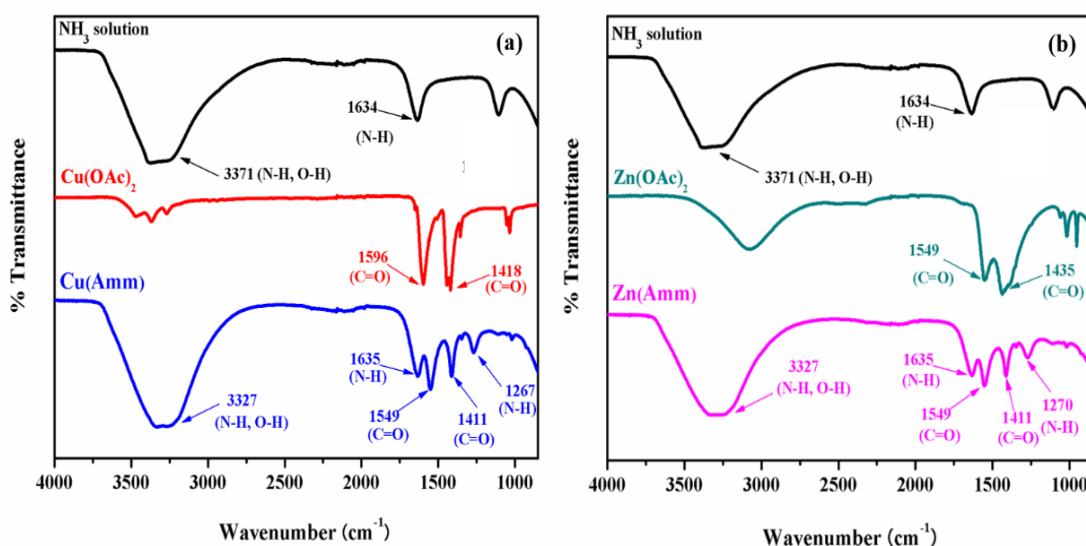
Figure 4.8 IR spectra of (a) Cu(Amm) and (b) Zn(Amm) aqueous solutions compared to metal acetate (solid) and NH$_3$ solution.

4.2 Preparation of rigid PUR foams using metal-ammonia complexes as catalysts

In the second section, Cu(Amm) and Zn(Amm) solutions were applied as catalysts for the preparation of rigid PUR foams. The main functions of catalyst use to accelerate and to balance the reaction rate between blowing and gelling reactions of the foam. Equimolar of isocyanate and hydroxyl compounds (isocyanate index of 100) was used to prepare rigid PUR foams.

4.2.1 Reaction time and properties of rigid PUR foam accelerated by metal-ammonia complexes

The reaction time and physical properties of rigid PUR foam accelerated by constant amount of Cu(Amm) and Zn(Amm) at 1.0 pbw were investigated and compared to those accelerated by Cu(OAc)$_2$, Zn(OAc)$_2$, NH$_3$ and DMCHA (the

industrial catalyst) as shown in Table 4.3 and Figure 4.9. According to ASTM standard method of rigid PUR foams, the reaction time in the foaming reactions should be recorded as follows: cream time is the starting point of blowing reaction at which the foam height increases approximately 5% of total height. Gel time is the beginning point of crosslink formation (gelling reaction) via urethane linkages. At this time, stable shape of the foam mixture is observed. Rise time is the time when blowing reaction is completed and the foams no longer rise. Tack free time is the time when gelling reaction is completed and the foams totally become dry solid (34, 86, 87). Among the reaction time, tack free time and rise time indicate the time at which gelling reaction and blowing reaction, respectively, are accomplished. Therefore, the catalytic efficiency in gelling and blowing reactions of each catalyst was considered via tack free time and rise time, respectively.

Table 4.3 Reaction time and properties of rigid PUR foam obtained from various catalysts.

Catalysts	Reaction time (s)				Density (kg/m^3)	Foam height (%)	Isocyanate conversion (%)
	Cream time	Gel time	Tack free time	Rise time			
No catalyst	38±1	359±8	1682±13	779±10	58.7±1.9	65.0	86.7
DMCHA	21±0	34±1	165±3	112±4	39.4±0.5	95.8	99.1
Cu(Amm)	27±1	69±2	142±3	156±2	41.8±0.4	87.4	99.2
Zn(Amm)	25±1	95±1	192±2	215±2	38.5±0.8	100	98.5
Cu(OAc)$_2$	35±1	237±4	880±6	557±6	51.6±2.4	69.9	94.7
Zn(OAc)$_2$	30±1	256±4	775±10	527±9	44.4±2.1	83.9	91.7
NH$_3$	28±0	165±1	859±3	403±4	43.6±2.0	80.4	92.7
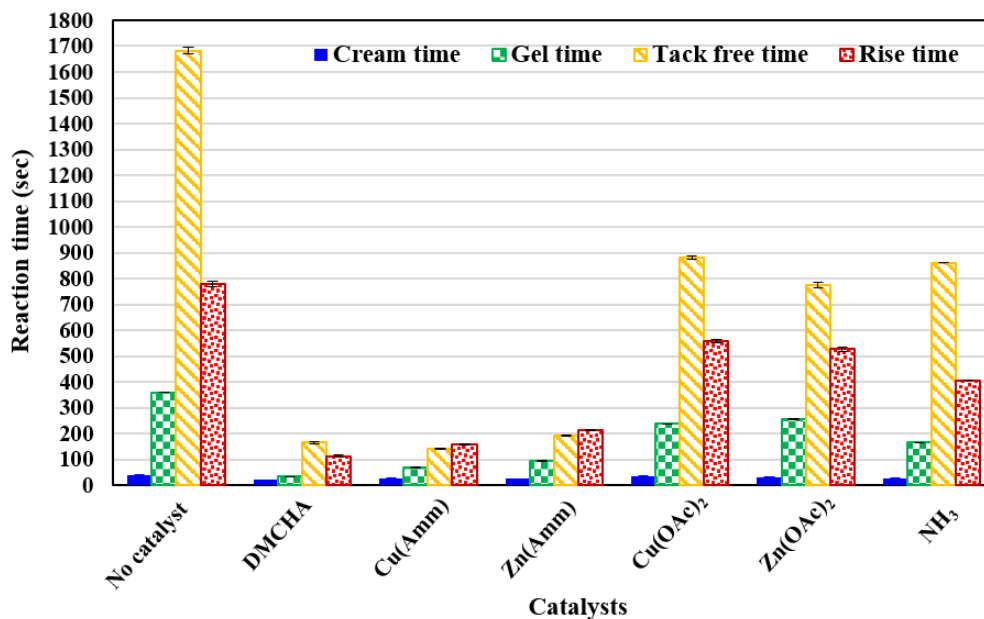
Figure 4.9 Trend of reaction time of rigid PUR foam catalyzed by various catalysts.

It was found that NH_3, metal acetates [$Cu(OAc)_2$ and $Zn(OAc)_2$] and metal-ammonia complexes could catalyze the reactions of rigid PUR foam since they reduced the reaction time in comparison to those of the foam without catalyst. However, their catalytic activity showed the large difference. Without complex structure, NH_3, $Cu(OAc)_2$ and $Zn(OAc)_2$ showed very poor catalytic activity resulting in very long reaction time, whereas Cu(Amm) and Zn(Amm) obviously showed better catalytic activity to effectively reduce the reaction time of the foams. This result might be attributed to reason that copper and zinc ions had strong interaction with NH_3 ligands and could maintain their complex structures without ligand detachment throughout their catalytic processes. Therefore, it might be concluded that the complex structure was necessary and could enhance the catalytic properties of copper- and zinc-based catalysts in this study. The consistent result was also reported by Schellekens et al., who used iron(II) complex catalysts having several ligand types to catalyze the polymerization (gelling reaction) of thermoplastic polyurethane. They found that the iron(II)-complexes with the stable complex structures could prevent the deactivation of central iron(II) ion during polymerization process and showed better catalytic activity, especially at high temperature, than iron(II)-complexes with ligand

detachment (49). The foam appearance obtained from those catalysts was also investigated as presented in Figures 4.10. The foam without catalyst as well as the foams accelerated by $Cu(OAc)_2$, $Zn(OAc)_2$ and NH_3 were brittle materials. This indicated that $Cu(OAc)_2$, $Zn(OAc)_2$ and NH_3 were not good catalysts for rigid PUR foams. In contrast, the foams processed by Cu(Amm) and Zn(Amm) had proper appearance with stable shape and did not have the fracture surface.
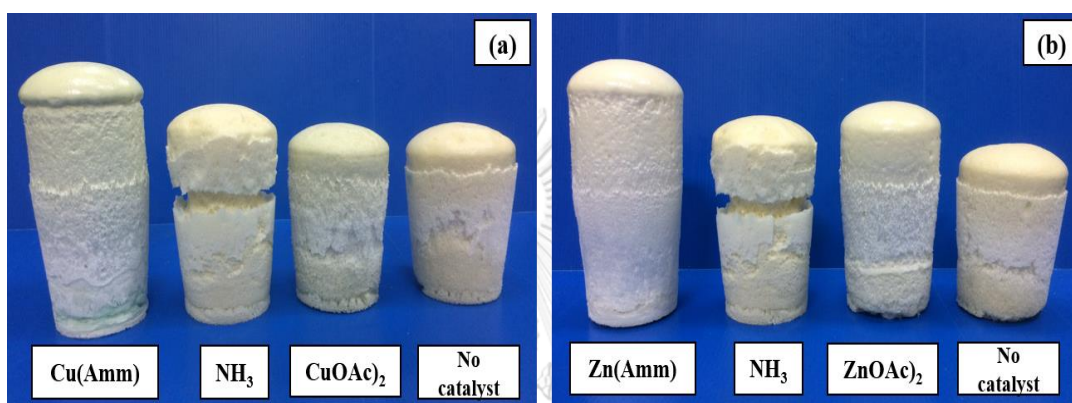
Figure 4.10 Appearance of rigid PUR foams accelerated by (a) Cu(Amm) and (b) Zn(Amm) in comparison with their unaccelerated foams and those accelerated by $Cu(OAc)_2$, $Zn(OAc)_2$ and NH_3.

Then, the catalytic efficiency of the synthesized complexes [Cu(Amm) and Zn(Amm)] was compared to that of industrial catalyst (DMCHA). Considering the catalytic efficiency in gelling reaction, gel time and tack free time obtained from these catalysts followed the orders DMCHA < Cu(Amm) < Zn(Amm) and Cu(Amm) < DMCHA < Zn(Amm), respectively. Cu(Amm) and Zn(Amm) appeared to start the gelling reaction slower than DMCHA resulting in longer gel time, which was good for the processing of samples in large mold since longer mixing time was obtained. However, according to the fastest tack free time of Cu(Amm), it could improve its catalytic activity along the reaction time and accomplished the gelling reaction before DMCHA and Zn(Amm). This indicated that Cu(Amm) gave the fastest catalytic activity in gelling reaction. In case of cream time and rise time, DMCHA had the highest catalytic activity and appeared to overwhelm Cu(Amm) and Zn(Amm) for

catalyzing the CO_2 generation. Nevertheless, the foam density obtained from Cu(Amm), Zn(Amm) and DMCHA is quite similar. This result indicated that the catalytic efficiency in blowing reaction of Cu(Amm) and Zn(Amm) was enough to obtain rigid PUR foams with appropriate density.

The isocyanate conversion of rigid PUR foam (Table 4.3) is another parameter which can indicate the efficiency of catalyst to complete gelling and blowing reactions of the foams. After all reactions of the foams took place, isocyanate conversion was computed from the normalized absorption peak of remaining isocyanate group at 2277 cm^{-1} in IR spectra as shown in Figure 4.11 using the following equation (88):

$$\text{Isocyanate conversion (\%)} = [1 - (A^t_{\text{isocyanate}}/A^0_{\text{isocyanate}})] \times 100 \qquad (4.1)$$

where $A^t_{\text{isocyanate}}$ is the normalized absorption peak of isocyanate group at time t. $A^0_{\text{isocyanate}}$ is the normalized absorption peak of isocyanate group at initial time. The results in Figure 4.11(a) showed that there was the large decrease in isocyanate absorption peak of the foams accelerated by Cu(Amm) and Zn(Amm) in comparison to those accelerated by the other catalysts in Figure 4.11(b). Considering % isocyanate conversion, rigid PUR foam without catalyst showed the lowest % isocyanate conversion of 86.7%. The isocyanate conversion of the foams accelerated by Cu(Amm), Zn(Amm) and DMCHA increased to 99.2%, 98.5% and 99.1%, respectively. More than 98% of isocyanate conversionreduc accompanying with the other previous results indicated that Cu(Amm) and Zn(Amm) could act as the suitable catalysts for the preparation of rigid PUR foam.
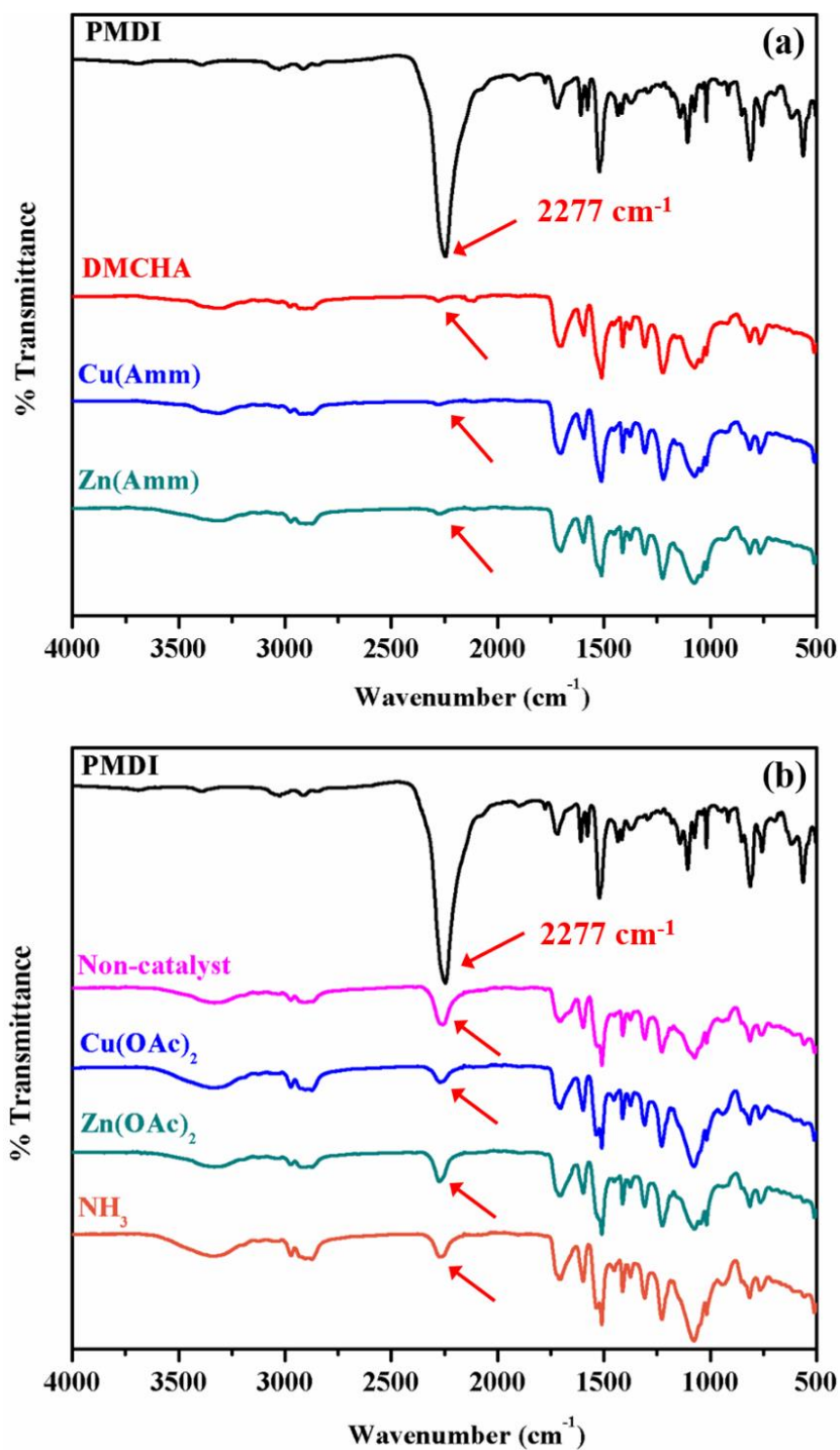
Figure 4.11 IR spectra of rigid PUR foams accelerated by (a) Cu(Amm), DMCHA and Zn(Amm) and (b) other catalysts in comparison to isocyanate starting material (PMDI).

4.2.2 Rise profiles of rigid PUR foam accelerated by metal-ammonia complexes

Figure 4.12 presents rise profiles of rigid PUR foam accelerated by Cu(Amm), Zn(Amm) and DMCHA. The result revealed that the foams processed by Cu(Amm), Zn(Amm) and DMCHA had the similar rise profiles which exhibited smooth rise profiles with uninterrupted pattern during rising process. The order of the foams arriving to their total height is Zn(Amm) > Cu(Amm) > DMCHA. DMCHA drove the foam height very fast at initial time. Cu(Amm) and Zn(Amm) initiated the blowing reaction and increased the foam height slower than DMCHA at the initial time, however, they could give faster rise curves in the latter stage.
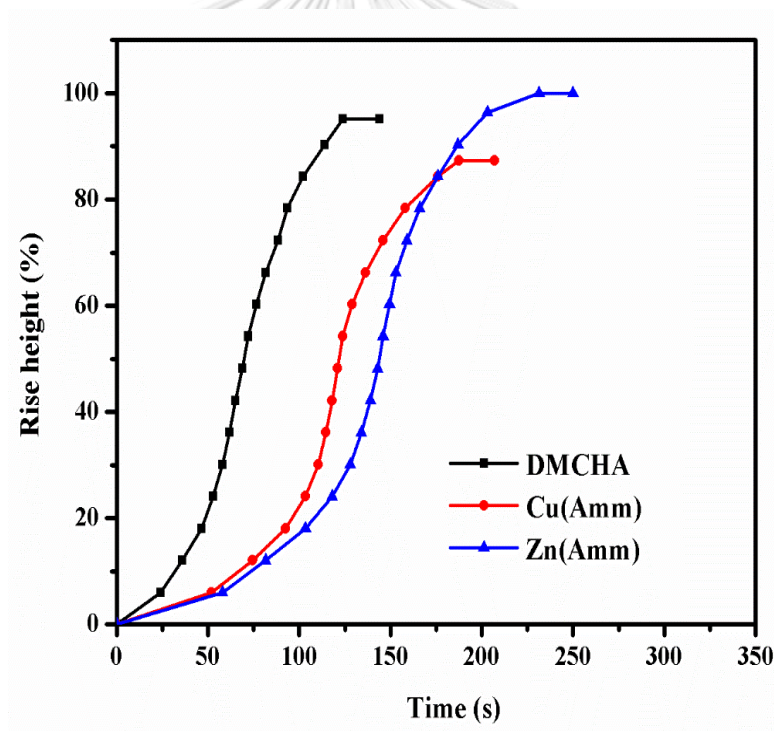
Figure 4.12 Rise profiles of rigid PUR foam accelerated by different catalysts.

4.2.3 Temperature profiles of rigid PUR foam accelerated by metal-ammonia complexes

Because both gelling reaction and blowing reaction of rigid PUR foam are exothermic reaction, the study of heat release during foaming process is necessary. Temperature profiles of the foams accelerated by Cu(Amm), Zn(Amm) and DMCHA are shown in Figure 4.13. It was found that the reaction temperature increased along with the time until the reactions almost completed. The maximum core temperatures of the foam accelerated by Cu(Amm), Zn(Amm) and DMCHA were 123.8, 124.5 and 127.8 °C, respectively, and appeared close to each other.
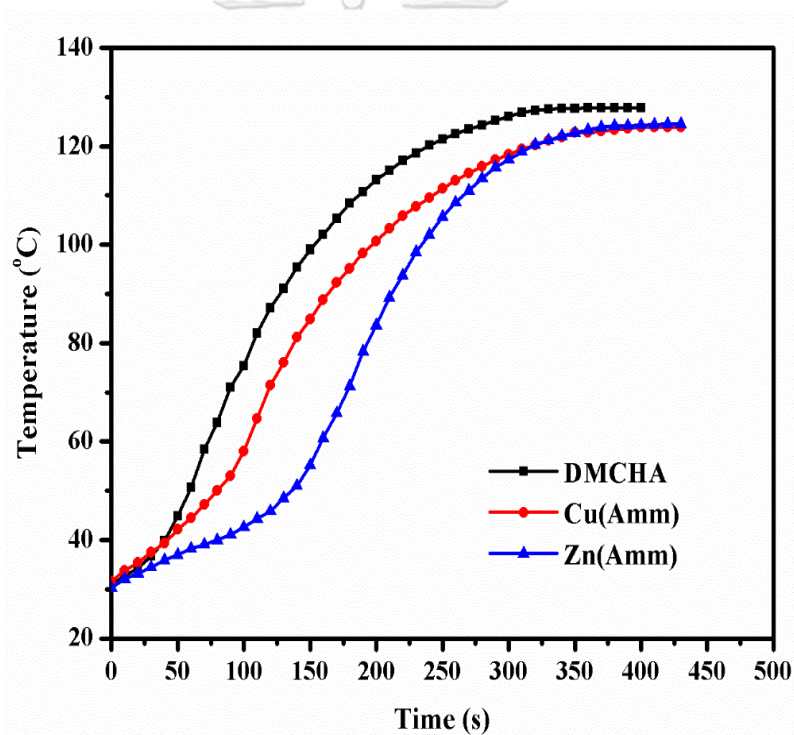
Figure 4.13 Temperature profiles of rigid PUR foam accelerated by different catalysts.

4.2.4 Effect of catalyst amount on rigid PUR foam properties

Effect of amount of Cu(Amm) and Zn(Amm) on reaction time and the appearance of the foams was investigated as shown in Figures 4.14 and 4.15,

respectively. The same result was observed for both Cu(Amm) and Zn(Amm) that the reaction time decreased with increasing catalyst amount in foam formulation. The large decrease in gel time and tack free time affirmed that Cu(Amm) and Zn(Amm) were effective catalysts for accelerating the gelling reaction.
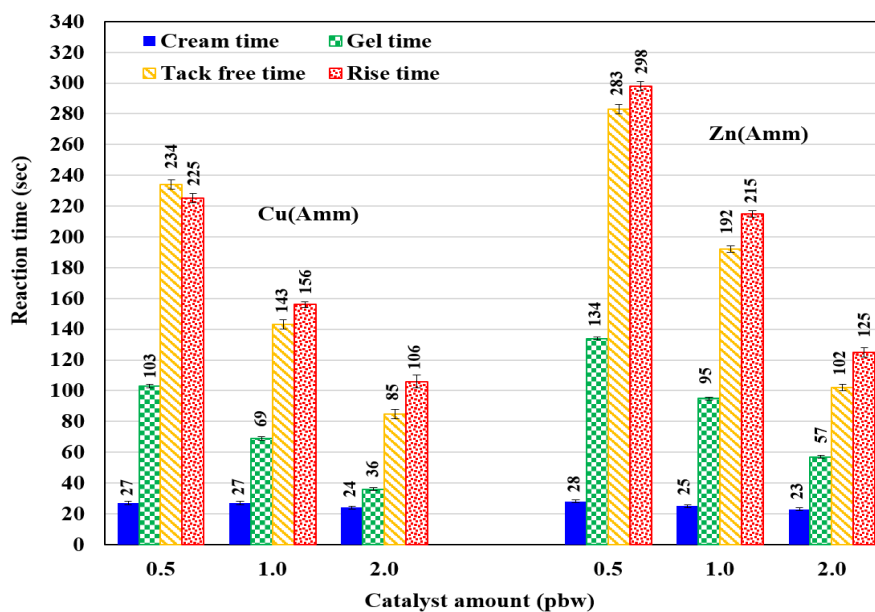
Figure 4.14 Effect of catalyst amount on reaction time of rigid PUR foam.
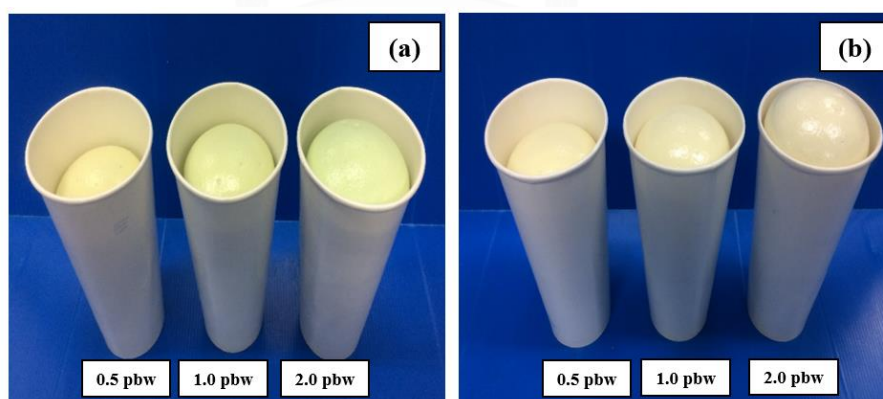
Figure 4.15 Appearance of rigid PUR foams obtained from different amount of (a) Cu(Amm) and (b) Zn(Amm) catalysts at the constant blowing agent content of 3.0 pbw.

Foam density decreased with higher amount of catalyst as shown in Figure 4.16. The increase of catalyst amount caused the increase of foaming temperature, which could promote the kinetic rate of CO_2 diffusion into the foam cells resulting in reduction of foam density (89).
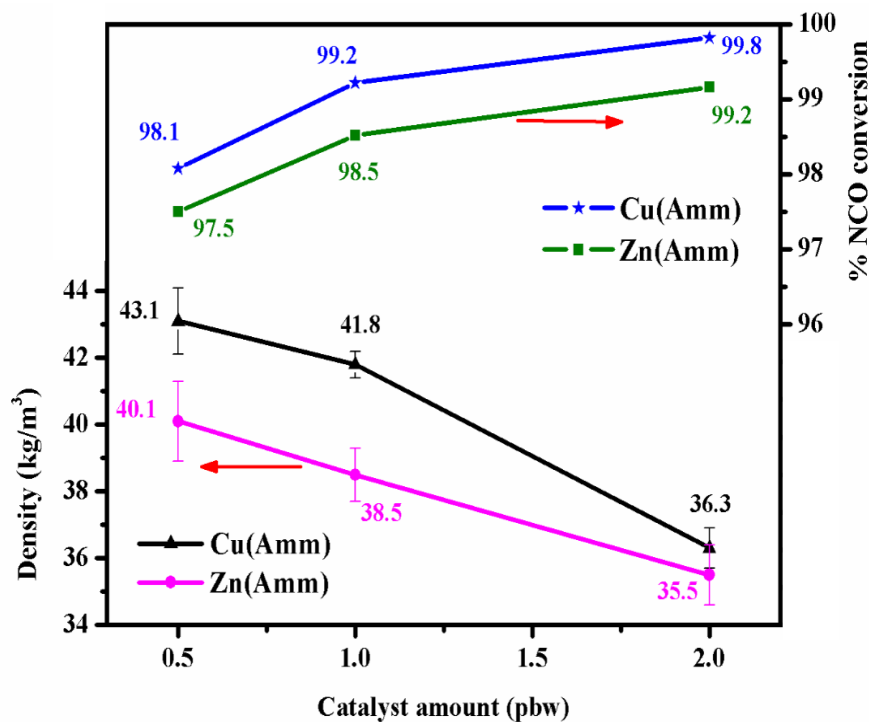
Figure 4.16 Effect of catalyst amount on density of rigid PUR foam and % isocyanate conversion.

The effect of catalyst amount on % isocyanate conversion was studied as shown in Figure 4.16. It was found that % isocyanate conversion slightly increased with increasing catalyst amount from 0.5-2.0 pbw. Although higher catalyst amount of both Cu(Amm) and Zn(Amm) at 2.0 pbw could almost complete the reaction of isocyanate and also gave faster reaction time, rigid PUR foams processed using this catalyst amount had poor properties. The large holes appeared at the bottom of the foam as shown in Figure 4.17. Therefore, the suitable amount of Cu(Amm) and Zn(Amm) for the processing of rigid PUR foams is 1.0 pbw.
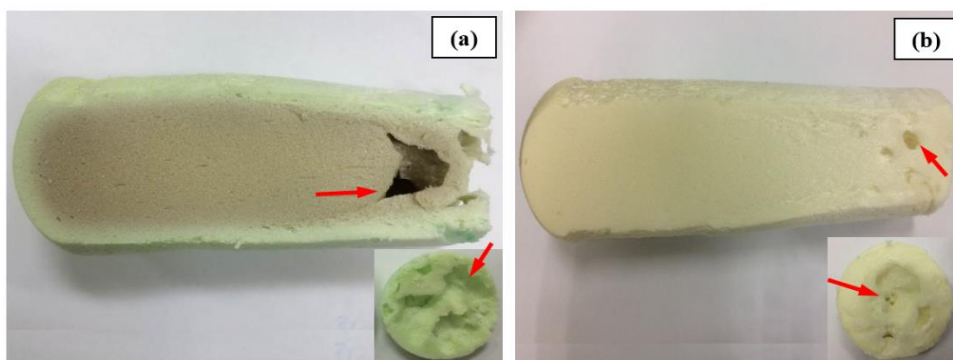
Figure 4.17 The large holes at the bottom of rigid PUR foam accelerated by 2.0 pbw of (a) Cu(Amm) and (b) Zn(Amm).

4.2.5 Proposed catalytic mechanism of metal-ammonia complexes

Catalytic mechanism in gelling and blowing reactions of metal-ammonia complexes is presented based on the information of alternative catalysts suggested in several works. For example, Barman et al., Schellekens et al. and Sardon et al. developed copper(II)-, iron(II)-based and zirconium(IV)-based catalysts, respectively, for catalyzing urethane formation (49, 90, 91). They reported that their transition metal ions of catalyst could be electrophilic activators by accepting electron pair from isocyanate. Whereas cyclic guanidines, which is the tertiary amines, were used by Alsarraf et al. as the nucleophilic activators for donating electron pair to the proton of alcohol (51).

Based on these evidences, Cu(Amm) and Zn(Amm) were proposed to be electrophilic activator and nucleophilic activator for gelling reaction (Scheme 4.3) and blowing reaction (Scheme 4.4) as they contained both metal ions and amines in their structures (24, 92). After Cu(Amm) and Zn(Amm) detached their axial ligands (H_2O) to have square planar structures, Cu^{2+} or Zn^{2+} could perform as electrophilic activators (Lewis acid) by coordinating with an oxygen atom of isocyanate compound. This led a carbon atom of isocyanate compound to be more electrophilic. Meanwhile, NH_3 could be nucleophilic activators (Lewis base) by interacting with the proton of hydroxyl compound. This led the oxygen atom of hydroxyl compound to be more nucleophilic for interacting with the carbon atom of isocyanate compounds.
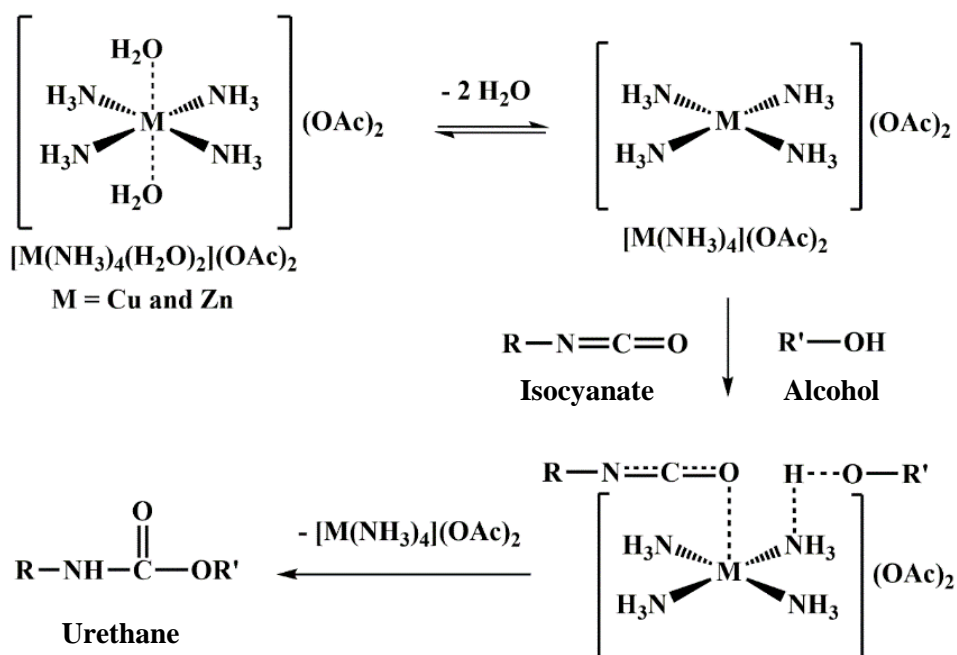
Scheme 4.3 Proposed catalytic mechanism in gelling reaction of metal-ammonia complexes.
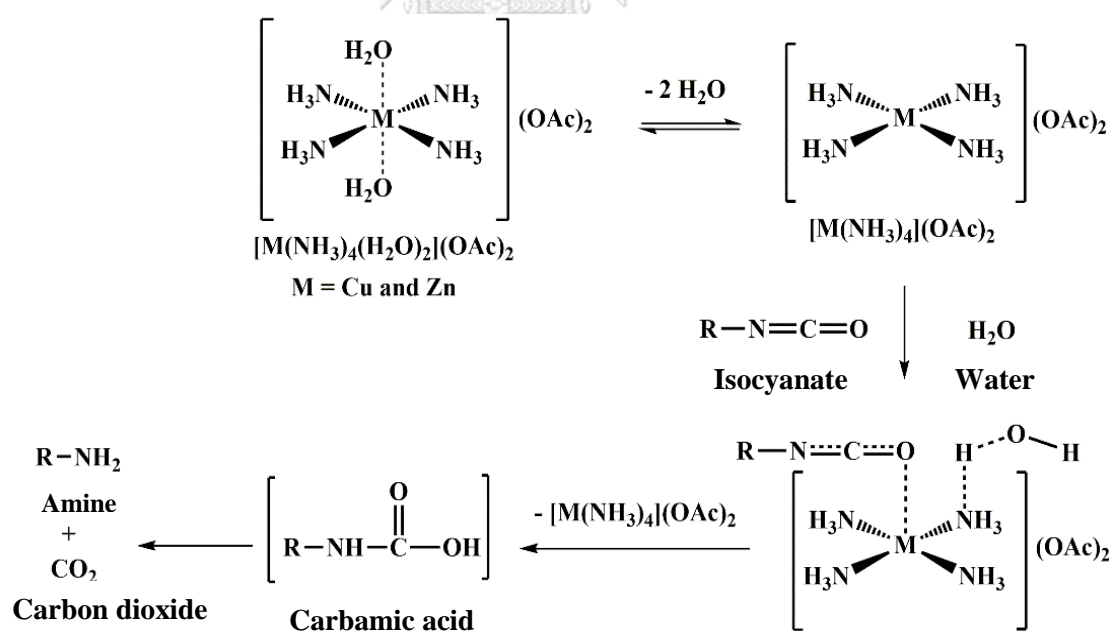
Scheme 4.4 Proposed catalytic mechanism in blowing reaction of metal-ammonia complexes.

4.2.6 Effect of blowing agent amount on rigid PUR foam properties

The effect of blowing agent amount on reaction time and properties of the foam accelerated by constant amount of metal-ammonia complex at 1.0 pbw was also studied as shown in Figures 4.18-4.20. It was found that gel time, tack free time and rise time increased with increasing blowing agent amount, whilst the change in cream time was negligible. The blowing reaction between isocyanate with water needs suitable catalyst quantity in acceleration (46). Increase of water amount employs more catalyst content to complete the blowing reaction. Therefore, in the case of using the constant amount of catalyst at 1.0 pbw, the duration for completing blowing reaction at higher amount of water was extended resulting in longer reaction time. The isocyanate conversion slightly decreased with increasing blowing agent as presented in Figure 4.19. This result indicated that the catalytic activity of catalysts slightly reduced at the higher amount of blowing agent. Density of the foams decreased with increasing of blowing agent content due to the fact that more CO_2 was generated (93, 94) resulting in higher rigid PUR foams as shown in Figure 4.20.
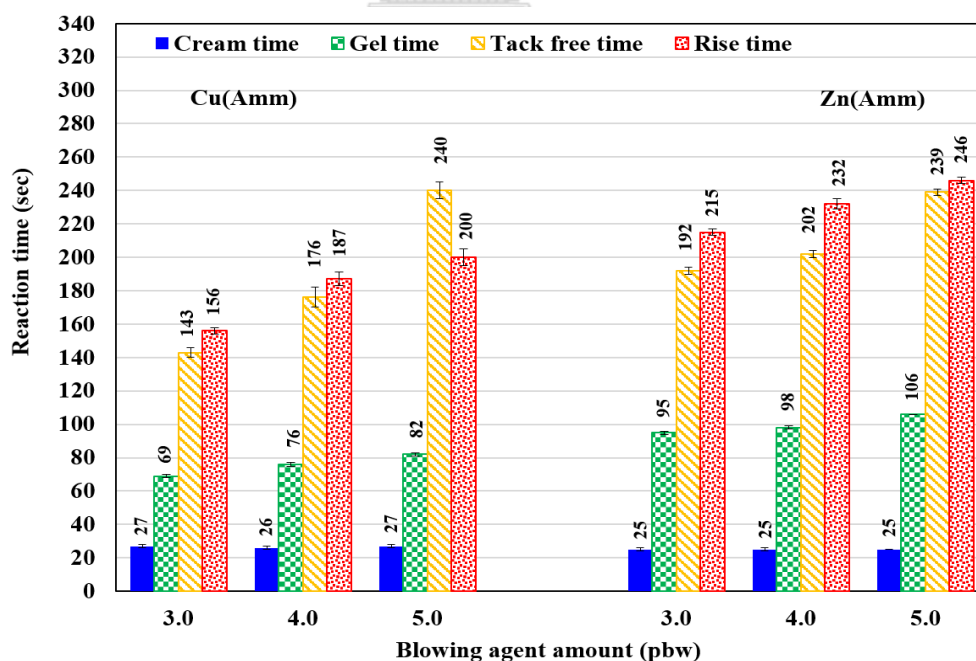
Figure 4.18 Effect of blowing agent amount on reaction time of rigid PUR foam.
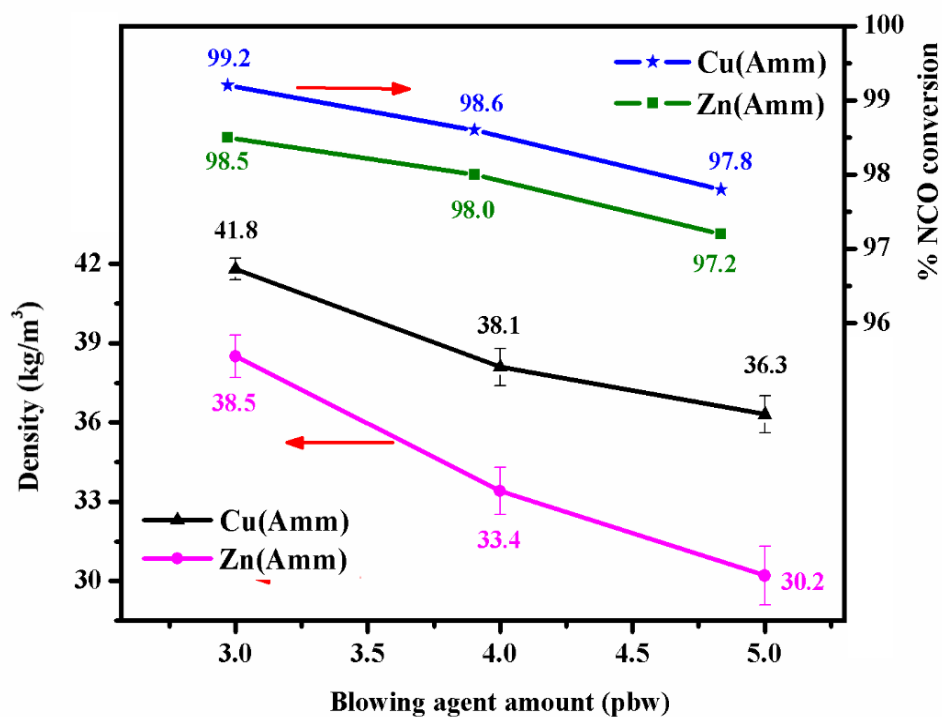
Figure 4.19 Effect of blowing agent amount on density of rigid PUR foams and % isocyanate conversion.
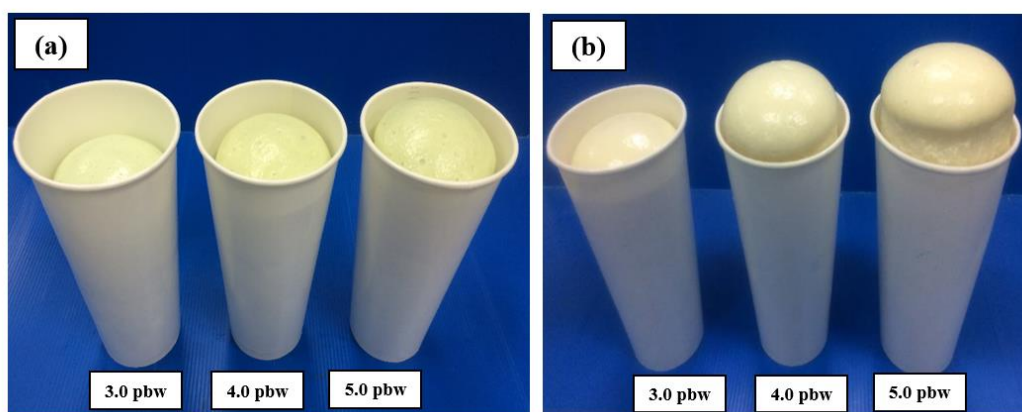
Figure 4.20 Appearance of rigid PUR foams accelerated by (a) Cu(Amm) and (b) Zn(Amm) using different blowing agent contents.

4.2.7 Morphology of rigid PUR foams accelerated by metal-ammonia complexes

Morphology of the foams is affected by several parameters, such as catalytic activity of catalysts, blowing agent amount and foam-rising direction. The foam morphology with small cell size and high number of close cell could improve the mechanical properties of rigid PUR foam (95).

Figure 4.21 presents the SEM micrographs of rigid PUR foam processed by different catalysts, blowing agent amount and foam-rising direction. It was observed that all rigid PUR foams composed of close cell structures and had dissimilar morphology when observed in different views. The cell morphology in the same to foam-rising direction (side view) had extended shape, whilst that in the opposite to foam-rising direction (top view) appeared rounded shape.
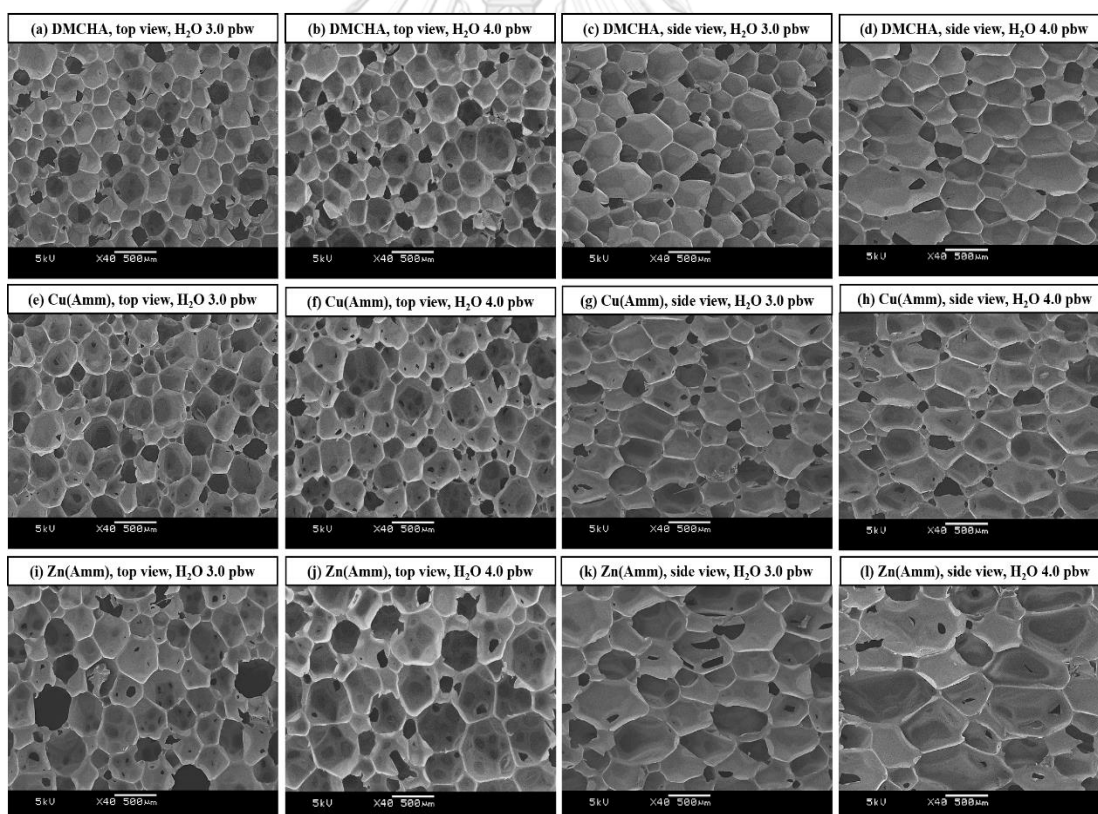
Figure 4.21 SEM micrographs of rigid PUR foam accelerated by DMCHA, Cu(Amm) and Zn(Amm) at different views and amount of blowing agent.

The average cell size of those foams calculated from the SEM micrographs is shown in Table 4.4. At constant amount of blowing agent, the effect of different catalyst types on morphology could be observed. The order of average cell size obtained from different catalyst types in both top and side views is Zn(Amm) > DMCHA > Cu(Amm). The average cell size of the foams accelerated by Cu(Amm) was very close to that accelerated by DMCHA, whilst the foams accelerated by Zn(Amm) distinctly showed the largest average cell size. The smallest cell size of the foams accelerated by Cu(Amm) might be corresponded to the fastest tack free time given by this catalyst, which could confine the foam cells to increase their volume and prevent the coalescence of foam cells resulting in the final foams with the smallest average cell size (96, 97). For the foams accelerated by Zn(Amm), their reaction time was the longest. Therefore, the coalescence of their foam cells could occur owing to the slowest viscosity increase resulting in the largest average cell size.

The effect of blowing agent (water) amount on morphology of the foams was also examined. It was observed that all foam cells were larger (Figure 4.21) and the average cell size in both top and side views increased (Table 4.4) when increasing water amount from 3.0 to 4.0 pbw. Water is the chemical blowing agent, which produces CO_2 through the exothermic reaction with isocyanate compounds. Due to the increase of water amount, more CO_2 was generated and trapped into the foam cells resulting in larger foam cells (32, 98).

Table 4.4 Average cell size of rigid PUR foams accelerated by DMCHA, Cu(Amm) and Zn(Amm) at different views and amount of blowing agent.

Catalysts	Average cell size (μm)			
	Top view		Side view	
	3.0	4.0	3.0	4.0
DMCHA	310.2±62.5	330.9±73.2	502.0±70.4	546.0±175.6
Cu(Amm)	308.7±53.8	341.5±70.4	498.5±81.1	539.5±109.8
Zn(Amm)	402.5±67.3	484.6±88.6	660.1±136.7	993.9±187.7

4.2.8 Compression properties of rigid PUR foam accelerated by metal-ammonia complexes

Compression stress-strain graphs of rigid PUR foam accelerated by metal-ammonia complexes in the same and the opposite to foam-rising direction are illustrated in Figure 4.22. This figure also shows the effect of blowing agent amount, 3.0 and 4.0 pbw, on compression properties of the foam. Compression strength was collected at 10% strain as reported in Figure 4.23.
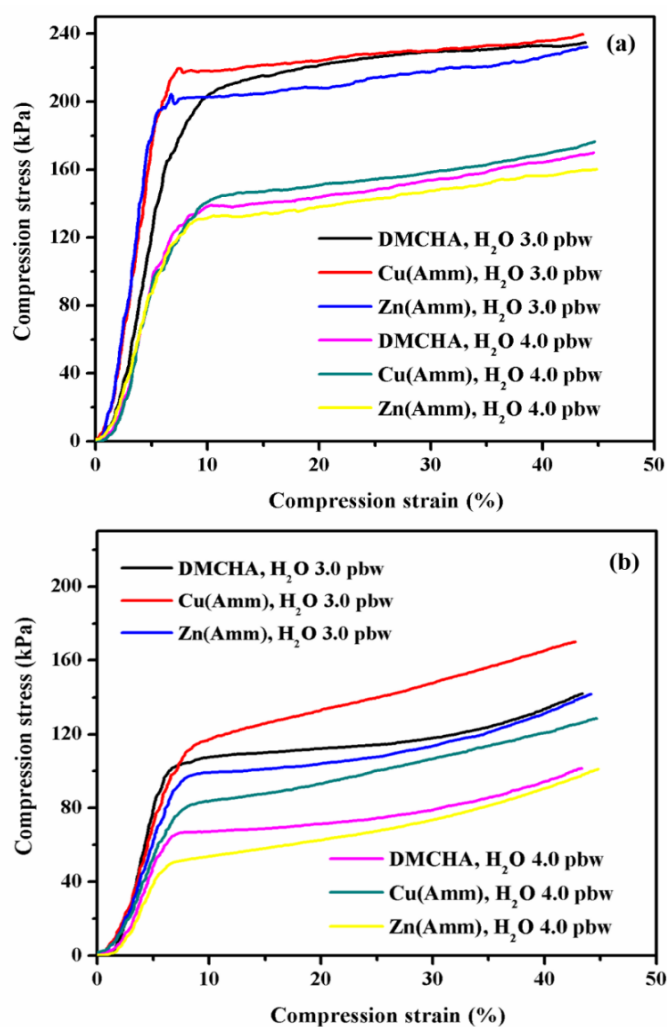
Figure 4.22 Compression behavior of rigid PUR foam obtained using different catalyst types and blowing agent amount in (a) the same and (b) the opposite to foam-rising direction.
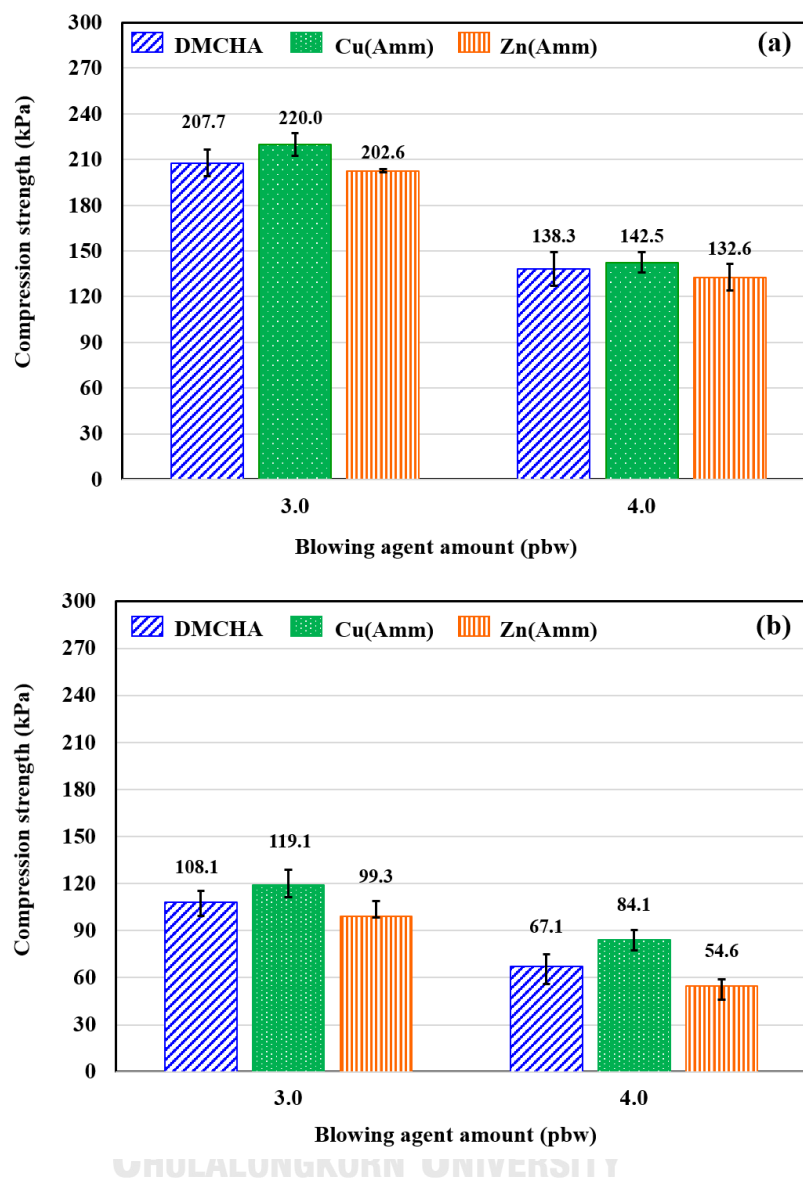
Figure 4.23 Compression strength of rigid PUR foam obtained using different catalyst types and blowing agent amount in (a) the same and (b) the opposite to foam-rising direction.

It was found that the foams processed using the same catalyst type and constant blowing agent amount had higher compression strength in the same to foam-rising direction [Figures 4.22(a) and 4.23 (a)] than that in the opposite to foam-rising direction [Figures 4.22(b) and 4.23 (b)]. This might be corresponded to the dissimilar cell structures of the foam. Lin et al. suggested that the foam cells with extended shape could resist with the compression better than the foam cells with rounded shape

as they could freely rise without restriction by the mold wall and therefore contained higher degree of cell orientation (99).

At constant blowing agent amount, various catalyst types affected the compression properties of the foam. The order of compression strength obtained from various catalysts in the same and the opposite to foam-rising direction is Cu(Amm) > DMCHA > Zn(Amm). The maximum compression strength of the foam accelerated by Cu(Amm) was due to its highest density and smallest average cell size. On the other hand, the foam accelerated by Zn(Amm) had lowest density and largest average cell size, and therefore it showed the lowest compression strength in the same and the opposite to foam-rising direction. In general, the higher foam density (34, 98) and smaller average cell size (100-102) could improve compression properties of the foam. The smaller foam cells had the thicker cell walls as they expanded less than the larger foam cells during foaming process. Therefore, they could resist with the compression better than the larger foam cells resulting in higher compression strength. However, the compression strength of the foam processed by Zn(Amm) at 3.0 pbw of blowing agent is practical since it reaches the recommended value at 100 kPa (42).

Considering effect of blowing agent amount on compression properties, with increasing blowing agent amount from 3.0 to 4.0 pbw, the compression strength in the same and the opposite to foam-rising direction decreased due to the decrease in foam density together with larger average cell size.

4.2.9 Dimensional stability of rigid PUR foam accelerated by metal-ammonia complexes

Tables 4.5 and 4.6 summarize dimensional variation of rigid PUR foam accelerated by metal-ammonia complexes, when they were kept according to the ASTM standard method for 14 days at -25 and 70 °C, respectively. The foam appearance (Figure 4.24) after 14 days showed that the foams accelerated by Cu(Amm) and Zn(Amm) still had dimensional stability without any visible damage or crack on the surface. The foams processed from Cu(Amm) showed good dimensional stability at both high and low temperatures. The % dimensional variation of the foams processed by Zn(Amm) was higher than that of the foams processed by Cu(Amm).

For instance, % volume and % mass variation at 70 °C after 14 days of the foams obtained from Zn(Amm) were -3.33% and - 2.65%, respectively, which were higher than those obtained from Cu(Amm) of -2.41% and -1.82%, respectively. However, the highest % linear variation (width, length and thickness) of the foams accelerated by Zn(Amm) did not exceed the values recommended by commercial standard (BS4370: Part 1), which reported that the foams should have % linear change lower than 3.0% and 1.0% at 70 °C and -15 °C, respectively (103).

According to the results, our foams shrank at both high and low temperatures. This is different from the foams blown with CFC, which shrank at low temperature but expanded their volume at high temperature. CFC-blown foams decreased internal pressure at low temperature due to the condensation of CFC resulting in volume reduction of foams. In contrast, the volume of the CFC-blown foams increased at high temperature because CFC tried to evaporate when temperature increased (104, 105). For the H_2O-blown foams, CO_2 did not condense at -25 °C, but tried to outwardly diffuse from foam cells at both high temperature and low temperature (106, 107). Therefore, the shrinkage of the foams was found at the testing temperatures. This result is in agreement with that of H_2O-blown foam reported in another study (108).

Table 4.5 Dimensional variation of rigid PUR foam accelerated by Cu(Amm) and Zn(Amm) at -25 °C.

Catalyst	Duration (days)	% Variation at -25 °C				
		Width	Length	Thickness	Volume	Mass
	1	-0.02±0.01	-0.05±0.02	-0.09±0.06	-0.16±0.07	-0.18±0.04
Cu(Amm)	7	-0.11±0.04	-0.09±0.01	-0.13±0.02	-0.33±0.05	-0.49±0.12
	14	-0.10±0.04	-0.14±0.06	-0.19±0.10	-0.44±0.07	-0.58±0.10
	1	-0.04 ± 0.04	-0.14 ± 0.03	-0.17 ± 0.05	-0.51 ± 0.16	-0.60 ± 0.12
Zn(Amm)	7	-0.16 ± 0.09	-0.25 ± 0.08	-0.28 ± 0.08	-0.95 ± 0.26	-1.27 ± 0.17
	14	-0.22 ± 0.06	-0.21 ± 0.10	-0.45 ± 0.09	-1.30 ± 0.23	-1.44 ± 0.19

Table 4.6 Dimensional variation of rigid PUR foam accelerated by Cu(Amm) and Zn(Amm) at 70 °C.

Catalyst	Duration (days)	% Variation at 70 °C				
		Width	Length	Thickness	Volume	Mass
Cu(Amm)	1	-0.06±0.03	0.01±0.03	-0.08±0.04	-0.13±0.05	0.09±0.15
	7	-0.30±0.10	-0.16±0.04	-0.32±0.09	-0.79±0.13	-0.63±0.06
	14	-0.25±0.08	-0.22±0.06	-0.46±0.05	-0.92±0.13	-0.83±0.08
Zn(Amm)	1	-0.22±0.02	-0.24±0.09	-0.38±0.09	-1.19±0.29	-1.37±0.22
	7	-0.52±0.06	-0.50±0.06	-0.80±0.13	-2.57±0.21	-2.01±0.15
	14	-0.74±0.06	-0.63±0.04	-1.01±0.07	-3.33±0.19	-2.65±0.28
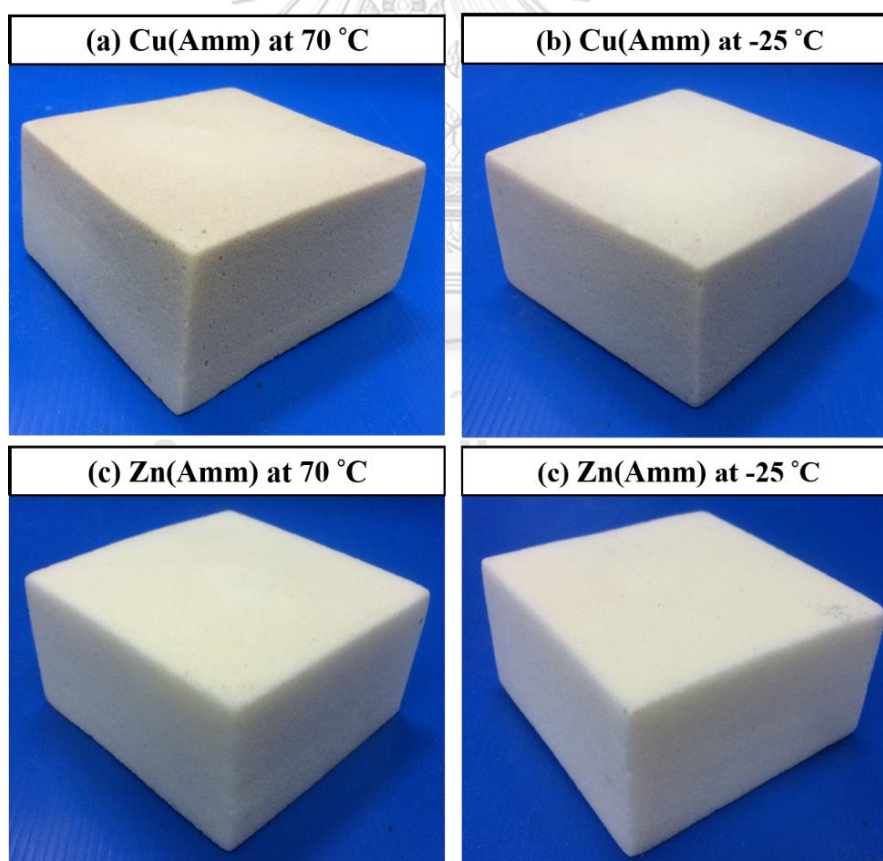
Figure 4.24 Rigid PUR foams after dimensional variation test (14 days).

4.3 Preparation of PIR foam using the mixtures of potassium octoate with metal-ammonia complexes as catalysts

In the third section, the processing of PIR foam has been done. The catalyst systems used for PIR foam processing composed of isocyanurate catalyst, gelling catalyst and blowing catalyst. Isocyanurate catalyst is the main catalyst for increasing the reaction rate of trimerization in order to obtain PIR crosslinks. Whilst, gelling and blowing catalysts are the co-catalysts for accelerating the reaction rate of gelling and blowing reactions, respectively, resulting in PUR crosslinks and entrapped CO_2. In the foam processing, potassium octoate was applied as isocyanurate catalyst, whilst metal-ammonia complexes were applied as gelling and blowing catalysts. Excess amount of isocyanate (isocyanate indices of 160, 200 and 250) was used for PIR foams. Physical properties, PIR/PUR proportion, morphology, compression properties, fire-retarded properties and thermal properties of PIR foam were compared to their relating rigid PUR foams in order to ensure that the properties of PIR foam were improved.

4.3.1 Reaction time and density of PIR foam accelerated by the mixtures of potassium octoate with metal-ammonia complexes

Table 4.7 summarizes the reaction time of PIR foam processed at different isocyanate indices and catalyst systems. The foam appearance is presented in Figures 4.25-4.27. When comparing between PIR foams and their relating rigid PUR foams, it could be observed the different results between PIR foams accelerated by the mixtures of potassium octoate with metal-ammonia complexes and PIR foams accelerated by the mixture of potassium octoate with DMCHA. In the case of PIR foams accelerated by the mixtures of potassium octoate with Cu(Amm) or Zn(Amm), gel time, tack free time and rise time were obviously decreased from those of their relating rigid PUR foams, whilst the change in cream time was negligible. For instance, the gel time, tack free time and rise time of PIR foam processed using the mixture of potassium octoate with Cu(Amm) at isocyanate index of 160 were shorter than those of rigid PUR foam processed using Cu(Amm) by 45, 130 and 120 s, respectively. Higher proportion of PIR crosslink caused the decrease in gel time and tack free time (52). Incorporation of

potassium octoate catalyst increased PIR crosslinks which could lead the viscosity of the reaction mixture of PIR foam to increase and to become gel faster than that of their relating rigid PUR foams. The decrease in rise time of PIR foam might be affected by faster tack free time. When the crosslink reactions seemed to complete faster, the foams were more difficult to expand their volume during rising process resulting in faster stop in rising.

Considering the different result of PIR foams accelerated by the mixture of potassium octoate with DMCHA, the gel time of these PIR foams was extended in comparison to their relating rigid PUR foam accelerated by only DMCHA. Moreover, at the same isocyanate index, the mixture of potassium octoate with DMCHA seemed to have less catalytic activity than the mixtures of potassium octoate with metal-ammonia complexes resulting in longer reaction time. These results pointed out that the catalytic activity of DMCHA for gelling reaction might be partially lost when used with potassium octoate catalyst. The drop of DMCHA's catalytic activity for gelling reaction was also reported in another work (109). Furthermore, the solubility of DMCHA with potassium octoate solution in diethylene glycol and H_2O (blowing agent of PIR foam) is limited (13). This might cause the insufficient compatibility between catalyst components as well as the reactant of PIR foam and could influence the DMCHA's catalytic activity. For Cu(Amm) and Zn(Amm) solutions, they could be completely soluble with potassium octoate solution in diethylene glycol and H_2O owing to the intermolecular interaction (H-bond) of diethylene glycol, NH_3 and H_2O. Therefore, the homogeneously catalytic systems for PIR foams could be obtained.

The effect of isocyanate index on reaction time and foam density was examined (Table 4.7). It was found that tack free time and rise time of all PIR foams were longer with increasing isocyanate indices from 160 to 250. After the gel time, the polymerization rate of PIR foam was slightly retarded owing to the denser polymer crosslinks (38). Thus, the period to complete all reactions was prolonged with increasing isocyanate index. The retardation in gelling and blowing reactions affected by higher isocyanate index was reported in other studies (38, 110, 111). Density of PIR foams increased with increasing isocyanate index regardless of catalyst systems because more density of PIR crosslinks was obtained with increasing isocyanate index (112).

Table 4.7 Reaction time and density of PIR foam obtained from various catalysts in comparison to their relating rigid PUR foams.

Catalysts	isocyanate indices	Reaction time (s)				Density (kg/m^3)
		Cream time	Gel time	Tack free time	Rise time	
Rigid PUR foams						
DMCHA	100	21±1	35±2	196±3	125±3	34.7±0.7
Cu(Amm)	100	26±1	76±2	176±6	187±4	38.1±0.7
Zn(Amm)	100	25±1	98±1	202±2	232±3	33.4±0.9
PIR foams						
DMCHA & potassium octoate	160	24±1	40±1	85±2	122±2	38.5±0.9
	200	25±1	46±1	97±2	141±2	42.6±0.6
	250	28±1	53±1	122±2	181±2	51.6±0.7
Cu(Amm) & potassium octoate	160	24±1	31±1	46±1	67±2	38.7±0.8
	200	25±0	36±1	49±1	70±1	43.6±0.9
	250	28±1	43±1	70±2	98±2	52.7±1.3
Zn(Amm) & potassium octoate	160	23±1	33±1	62±2	89±2	37.5±0.7
	200	24±0	37±1	68±1	97±2	39.9±0.9
	250	27±0	46±0	92±1	125±2	50.4±0.8
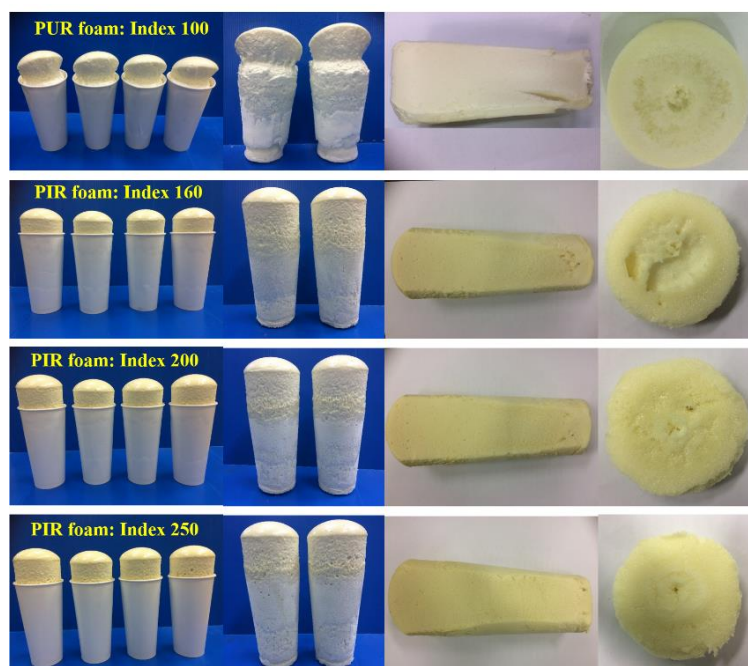
Figure 4.25 Appearance of PIR foams accelerated by the mixture of potassium octoate with DMCHA in comparison to their relating rigid PUR foams.
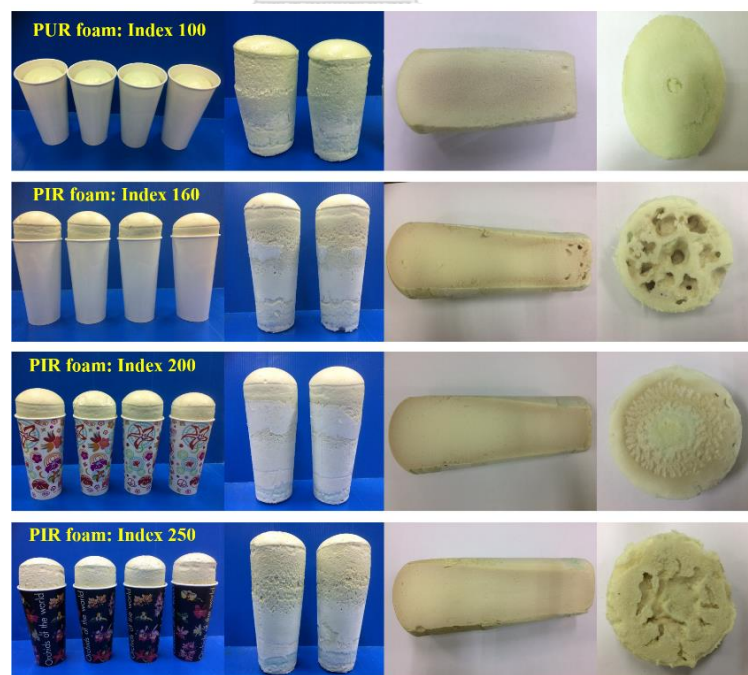
Figure 4.26 Appearance of PIR foams accelerated by the mixture of potassium octoate with Cu(Amm) in comparison to their relating rigid PUR foams.
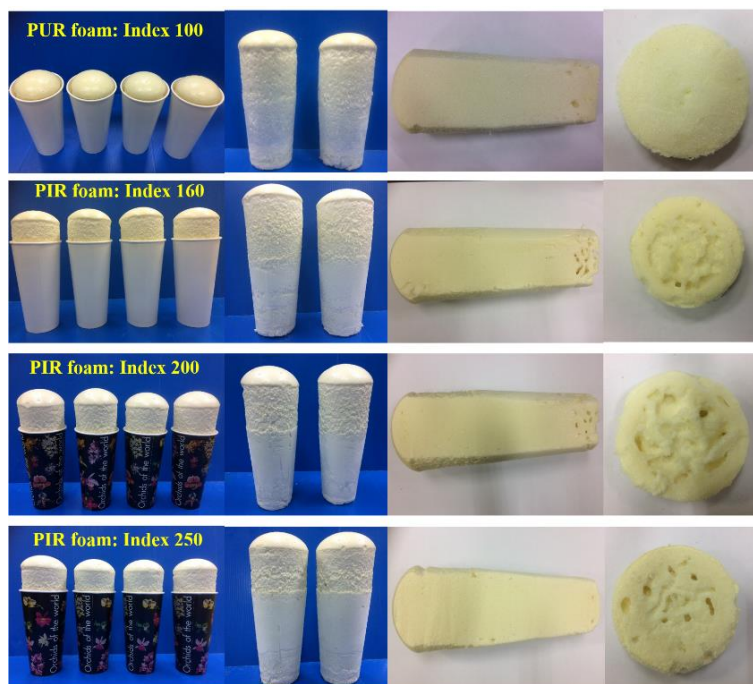
Figure 4.27 Appearance of PIR foams accelerated by the mixture of potassium octoate with Zn(Amm) in comparison to their relating rigid PUR foams.

4.3.2 Calculation of PIR/PUR proportion and % isocyanate conversion of PIR foams accelerated by the mixtures of potassium octoate with metal-ammonia complexes

Effect of different catalyst systems and isocyanate indices on PIR/PUR proportions and % isocyanate conversion was studies as shown in Figure 4.28 and Table 4.8. PIR foams showed the increase in PIR/PUR proportions in comparison to those of their relating rigid PUR foams for all catalyst systems. However, at isocyanate index of 160, PIR/PUR proportions of PIR foam were not significantly different and had similar values to those of their relating rigid PUR foams. The effect of different catalyst systems on PIR/PUR proportions of PIR foam could be compared at higher isocyanate indices of 200 and 250. For example, PIR foams processed at isocyanate index of 250 and accelerated by the mixtures of potassium octoate with Cu(Amm), DMCHA or Zn(Amm) had PIR/PUR proportions of 3.31, 3.19 and 2.58, respectively. This result revealed that the mixtures of potassium octoate with

Cu(Amm) or DMCHA gave better catalytic activity toward PIR/PUR proportions than the mixture of potassium octoate with Zn(Amm).

The change in isocyanate indices was another factor that strongly influenced PIR/PUR proportions (35). It was found that the PIR/PUR proportions of PIR foam increased with increasing isocyanate indices from 160 to 250 for all catalyst systems. Nonetheless, the % NCO conversion of PIR foam slightly decreased when increasing NCO indices. The % NCO conversion of PIR foam at maximum isocyanate index of 250 decreased approximately 1.8 – 5.6 % as compared to those of their relating rigid PUR foams. The PIR foam accelerated by the mixture of potassium octoate with DMCHA seemed to have the lowest % isocyanate conversion, which could be attributed to the loss of reactivity of DMCHA in gelling reaction and blowing reaction as previously discussed.
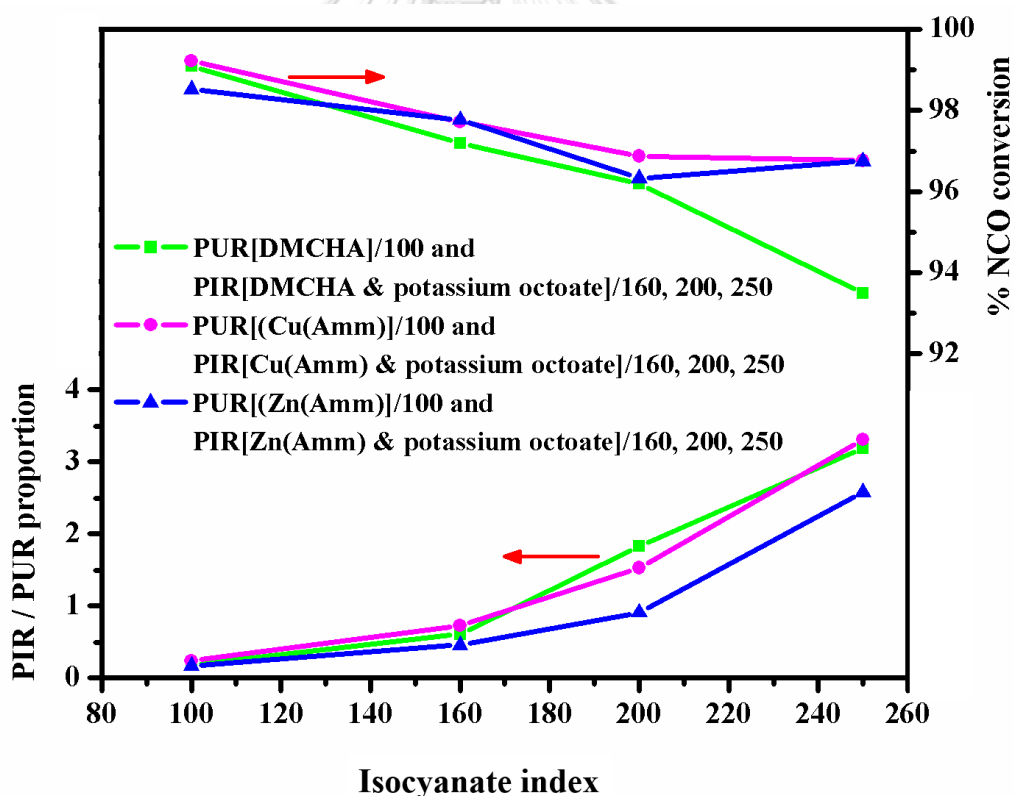
Figure 4.28 Trend of PIR/PUR proportions and % isocyanate conversion of PIR foams obtained from various catalysts as compared to their relating rigid PUR foams.

Table 4.8 PIR/PUR proportions and % isocyanate conversion of PIR foam obtained from various catalysts as compared to their relating rigid PUR foams.

Catalysts	Isocyanate indices	PIR/PUR proportions	% isocyanate conversion
Rigid PUR foams			
DMCHA	100	0.18	99.1
Cu(Amm)	100	0.24	99.2
Zn(Amm)	100	0.17	98.5
PIR foams			
DMCHA & potassium octoate	160	0.61	97.2
	200	1.83	96.2
	250	3.19	93.5
Cu(Amm) & potassium octoate	160	0.73	97.7
	200	1.53	96.9
	250	3.31	96.8
Zn(Amm) & potassium octoate	160	0.46	97.8
	200	0.91	96.3
	250	2.58	96.8

4.3.3 Fire-retarded properties of PIR foam accelerated by the mixtures of potassium octoate with metal-ammonia complexes

Fire-retarded behavior of PIR foams was investigated via the results of horizontally-oriented burning test and % LOI as illustrated in Figures 4.30 -4.33. In addition, the appearance of burned PIR foams as compared to burned rigid PUR foams after horizontally-oriented burning test is shown in Figure 4.29. It could be observed from Figure 4.29 that fire-retarded behavior of those foams depends on catalyst systems and isocyanate indices. All rigid PUR foams, especially the foam processed from Zn(Amm), lacked fire-retarded properties and suddenly caught fire with severe burning due to their highly combustible characteristics (5, 113). The flame propagation occurred very fast and burned out 15.0 cm throughout of sample

length for all catalysts (Figure 4.29). The total time for burning out of rigid PUR foams accelerated by DMCHA, Cu(Amm) and Zn(Amm) was 57.0, 63.0 and 46.5 s, respectively (Figure 4.32). After burned out, the surface of foams peeled off and a lot of voids were observed.
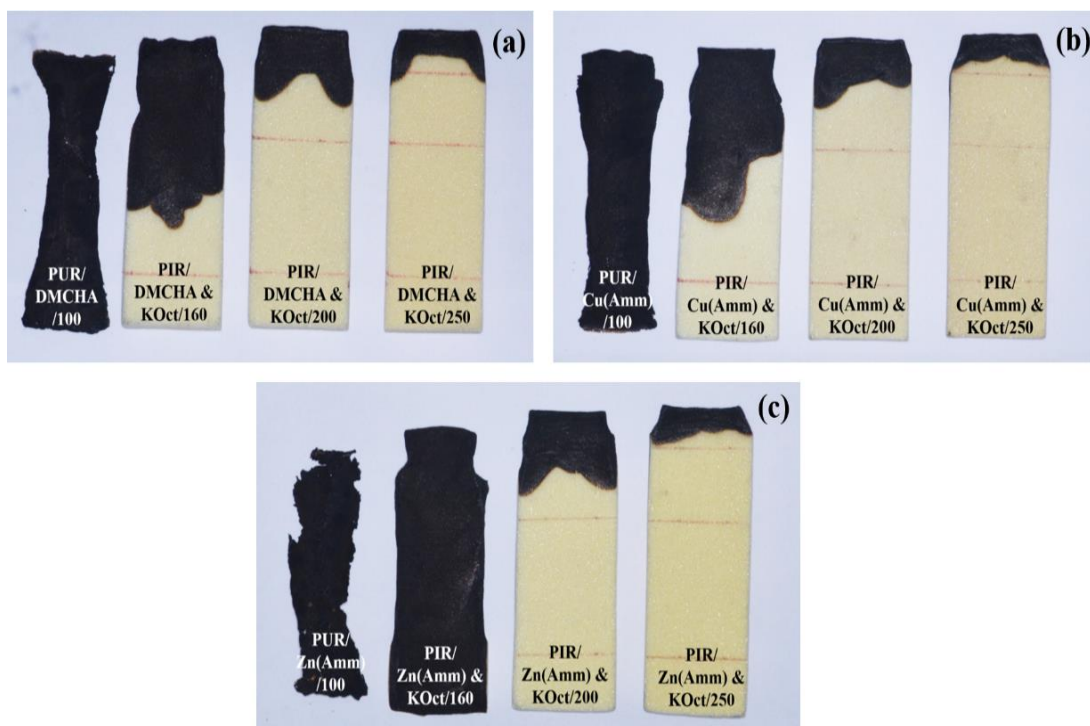
Figure 4.29 Appearance of burned foams after burning test; (a), (b) and (c) are PIR foams at different isocyanate indices accelerated by the mixtures of potassium octoate (KOct) with DMCHA, Cu(Amm) or Zn(Amm), respectively, in comparison to their relating rigid PUR foams.

For PIR foams, their damage areas were reduced. However, the foams processed using isocyanate index of 160 still showed combustible characteristic due to the low PIR/PUR proportions resulting in long burning lengths (Figure 4.30) and afterglow time (Figure 4.32). The effect of different catalyst systems on fire-retarded properties could be found in the case of foams processed at isocyanate indices of 100 and 160. For both indices, the order of fire-retarded properties of the foams is Cu(Amm)-based foams $\cong$ DMCHA-based foams > Zn(Amm)-based foams. The PIR

and the rigid PUR foams processed using Zn(Amm) as gelling and blowing catalysts had the worst fire-retarded properties because of the least PIR/PUR proportions and the lowest density. In general, the fire-retarded properties of foam relate to not only the PIR/PUR proportion but also the foam density. The foam having higher density is more difficult to ignite, can retard the flame propagation and therefore shows better fire-retarded behaviors (113). This result indicated that the catalytic activity of metal-ammonia complexes could influence the fire-retarded properties of the foam by giving different foam density.

The improvement in fire-retarded properties of PIR foam processed at isocyanate indices of 200 and 250 could be obviously observed for all catalyst systems. In comparison to their relating rigid PUR foams, all PIR foams showed large reduction in burning length (Figure 4.30), burning rate (Figure 4.31) as well as afterglow time (Figure 4.32) and could extinguish by themselves. For example, burning length, burning rate and afterglow time of PIR foam processed by the mixture of potassium octoate with Zn(Amm) at isocyanate index of 200 decreased from those of rigid PUR foam processed by Zn(Amm) at isocyanate index of 100 by 10.5 cm, 17.1 cm/min and 23.8 s, respectively. In case of Cu(Amm)-based foams, burning length, burning rate and afterglow time of PIR foam processed by the mixture of potassium octoate with Cu(Amm) at isocyanate index of 200 decreased from those of rigid PUR foam processed by Cu(Amm) at isocyanate index of 100 by 11.2 cm, 10.3 cm/min and 44 s, respectively. For PIR foams processed at isocyanate index of 250, their fire-retarded properties were higher than those of PIR foams processed at isocyanate index of 200 for all catalyst systems. All PIR foams processed at isocyanate index of 250 could almost suddenly extinguish when the fire source was taken away. Therefore, their afterglow time was 0.0 s and their burning rate was unable to calculate. The enhancement of fire-retarded properties of PIR foam over rigid PUR foam is owing to the increase of PIR crosslinks that can act as intrinsically fire-retarded structures (5).
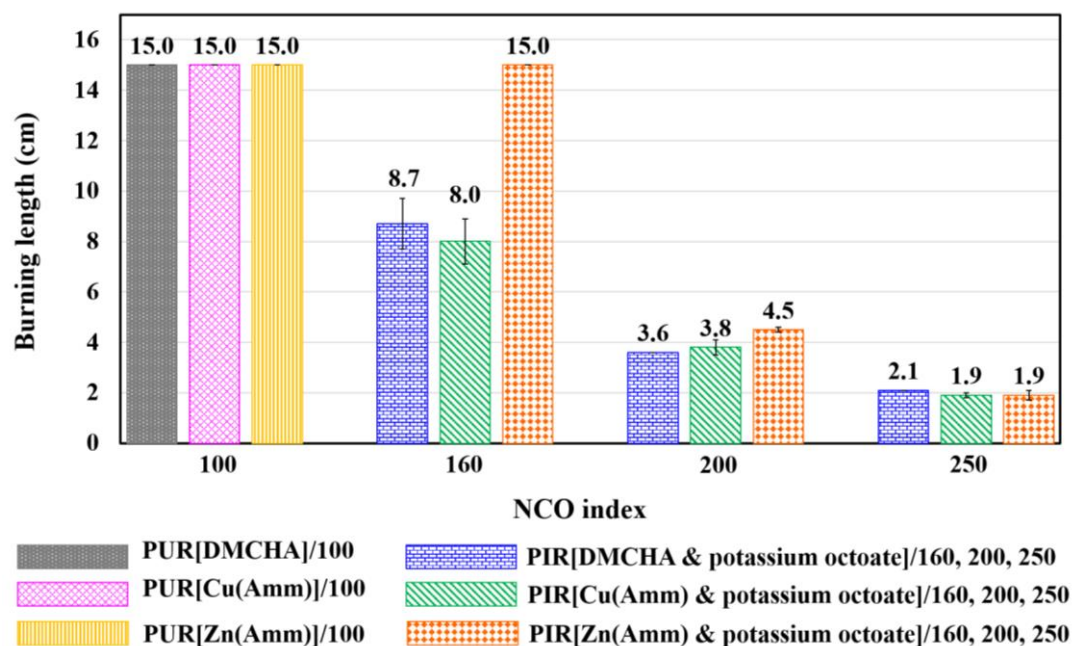
Figure 4.30 Burning length of the foams processed at various isocyanate indices and catalyst systems.
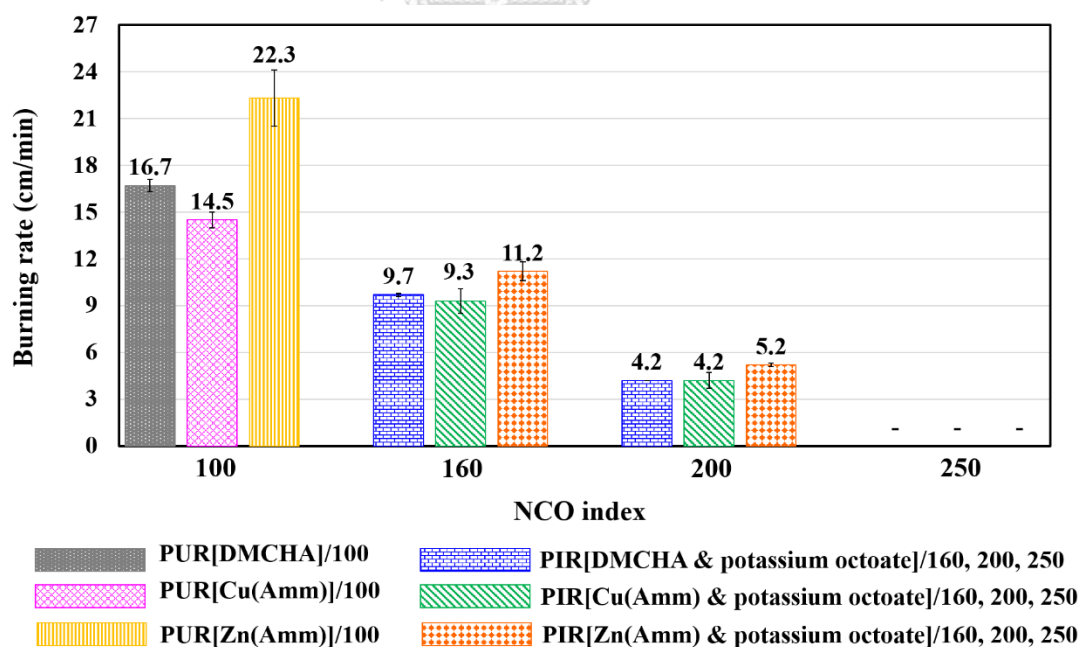
Figure 4.31 Burning rate of the foams processed at various isocyanate indices and catalyst systems.
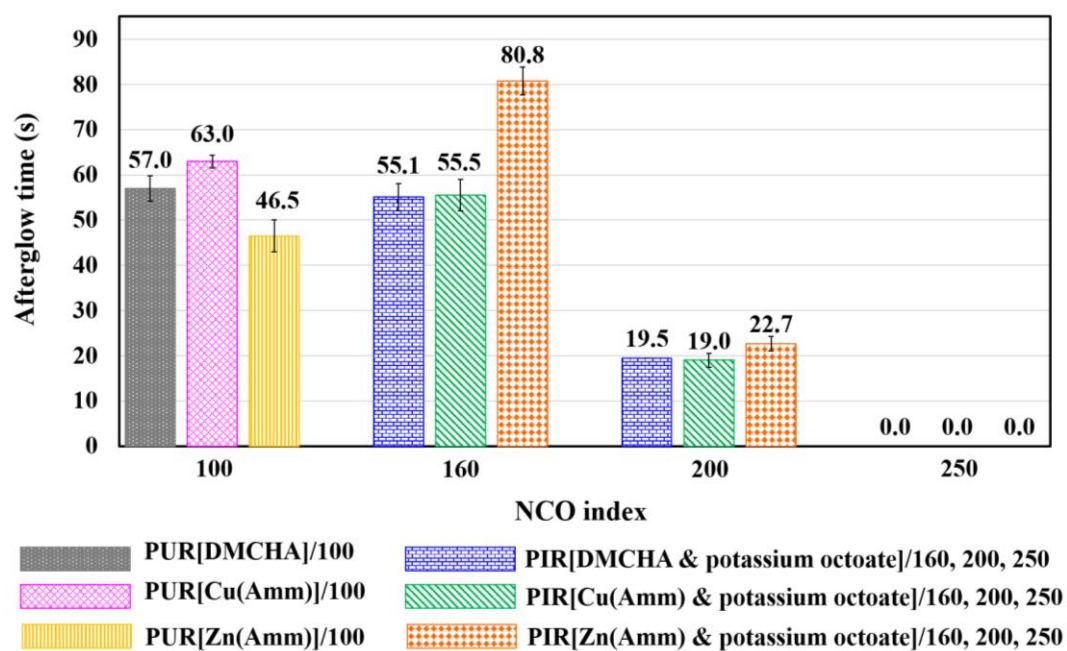
Figure 4.32 Afterglow time of the foams processed at various isocyanate indices and catalyst systems.

Table 4.9 Burning behavior of PIR and rigid PUR foams.

Catalysts	Isocyanate indices	Self-extinguishment	Burning behavior	Material rating
Rigid PUR foams				
DMCHA	100	Burn out	Fast and severely burn	No rating
Cu(Amm)	100	Burn out	Fast and severely burn	No rating
Zn(Amm)	100	Burn out	Fast and severely burn	No rating
PIR foams				
DMCHA &	160	Yes	Fast burn	HBF
potassium octoate	200	Yes	Slow burn	HF1
	250	Yes	Slow burn	HF1
Cu(Amm) &	160	Yes	Fast burn	HBF
potassium octoate	200	Yes	Slow burn	HF1
	250	Yes	Slow burn	HF1
Zn(Amm) &	160	Burn out	Fast burn	No rating
potassium octoate	200	Yes	Slow burn	HF1
	250	Yes	Slow burn	HF1

PIR and rigid PUR foams were categorized by their fire-retarded properties following ASTM D4986 as summarized in Table 4.9. It was found that all rigid PUR foams showed no rating because of the worst fire-retarded results. Whereas PIR foams accelerated by the mixtures of potassium octoate with Cu(Amm), Zn(Amm) or DMCHA at isocyanate indices 200 and 250 could achieve HF1 rating, which is the best rating of fire-retarded cellular polymers as they had burning length and afterglow time less than 6.0 cm and 30 s, respectively.

%LOI (Figure 4.33) of PIR and their relating rigid PUR foams was also investigated. PIR foams showed greater %LOI than their relating rigid PUR foams. The % LOI of PIR foams increased with increasing isocyanate indices from 160 to 250. The maximum %LOI values of PIR foam accelerated by the mixtures of potassium octoate with Cu(Amm), Zn(Amm) or DMCHA at isocyanate index of 250 were as high as 21.4%, 21.4% and 21.5%, respectively. The enhancement in %LOI of PIR foams is consistent with the results of horizontally-oriented burning test. This can confirm the improvement in fire-retarded properties of PIR foams in comparison to rigid PUR foams. The PIR crosslinks along with carbonaceous char occurred during foam burning of PIR foams might cause the improvement of these fire-retarded properties (1).
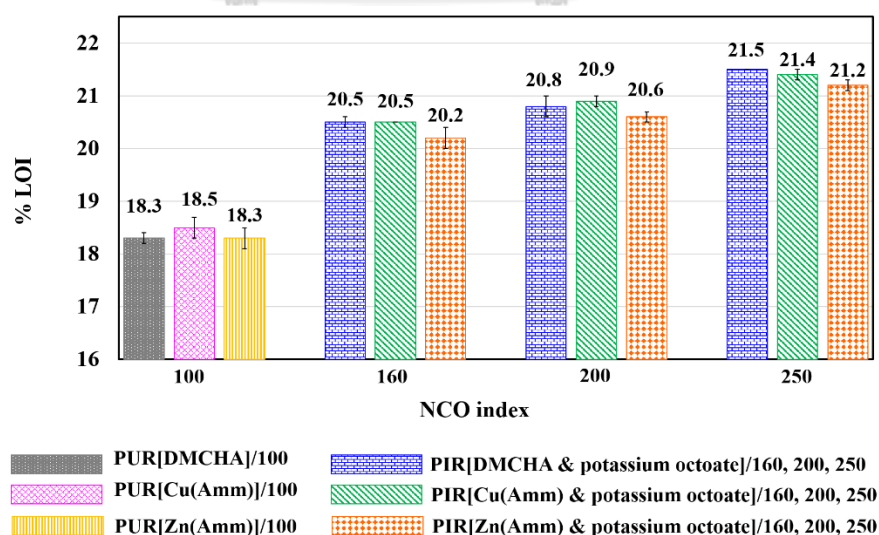
Figure 4.33 % LOI of the foams processed at various isocyanate indices and catalyst systems.

In order to confirm the above results, SEM micrographs of the carbonaceous char accumulated on burned areas of PIR foam at different isocyanate indices were investigated and compared to those of rigid PUR foams as presented in Figure 4.34. It was found that the foams processed at the same isocyanate index show similar morphology of the burned areas and the carbonaceous char, even though they were accelerated by different catalyst systems. However, the dissimilar morphology of the burned areas and the carbonaceous char among the foams processed at different isocyanate indices could be observed. More carbonaceous char tended to accumulate on burned areas when increasing isocyanate indices. For rigid PUR foams (isocyanate index of 100) and PIR foams (isocyanate index of 160) in Figures 4.34(a) - 4.34(f), less carbonaceous char content was obtained and their burned areas appeared to have a lot of voids due to the severe release of combustible gases through the char layers (52). In contrast, PIR foams (isocyanate indices of 200 and 250) appeared to have the intact char, which could cover throughout the foam surface. This intact char might be originated from the crosslinked isocyanurate, which is easy to yield the char during combustion (5, 52), and could improve the fire-retarded properties of PIR foam because it could restrain the release of combustible gases to fire, prevent the oxygen from attaching polymer to participate the combustion and reduce the heat transfer from fire source to polymer (1, 5, 52, 114).
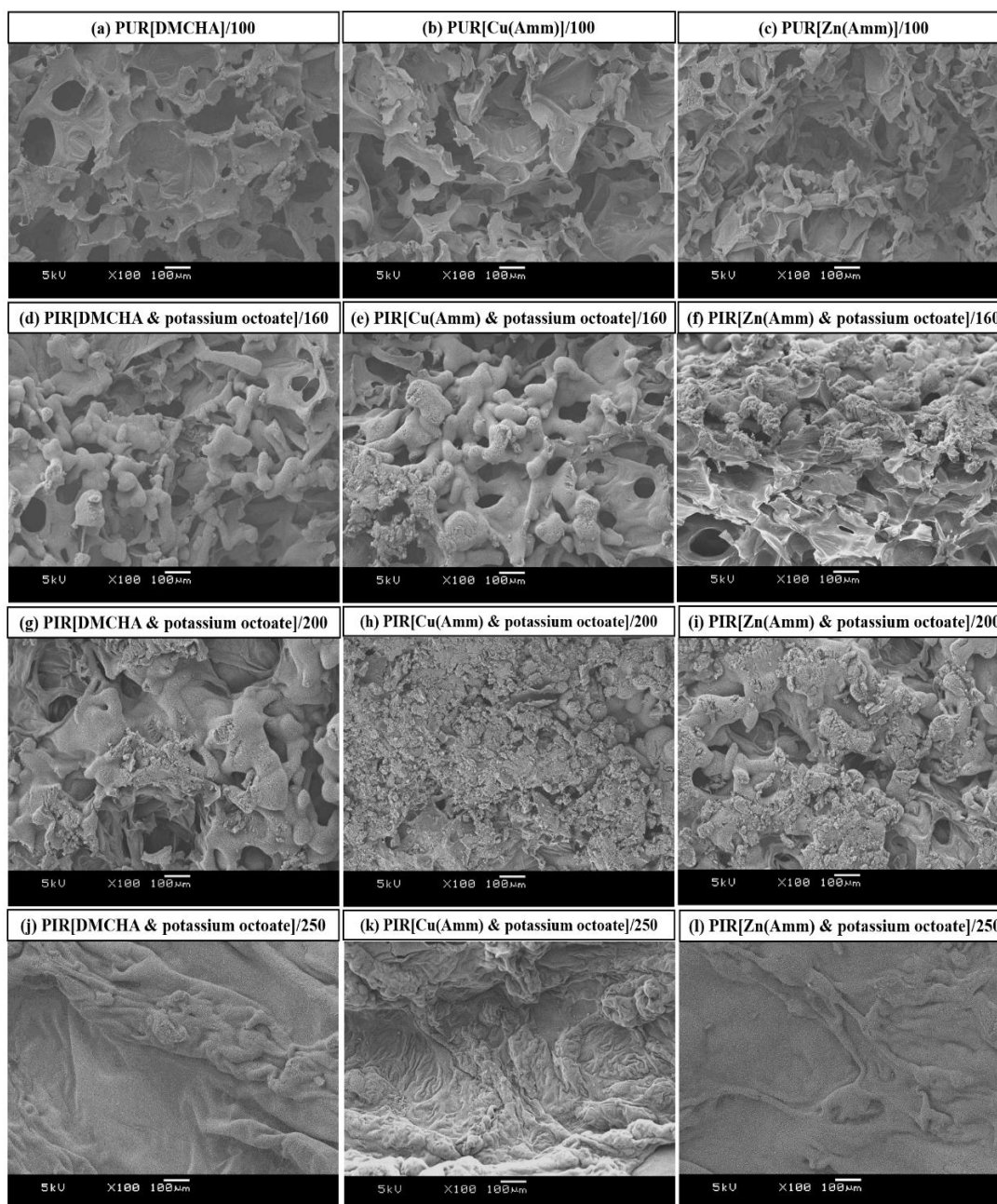
Figure 4.34 Morphology of char covering burned areas of the foam.

4.3.4 Morphology of PIR foams accelerated by the mixtures of potassium octoate with metal-ammonia complexes

Effect of various catalyst systems, isocyanate indices and foam-rising direction on morphology of PIR foams was investigated. The SEM micrographs of

cell morphology of PIR foams accelerated by the mixtures of potassium octate with DMCHA, Cu(Amm) or Zn(Amm) are presented in Figures 4.36-4.38, respectively. Average cell size of all foams in the same and the opposite to foam-rising direction is summarized in Figure 4.35. The results showed that the cell structures of PIR foam still appeared extended and rounded shape in the same (side view) and the opposite (top view) to foam-rising direction, respectively.

Considering trend of average cell size, all PIR foams at isocyanate index of 160 had the significant decrease in average cell size in the same and the opposite to foam-rising direction when compared to their relating rigid PUR foams processed at isocyanate index of 100. It is postulated that the average cell size can depend on several factors, such as reaction time (gel time), density of crosslinks and viscosity of reactants. Faster gel time and high density of crosslinks lead to the foams with smaller cell size, whereas low viscosity of reactants leads to the foams with larger cell size (110, 115-117). The reduction of average cell size of PIR foams in comparison to that of rigid PUR foams was due to the faster gel time along with the increase of PIR crosslinks, which could restrain CO_2 growth to coalesce with each other and reduce the ability of cell walls to expand themselves (110, 115, 117).

In the case of average cell size of PIR foams accelerated by potassium octoate and DMCHA at different isocyanate indices, the average cell size of the foams continually increased with increasing isocyanate indices from 160 to 250 (Figures 4.35 and 4.36). This result revealed that effect of longer gel time resulted from this catalyst system and the viscosity decrease of reaction mixture when increasing isocyanate indices could overwhelm the effect of PIR crosslink density.

However, the contrast results were observed for PIR foams accelerated by the mixtures of potassium octoate with Cu(Amm) (Figures 4.35 and 4.37) or Zn(Amm) (Figures 4.35 and 4.38). The average cell size of these PIR foams decreased until the isocyanate index was risen to 200, but then slightly increased at the higher isocyanate index of 250. Unlike the industrial catalyst system (the mixture of potassium octoate with DMCHA), the developed catalyst systems of potassium octoate with Cu(Amm) or Zn(Amm) did not seem to lose their reactivity in PIR foam system. The gel time given by both alternative catalysts was faster than that obtained from the industrial catalyst system, and therefore they could hold the decrease of foam

cell size until isocyanate index was risen to 200. However, when the viscosity of reaction mixture was further reduced and polymerization rate (reaction time) was slightly delayed by adding larger amount of isocyanate reactant, the foam cells could expand their volume and coalesce into the larger cells. These results pointed out the complex interaction among those parameters, namely reaction time, density of PIR crosslinks and viscosity of reactants, in determination of the cell size of the foams.
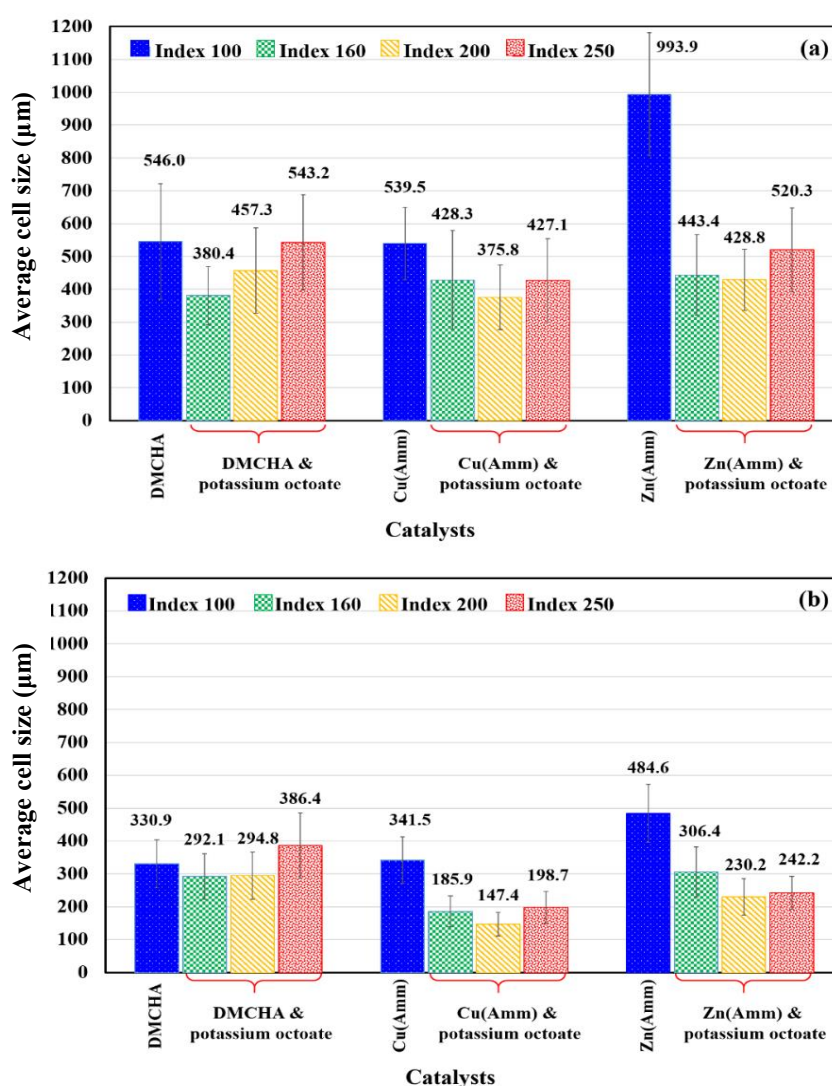
Figure 4.35 Average cell size in (a) the same (side view) and (b) the opposite (top view) to foam-rising direction.
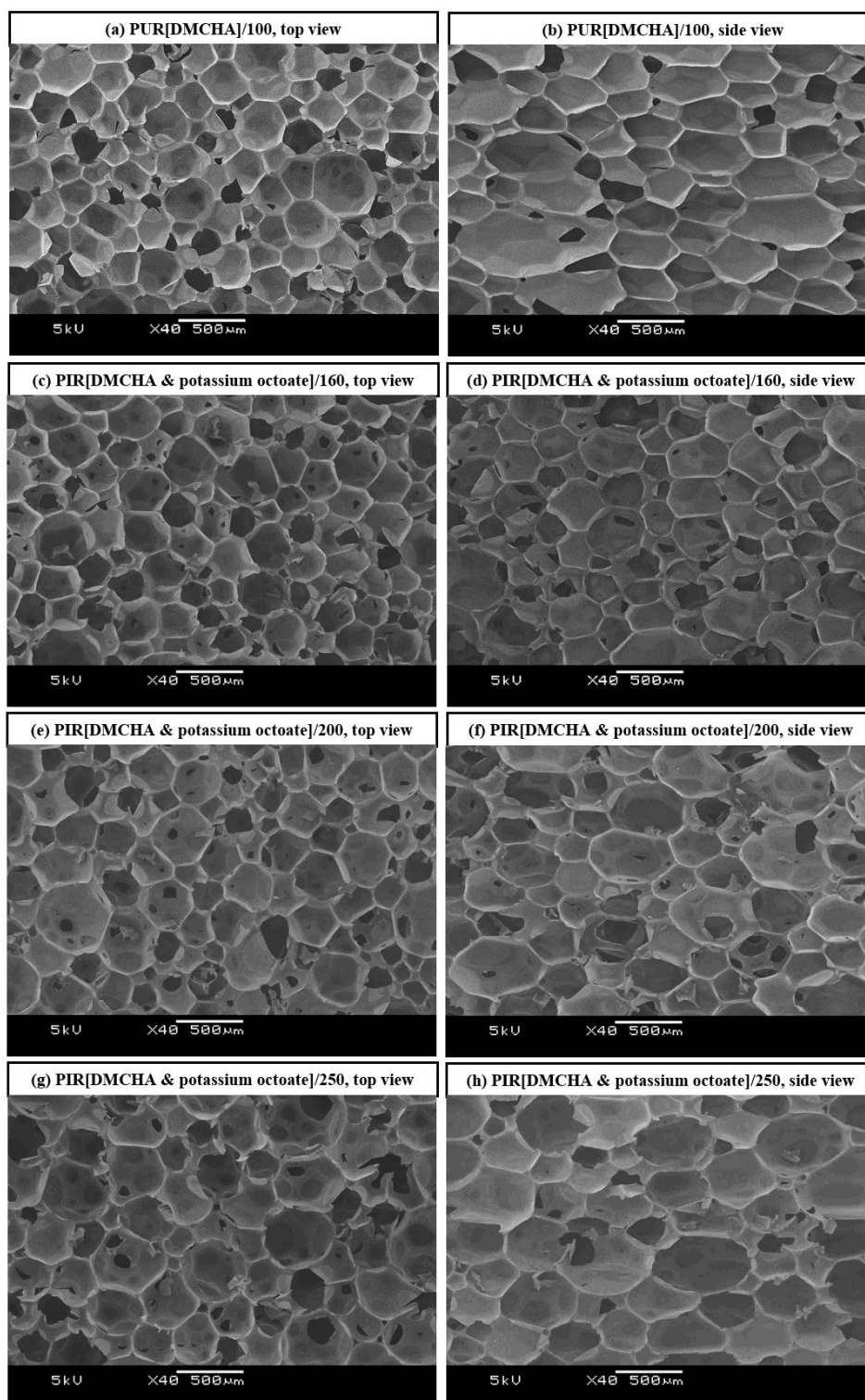
Figure 4.36 SEM micrographs of PIR foam accelerated by potassium octoate and DMCHA (indices 160, 200 and 250) and rigid PUR foam accelerated by DMCHA (index 100) and at different views.

(a) PUR[Cu(Amm)]/100, top view

(b) PUR[Cu(Amm)]/100, side view

(c) PIR[Cu(Amm) & potassium octoate]/160, top view

(d) PIR[Cu(Amm) & potassium octoate]/160, side view

(e) PIR[Cu(Amm) & potassium octoate]/200, top view

(f) PIR[Cu(Amm) & potassium octoate]/200, side view

(g) PIR[Cu(Amm) & potassium octoate]/250, top view

(h) PIR[Cu(Amm) & potassium octoate]/250, side view
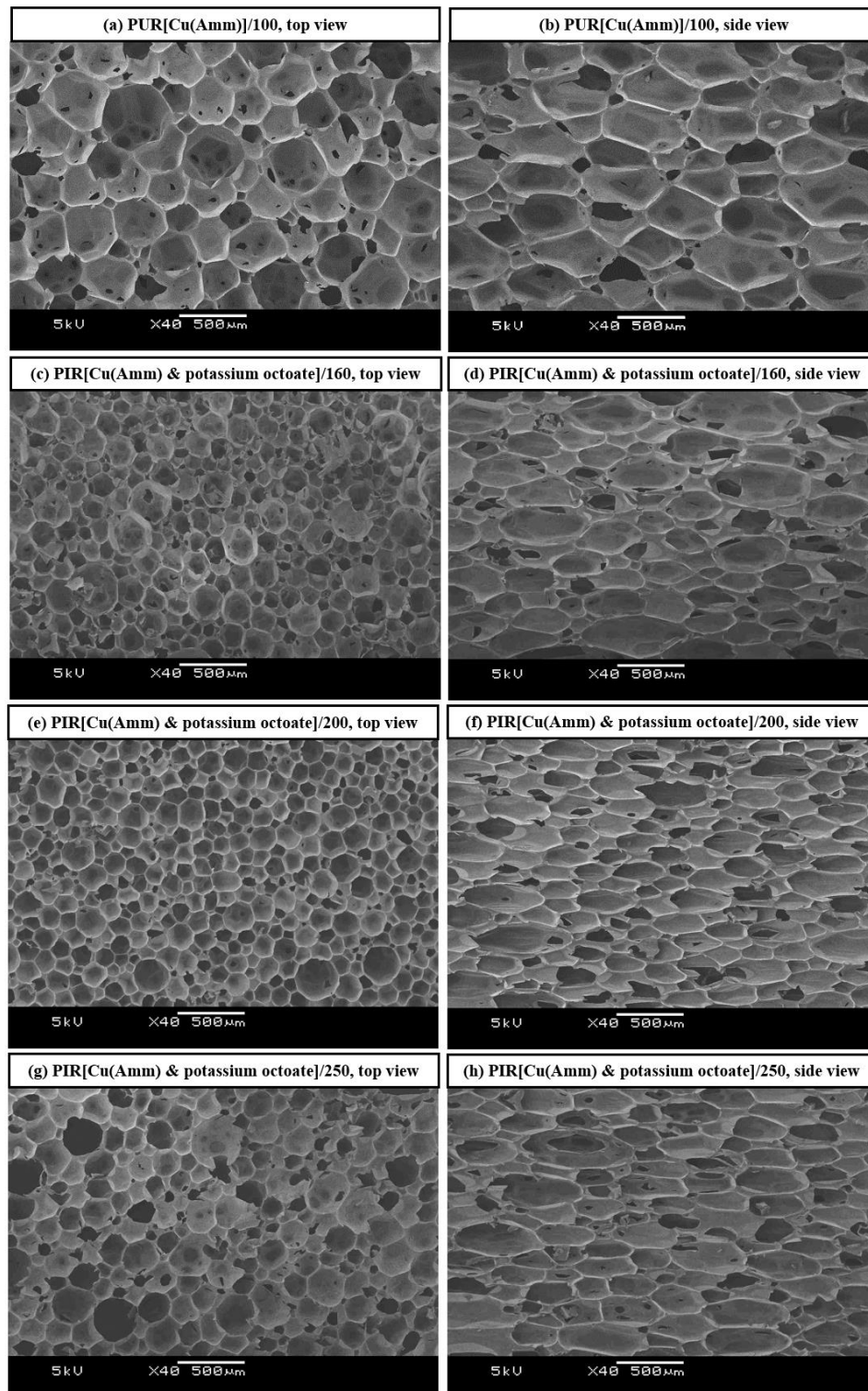
Figure 4.37 SEM micrographs of PIR foam accelerated by potassium octoate and Cu(Amm) (indices 160, 200 and 250) and rigid PUR foam accelerated by Cu(Amm) (index100) and at different views.
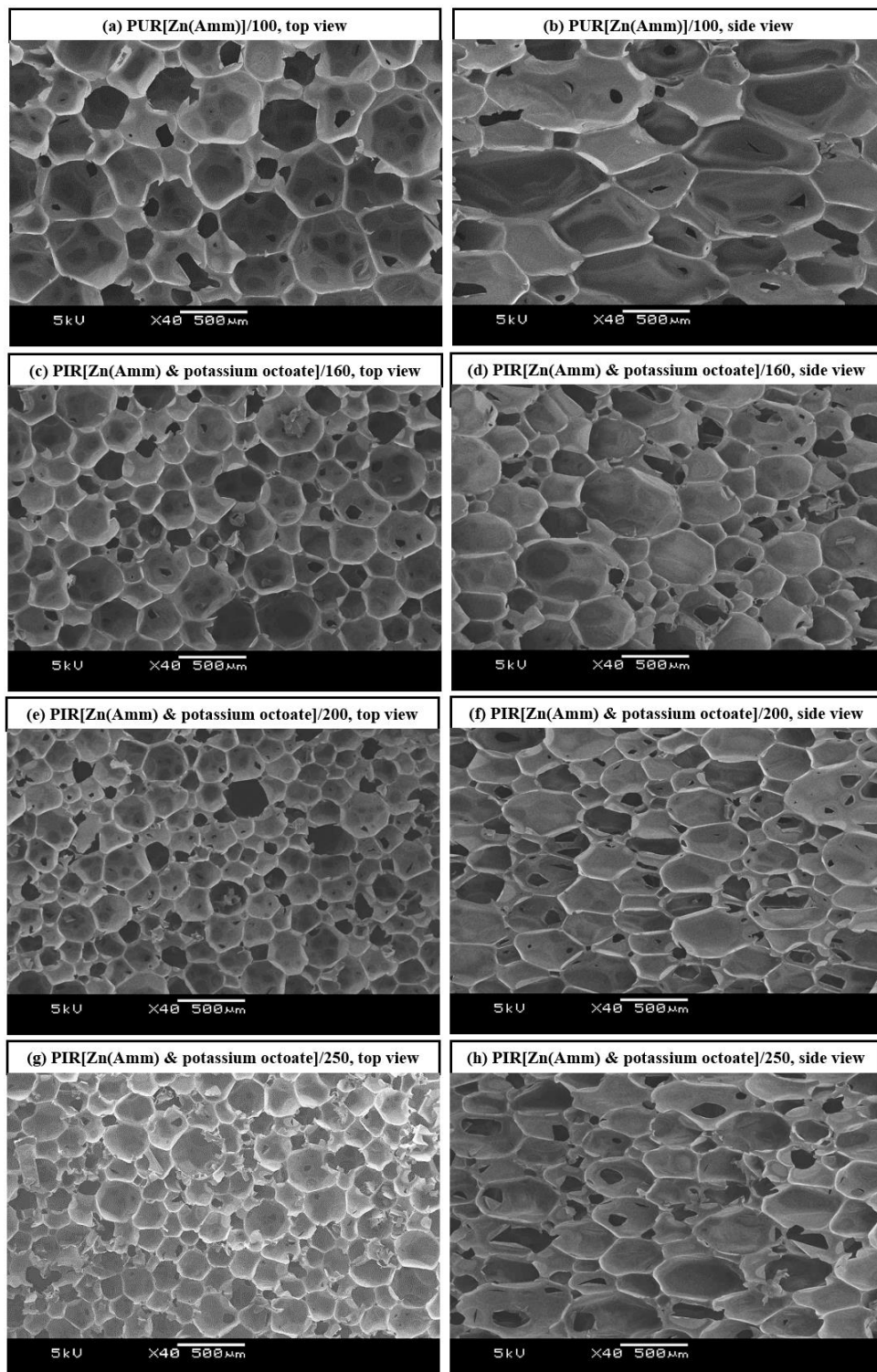
Figure 4.38 SEM micrographs of PIR foam accelerated by potassium octoate and Zn(Amm) (indices 160, 200 and 250) and rigid PUR foam accelerated by Zn(Amm) (index100) and at different views.

4.3.5 Compression properties of PIR foam accelerated by the mixtures of potassium octoate with metal-ammonia complexes

In order to investigate whether compression properties of PIR foams are improved in comparison to their relating rigid PUR foams, their compression stress-strain graphs in the same and the opposite to foam-rising direction were studied as shown in Figure 4.39. Their compression strength, which was recorded at 10% of strain, is reported as the function of foam density and catalyst systems in Figure 4.40. In this section, PIR foams processed at isocyanate index of 200 are chosen to study since their apparent density was suitable for application, which was between 30 to 50 kg/m^3 (114). As expected, the compression strength of PIR foam in the same to foam-rising direction (Figures 4.39a and 4.40a) was higher than that in the opposite to foam-rising direction (Figures 4.39b and 4.40b) due to the higher degree of cell orientation in the same to foam-rising direction (99). When compared to their relating rigid PUR foams, PIR foams gave superior compression strength in the same and the opposite to foam-rising direction. This could be attributed to the higher foam density and the increase of PIR crosslink density, which might cause PIR foams to become denser polymer network and could resist with the compression force better than their relating rigid PUR foams (38). This result pointed out that PIR foams were stronger than rigid PUR foams.

Considering the compression properties among PIR foams accelerated by different catalyst systems, It was observed that PIR foams processed from the mixture of potassium octoate with Cu(Amm) or Zn(Amm) were tough and did not rupture when compressed resulting in hard and tough stress-strain graphs (Figures 4.39a). The compression strength in the same to foam-rising direction of PIR foams processed from the mixtures of potassium octoate with Cu(Amm) or Zn(Amm) was 228.0 and 218.5 kPa, respectively (Figures 4.40a). These values are higher than the recommended value at 100 kPa (42). However, the PIR foam accelerated by the mixture of potassium octoate with DMCHA had the lowest compression strength in the same to foam-rising direction of 193.9 kPa (Figures 4.40a). Moreover, this foam ruptured at ≈ 7.0 % of strain during compression test and showed brittle stress-strain

graphs (Figures 4.39a). This result indicated undesirable mechanical properties of PIR foam obtained from this catalyst system.
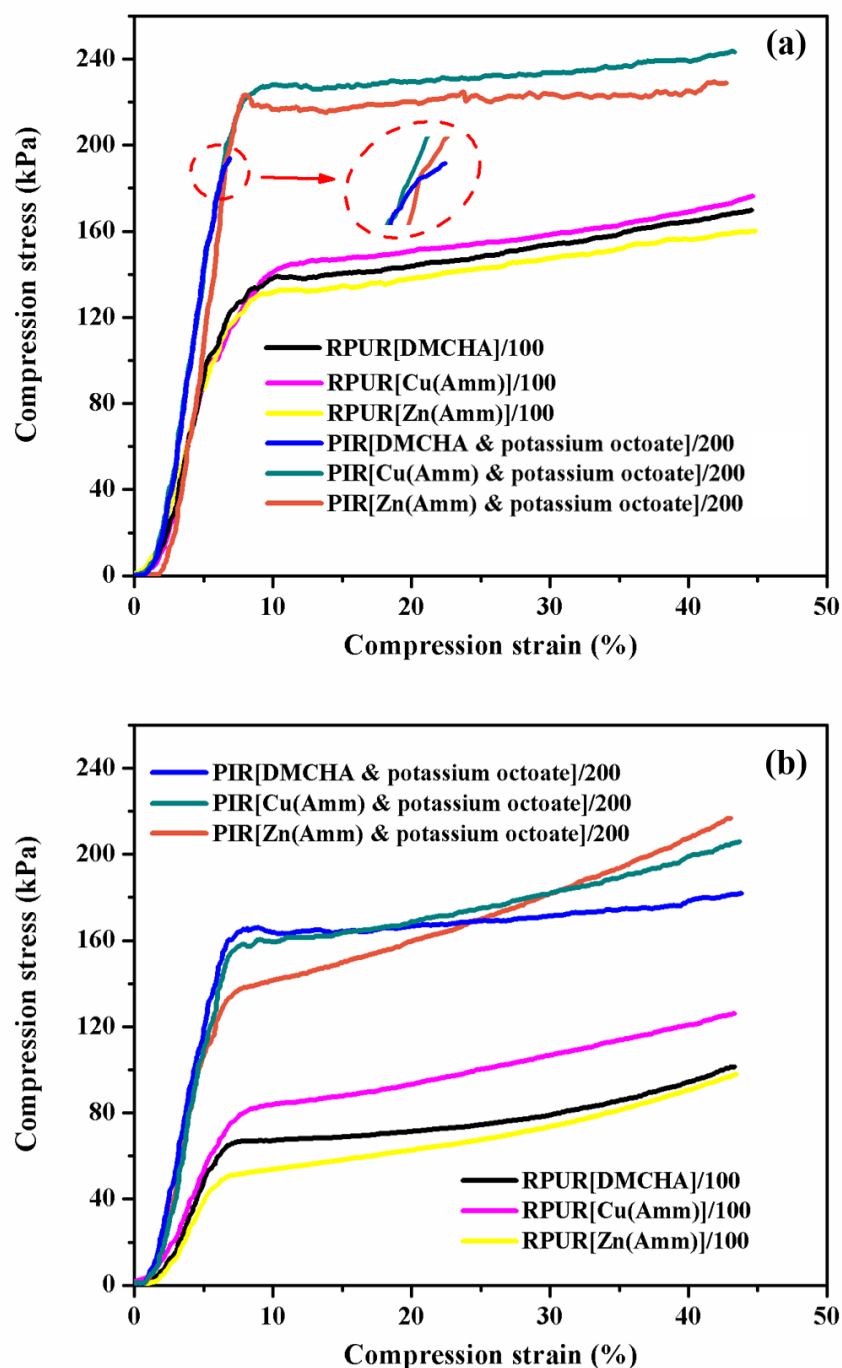
Figure 4.39 Stress-strain graphs of foam obtained using different catalyst systems in (a) the same and (b) the opposite to foam-rising direction.
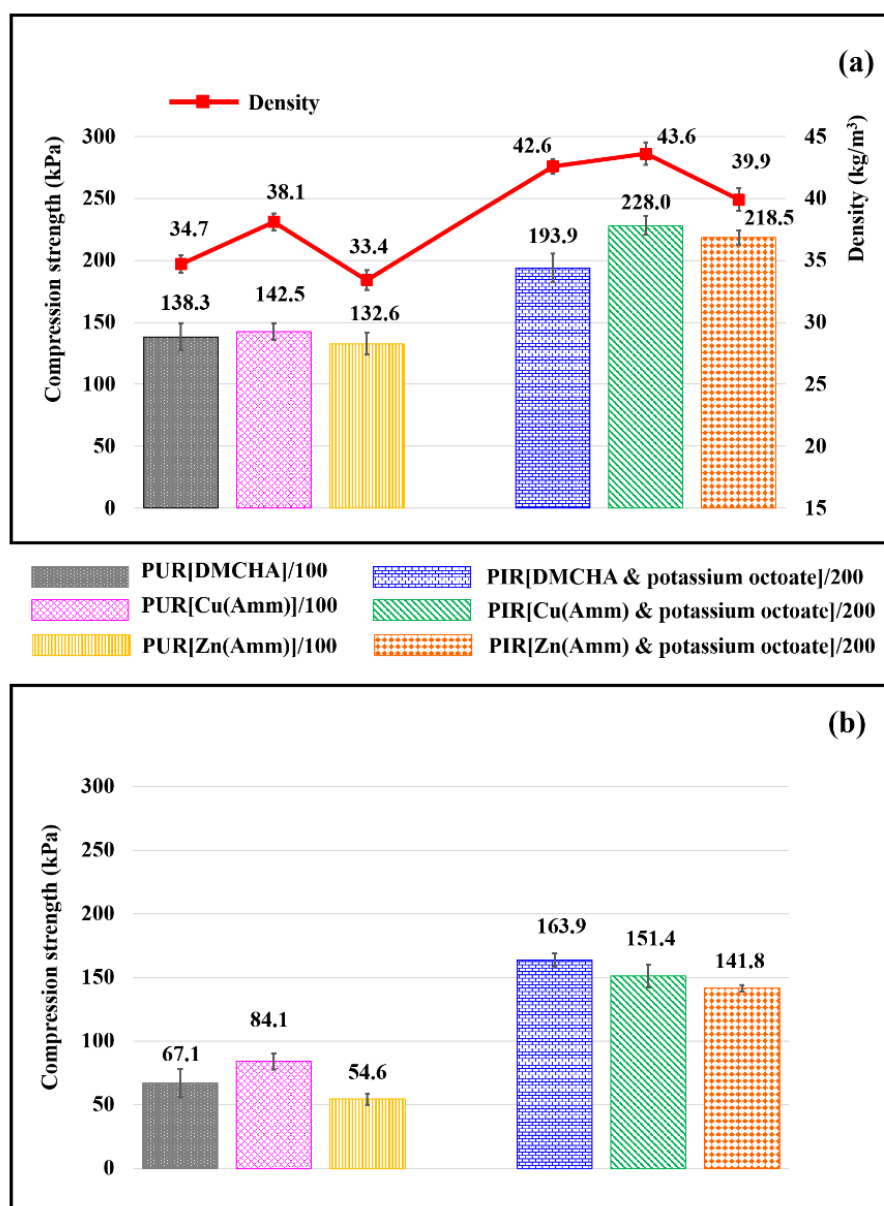
Figure 4.40 Compression strength of foams obtained using different catalyst systems in (a) the same and (b) the opposite to foam-rising direction.

4.3.6 Thermal properties of PIR foam accelerated by the mixtures of potassium octoate with metal-ammonia complexes

As the PIR foams processed from the mixtures of potassium octoate with metal-ammonia complexes at isocyanate index of 200 showed proper density, mechanical properties and fire-retarded properties, the thermal stability of these PIR

foams was further studied by TGA and compared the results to those of their relating rigid PUR foams in order to understand the improvement of thermal stability related with PIR structures. TG and DTG curves of PIR foam are presented in Figures 4.41a and 4.41b, respectively, whose thermal degradation data are summarized in Table 4.10. The results showed that two steps of thermal degradation were observed for both PIR and rigid PUR foams. The first degradation step occurred in the range of 250-400 °C that corresponds to the thermal degradation of urethane segments and polyol chains. The second thermal degradation step occurred in the range of 450-600 °C that relates with the decomposition of isocyanurate, aromatic and isocyanate segments (1, 52).

The temperature recorded at 5 wt% loss ($T_{5\%}$) can be used to indicate thermal stability of the foams (118). When considering $T_{5\%}$ of the foam in Table 4.10, PIR foams initiated their thermal degradation processes between 260-266 °C, which was higher than that of the their relating rigid PUR foams (238-259 °C). This indicated that PIR foams could withstand thermal better than RPUR foams. The higher degree of PIR crosslink in PIR foams can strengthen overall polymer network by increasing dense crosslinks. Therefore, higher thermal energy is needed for PIR foams to initiate their chain movement at the initial thermal degradation processes. The temperatures at maximum rate of weight loss (T_{max1} and T_{max2}) were investigated for both thermal degradation steps. It was found that T_{max1} of PIR foams was close to that of rigid PUR foams and appeared in the range of 307-314 °C, whereas T_{max2} of PIR foams was significantly higher than that of their relating PUR foams by 15-22 °C owing to the higher PIR/PUR proportion. Moreover, calculation of char residue from TGA is the relatively simple method to assess fire-retarded properties of polymeric foams (5). The % char residue of PIR foams after thermal analysis was higher than that of their relating rigid PUR foams by 8.8-14.0 %. This result is consistent with the results of horizontally-oriented burning test and could indicate the improvement in not only fire-retarded properties but also thermally-stable properties of PIR foams.

Horowitz-Metzger's method was applied to calculate the activation energy (E_a) of those foams by the equation as follows (119):

$$ln[ln(W_0 - W_t^f) / (W - W_t^f)] = E_a\theta / RT_s^2 \qquad (4.2)$$

where W_0 and W_t^f is the initial and final weight, respectively, of each thermal decomposition step. W is the weight at temperature (T). θ is T-T_s, where T_s is T_{max1} or T_{max2}. E_a of thermal degradation reported in Table 4.10 could be calculated from the slope of the graphs plotted between $ln[ln(W_0 - W_t^f)/(W - W_t^f)]$ and θ as shown in Figure 4.42. The slope of graphs could be used for E_a evaluation due to the reasonable correlation coefficients (R^2) as reported along with E_a in Table 4.10. The results showed that the E_a for the latter degradation step was higher than that for the first degradation step for all foam samples due to the fact that the isocyanurate linkage is more thermally stable and require more energy to decompose in comparison with the urethane linkage (4, 5, 52). Therefore, it could be concluded from this result that the incorporation of isocyanurate structures could help PIR foams to enhance their thermal stability.

Table 4.10 Thermal properties of PIR and rigid PUR foams obtained from TGA.

| Catalysts | $T_{5\%}$ (°C) | 1st Step | | | | 2nd Step | | | | Char at 800 °C (%) |
		T_{max1} (°C)	wt% loss	E_a (kJ/ mol)	R^2	T_{max2} (°C)	wt% loss	E_a (kJ/ mol)	R^2	
Cu(Amm)	259	314	76.1	256.0	0.9995	466	11.9	306.1	0.9975	12.0
Zn(Amm)	238	307	76.0	254.3	0.9993	465	12.4	331.7	0.9995	11.6
Potassium octoate and Cu(Amm)	266	314	61.6	357.7	0.9981	488	12.4	384.0	0.9975	26.0
Potassium octoate and Zn(Amm)	260	311	64.4	350.9	0.9981	480	15.2	380.2	0.9982	20.4
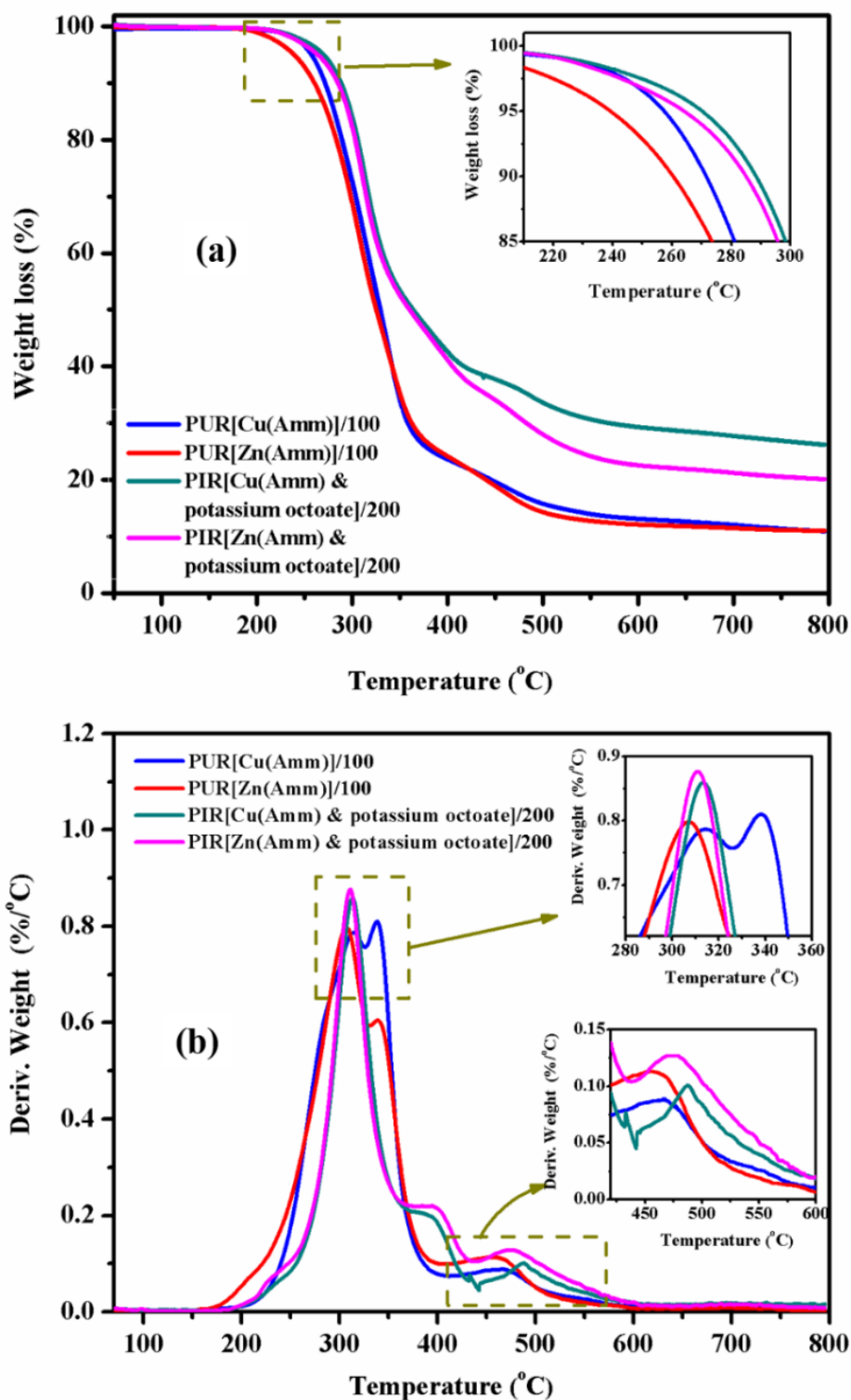
Figure 4.41 Thermograms of (a) TG and (b) DTG of PIR foams as compared to rigid PUR foams.
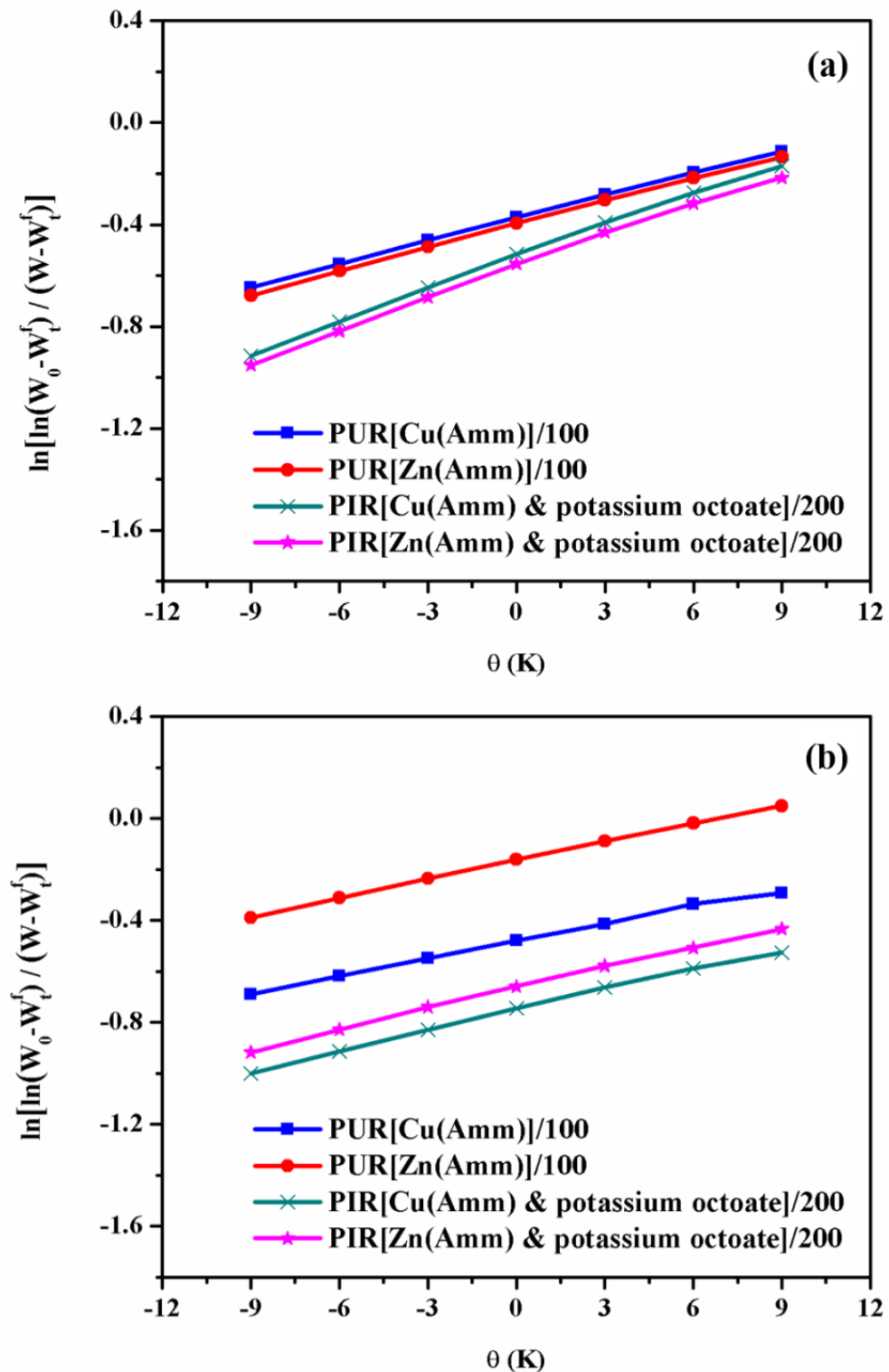
Figure 4.42 Plots by Horowitz-Metzger's method to evaluate degradation activation energy of (a) first-step degradation (b) second-step degradation.

CHAPTER 5

THEORETICAL STUDY OF CATALYTIC PROPERTIES OF METAL-AMMONIA COMPLEXES IN GELLING AND BLOWING REACTIONS

According to the experimental results in the previous chapter, Cu(Amm) and Zn(Amm) were able to accelerate gelling and blowing reactions of rigid PUR and PIR foams. In this section, the DFT computational study at CAM–B3LYP/6–31G(d) level of theory was conducted to investigate their catalytic mechanism as well as the thermodynamic properties of catalyzed gelling and blowing reactions. The transition state of each reaction was studied in order to reach better understanding on the reaction pathways of urethane formation and CO_2 generation.

5.1 Reaction mechanism of gelling reaction over metal-ammonia complexes

The computational study for gelling reaction (urethane formation) was carried out using a model reaction (Scheme 5.1). Methanol is employed as the model of polyol while phenyl isocyanate substitutes PMDI. Methyl phenyl carbamate (urethane) is the product. $[Cu(NH_3)_4]^{2+}$ and $[Zn(NH_3)_4]^{2+}$ are the structures of catalysts used in gelling reaction since $[Cu(NH_3)_4(H_2O)_2]^{2+}$ and $[Zn(NH_3)_4(H_2O)_2]^{2+}$ can readily liberate their H_2O ligands (83, 85) to have vacant sites for interacting with the methanol and phenyl isocyanate reactants as discussed in the previous chapter. The noncatalytic system for gelling reaction was also studied in order to confirm that whether $[Cu(NH_3)_4]^{2+}$ and $[Zn(NH_3)_4]^{2+}$ can effectively increase the rate of gelling reaction.
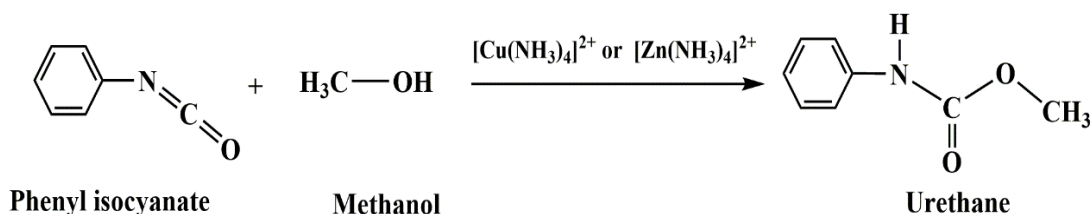
Scheme 5.1 A model reaction for gelling reaction.

Based on the computational investigation, the reaction mechanism for the gelling reaction accelerated by $[Cu(NH_3)_4]^{2+}$ can be constructed as shown in Figure 5.1. The reaction pathway composes of four reaction steps, namely 1) the primary coordination between the reactants and $[Cu(NH_3)_4]^{2+}$, 2) the reaction between activated reactants toward the transition state, 3) the urethane formation over $[Cu(NH_3)_4]^{2+}$ and 4) the liberation of urethane product from $[Cu(NH_3)_4]^{2+}$. The reaction pathway for the gelling reaction accelerated by $[Zn(NH_3)_4]^{2+}$ is similar to that obtained from $[Cu(NH_3)_4]^{2+}$as shown in Figure 5.2. In the case of uncatalyzed gelling reaction (Figure 5.3), the reaction mechanism appears different. The reaction pathway composes of three reaction steps, namely 1) the primary interaction between phenyl isocyanate and methanol reactants, 2) the reaction toward the transition state and 3) the urethane formation. The details about all configurations included in these reaction pathways are further discussed in the sections 5.1.1 and 5.1.2.
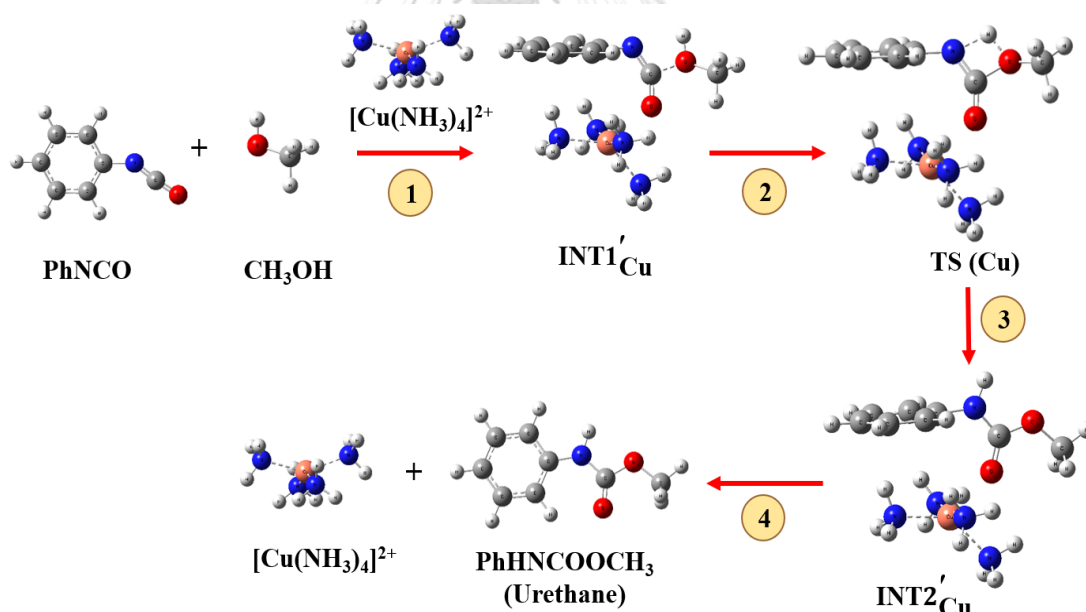
Figure 5.1 Reaction mechanism for gelling reaction accelerated by $[Cu(NH_3)_4]^{2+}$.
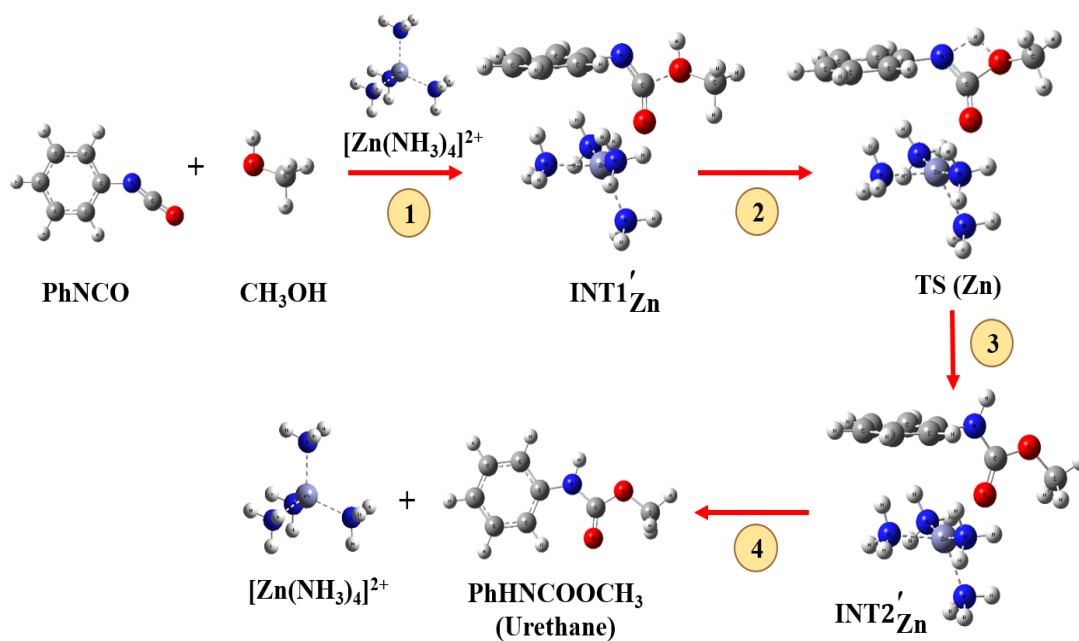
Figure 5.2 Reaction mechanism for gelling reaction accelerated by $[Zn(NH_3)_4]^{2+}$.
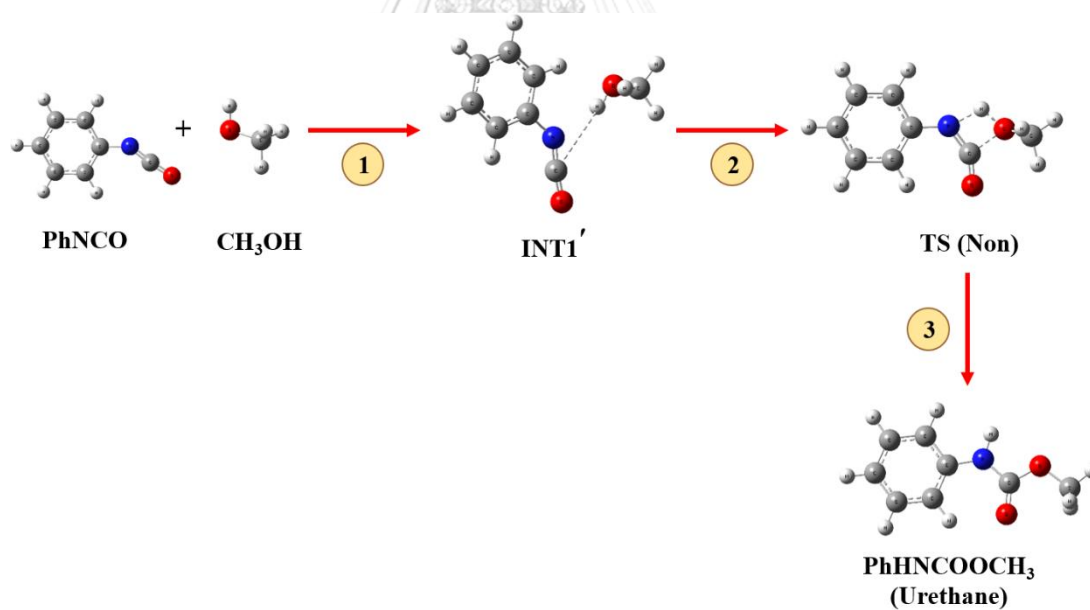
Figure 5.3 Reaction mechanism for unaccelerated gelling reaction.

5.1.1 Optimized structures of reactant, product and catalyst for gelling reaction

The optimized structures of phenyl isocyanate, methanol, urethane product and metal-ammonia complexes obtained at CAM–B3LYP/6–31G(d) level of theory are presented in Figure 5.4. Phenyl isocyanate is the planar structure. A bond angle of N=C=O group is 173.55°, which almost appears as a linear bond before it is activated by metal-ammonia complexes. Bond distances between N=C and C=O of phenyl isocyanate are 1.20 and 1.17 Å, respectively. For methanol, the bond distance of O–H is shorter at 0.97 Å. In the case of $[Cu(NH_3)_4]^{2+}$ and $[Zn(NH_3)_4]^{2+}$, the coordinated bond distances between Cu---N and Zn---N are 2.01 and 2.04 Å, respectively.
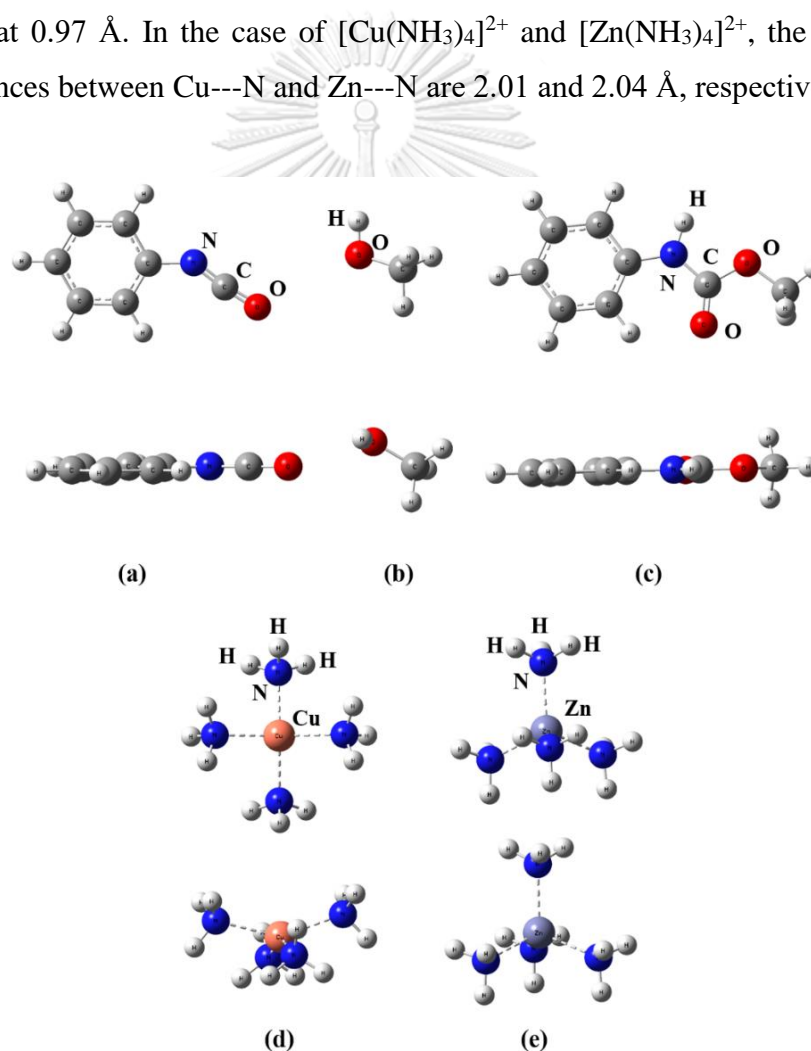
Figure 5.4 CAM–B3LYP/6–31G(d)-optimized structures of (a) phenyl isocyanate (b) methanol, (c) urethane product, (d) $[Cu(NH_3)_4]^{2+}$ and (e) $[Zn(NH_3)_4]^{2+}$. The optimized structures in top and bottom rows are top and side views, respectively.

5.1.2 Optimized structures of involved configuration in gelling reaction

According to the reaction mechanism, it is found that the gelling reaction accelerated by $[Cu(NH_3)_4]^{2+}$ and $[Zn(NH_3)_4]^{2+}$ composes of three involved configurations (Figures 5.5 and 5.6) as follows: 1) the intermediate ($INT1'_{Cu}$ or $INT1'_{Zn}$) which occurs before the transition state when the phenyl isocyanate is activated by the catalysts and the reactants move closer to each other. 2) the transition state [TS(Cu) or TS(Zn)] which occurs when the oxygen of methanol interacts with the carbon of phenyl isocyanate to have the C–O bond and tries to transfer its proton to nitrogen of phenyl isocyanate to form urethane linkage. 3) the intermediate ($INT2'_{Cu}$ or $INT2'_{Zn}$) which occurs after transition state when the urethane product is formed and tries to release from the catalyst. For uncatalyzed gelling reaction, only two involved configurations, namely INT1′ (the closer reactants) and TS(Non) (the structure with proton transfer process) are found as shown in Figure 5.7.

Considering $INT1'_{Cu}$ [Figure 5.5(a)] and $INT1'_{Zn}$ structures [Figure 5.6(a)], it can be observed that their N=C=O groups tend to bend toward the $[Cu(NH_3)_4]^{2+}$ and $[Zn(NH_3)_4]^{2+}$ catalysts, respectively. The bond angle of N=C=O group of $INT1'_{Cu}$ and $INT1'_{Zn}$ changes from 173.55 ° to 143.33° when compared to that of phenyl isocyanate reactant. The oxygen of N=C=O group obviously points to the metal ion of each metal complex for coordinating. The distances between carbon of phenyl isocyanate and oxygen of methanol (C---O) in $INT1'_{Cu}$ and $INT1'_{Zn}$ are 1.57 and 1.56 Å, respectively. These distances are much shorter than that of INT1′ in uncatalyzed gelling reaction (3.81 Å). The distance between reacting atoms is one of the physical factors that indicates whether the reaction is easily taken place (58). This result reveals that $[Cu(NH_3)_4]^{2+}$ and $[Zn(NH_3)_4]^{2+}$ can activate the N=C=O group through the oxygen coordination and decrease the distance between the reactants by inducing the methanol to move closer to activated phenyl isocyanate. Therefore, the urethane formation between methanol and phenyl isocyanate tends to occur easier in comparison to the uncatalyzed gelling reaction.

In the case of transition state configurations of $[Cu(NH_3)_4]^{2+}$-catalyzed, $[Zn(NH_3)_4]^{2+}$-catalyzed and uncatalyzed gelling reactions, namely TS(Cu) [Figure 5.5(b)], TS(Zn) [Figure 5.6(b)] and TS(Non) [Figure 5.7(b)], respectively, appear as

the four-membered ring structures with the single negative imaginary frequency of 1640.99i, 1642.91i and 1517.21i cm^{-1}, respectively. The intrinsic reaction coordinate (IRC) of TS(Cu), TS(Zn) and TS(Non), which can track the minimum energy paths from transition state structures to the corresponding minimum, are presented in Figures B1, B2 and B3, respectively, in Appendix B. It is found that the transition state for gelling reaction proceeds through the proton transfer process from the oxygen of methanol to the nitrogen of phenyl isocyanate. These obtained four-membered ring structures with the proton transfer at the transition state of urethane formation are in good agreement with the previous results studied using the different systems in the other works (57, 64, 120). The urethane products catalyzed by [Cu(NH$_3$)$_4$]$^{2+}$and [Zn(NH$_3$)$_4$]$^{2+}$ catalysts as shown in Figures 5.5(c) and 5.6(c), respectively, have the similar geometry to that obtained from uncatalyzed gelling reaction as shown in Figure 5.7(c).
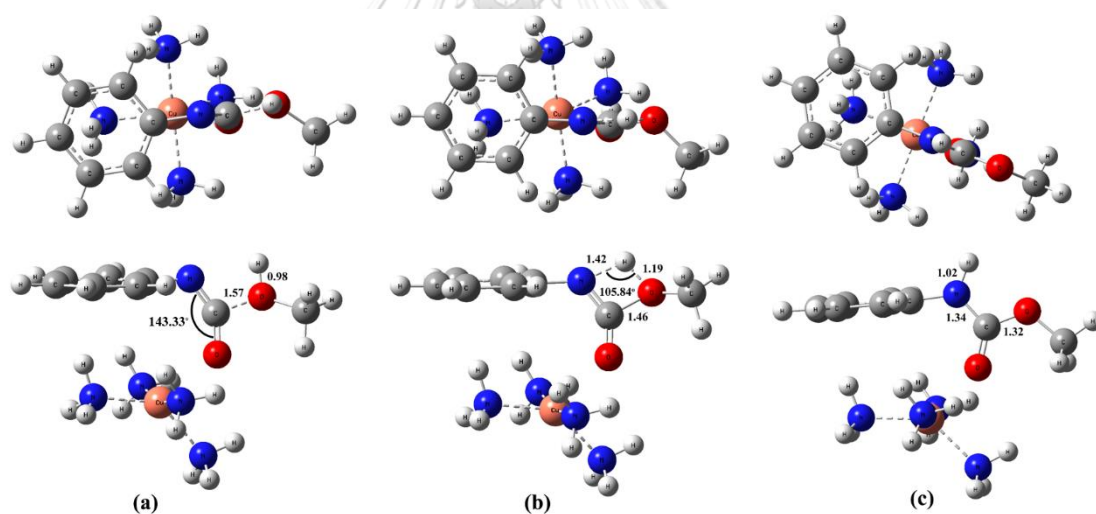
Figure 5.5 CAM–B3LYP/6–31G(d)-optimized structures of (a) INT1$'_{Cu}$, (b) TS(Cu) and (c) INT2$'_{Cu}$. The optimized structures in top and bottom rows are top and side views, respectively. The bond distances are in Å.
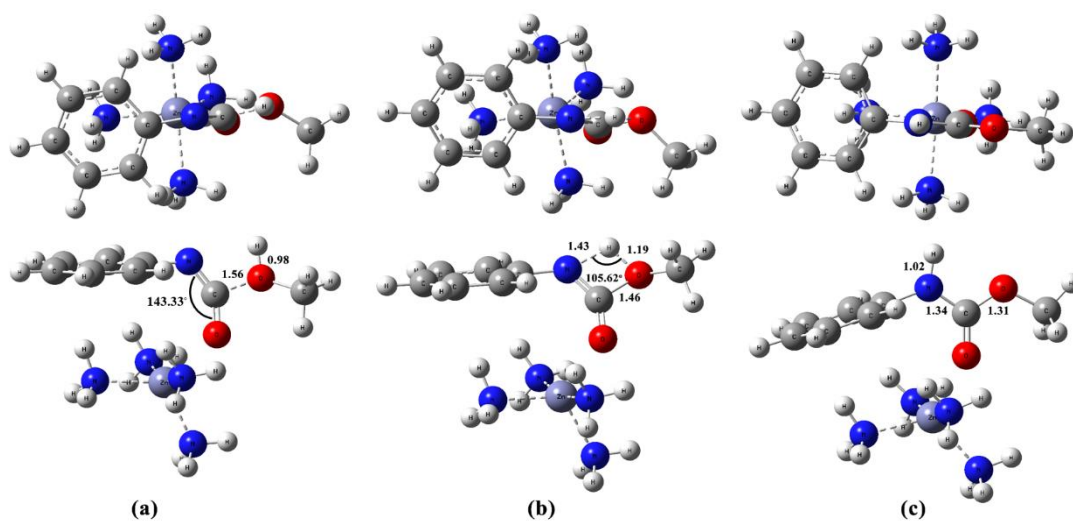
Figure 5.6 CAM–B3LYP/6–31G(d)-optimized structures of (a) $INT1'_{Zn}$, (b) TS(Zn) and (c) $INT2'_{Zn}$. The optimized structures in top and bottom rows are top and side views, respectively. The bond distances are in Å.
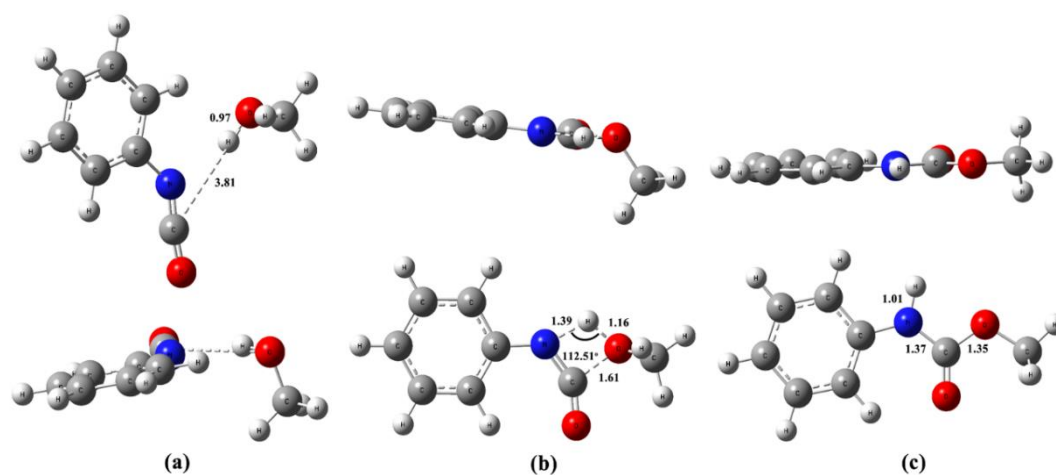
Figure 5.7 CAM–B3LYP/6–31G(d)-optimized structures of (a) INT1′, (b) TS(Non) and (c) urethane product. The optimized structures in top and bottom rows are top and side views, respectively. The bond distances are in Å.

5.1.3 Natural bond orbital (NBO) analysis for gelling reaction accelerated by $[Cu(NH_3)_4]^{2+}$ and $[Zn(NH_3)_4]^{2+}$

The population of charge on the atoms of TS(Cu), TS(Zn) and TS(Non) structures is presented in Figures 5.8(a), (b) and (c), respectively. The atoms relating with the reaction site of the urethane formation are focused as labeled in these Figures. The positive charges are accumulated on Cu, Zn, C and H and appear as the green atoms, while the negative charges are accumulated on O1, N and O2 and appear as the red atoms. The charge values are summarized in Table 5.1.

The investigation for donating and accepting of electrons between molecules could be conducted through the NBO analysis, which gives the appropriate basis to predict the partial charge transfer (Q_{PCT}) between the catalysts and their accelerated molecules and can indicate the catalytic mechanism of $[Cu(NH_3)_4]^{2+}$ and $[Zn(NH_3)_4]^{2+}$ in the urethane formation. The Q_{PCT} is calculated using the following equation:

$$Q_{PCT} = Q_{catalyst/PhNCO/CH_3OH} - Q_{catalyst} \qquad (5.1)$$

where $Q_{catalyst/PhNCO/CH_3OH}$ is the total charge (in e) of catalysts, $[Cu(NH_3)_4]^{2+}$ or $[Zn(NH_3)_4]^{2+}$, during accelerating the reaction of phenyl isocyanate and methanol at the transition state, while $Q_{catalyst}$ is the charge of $[Cu(NH_3)_4]^{2+}$ or $[Zn(NH_3)_4]^{2+}$ in free case. It is found that $[Cu(NH_3)_4]^{2+}$ and $[Zn(NH_3)_4]^{2+}$ catalysts can withdraw electrons from phenyl isocyanate, and Q_{PCT} is transferred to $[Cu(NH_3)_4]^{2+}$ and $[Zn(NH_3)_4]^{2+}$ of -0.155 and -0.168 e, respectively [Figures 5.8(a) and (b)]. The electron transfer to $[Zn(NH_3)_4]^{2+}$ is slightly more than $[Cu(NH_3)_4]^{2+}$ owing to the reason that the zinc ion coordinates with the oxygen atom of phenyl isocyanate closer than the copper ion.

Based on this result obtained from NBO analysis along with the optimized geometries of TS(Cu) and TS(Zn), which obviously point the oxygen atom of phenyl isocyanate to each metal ion of the catalyst, the catalytic mechanism of $[Cu(NH_3)_4]^{2+}$ and $[Zn(NH_3)_4]^{2+}$ can be deduced that the metal ions (copper and zinc ions) of $[Cu(NH_3)_4]^{2+}$ and $[Zn(NH_3)_4]^{2+}$ act as the Lewis acid to coordinate with the oxygen atom of phenyl isocyanate. This causes the carbon atom of phenyl isocyanate to be

more electrophilic, which enhances the nucleophilic attack from the oxygen of methanol to form the urethane linkage. The data of NBO charge in Table 5.1 show that the carbon atoms of phenyl isocyanate accelerated by $[Cu(NH_3)_4]^{2+}$ and $[Zn(NH_3)_4]^{2+}$ have more positive charge values of 0.938 and 0.941 e, respectively, in comparison to that of carbon atom in noncatalytic system (0.919 e).
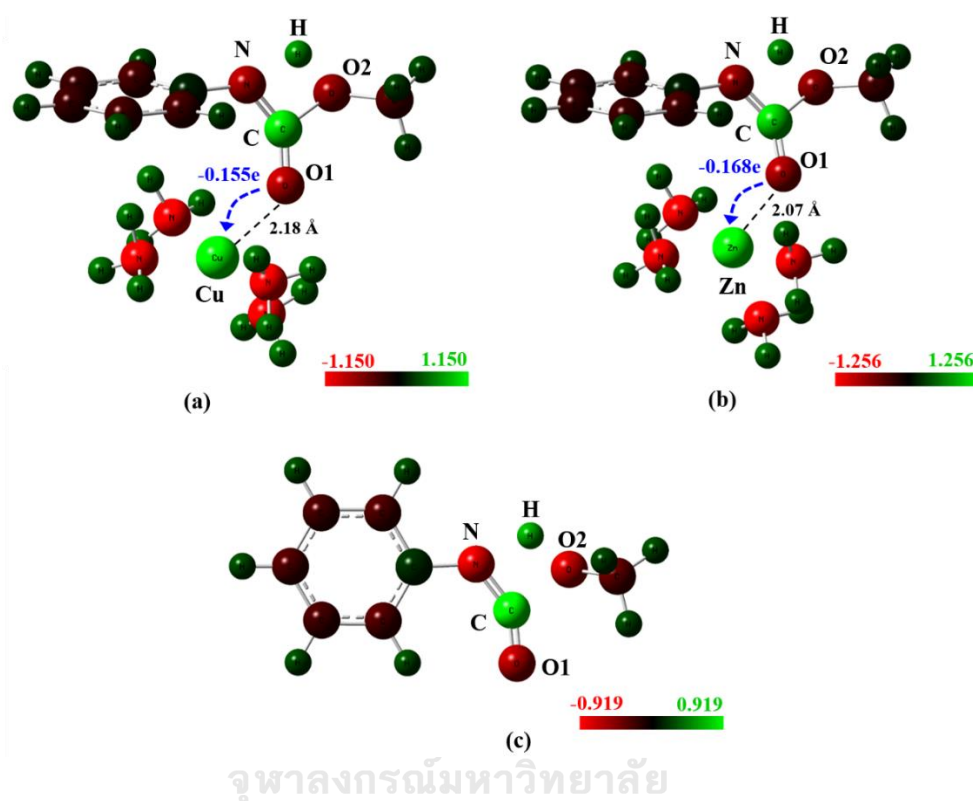
Figure 5.8 NBO atomic charges at the transition state of urethane formation accelerated by (a) $[Cu(NH_3)_4]^{2+}$, (b) $[Zn(NH_3)_4]^{2+}$ and (c) noncatalytic system.

Table 5.1 Selected NBO charges (in e) of the relating atoms around the reaction site of urethane formation obtained using CAM–B3LYP/6–31G(d) level of theory.

Configurations	Cu	Zn	O1	C	N	O2	H
TS(Non)	-	-	-0.578	0.919	-0.729	-0.656	0.542
TS(Cu)	1.113	-	-0.726	0.938	-0.667	-0.597	0.565
TS(Zn)	-	1.256	-0.741	0.941	-0.654	-0.594	0.565

5.1.4 Frontier molecular orbital (FMO) analysis for gelling reaction accelerated by $[Cu(NH_3)_4]^{2+}$ and $[Zn(NH_3)_4]^{2+}$

FMO analysis was carried out for better understanding about the electronic properties of $[Cu(NH_3)_4]^{2+}$ and $[Zn(NH_3)_4]^{2+}$ catalysts in gelling reaction. HOMO and LUMO orbital distributions of TS(Cu), TS(Zn) and TS(Non) are shown in Figures 5.9(a), (b) and (c), respectively. The difference result of orbital distributions between the catalyzed and the uncatalyzed transition state is found. For catalyzed transition state, namely TS(Cu) and TS(Zn), the electron delocalization between HOMO and LUMO is obviously changed. Their HOMOs are delocalized on the phenyl group and around the interacting site between phenyl isocyanate and methanol, while their LUMOs are delocalized on $[Cu(NH_3)_4]^{2+}$ or $[Zn(NH_3)_4]^{2+}$. For uncatalyzed transition state or TS(Non), the electron delocalization between HOMO and LUMO is not obviously changed, which locates on phenyl isocyanate and the oxygen atom of methanol. This result indicates that the use of $[Cu(NH_3)_4]^{2+}$ and $[Zn(NH_3)_4]^{2+}$ catalysts for urethane formation can lead the electron delocalization at the transition state of urethane formation.
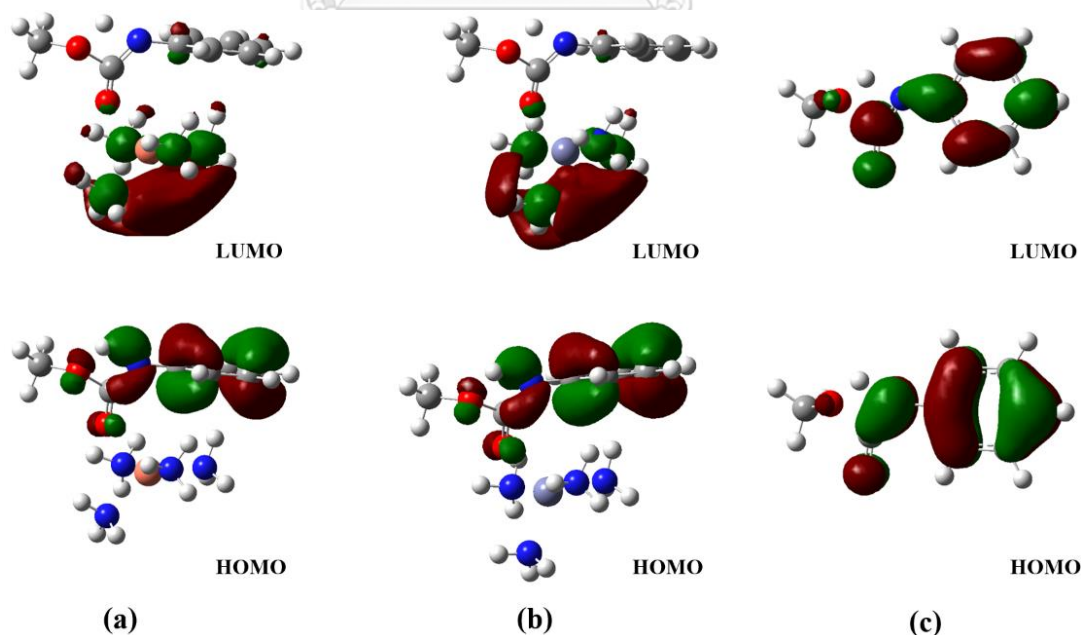
Figure 5.9 Frontier molecular orbitals of (a) TS(Cu), (b) TS(Zn) and (c) TS(Non) investigated at the transition state of urethane formation.

Moreover, the HOMO and LUMO orbital distributions relating to some crucial step in the reaction pathway of urethane formation were investigated. As previous discussed, $[Cu(NH_3)_4]^{2+}$ or $[Zn(NH_3)_4]^{2+}$ can act as the Lewis acid to activate the carbon atom of phenyl isocyanate to be more electrophilic for enhancing the nucleophilic attack from oxygen atom of methanol in the activating step of urethane formation. Therefore, this activating step is important to calculate the energy gab (E_g) between the LUMO of activated phenyl isocyanate and the HOMO of methanol in order to evaluate the reactivity of the catalysts and to indicate whether urethane formation is easier to occur in comparison to the uncatalyzed reaction. The LUMO of activated phenyl isocyanate is the innermost empty orbital which can accept the electron from the HOMO of methanol, and the HOMO of methanol is the outermost orbital which contains the electron for giving to the LUMO of activated phenyl isocyanate for constructing the C–O bond of urethane linkage.

Figures 5.10(a), (b) and (c) show the calculated energy gap ($E_g = \Delta E_{HOMO-LUMO}$) obtained from $[Cu(NH_3)_4]^{2+}$-catalyzed, $[Zn(NH_3)_4]^{2+}$-catalyzed and uncatalyzed reactions, respectively. It is found that the E_g between the LUMO of phenyl isocyanate and the HOMO of methanol largely decreases from 9.636 eV (uncatalyzed reaction) to 2.671 and 2.737 eV when using $[Cu(NH_3)_4]^{2+}$ and $[Zn(NH_3)_4]^{2+}$ catalysts, respectively. This narrower E_g can indicate that the reaction between activated phenyl isocyanate with methanol to form urethane can occur easier when using $[Cu(NH_3)_4]^{2+}$ and $[Zn(NH_3)_4]^{2+}$ catalysts. The slightly narrower E_g obtained from $[Cu(NH_3)_4]^{2+}$ reveals that $[Cu(NH_3)_4]^{2+}$ had slightly more reactivity than $[Zn(NH_3)_4]^{2+}$.
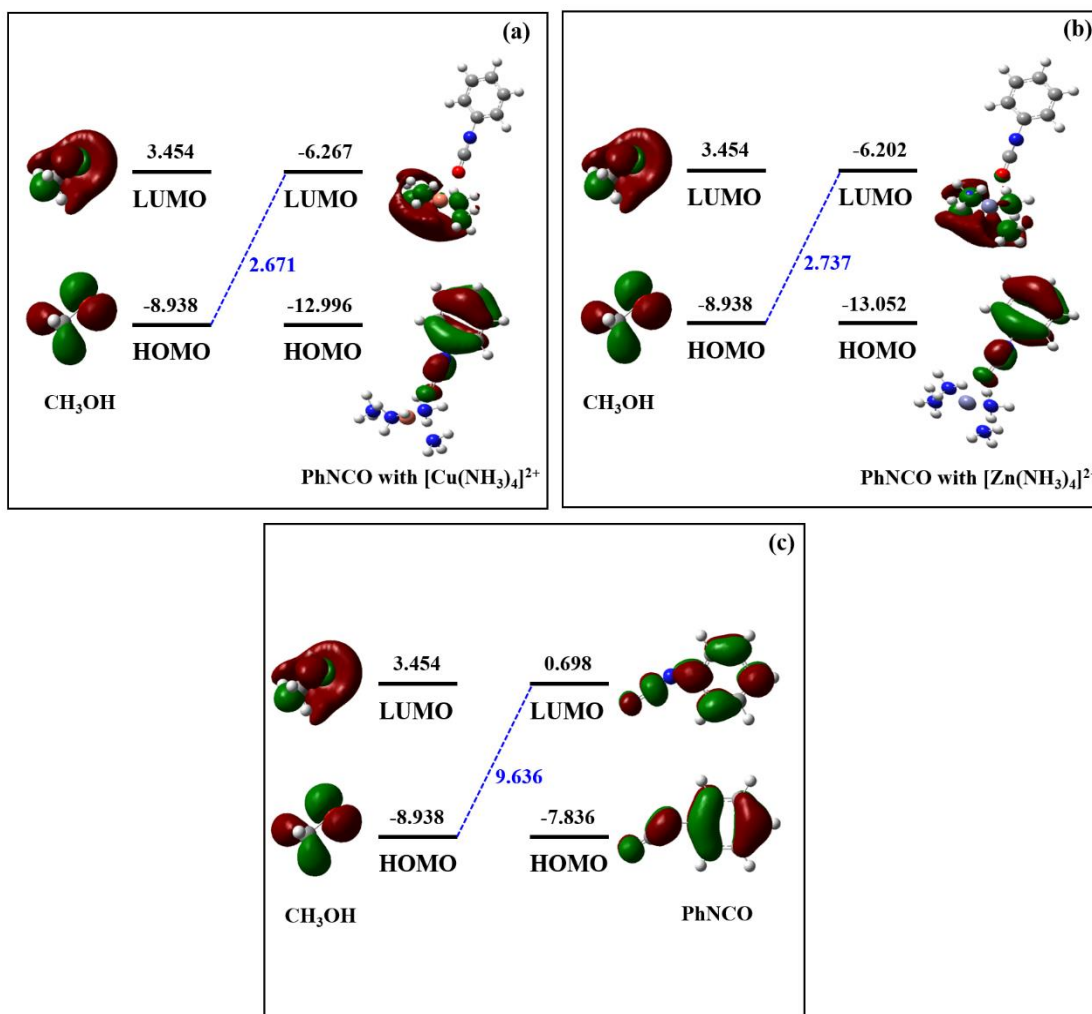
Figure 5.10 Frontier molecular orbitals of phenyl isocyanate and methanol in the case of (a) $[Cu(NH_3)_4]^{2+}$-catalyzed, (b) $[Zn(NH_3)_4]^{2+}$-catalyzed and (c) uncatalyzed reactions. The unit of energy gap (E_g) is eV.

5.1.5 Thermodynamic and kinetic investigation of gelling reaction accelerated by $[Cu(NH_3)_4]^{2+}$ and $[Zn(NH_3)_4]^{2+}$

Potential energy profiles of gelling reaction obtained from $[Cu(NH_3)_4]^{2+}$-catalyzed, $[Zn(NH_3)_4]^{2+}$-catalyzed and uncatalyzed systems are presented in Figures 5.11, 5.12 and 5.13, respectively. The reaction energy, thermodynamic property, reaction rate constant and equilibrium constant for each system are summarized in Table 5.2. It can be observed from the potential energy profiles that the rate

determining step for gelling reaction in both catalytic and noncatalytic systems is the step at which the $INT1'_{Cu}$, $INT1'_{Zn}$ and $INT1'$ transform to the $INT2'_{Cu}$, $INT2'_{Zn}$ and $INT2'$, respectively, via the transition state of each reaction. According to the data in Table 5.2, the reaction rate constants for the rate determining step via TS(Cu), TS(Zn) and TS(Non) are 1.28×10^7, 3.51×10^6 and 9.43×10^{-10} s^{-1}, respectively. The equilibrium constants for the rate determining step via TS(Cu), TS(Zn) and TS(Non) are 2.58×10^{33}, 2.07×10^{32} and 2.98×10^{16}, respectively. The activation energies for the $[Cu(NH_3)_4]^{2+}$-catalyzed, $[Zn(NH_3)_4]^{2+}$-catalyzed and uncatalyzed gelling reactions are 9.49, 9.58 and 27.54 kcal/mol, respectively. The gelling reaction without any catalyst shows the largest activation energy accompanying with the minimum reaction rate constant. This result proves that $[Cu(NH_3)_4]^{2+}$ and $[Zn(NH_3)_4]^{2+}$ are good catalysts for the gelling reaction since they show the activities of the catalyst, which can reduce the activation energy and also increase the rate constant of the gelling reaction in comparison to the uncatalyzed reaction.
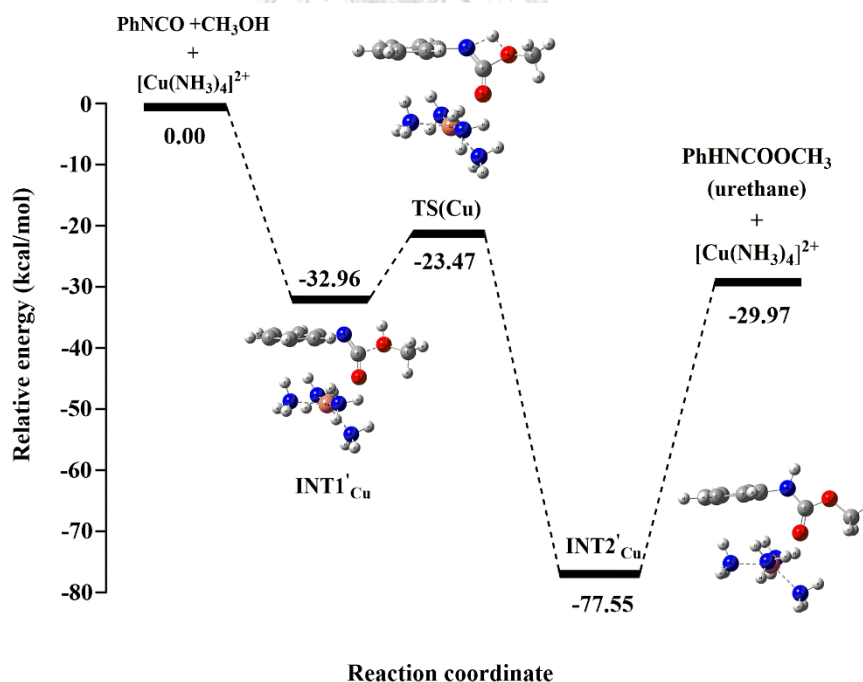
Figure 5.11 The potential energy profile for gelling reaction accelerated by $[Cu(NH_3)_4]^{2+}$.
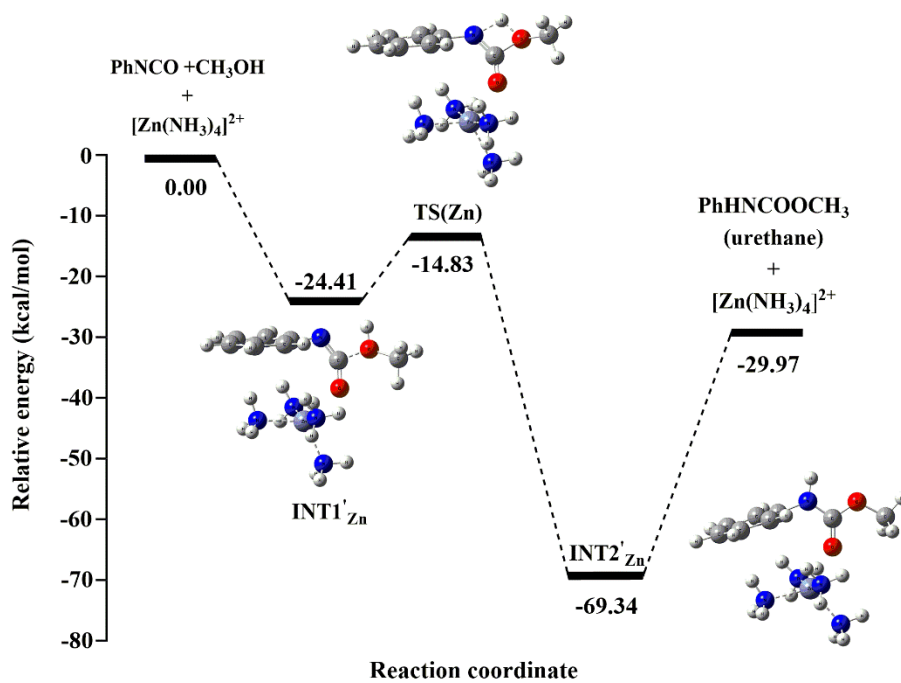
Figure 5.12 The potential energy profile for gelling reaction accelerated by $[Zn(NH_3)_4]^{2+}$.
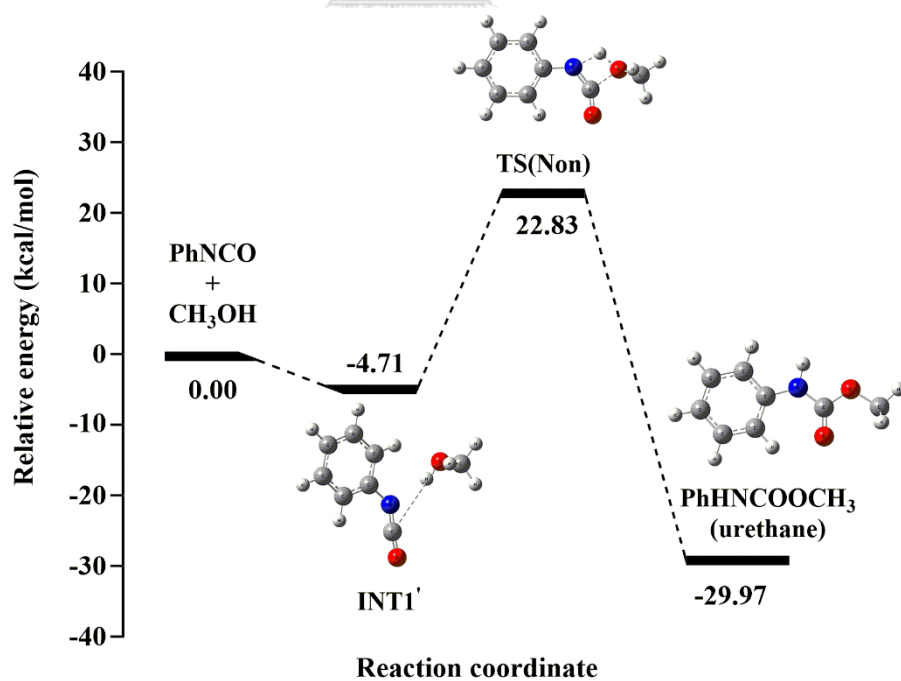
Figure 5.13 The potential energy profile for uncatalyzed gelling reaction.

Table 5.2 Activation energies, reaction energies, thermodynamic quantities, rate constants and equilibrium constants of catalyzed and uncatalyzed gelling reaction, computed at the CAM–B3LYP/6–31G(d) level of theory.

Reaction	$\Delta E^{\ddagger}$ a,b	$\Delta G^{\ddagger}$ a,b	k_{298} c	ΔE a	ΔH^{o}_{298} a	ΔG^{o}_{298} a	K_{298}
Noncatalytic system:							
PhNCO + CH₃OH → INT1'	–	–	–	–4.71	–4.40	4.36	6.41×10^{-4}
INT1' → TS(Non) → urethane	27.54	30.26	9.43×10^{-10}	–25.26	–26.43	–22.47	2.98×10^{16}
Catalytic system:							
[Cu(NH₃)₄]²⁺ catalyst:							
PhNCO + CH₃OH + [Cu(NH₃)₄]²⁺ → INT1'$_{Cu}$	–	–	–	–32.96	–33.21	–8.89	3.27×10^{6}
INT1'$_{Cu}$ → TS(Cu) → INT2'$_{Cu}$	9.49	9.30	1.28×10^{7}	–44.59	–44.64	–45.58	2.58×10^{33}
INT2'$_{Cu}$ → urethane + [Cu(NH₃)₄]²⁺	–	–	–	47.58	47.01	36.35	2.26×10^{-27}
[Zn(NH₃)₄]²⁺ catalyst:							
PhNCO + CH₃OH + [Zn(NH₃)₄]²⁺ → INT1'$_{Zn}$	–	–	–	–24.41	–24.24	–0.17	1.32×10^{0}
INT1'$_{Zn}$ → TS(Zn) → INT2'$_{Zn}$	9.58	9.33	3.51×10^{6}	–44.93	–45.55	–44.08	2.07×10^{32}
INT2'$_{Zn}$ → urethane + [Zn(NH₃)₄]²⁺	–	–	–	39.37	38.96	26.13	6.98×10^{-20}

[a] In kcal/mol.

[b] Activation energy.

[c] In s⁻¹.

5.2 Reaction mechanism of blowing reaction over metal-ammonia complexes

According to the results of gelling reaction obtained from computational study in the previous section, $[Cu(NH_3)_4]^{2+}$ showed better catalytic efficiency than $[Zn(NH_3)_4]^{2+}$. Therefore, the catalytic mechanism in blowing reaction was studied using $[Cu(NH_3)_4]^{2+}$ as the catalyst. The model reaction for computational study of blowing reaction is shown in Scheme 5.2. Water (H_2O) reacts with phenyl isocyanate to obtain the carbamic acid (intermediate molecule), which further decomposes to give carbon dioxide (CO_2) and phenyl amine. CO_2 product is the blowing gas providing the cellular structure of the foams.

Scheme 5.2 A model reaction for blowing reaction.

From the result of computational study, the reaction mechanism for the blowing reaction accelerated by $[Cu(NH_3)_4]^{2+}$ can be obtained as shown in Figure 5.14. The reaction pathway composes of eight reaction steps, namely 1) the primary coordination between the reactants and $[Cu(NH_3)_4]^{2+}$, 2) the reaction of activated reactants toward the first transition state, 3) the carbamic acid formation over $[Cu(NH_3)_4]^{2+}$ catalyst, 4) the rotation of proton of carbamic acid toward the second transition state, 5) the change of second transition state toward the intermediate, 6) the reaction of intermediate toward the third transition state, 7) the CO_2 generation and phenyl amine formation over $[Cu(NH_3)_4]^{2+}$ catalyst and 8) the liberation of CO_2 and phenyl amine products from $[Cu(NH_3)_4]^{2+}$. The details about all configurations involved in the blowing reaction pathway are further discussed in the section 5.2.1.

Figure 5.14 Reaction mechanism for blowing reaction accelerated by $[Cu(NH_3)_4]^{2+}$.

5.2.1 Optimized structures of reactant, product and involved configuration in blowing reaction accelerated by $[Cu(NH_3)_4]^{2+}$

The optimized structures of phenyl isocyanate, H_2O, phenyl amine and CO_2 obtained at CAM–B3LYP/6–31G(d) level of theory are presented in Figure 5.15.
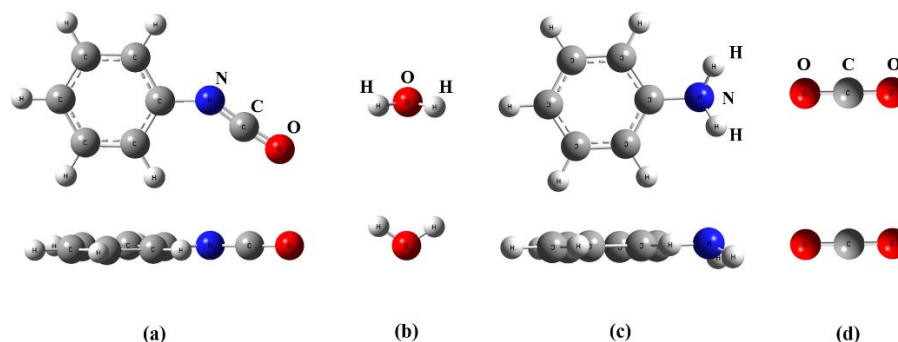
Figure 5.15 CAM–B3LYP/6–31G(d)-optimized structures of (a) phenyl isocyanate (b) H_2O, (c) phenyl amine and (d) CO_2. The optimized structures in top and bottom rows are top and side views, respectively.

The seven optimized geometies of involved configurations in blowing reaction are shown in Figures 5.16. This number of involved configurations in blowing reaction is more than that of gelling reaction, which points out that the reaction pathway of blowing reaction might be more complex than that of the gelling reaction. The details of the configurations in the blowing reaction pathway are as follows: 1) the intermediate $[INT1'_{(Cu,CO_2)}]$ which occurs when the phenyl isocyanate is activated by the $[Cu(NH_3)_4]^{2+}$, and the H_2O reactant is induced to move closer to the activated phenyl isocyanate. 2) the first transition state $[TS1(Cu,CO_2)]$ which occurs when the oxygen atom of H_2O interacts with the carbon atom of phenyl isocyanate to obtain C–O bond and tries to transfer its proton to nitrogen atom of phenyl isocyanate to form carbamic acid. 3) the obtained carbamic acid $[INT2'_{(Cu,CO_2)}]$ which is the thermally unstable structure and the main intermediate of blowing reaction (8, 10, 121). 4) the rotational transition state $[TS2(Cu,CO_2)]$ which is the second transition state and occurs when carbamic acid tries to rotate its hydroxyl

group. 5) the intermediate [INT3$'_{(Cu,CO_2)}$] whose hydroxyl proton locates in the same planar to the N–H. 6) the third transition state [TS3(Cu,CO$_2$)] which occurs when the C–N bond of carbamic acid is weaker and the oxygen atom tries to transfer the second proton to nitrogen atom in the same carbamic acid molecule. 7) the intermediate [INT4$'_{(Cu,CO_2)}$] which composes of CO$_2$ and phenyl amine products over the [Cu(NH$_3$)$_4$]$^{2+}$ catalyst.

The result reveals that all intermediates in the blowing reaction pathway still point their N=C=O groups toward the [Cu(NH$_3$)$_4$]$^{2+}$ catalyst. This is similarly to the case of gelling reaction. However, the distance between the activated phenyl isocyanate and the H$_2$O (2.21 Å) in the case of blowing reaction shown in INT1$'_{(Cu,CO_2)}$ is longer than that of the activated phenyl isocyanate and the methanol (1.57 Å) in the case of gelling reaction shown in INT1$'_{Cu}$ even though both reactions are accelerated by the same catalyst. In addition, the blowing reaction undergoes three transition state configurations, namely TS1(Cu,CO$_2$), TS2(Cu,CO$_2$) and TS3(Cu,CO$_2$), with the single negative imaginary frequency of 1605.29i, 504.45i and 1777.99i cm^{-1}, respectively. The intrinsic reaction coordinate (IRC) of these transition state structures are presented in Figures B4-B6 in Appendix B. TS1(Cu,CO$_2$) and TS3(Cu,CO$_2$) are the proton transfer transition states with four-membered ring structures, whereas TS2(Cu,CO$_2$) is hydroxyl rotational transition state. Generally, the optimized structure of the CO$_2$ should be the linear structure as shown in the Figure 5.15(d), but, the CO$_2$ product decomposed from the carbamic acid in INT4$'_{(Cu,CO_2)}$ locates at the middle between the phenyl amine product and [Cu(NH$_3$)$_4$]$^{2+}$ catalyst. This leads the CO$_2$ structure to slightly bend its oxygen atoms toward the [Cu(NH$_3$)$_4$]$^{2+}$ catalyst with the bond angle of 133.9°.
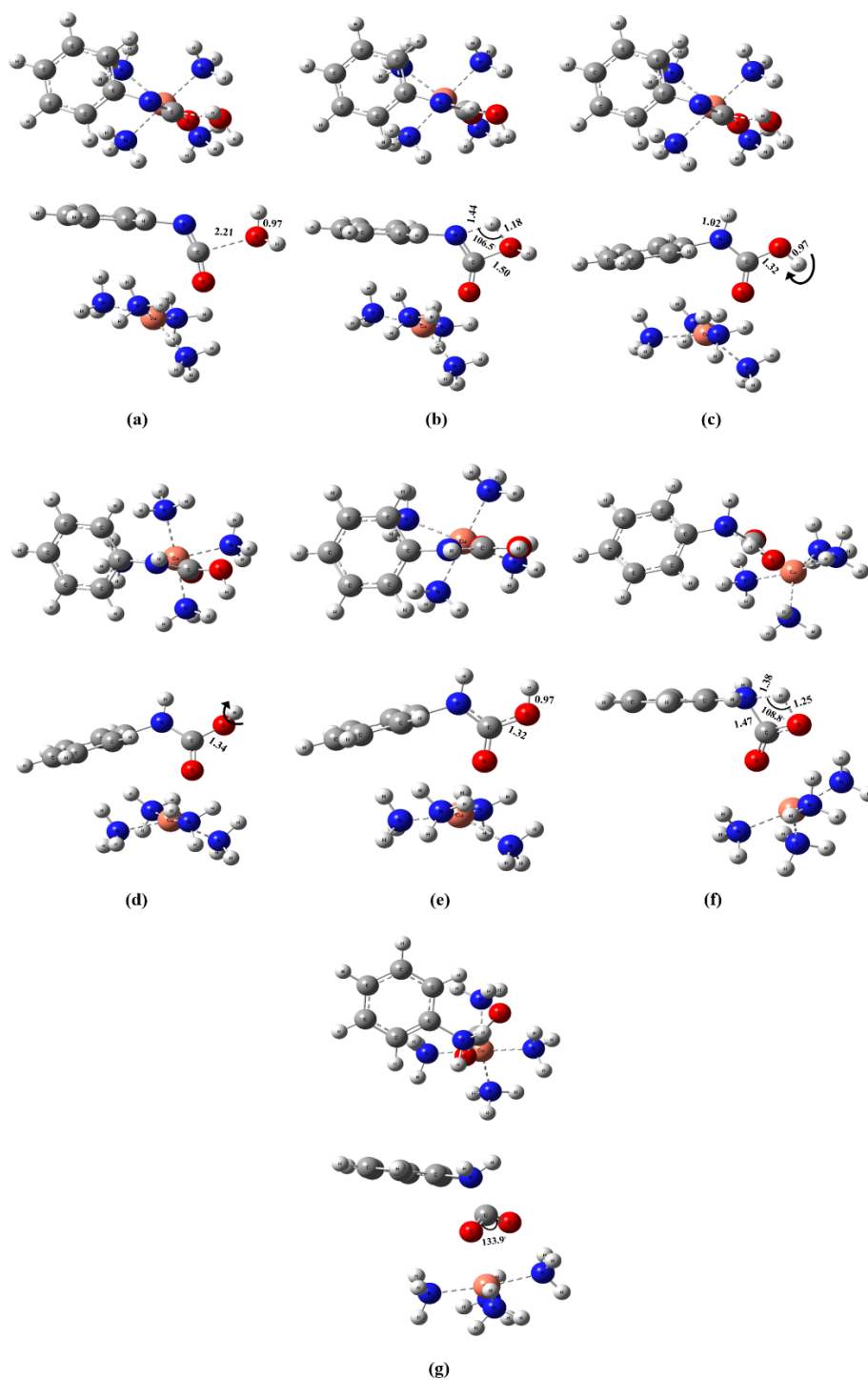
Figure 5.16 CAM–B3LYP/6–31G(d)-optimized structures of (a) $INT1'_{(Cu,CO_2)}$, (b) TS1(Cu,CO$_2$), (c) $INT2'_{(Cu,CO_2)}$, (d) TS2(Cu,CO$_2$), (e) $INT3'_{(Cu,CO_2)}$, (f) TS3(Cu,CO$_2$) and (g) $INT4'_{(Cu,CO_2)}$. The optimized structures in top and bottom rows are top and side views, respectively. The bond distances are in Å.

5.2.2 Natural bond orbital (NBO) analysis for blowing reaction accelerated by $[Cu(NH_3)_4]^{2+}$

The population of charge at the transition state of blowing reaction was investigated. The NBO charges on the atoms of TS1(Cu,CO$_2$), TS2(Cu,CO$_2$) and TS3(Cu,CO$_2$) are presented in Figures 5.17(a), (b) and (c), respectively. The atoms relating with the blowing reaction are focused as labeled in these Figures. Their charge values are summarized in Table 5.3. The partial charge transfer (Q_{PCT}) between the catalyst and their accelerated molecules (in e) is calculated using the same equation of gelling reaction as shown in the Figure 5.17. As expected, $[Cu(NH_3)_4]^{2+}$ also shows the Lewis acid characteristic for catalyzing the blowing reaction, which can withdraw electrons from the phenyl isocyanate reactant. In the case of blowing reaction, Q_{PCT} is transferred to $[Cu(NH_3)_4]^{2+}$ of -0.145, -0.149 and -0.140 e for TS1(Cu,CO$_2$), TS2(Cu,CO$_2$) and TS3(Cu,CO$_2$), respectively. These Q_{PCT} values are slightly less than that transferred to $[Cu(NH_3)_4]^{2+}$ in the case of gelling reaction (-0.155 e).
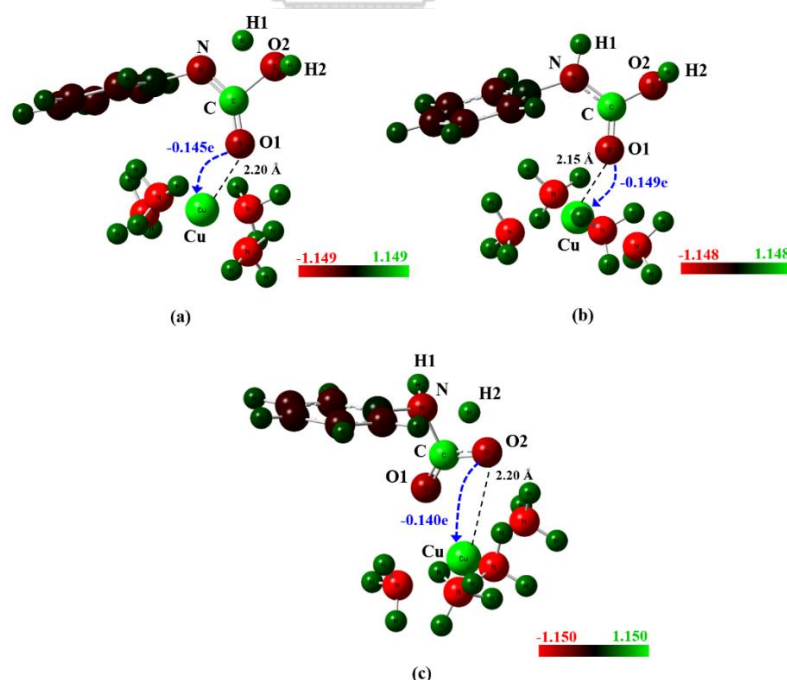
Figure 5.17 NBO atomic charges of (a) TS1(Cu,CO$_2$), (b) TS2(Cu,CO$_2$) and (c) TS3(Cu,CO$_2$) investigated at the transition states of blowing reaction.

Table 5.3 Selected NBO charges (in e) of the relating atoms around the reaction site of blowing reaction obtained using CAM–B3LYP/6–31G(d) level of theory.

Configurations	Cu	O1	C	N	O2	H1	H2
TS1(Cu,CO$_2$)	1.113	-0.715	0.933	-0.664	-0.759	0.568	0.560
TS2(Cu,CO$_2$)	1.111	-0.731	1.006	-0.646	-0.738	0.468	0. 540
TS3(Cu,CO$_2$)	1.101	-0.656	0.996	-0.759	-0.740	0.471	0. 544

5.2.3 Frontier molecular orbital (FMO) analysis for blowing reaction accelerated by [Cu(NH$_3$)$_4$]$^{2+}$

HOMO and LUMO orbital distributions of TS1(Cu,CO$_2$), TS2(Cu,CO$_2$) and TS3(Cu,CO$_2$) are shown in Figures 5.18(a), (b) and (c), respectively. The orbital distributions for the transition state configurations of blowing reaction are similar to those of the gelling reaction. The Homos are delocalized on the phenyl group and around the interacting site between activated phenyl isocyanate and H$_2$O, while their LUMOs are delocalized on [Cu(NH$_3$)$_4$]$^{2+}$ due to the Lewis acid nature of this catalyst.
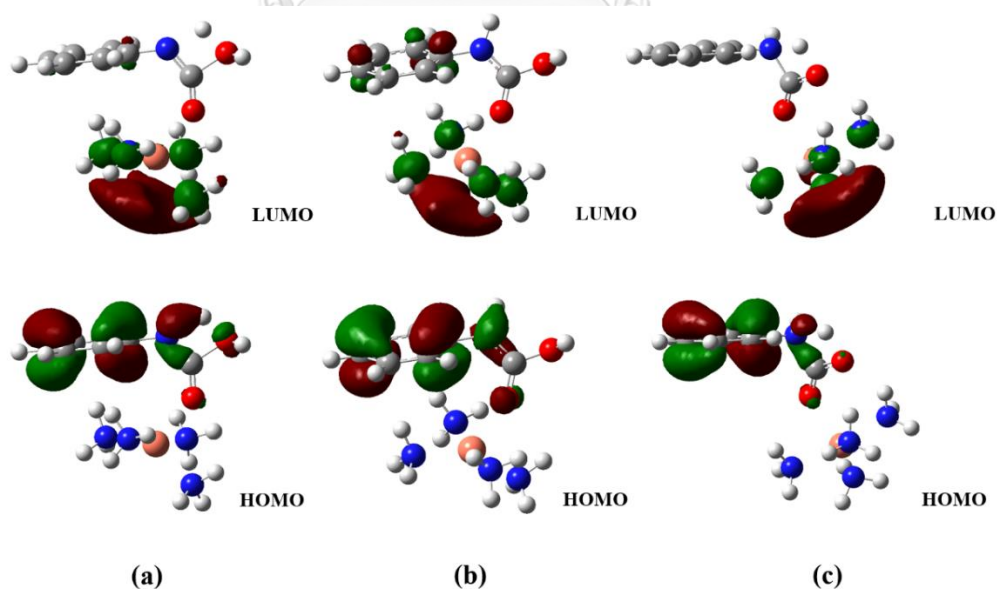
Figure 5.18 Frontier molecular orbitals of (a) TS1(Cu,CO$_2$), (b) TS2(Cu,CO$_2$) and (c) TS3(Cu,CO$_2$) investigated at the transition states of blowing reaction.

The calculated E_g ($\Delta E_{HOMO-LUMO}$) between LUMO of activated phenyl isocyanate and the HOMO of H_2O is shown in Figure 5.19(a) and compared to that of uncatalyzed blowing reaction as shown in Figure 5.19(b). This calculated E_g decreases from 10.443 eV of uncatalyzed blowing reaction to 3.479 eV with using $[Cu(NH_3)_4]^{2+}$ catalyst. In comparison to the gelling reaction catalyzed by $[Cu(NH_3)_4]^{2+}$, the E_g of blowing reaction is wider than that of the gelling reaction (2.671 eV). This result indicates that the reactivity of $[Cu(NH_3)_4]^{2+}$ in gelling reaction is better than that in the blowing reaction.
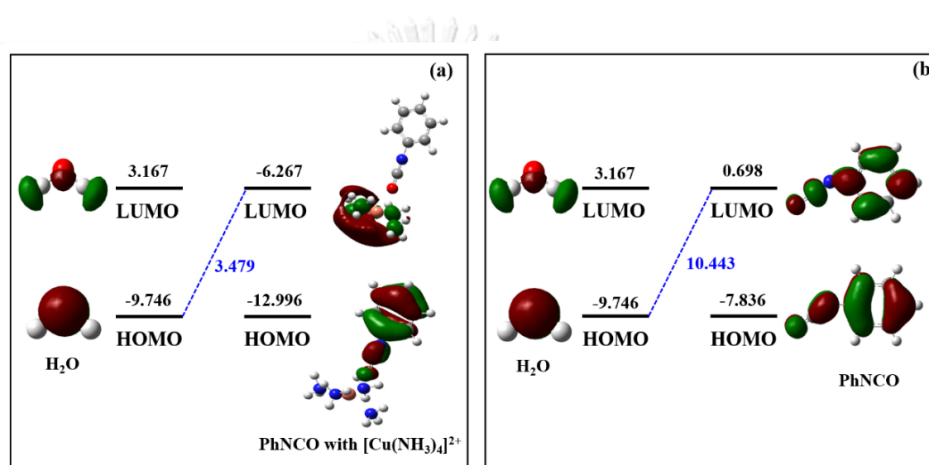
Figure 5.19 Frontier molecular orbitals of phenyl isocyanate and H_2O in the case of (a) $[Cu(NH_3)_4]^{2+}$-catalyzed and (b) uncatalyzed reactions. A unit of energy gab (E_g) is eV.

5.2.4 Thermodynamic and kinetic investigation of blowing reaction accelerated by $[Cu(NH_3)_4]^{2+}$

The potential energy profile of blowing reaction accelerated by $[Cu(NH_3)_4]^{2+}$ are presented in Figures 5.20. The reaction energies, thermodynamic properties, reaction rate constants and equilibrium constants are summarized in Table 5.4. The result of the potential energy profile reveals that the rate determining step for the blowing reaction accelerated by $[Cu(NH_3)_4]^{2+}$ is the step at which the rotated carbamic acid $[INT3'_{(Cu,CO_2)}]$ transforms to CO_2 and phenyl amine $[INT4'_{(Cu,CO_2)}]$ via the proton transfer transition state $[TS3(Cu,CO_2)]$. The reaction rate constant, the

equilibrium constant and the activation energy for this rate determining step of blowing reaction are 9.71×10^{-15} s^{-1}, 4.35×10^{-3} and 36.42 kcal/mol, respectively. The calculated reaction rate constant is rather low because our computational study of blowing model reaction was conducted at 298.15 K. However, the real temperature obtained from the reactions of rigid PUR foam catalyzed by $[Cu(NH_3)_4]^{2+}$ is 396.9 K. Therefore, the reaction rate constant for the real blowing reaction can increase with this higher temperature. In comparison to the gelling reaction catalyzed by the same catalyst, the blowing reaction show the lower reaction rate constant accompanying with the higher activation energy. This result points out that $[Cu(NH_3)_4]^{2+}$ can catalyze the gelling reaction better than the blowing reaction.

According to all data of computational study, it can be concluded that the results of experimental study are in good agreement with the results of computational study, which reveals that the metal-ammonia complex can catalyze the gelling reaction better than the blowing reaction. The catalytic mechanism of both gelling and blowing reaction can be obtained. However, only Lewis acid characteristic of catalyst can be confirmed by this computational study.
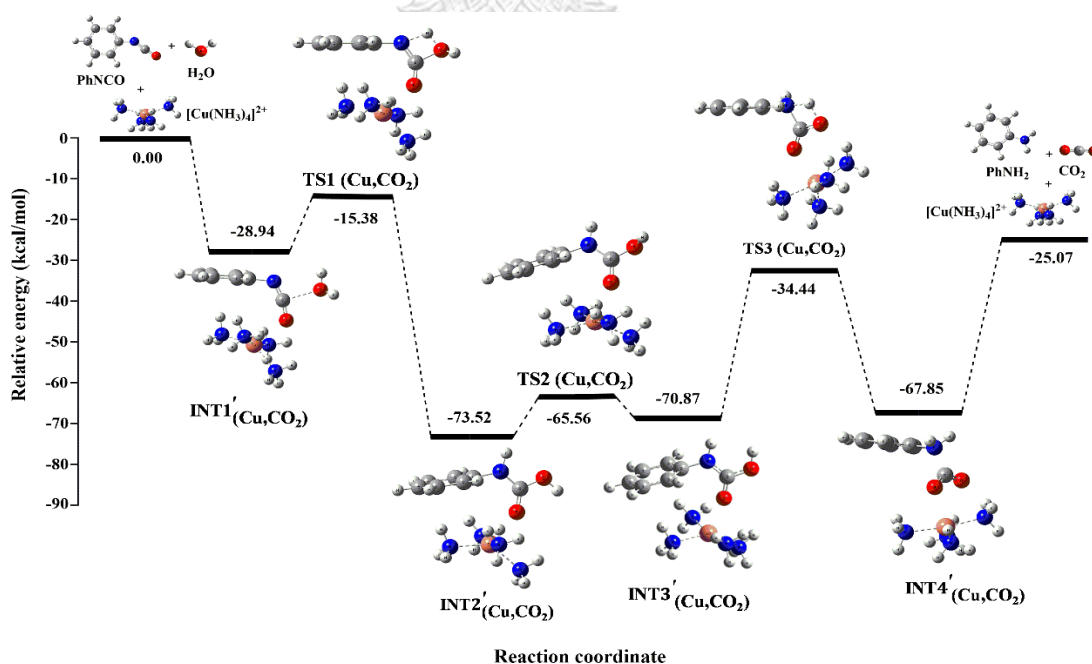
Figure 5.20 The potential energy profile for blowing reaction accelerated by $[Cu(NH_3)_4]^{2+}$.

Table 5.4 Activation energies, reaction energies, thermodynamic quantities, rate constants and equilibrium constants of blowing reaction accelerated by $[Cu(NH_3)_4]^{2+}$, computed at the CAM–B3LYP/6–31G(d) level of theory.

Reaction	$\Delta E^{\ddagger}$ [a,b]	$\Delta G^{\ddagger}$ [a,b]	k_{298} [c]	ΔE [a]	ΔH^{o}_{298} [a]	ΔG^{o}_{298} [a]	K_{298}
Blowing reaction (CO₂ generation):							
$[Cu(NH_3)_4]^{2+}$ catalyst:							
$PhNCO + H_2O + [Cu(NH_3)_4]^{2+} \rightarrow INT1'_{(Cu,CO_2)}$	-	-	-	-28.94	-28.88	-9.77	1.46×10^{7}
$INT1'_{(Cu,CO_2)} \rightarrow TS1(Cu,CO_2) \rightarrow INT2'_{(Cu,CO_2)}$	13.56	16.82	2.90×10^{0}	-44.57	-45.72	-42.88	2.74×10^{31}
$INT2'_{(Cu,CO_2)} \rightarrow TS2(Cu,CO_2) \rightarrow INT3'_{(Cu,CO_2)}$	7.95	9.36	8.57×10^{5}	2.65	2.71	3.33	3.61×10^{-3}
$INT3'_{(Cu,CO_2)} \rightarrow TS3(Cu,CO_2) \rightarrow INT4'_{(Cu,CO_2)}$	36.42	36.57	9.71×10^{-15}	3.01	2.66	3.22	4.35×10^{-3}
$INT4'_{(Cu,CO_2)} \rightarrow CO_2 + PhNH_2 + [Cu(NH_3)_4]^{2+}$	-	-	-	42.78	43.21	21.18	2.99×10^{-16}

[a] In kcal/mol.

[b] Activation energy.

[c] In s⁻¹.
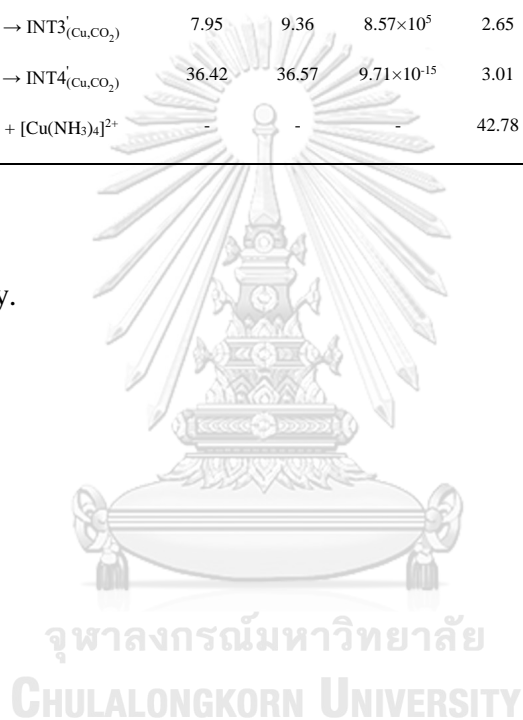
CHAPTER 6

CONCLUSIONS

The conclusions of all experiment and computational parts are as follows:

6.1 Synthesis and characterization of metal-ammonia complex solutions

Copper- and Zinc-ammonia complexes, namely Cu(Amm) and Zn(Amm), respectively, were synthesized using water as a solvent in order to yield the solution form of these metal complexes, which could be utilized as the homogeneous catalysts for the processing of rigid PUR and PIR foams. According to the catalyst synthesis, the metal acetate [$Cu(OAc)_2$ and $Zn(OAc)_2$] could *in situ* coordinate with NH_3 in water with the optimum mole ratio of metal acetate:NH_3 of 1:6. Cu(Amm) and Zn(Amm) solutions could be characterized by MALDI-TOF mass spectrometry and UV-visible spectroscopy, which indicated that the main structures of metal complex were [$Cu(NH_3)_4(H_2O)_2$]($OAc)_2$ and [$Zn(NH_3)_4(H_2O)_2$]($OAc)_2$. Density functional theory (DFT) calculations at B3LYP/6-311+g(d,p) level of theory confirmed that these structures were the most stable species of the metal complex in water.

6.2 Preparation of rigid PUR foams using metal-ammonia complexes as catalysts

Cu(Amm) and Zn(Amm) could be homogeneously mixed with all reactants of the foam. Cu(Amm) and Zn(Amm) showed adequately catalytic activity toward both gelling and blowing reactions in comparison to DMCHA (the industrial catalyst). Zn(Amm) slightly had lower catalytic activity than DMCHA, whilst Cu(Amm) showed higher catalytic activity than DMCHA. The coordinated structures were necessary for copper-based and zinc-based catalysts in this work since the metal acetates without the complex structures showed very poor catalytic activity. H_2O merely existed as a solvent in catalyst solutions, but did not interfere the catalytic activity of metal-ammonia complexes. Both Cu(Amm) and Zn(Amm) showed the

characteristic of catalyst, which could obviously decrease the reaction time of the foams with increasing catalyst contents. The optimum catalyst content for processing of rigid PUR foam is 1.0 pbw. Density of rigid PUR foams obtained from Cu(Amm) and Zn(Amm) was comparable to that of DMCHA. More than 98% of isocyanate conversion of rigid PUR foam could be obtained with using Cu(Amm) and Zn(Amm) catalysts. The reactions of rigid PUR foams were exothermic reactions, which gave the maximum core temperature of the foam in the range of 123.8-127.8 $^{\circ}$C. All rigid PUR foams composed of close cells, which had dissimilar morphology in different foam-rising direction. The compression strength of rigid PUR foams in the same to foam-rising direction was higher than that in the opposite to foam-rising direction. This probably related to the dissimilar morphology of foam in different foam-rising direction. The compression strength of the foams decreased when using higher water content in foam formulation. The prepared rigid PUR foams using Cu(Amm) and Zn(Amm) as the catalysts had suitable dimensional stability that was in the range of commercial standard.

6.3 Preparation of PIR foam using the mixtures of potassium octoate with metal-ammonia complexes as catalysts

Cu(Amm) and Zn(Amm) solutions were completely soluble with potassium octoate solution in diethylene glycol (the trimerization catalyst) and could be used as co-catalysts for accelerating the urethane formation and CO_2 production of PIR foam. Their catalytic activity was compared to the mixture of potassium octoate with DMCHA, which was the industrial catalyst system. PIR foams prepared by the mixtures of potassium octoate with Cu(Amm) or Zn(Amm) showed shorter reaction time than their relating rigid PUR foams. However, PIR foams obtained from the mixture of potassium octoate with DMCHA showed longer gel time than their relating rigid PUR foam. This result indicated the partial loss of catalytic activity for gelling reaction of DMCHA when used in PIR foam system. Higher isocyanate index increased PIR/PUR proportions, but decreased % isocyanate conversion. However, all catalyst mixtures gave >90% of isocyanate conversion at the highest isocyanate index of 250. The PIR foam processed by the mixture of potassium octoate with Cu(Amm)

had similar fire-retarded properties to that processed by mixture of potassium octoate with DMCHA, but showed better compression properties which did not rupture with the compression force. All prepared PIR foams showed better compression properties, fire-retarded properties as well as thermal stability in comparison to rigid PUR foams.

6.4 Theoretical study of catalytic properties of metal-ammonia complexes in gelling and blowing reactions

The reaction mechanism for gelling and blowing reactions accelerated by Cu(Amm) and Zn(Amm) could be obtained by theoretical study using DFT calculations at CAM–B3LYP/6–31G(d) level of theory. The reaction pathway of catalyzed gelling reaction composed of four reaction steps and three configurations, while reaction pathway of catalyzed blowing reaction composed of eight reaction steps and seven configurations. The blowing reaction pathway was more complex than the gelling reaction and had three transition states of the reaction. NBO analysis confirmed that Cu(Amm) and Zn(Amm) showed the Lewis acid characteristic in the catalysis, which could withdraw the electron from their activated isocyanate compounds resulting in more electrophilic carbon of isocyanate compound. FMO analysis indicated that the energy gab between the reactants of both gelling and blowing reactios decreased with using Cu(Amm) and Zn(Amm) catalysts. Thermodynamic and kinetic investigation revealed that the reaction rate constant increased, while the activation energy of the reactions decreased with using Cu(Amm) and Zn(Amm) catalysts. This could prove the catalytic activity of Cu(Amm) and Zn(Amm) catalysts in gelling and blowing reactions. The results of experimental study are in good agreement with the results of computational study, which reveals that the metal-ammonia complexes can catalyze the gelling reaction better than the blowing reaction. However, only Lewis acid characteristic of catalyst in the proposed catalytic mechanism can be confirmed by the computational study.

In summary, the advantages of Cu(Amm) and Zn(Amm) solutions in the processing of rigid PUR and PIR foams are as follows: The catalytic mechanism of these catalysts in gelling and blowing reactions is known. These catalysts were obtained in the form of aqueous solution which was homogeneous and could be

applied for the foam processing without purifying step. H_2O solvent in the catalyst solutions was able to blow both rigid PUR and PIR foams. This gave more convenient procedure for the foam processing and showed the potential to reduce the use of hydrochlorofluorocarbons (HCFCs), which is the physical blowing agent of the foams and can cause ozone depletion. Both Cu(Amm) and Zn(Amm) solutions had much weaker odor than the DMCHA industrial catalyst and could improve the working environment in the foam processing. The catalytic activity in gelling and blowing reactions of these catalysts was enough resulting in rigid PUR and PIR foams with good properties.

6.5 Suggestion for future work

The other compounds of transition metal, namely $Mn(acac)_2$, $Fe(acac)_3$, $FeCl_3$ and $Zr(acac)_4$, may be further studied for using instead of $Cu(OAc)_2$ and $Zn(OAc)_2$ in the synthesis of metal-ammonia complexes in order to obtain more variety of the catalytic activity of catalyst.
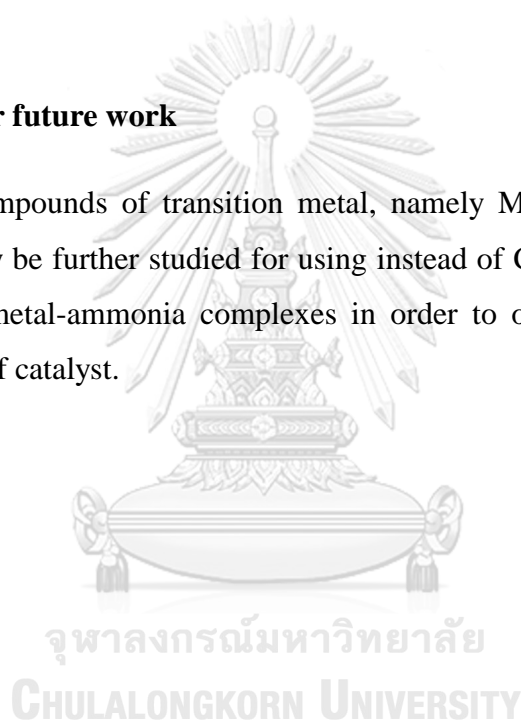
REFERENCES

1. Gao L, Zheng G, Zhou Y, Hu L, Feng G, Zhang M. Synergistic effect of expandable graphite, diethyl ethylphosphonate and organically-modified layered double hydroxide on flame retardancy and fire behavior of polyisocyanurate-polyurethane foam nanocomposite. Polym Degrad Stab. 2014;101:92-101.

2. Naruse A, Nanno H, Kurita M, Inohara H, Fukami T. Development of all water-blown polyisocyanurate foam system for metal-faced continuous sandwich panels. J Cell Plast. 2002;38(5):385-401.

3. Okuzono S, Tokumoto K, Tamano Y, Lowe DW. New polyisocyanurate catalysts which exhibit high activity at low temperature. J Cell Plast. 2001;37(1):72-89.

4. Ashida K. Polyurethane and related foams: chemistry and technology. New York: CRC press; 2006.

5. Chattopadhyay D, Webster DC. Thermal stability and flame retardancy of polyurethanes. Prog Polym Sci. 2009;34(10):1068-133.

6. Singh H, Jain A. Ignition, combustion, toxicity, and fire retardancy of polyurethane foams: a comprehensive review. J Appl Polym Sci. 2009;111(2):1115-43.

7. Cear S, Feltzin J, Baldino JP. Polyisocyanurate foams having low friability and flame spread. J Cell Plast. 1977;13(1):21-5.

8. Randall D, Lee S, editors. Huntsman polyurethanes – the polyurethanes book. United Kingdom: John Wiley & Sons; 2002.

9. Maris RV, Tamano Y, Yoshimura H, Gay KM. Polyurethane catalysis by tertiary amines. J Cell Plast. 2005;41(4):305-22.

10. Silva AL, Bordado JC. Recent developments in polyurethane catalysis: catalytic mechanisms review. Catal Rev. 2004;46(1):31-51.

11. Lövenich CJ, Raffel B. A quantitative investigation of the effect of the recipe on the trimer-yield in polyisocyanurate foams. J Cell Plast. 2006;42(4):289-305.

12. Modesti M, Lorenzetti A. Flame retardancy of polyisocyanurate–polyurethane foams: use of different charring agents. Polym Degrad Stab.

2002;78(2):341-7.

13. Góral M, Shaw DG, Mączyński A, Wiśniewska-Gocłowska B, Oracz P. IUPAC-NIST solubility data series. 96. Amines with water part 2. C_7–C_{24} aliphatic amines. J Phys Chem Ref Data. 2012;41(4):043107.

14. Strachota A, Strachotová B, Špírková M. Comparison of environmentally friendly, selective polyurethane catalysts. Materials and Manufacturing Processes. 2008;23(6):566-70.

15. Wegener G, Brandt M, Duda L, Hofmann J, Kleszczewski B, Koch D, Kumpf R-J, Orzesek H, Pirkl H-G, Six C, Steinlein C, Weisbeck M. Trends in industrial catalysis in the polyurethane industry. Applied Catalysis A: General. 2001;221(1):303-35.

16. Dworakowska S, Bogdał D, Zaccheria F, Ravasio N. The role of catalysis in the synthesis of polyurethane foams based on renewable raw materials. Catalysis Today. 2014;223:148-56.

17. Sardon H, Pascual A, Mecerreyes D, Taton D, Cramail H, Hedrick JL. Synthesis of polyurethanes using organocatalysis: a perspective. Macromolecules. 2015;48(10):3153-65.

18. Blank WJ, He ZA, Hessell ET. Catalysis of the isocyanate-hydroxyl reaction by non-tin catalysts. Prog Org Coat. 1999;35(1):19-29.

19. Cakic SM, Stamenkovic JV, Djordjevic DM, Ristic IS. Synthesis and degradation profile of cast films of PPG-DMPA-IPDI aqueous polyurethane dispersions based on selective catalysts. Polym Degrad Stab. 2009;94(11):2015-22.

20. Inoue S, Nagai Y, Okamoto H. Amine-manganese complex as an efficient catalyst for polyurethane syntheses. Polym J. 2002;34(4):298-301.

21. Liao A, Qiao L, He R, Lan P, Lan L, Lu Y, Li M. $NdCl_3$-schiff base complex as catalyst for formation of water-blown semi-rigid polyurethane foam. Asian J Chem. 2015;27(9):3361-4.

22. Meskinfam M, Bertoldi S, Albanese N, Cerri A, Tanzi M, Imani R, Baheiraei N, Farokhi M, Fare S. Polyurethane foam/nano hydroxyapatite composite as a suitable scaffold for bone tissue regeneration. Mater Sci Eng C. 2018;82:130-40.

23.   Belmokaddem F-Z, Dagonneau J, Lhomme J, Blanc R, Garduno-Alva A, Maliverney C, Baceiredo A, Maerten E, Fleury E, Méchin F. Novel nucleophilic/basic and acidic organocatalysts for reaction between poorly reactive diisocyanate and diols. Des Monomers Polym. 2016;19(4):347-60.

24.   Pengjam W, Saengfak B, Ekgasit S, Chantarasiri N. Copper–amine complexes as new catalysts for rigid polyurethane foam preparations. J Appl Polym Sci. 2012;123(6):3520-6.

25.   Sridaeng D, Jitaree W, Thiampanya P, Chantarasiri N. Preparation of rigid polyurethane foams using low-emission catalysts derived from metal acetates and ethanolamine. e-Polymers. 2016;16(4):265-75.

26.   Kauffman GB. Eduard Schweizer (1818-1860): the unknown chemist and his well-known reagent. J Chem Educ. 1984;61(12):1095-7.

27.   Chen J, Wu X, Gong Y, Wang P, Li W, Mo S, Peng S, Tan Q, Chen Y. General synthesis of transition-metal oxide hollow nanospheres/nitrogen-doped graphene hybrids by metal–ammine complex chemistry for high-performance lithium-ion batteries. Chem Eur J. 2018;24(9):2126-36.

28.   Armbruster T, Simoncic P, Döbelin N, Malsy A, Yang P. Cu^{2+}-acetate and Cu^{2+}-ammine exchanged heulandite: a structural comparison. Micropor Mesopor Mater. 2003;57(2):121-31.

29.   Yashnik S, Ismagilov Z. Cu-substituted ZSM-5 catalyst: controlling of DeNOx reactivity via ion-exchange mode with copper–ammonia solution. Appl Catal B. 2015;170:241-54.

30.   Zhang Q, Peng R, Zhang C, Chen D, Lin Z, Chang J, Zhang J, Hao Y. Inverted organic solar cells with low-temperature Al-doped-ZnO electron transport layer processed from aqueous solution. Polymers. 2018;10(2):127.

31.   Park SY, Kim S, Yoo J, Lim K-H, Lee E, Kim K, Kim J, Kim YS. Aqueous zinc ammine complex for solution-processed ZnO semiconductors in thin film transistors. RSC Adv. 2014;4(22):11295-9.

32.   Woods G. The ICI polyurethane handbook. 2nd ed. New York: John Wiley & Sons; 1990.

33.   Nicholas L, Gmitter GT. Heat resistant rigid foams by trimerization of

isocyanate terminated prepolymers. J Cell Plast. 1965;1(1):85-90.

34. Szycher M. Szycher's handbook of polyurethanes. 2nd ed. Florida: CRC press; 2012.

35. Park DH, Park GP, Kim SH, Kim WN. Effects of isocyanate index and environmentally-friendly blowing agents on the morphological, mechanical, and thermal insulating properties of polyisocyanurate-polyurethane foams. Macromol Res. 2013;21(8):852-9.

36. Oertel G. Polyurethane handbook: chemistry, raw materials, processing, application. New York: Macmillan Publishing Co. Inc.; 1985.

37. Akindoyo JO, Beg M, Ghazali S, Islam M, Jeyaratnam N, Yuvaraj A. Polyurethane types, synthesis and applications–a review. RSC Adv. 2016;6(115):114453-82.

38. Modesti M, Lorenzetti A. An experimental method for evaluating isocyanate conversion and trimer formation in polyisocyanate–polyurethane foams. Eur Polym J. 2001;37(5):949-54.

39. Kalaimani S, Nasar AS. Catalysis of deblocking and cure reactions of easily cleavable phenol blocked polyisocyanates with poly(polytetrahydrofuran carbonate) diol. Eur Polym J. 2017;91:221-31.

40. Strachota A, Strachotova B, Špírková M. Comparison of environmentally friendly, selective polyurethane catalysts. Mater Manuf Process. 2008;23(6):566-70.

41. Tarasov DN, Tiger RP, Chirkov YN, Entelis SG, Tondeur J-J. Molecular organization of reactants in the kinetics and catalysis of liquid phase reactions: X. Synergism in the combined catalysis of urethane formation by organotin compounds and tertiary amines. Kinetics and Catalysis. 2000;41(3):355-8.

42. Kim SH, Lim H, Song JC, Kim BK. Effect of blowing agent type in rigid polyurethane foam. J Macromol Sci A. 2008;45(4):323-7.

43. Weil ED, Levchik SV. Commercial flame retardancy of polyurethanes. J Fire Sci. 2004;22(3):183-210.

44. Han MS, Choi SJ, Kim JM, Kim YH, Kim WN, Lee HS, Sung JY. Effects of silicone surfactant on the cell size and thermal conductivity of rigid polyurethane

foams by environmentally friendly blowing agents. Macromol Res. 2009;17(1):44-50.

45.   Chen M-J, Chen C-R, Tan Y, Huang J-Q, Wang X-L, Chen L, Wang Y-Z. Inherently flame-retardant flexible polyurethane foam with low content of phosphorus-containing cross-linking agent. Ind Eng Chem Res. 2014;53(3):1160-71.

46.   Pentrakoon D, Ellis JW. An introduction to plastic foams. Bangkok: Chulalongkorn University Press; 2005.

47.   Pengjam W. Preparation of rigid polyurethane foam catalyzed by Cu-amine and Mn-amine complexes [Thesis]. Bangkok: Chulalongkorn University; 2010.

48.   Finkel E. Quantum chemistry. 3rd ed. New York: Allyn and Bacon; 1985.

49.   Schellekens Y, Van Trimpont B, Goelen P-J, Binnemans K, Smet M, Persoons M-A, De Vos D. Tin-free catalysts for the production of aliphatic thermoplastic polyurethanes. Green Chem. 2014;16(9):4401-7.

50.   Sardon H, Engler AC, Chan JM, García JM, Coady DJ, Pascual A, Mecerreyes D, Jones GO, Rice JE, Horn HW. Organic acid-catalyzed polyurethane formation via a dual-activated mechanism: unexpected preference of N-activation over O-activation of isocyanates. J Am Chem Soc. 2013;135(43):16235-41.

51.   Alsarraf J, Ammar YA, Robert F, Cloutet E, Cramail H, Landais Y. Cyclic guanidines as efficient organocatalysts for the synthesis of polyurethanes. Macromolecules. 2012;45(5):2249-56.

52.   Xu Q, Hong T, Zhou Z, Gao J, Xue L. The effect of the trimerization catalyst on the thermal stability and the fire performance of the polyisocyanurate-polyurethane foam. Fire Mater. 2018;42(1):119-27.

53.   Hathaway BJ, Tomlinson AAG. Copper(II) ammonia complexes. Coord Chem Rev. 1970;5(1):1-43.

54.   Bjerrum J. On the tendency of the metal ions toward complex formation. Chem Rev. 1950;46(2):381-401.

55.   Vazquez-Arenas J, Lazaro I, Cruz R. Electrochemical study of binary and

ternary copper complexes in ammonia-chloride medium. Electrochim Acta. 2007;52(20):6106-17.

56. Fan D, Zhou Q, Lv X, Jing J, Ye Z, Shao S, Xie J. Synthesis, thermal conductivity and anti-oxidation properties of copper nanoparticles encapsulated within few-layer h-BN. Ceram Int. 2018;44(1):1205-8.

57. Çoban M, Konuklar FAS. A computational study on the mechanism and the kinetics of urethane formation. Comput Theor Chem. 2011;963(1):168-75.

58. Lu M-Y, Surányi A, Viskolcz B, Fiser B. Molecular design of sugar-based polyurethanes. Croat Chem Acta. 2018;91(3):1-9.

59. Samuilov AY, Balabanova F, Kamalov T, Samuilov YD, Konovalov A. Quantum-chemical study on reactions of isocyanates with linear methanol associates: III.* reaction of methyl isocyanate with linear methanol associates. Russ J Org Chem. 2010;46(10):1452-60.

60. Wang X, Hu W, Gui D, Chi X, Wang M, Tian D, Liu J, Ma X, Pang A. DFT study of the proton transfer in the urethane formation between 2, 4-diisocyanatotoluene and methanol. Bull Chem Soc Jpn. 2013;86(2):255-65.

61. Zhao Y, Suppes GJ. Computational study on reaction enthalpies of urethane-forming reactions. Polym Eng Sci. 2015;55(6):1420-8.

62. Devendra R, Edmonds NR, Söhnel T. Organotin carboxylate catalyst in urethane formation in a polar solvent: an experimental and computational study. RSC Adv. 2015;5(60):48935-45.

63. Devendra R, Edmonds NR, Söhnel T. Insight into the mechanism of the catalysis of urethane formation by organotin(IV) dicarboxylate. Reac Kinet Mech Cat. 2018;124(2):487-502.

64. Hatanaka M. DFT analysis of catalytic urethanation. Bull Chem Soc Jpn. 2011;84(9):933-5.

65. Sridaeng D, Sukkaneewat B, Chueasakol N, Chantarasiri N. Copper-amine complex solution as a low-emission catalyst for flexible polyurethane foam preparation. e-Polymers. 2015;15(2):119-26.

66. Baghban SA, Khorasani M, Sadeghi GMM. Acoustic damping flexible polyurethane foams: effect of isocyanate index and water content on the

soundproofing. J Appl Polym Sci. 2019;136(15):47363.

67. Davletbaeva IM, Zaripov II, Davletbaev RS, Balabanova FB. Polyurethanes based on anionic macroinitiators, aromatic isocyanates, and 4,4′-dihydroxy-2,2-diphenylpropane. Russ J Appl Chem. 2014;87(4):468-73.

68. Chaffanjon P, Grisgby RA, Rister EL, Zimmerman RL. Use of real-time FTIR to characterize kinetics of amine catalysts and to develop new grades for various polyurethane applications, including low emission catalysts. J Cell Plast. 2003;39(3):187-210.

69. Gosz K, Haponiuk J, Piszczyk Ł. The influence of substitution of a phosphorus-containing polyol with the bio-polyol on the properties of bio-based PUR/PIR foams. J Polym Environ. 2018;26(9):3877-88.

70. Frisch MJ, et al. Gaussian 09, Revision D.01. Wallingford, CT: Gaussian, Inc.; 2014.

71. Becke AD. Density-functional thermochemistry. III. The role of exact exchange. The Journal of Chemical Physics. 1993;98(7):5648-52.

72. Lee C, Yang W, Parr RG. Development of the Colle-Salvetti correlation-energy formula into a functional of the electron density. Physical Review B. 1988;37(2):785-9.

73. Yanai T, Tew DP, Handy NC. A new hybrid exchange–correlation functional using the coulomb-attenuating method (CAM-B3LYP). Chem Phys Lett. 2004;393(1):51-7.

74. Hehre WJ, Ditchfield K, Pople JA. Self-consistent molecular orbital methods. XII. Further extensions of gaussian-type basis sets for use in molecular orbital studies of organic molecules. The Journal of Chemical Physics. 1972;56(5):2257-61.

75. Yasarawan N, Thipyapong K, Ruangpornvisuti V. Exploring molecular structures, orbital interactions, intramolecular proton-transfer reaction kinetics, electronic transitions and complexation of 3-hydroxycoumarin species using DFT methods. J Mol Graph Model. 2014;51:13-26.

76. Gonzalez C, Schlegel HB. An improved algorithm for reaction path following. J Chem Phys. 1989;90(4):2154-61.

77.   Reed AE, Weinhold F. Natural bond orbital analysis of near-Hartree–Fock water dimer. J Chem Phys. 1983;78(6):4066-73.

78.   Foster JP, Weinhold F. Natural hybrid orbitals. J Am Chem Soc. 1980;102(24):7211-8.

79.   Bravo-Pérez G, Alvarez-Idaboy JR, Cruz-Torres A, Ruíz ME. Quantum chemical and conventional transition-state theory calculations of rate constants for the NO_3 + alkane reaction. J Phys Chem A. 2002;106(18):4645-50.

80.   Ruangpornvisuti V. A DFT study of transformation of nitrosothiol isomers and their decomposition to nitric oxide in gas phase. Int J Quantum Chem. 2009;109(2):275-84.

81.   Martell AE. The behavior of metal complexes in aqueous solutions. J Chem Educ. 1952;29(6):270.

82.   Yamaguchi T, Ohtaki H. X-Ray diffraction studies on the structures of tetra- and higher-ammine complexes of copper(II) ion in aqueous solution. Bull Chem Soc Jpn. 1979;52(2):415-9.

83.   Pavelka M, Burda JV. Theoretical description of copper Cu (I)/Cu (II) complexes in mixed ammine-aqua environment. DFT and ab initio quantum chemical study. Chem Phys. 2005;312(1-3):193-204.

84.   Bérces A, Nukada T, Margl P, Ziegler T. Solvation of Cu^{2+} in water and ammonia. Insight from static and dynamical density functional theory. J Phys Chem A. 1999;103(48):9693-701.

85.   Trevani LN, Roberts JC, Tremaine PR. Copper(II)–ammonia complexation equilibria in aqueous solutions at temperatures from 30 to 250°C by visible spectroscopy. J Sol Chem. 2001;30(7):585-622.

86.   Singh H, Sharma TP, Jain AK. Reactivity of the raw materials and their effects on the structure and properties of rigid polyurethane foams. J Appl Polym Sci. 2007;106(2):1014-23.

87.   Mondal P, Khakhar DV. Hydraulic resistance of rigid polyurethane foams. III. Effect of variation of the concentration of catalysts on foam structure and properties. J Appl Polym Sci. 2004;93(6):2838-43.

88.   Sung G, Kim JW, Kim JH. Fabrication of polyurethane composite foams with

magnesium hydroxide filler for improved sound absorption. J Ind Eng Chem. 2016;44:99-104.

89. Yan Y, Pang H, Yang X, Zhang R, Liao B. Preparation and characterization of water-blown polyurethane foams from liquefied cornstalk polyol. J Appl Polym Sci. 2008;110(2):1099-111.

90. Barman S, Parasar B, Kundu P, Roy S. A copper based catalyst for poly-urethane synthesis from discarded motherboard. RSC Adv. 2016;6(79):75749-56.

91. Sardon H, Irusta L, Fernández-Berridi M. Synthesis of isophorone diisocyanate (IPDI) based waterborne polyurethanes: comparison between zirconium and tin catalysts in the polymerization process. Prog Org Coat. 2009;66(3):291-5.

92. Sridaeng D, Limsirinawa A, Sirojpornphasut P, Chawiwannakorn S, Chantarasiri N. Metal acetylacetonate–amine and metal nitrate–amine complexes as low-emission catalysts for rigid polyurethane foam preparation. J Appl Polym Sci. 2015;132(31).

93. Thirumal M, Khastgir D, Singha NK, Manjunath BS, Naik YP. Effect of foam density on the properties of water blown rigid polyurethane foam. J Appl Polym Sci. 2008;108(3):1810-7.

94. Seo WJ, Jung HC, Hyun JC, Kim WN, Lee Y-B, Choe KH, Kim S-B. Mechanical, morphological, and thermal properties of rigid polyurethane foams blown by distilled water. J Appl Polym Sci. 2003;90(1):12-21.

95. Zhu M, Bandyopadhyay-Ghosh S, Khazabi M, Cai H, Correa C, Sain M. Reinforcement of soy polyol-based rigid polyurethane foams by cellulose microfibers and nanoclays. J Appl Polym Sci. 2012;124(6):4702-10.

96. Gwon JG, Kim SK, Kim JH. Development of cell morphologies in manufacturing flexible polyurethane urea foams as sound absorption materials. J Porous Mater. 2016;23(2):465-73.

97. Kraitape N, Thongpin C. Influence of recycled polyurethane polyol on the properties of flexible polyurethane foams. Energy Proc. 2016;89:186-97.

98. Seo WJ, Jung HC, Hyun JC, Kim WN, Lee YB, Choe KH, Kim SB. Mechanical, morphological, and thermal properties of rigid polyurethane foams blown by

distilled water. J Appl Polym Sci. 2003;90(1):12-21.

99. Lin Y, Hsieh F, Huff HE, Iannotti E. Physical, mechanical, and thermal properties of water-blown rigid polyurethane foam containing soy protein isolate. Cereal Chem. 1996;73(2):189-96.

100. Septevani AA, Evans DA, Chaleat C, Martin DJ, Annamalai PK. A systematic study substituting polyether polyol with palm kernel oil based polyester polyol in rigid polyurethane foam. Ind Crops Prod. 2015;66:16-26.

101. Ji D, Fang Z, He W, Luo Z, Jiang X, Wang T, Guo K. Polyurethane rigid foams formed from different soy-based polyols by the ring opening of epoxidised soybean oil with methanol, phenol, and cyclohexanol. Ind Crops Prod. 2015;74:76-82.

102. Marcovich N, Kurańska M, Prociak A, Malewska E, Kulpa K. Open cell semi-rigid polyurethane foams synthesized using palm oil-based bio-polyol. Ind Crops Prod. 2017;102:88-96.

103. Badri KH, Othman ZB, Razali IM. Mechanical properties of poyurethane composites from oil palm resources. Iran Polym J. 2005;14(5): 441-8.

104. Kim SH, Kim BK, Lim H. Effect of isocyanate index on the properties of rigid polyurethane foams blown by HFC 365mfc. Macromol Res. 2008;16(5):467-72.

105. Lim H, Kim SH, Kim BK. Effects of the hydroxyl value of polyol in rigid polyurethane foams. Polymers for Advanced Technologies. 2008;19(12):1729-34.

106. Li X, Cao H, Zhang Y. Structures and physical properties of rigid polyurethane foams with water as the sole blowing agent. Sci China Ser B. 2006;49(4):363-70.

107. Long Y, Sun F, Liu C, Xie X. A family of polypropylene glycol-grafted polyethyleneimines reversibly absorb and release carbon dioxide to blow polyurethanes. RSC Adv. 2016;6(28):23726-36.

108. Łukasiewicz B, Lubczak J. Polyurethane foams with purine ring and boron. J Cell Plast. 2014;50(4):337-59.

109. Carleton PS, Lockwood RJ, Reymore JHE, inventorsPolyisocyanate-based foam process using aminimides as catalyst patent 3,925,284. 1975.

110. Dusek K, Spirkova M, Havlicek I. Network formation of polyurethanes due to side reactions. Macromolecules. 1990;23(6):1774-81.

111. Hakim AA, Nassar M, Emam A, Sultan M. Preparation and characterization of rigid polyurethane foam prepared from sugar-cane bagasse polyol. Mater Chem Phys. 2011;129(1-2):301-7.

112. Nacas AM, Ito NM, Sousa RRD, Spinacé MA, Dos Santos DJ. Effects of NCO:OH ratio on the mechanical properties and chemical structure of Kraft lignin–based polyurethane adhesive. J Adhes. 2017;93(1-2):18-29.

113. Shi L, Li ZM, Xie BH, Wang JH, Tian CR, Yang MB. Flame retardancy of different-sized expandable graphite particles for high-density rigid polyurethane foams. Polym Int. 2006;55(8):862-71.

114. Zhang C, Bhoyate S, Ionescu M, Kahol PK, Gupta RK. Highly flame retardant and bio-based rigid polyurethane foams derived from orange peel oil. Polym Eng Sci. 2018;58(11):2078-87.

115. Mondal P, Khakhar D. Hydraulic resistance of rigid polyurethane foams. III. Effect of variation of the concentration of catalysts on foam structure and properties. J Appl Polym Sci. 2004;93(6):2838-43.

116. Chuayjuljit S, Maungchareon A, Saravari O. Preparation and properties of palm oil-based rigid polyurethane nanocomposite foams. J Reinf Plast Compos. 2010;29(2):218-25.

117. Paruzel A, Michałowski S, Hodan J, Horák P, Prociak A, Beneš H. Rigid polyurethane foam fabrication using medium chain glycerides of coconut oil and plastics from end-of-life vehicles. ACS Sustain Chem Eng. 2017;5(7):6237-46.

118. Zhang P, Tian S, Fan H, Chen Y, Yan J. Flame retardancy and hydrolysis resistance of waterborne polyurethane bearing organophosphate moieties lateral chain. Prog Org Coat. 2015;89:170-80.

119. Horowitz HH, Metzger G. A new analysis of thermogravimetric traces. Anal Chem. 1963;35(10):1464-8.

120. Samuilov AY, Zenitova L, Samuilov YD, Konovalov A. Quantum-chemical study on the reaction of phenyl isocyanate with linear methanol associates. Addition at the C= N bond. Russ J Org Chem. 2008;44(9):1316-22.

121. Zhao Y, Gordon MJ, Tekeei A, Hsieh F-H, Suppes GJ. Modeling reaction kinetics of rigid polyurethane foaming process. J Appl Polym Sci. 2013;130(2):1131-8.

APPENDICES

APPENDIX A

CALCULATIONS OF ISOCYANATE INDEX AND
ISOCYANATE CONVERSION

Isocyanate index calculation

The calculation of isocyanate index of 100 (for rigid PUR foams), 160, 200 and 250 (for PIR foams) requires the data of isocyanate compound and the reactive starting materials, which can react with the isocyanate compound, as follows:

- PMDI (B9001[®], molecular weight = 365.8, functionality = 2.7)
- Polyol (Polimaxx[®]4221, OH value = 440 mg KOH/g, functionality = 4.3)
- Blowing agent (water, molecular weight = 18.0 g/mole, functionality = 2)
- Solvent of trimerization catalyst (diethylene glycol molecular weight = 106.1 g/mole, functionality = 2

The chemical amount of each compound in foam formulation used for the calculation is presented in Table A1.

Table A1 Chemical content (pbw) of reactive compounds in foam formulations used for isocyanate calculation.

Chemicals	Rigid PUR foams	PIR foams		
Polyol	100.0	100.0	100.0	100.0
Diethylene glycol solvent in 70%wt potassium octoate solution (3.0 pbw)	-	0.9	0.9	0.9
Silicone surfactant	2.5	2.5	2.5	2.5
Water	4.0	4.0	4.0	4.0
Isocyanate index	100	160	200	250
PMDI	?	?	?	?

The example of the calculation can be shown as follows:

$$\text{Equivalent weight of polyol} = \frac{56.1}{440} \times 1000 = 127.5 \quad \text{(A1)}$$

$$\text{Equivalent weight of water} = \frac{18.0}{2} = 9.0 \quad \text{(A2)}$$

$$\text{Equivalent weight of diethylene glycol} = \frac{106.1}{2} = 53.1 \quad \text{(A3)}$$

Note: Surfactant, gelling and blowing catalysts are not required to calculate the equivalent weight since they do not react with isocyanate compounds.

$$\text{Number of equivalent in formulation} = \frac{\text{parts by weight (pbw)}}{\text{equivalent weight}} \quad \text{(A4)}$$

Number of equivalent in the formulation:

$$\text{Polyol} = \frac{100}{127.5} = 0.7843 \quad \text{(A5)}$$

$$\text{Water} = \frac{4.0}{9.0} = 0.4444 \quad \text{(A6)}$$

$$\text{Diethylene glycol (solvent)} = \frac{0.9}{53.1} = 0.0170 \quad \text{(A7)}$$

Total number of equivalent for rigid PUR foams = 0.7843 + 0.4444 = 1.2287

(A8)

Total number of equivalent for PIR foams = 0.7843 + 0.4444 + 0.0170 = 1.2457

(A9)

Therefore, the theorical amount of PMDI at isocyanate index of 100 for rigid PUR foams (without using trimerization catalysts) can be obtained as:

$$\text{PMDI (pbw)} = 1.2287 \times \frac{\text{PMDI molar mass}}{\text{functionality}} = 1.2287 \times \frac{365.8}{2.7} = 166.07$$

(A10)

The theorical amount of PMDI at isocyanate index of 100 for PIR foams can be obtained as:

$$\text{PMDI (pbw)} = 1.2457 \times \frac{\text{PMDI molar mass}}{\text{functionality}} = 1.2457 \times \frac{365.8}{2.7} = 168.77$$

(A11)

where;

$$\text{Isocyanate index} = \frac{\text{actual amount of isocyanate}}{\text{theoretical amount of isocyanate}} \times 100 \qquad \text{(A12)}$$

Thus, the actual amount of isocyanate at isocyanate index of 160 can be calculated as:

$$\text{Actual amount of isocyanate} = \frac{160.0}{100} \times 168.77 = 270.03 \text{ pbw} \qquad \text{(A13)}$$

The actual amount of isocyanate at isocyanate index of 200 can be calculated as:

$$\text{Actual amount of isocyanate} = \frac{200.0}{100} \times 168.77 = 337.54 \text{ pbw} \qquad \text{(A14)}$$

The actual amount of isocyanate at isocyanate index of 250 can be calculated as:

$$\text{Actual amount of isocyanate} \quad = \quad \frac{250.0}{100} \times 168.77 = 421.93 \text{ pbw} \qquad \text{(A15)}$$

Therefore, the actual amount of PMDI at isocyanate index of 100 for rigid PUR foams is 166.0 pbw, while the actual amount of PMDI at isocyanate index of 160, 200 and 250 for PIR foams are 270.0, 337.5 and 421.9 pbw, respectively.

Isocyanate conversion calculation

Isocyanate conversion is computed from the normalized absorption peak area of remaining isocyanate group at 2277 cm^{-1} using the following equation:

$$\text{Isocyanate conversion (\%)} = [1 - (A_{\text{isocyanate}}^{t}/A_{\text{isocyanate}}^{0})] \times 100 \qquad \text{(A16)}$$

where $A_{\text{isocyanate}}^{t}$ is the normalized absorption peak area of isocyanate group at time t. $A_{\text{isocyanate}}^{0}$ is the normalized absorption peak area of isocyanate group of PMDI at initial time. The normalization for obtaining $A_{\text{isocyanate}}^{0}$ is carried out using the absorption peak area of phenyl group (A_{phenyl}) at 1595 cm^{-1} as follows:

$$A_{\text{isocyanate}}^{0} = A_{\text{isocyanate}}/A_{\text{phenyl}} \qquad \text{(A17)}$$

where $A_{\text{isocyanate}}$ is the absorption peak area of isocyanate group of PMDI before normalization. Therefore, the $A_{\text{isocyanate}}^{0}$ can be calculated as:

$$A_{\text{isocyanate}}^{0} = 57.41/0.90 = 63.79 \qquad \text{(A18)}$$

This $A_{\text{isocyanate}}^{0}$ is used to calculate the isocyanate conversion for both rigid PUR and PIR foams. For example, rigid PUR foam prepared at isocyanate index of 100 and using Cu(Amm) as the catalyst has $A_{\text{isocyanate}}^{t}$ of

$$A_{\text{isocyanate}}^{t} = 0.91/1.82 = 0.50 \tag{A19}$$

The isocyanate conversion of this foam can be obtained by:

$$\text{Isocyanate conversion (\%)} = [1 - (A_{\text{isocyanate}}^{t}/A_{\text{isocyanate}}^{0})] \times 100 \tag{A20}$$

$$\text{Isocyanate conversion (\%)} = [1-(0.50/63.79] \times 100 = 99.22 \% \tag{A21}$$

PIR/PUR proportion

PIR/PUR proportion is calculated by the peak area proportion of PIR and PUR groups of each foam sample. For example, rigid PUR foam prepared at isocyanate index of 100 and using Cu(Amm) as the catalyst has peak areas of PIR and PUR of 1.06 and 4.37, respectively. Therefore, PIR/PUR proportion = 1.06/4.37 = 0.24.

Table A2-A4 show the calculated % isocyanate conversion and PIR/PUR proportion of all rigid PUR and PIR foams prepared in this work. The IR spectra whose peak areas are used to calculate these data are presented in Figure A1-A3.

Table A2 % Isocyanate conversion and PIR/PUR proportion of rigid PUR (isocyanate index 100) and PIR foams accelerated by Cu(Amm) and the mixture of potassium octoate solution with Cu(Amm), respectively.

NCO indices	Peak Areas					Isocyanate conversion (%)	PIR/PUR
	$A_{\text{isocyanate}}$ 2277 cm^{-1}	A_{phenyl} 1595 cm^{-1}	$A_{\text{isocyanate}}^{t}$ (Ph = 1.0)	A_{PIR} 1415 cm^{-1}	A_{PUR} 1220 cm^{-1}		
100	0.91	1.82	0.50	1.06	4.37	99.22	0.24
160	2.77	1.90	1.46	1.87	2.56	97.72	0.73
200	3.48	1.75	1.99	2.75	1.80	96.88	1.53
250	2.86	1.39	2.06	3.85	1.16	96.77	3.31

Table A3 % Isocyanate conversion and PIR/PUR proportion of rigid PUR (isocyanate index 100) and PIR foams accelerated by Zn(Amm) and the mixture of potassium octoate solution with Zn(Amm), respectively.

NCO indices	Peak Areas					Isocyanate conversion (%)	PIR/PUR
	$A_{isocyanate}$ 2277 cm^{-1}	A_{phenyl} 1595 cm^{-1}	$A^t_{isocyanate}$ (Ph = 1.0)	A_{PIR} 1415 cm^{-1}	A_{PUR} 1220 cm^{-1}		
100	1.73	1.83	0.94	0.57	3.40	98.52	0.17
160	2.96	2.08	1.42	1.31	2.83	97.77	0.46
200	4.10	1.75	2.34	2.11	2.32	96.33	0.91
250	3.23	1.56	2.07	2.90	1.13	96.75	2.57

Table A4 % Isocyanate conversion and PIR/PUR proportion of rigid PUR (isocyanate index 100) and PIR foams accelerated by DMCHA and the mixture of potassium octoate solution with DMCHA, respectively.

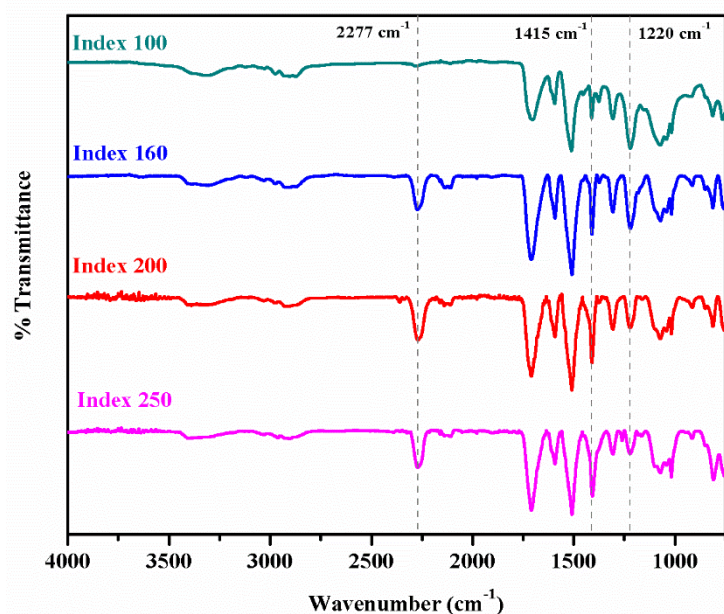| NCO indices	Peak Areas					Isocyanate conversion (%)	PIR/PUR
	$A_{isocyanate}$ 2277 cm^{-1}	A_{phenyl} 1595 cm^{-1}	$A^t_{isocyanate}$ (Ph = 1.0)	A_{PIR} 1415 cm^{-1}	A_{PUR} 1220 cm^{-1}		
100	1.11	1.94	0.57	0.95	5.30	99.10	0.18
160	3.40	1.90	1.79	1.69	2.76	97.19	0.61
200	4.39	1.81	2.42	4.42	2.41	96.20	1.83
250	6.34	1.53	4.14	5.29	1.66	93.51	3.19

Figure A1 IR spectra of rigid PUR foam accelerated by Cu(Amm) at isocyanate index 100 and PIR foams accelerated by the mixture of potassium octoate solution with Cu(Amm) at isocyanate index 160, 200 and 250.
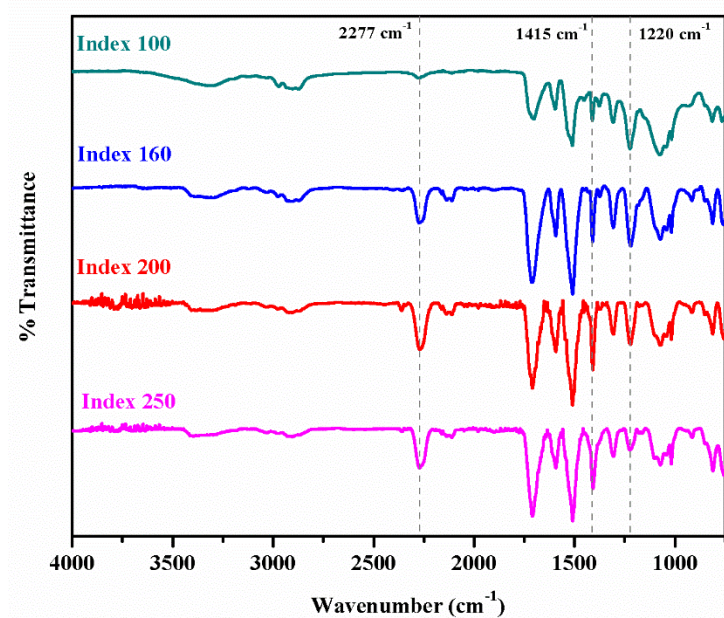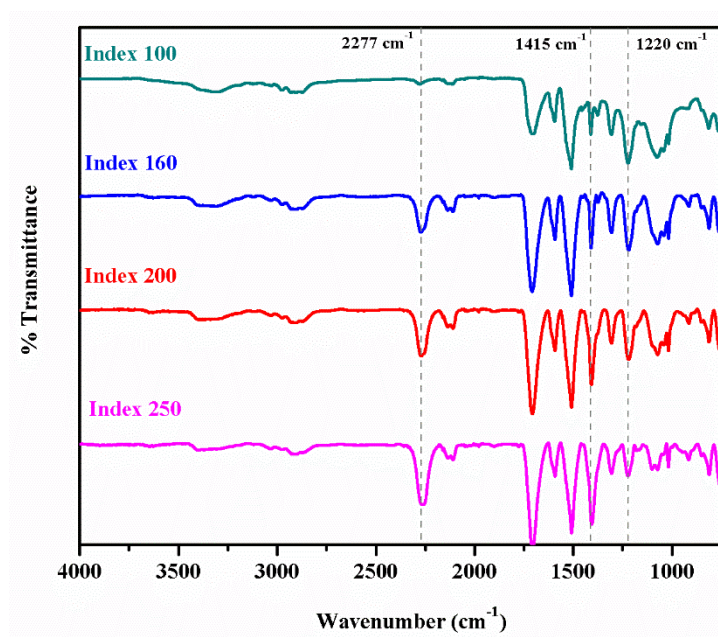

Figure A2 IR spectra of rigid PUR foam accelerated by Zn(Amm) at isocyanate index 100 and PIR foams accelerated by the mixture of potassium octoate solution with Zn(Amm) at isocyanate index 160, 200 and 250.

Figure A3 IR spectra of rigid PUR foam accelerated by DMCHA at isocyanate index 100 and PIR foams accelerated by the mixture of potassium octoate solution with DMCHA at isocyanate index 160, 200 and 250.

APPENDIX B

INTRINSIC REACTION COORDINATES FOR
TRANSITION STATE CONFIGURATIONS
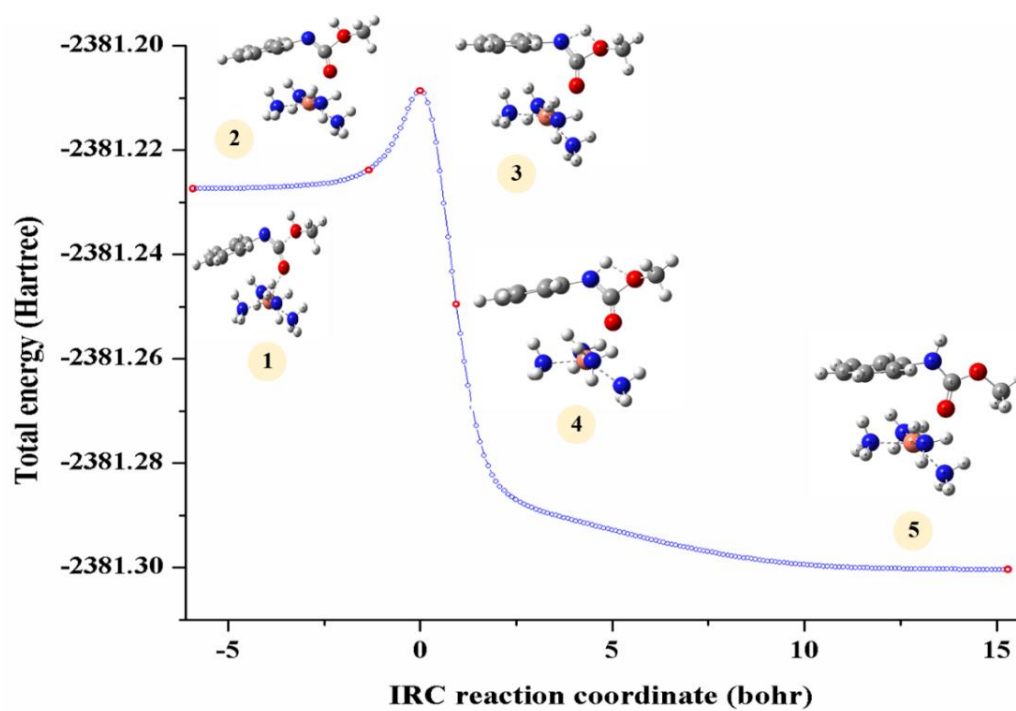
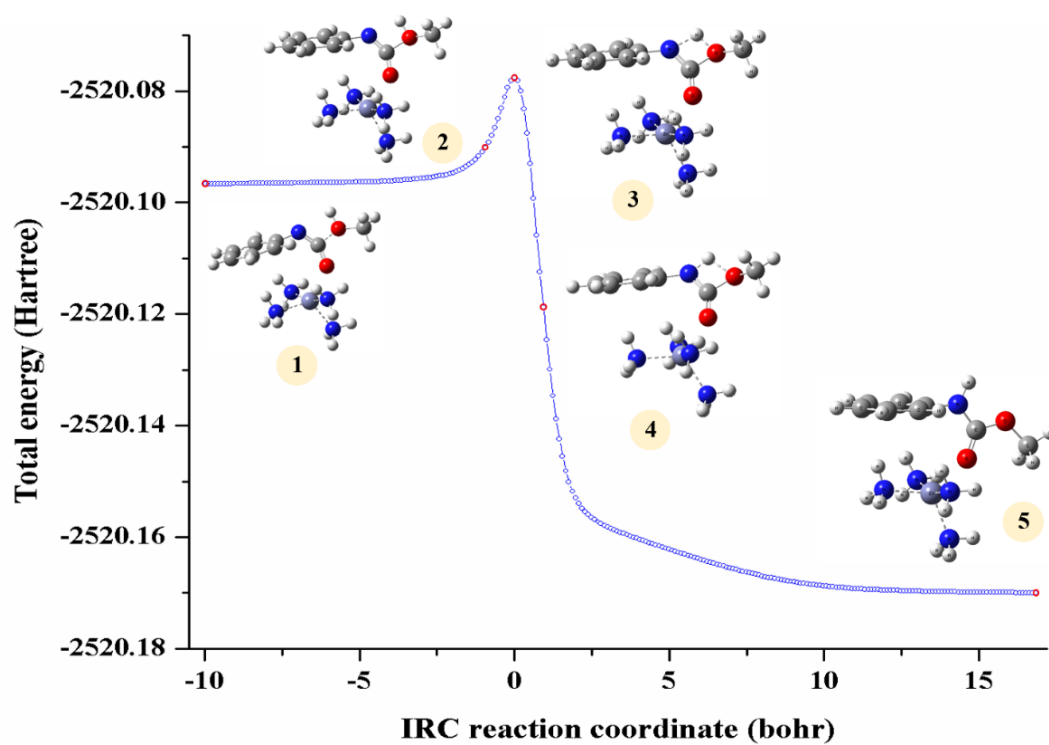**Figure B1** Intrinsic reaction coordinate of TS(Cu) for gelling reaction catalyzed by Cu(NH$_3$)$_4{}^{2+}$.

Figure B2 Intrinsic reaction coordinate of TS(Zn) for gelling reaction catalyzed by Zn(NH$_3$)$_4$$^{2+}$.
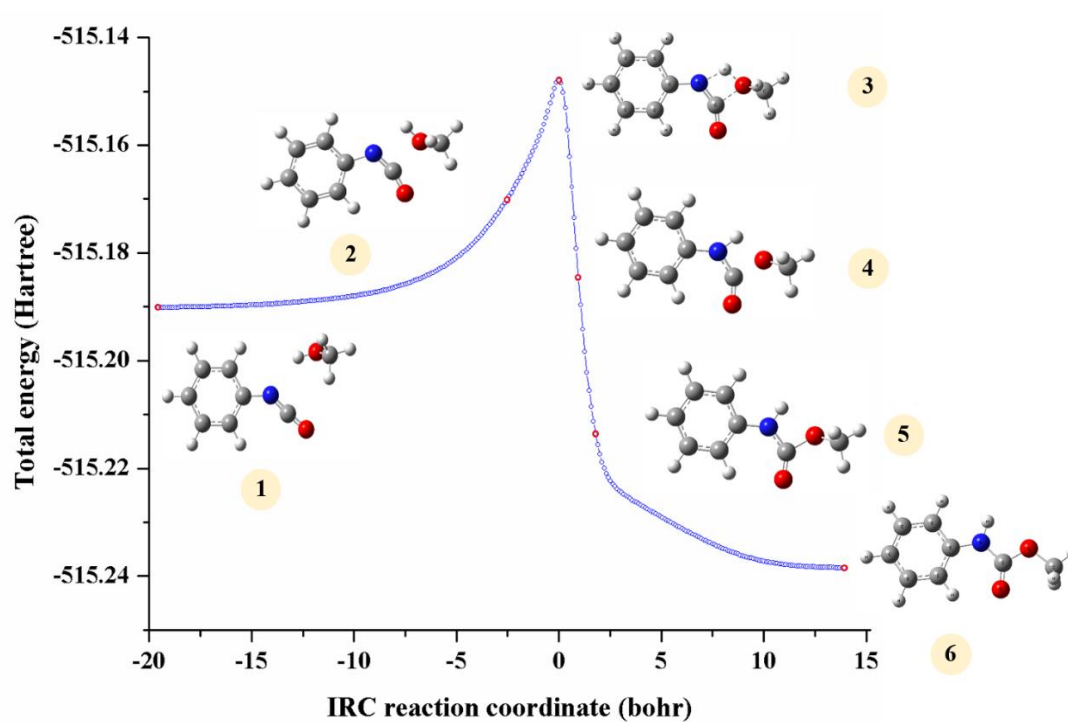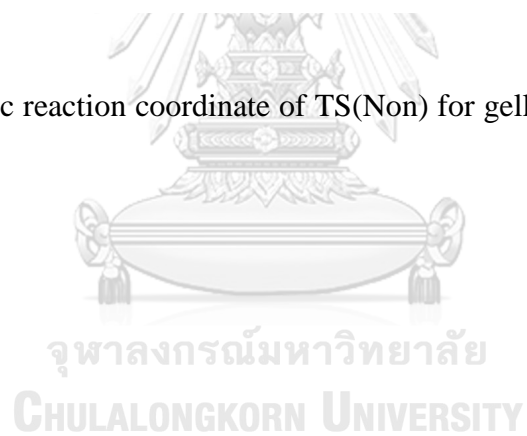
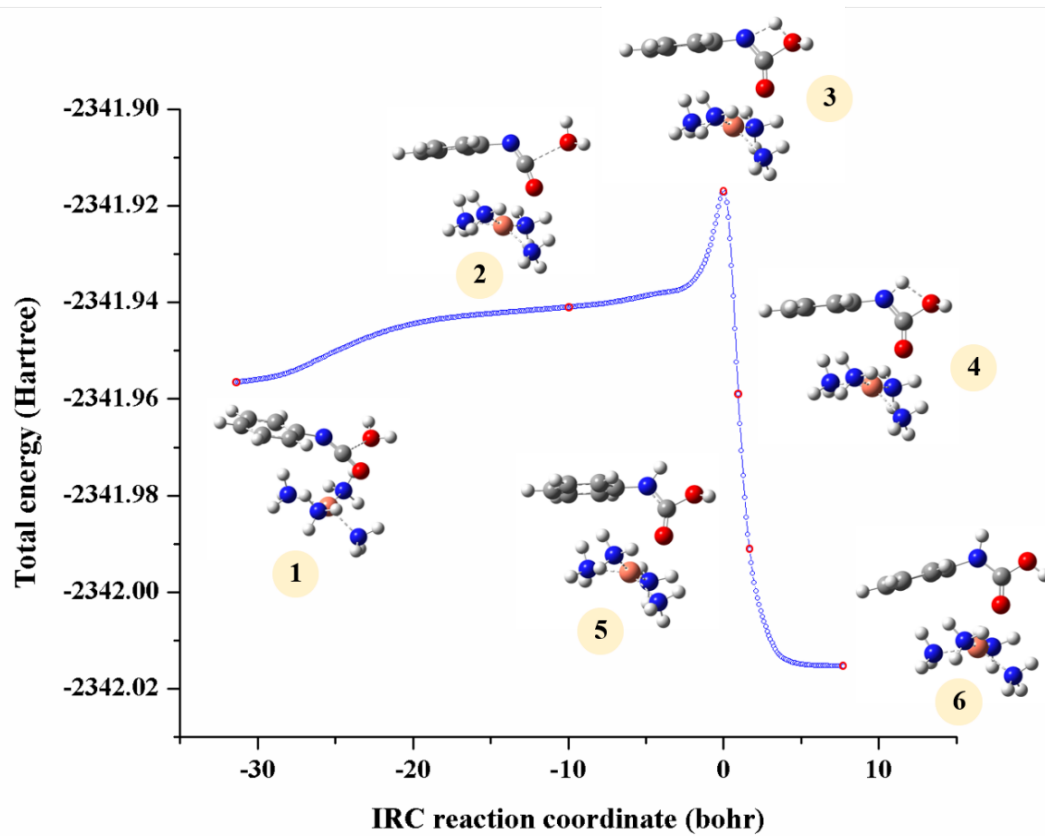**Figure B3** Intrinsic reaction coordinate of TS(Non) for gelling reaction without using catalyst**.**

Figure B4 Intrinsic reaction coordinate of TS1(Cu,CO$_2$) for blowing reaction catalyzed by Cu(NH$_3$)$_4^{2+}$.
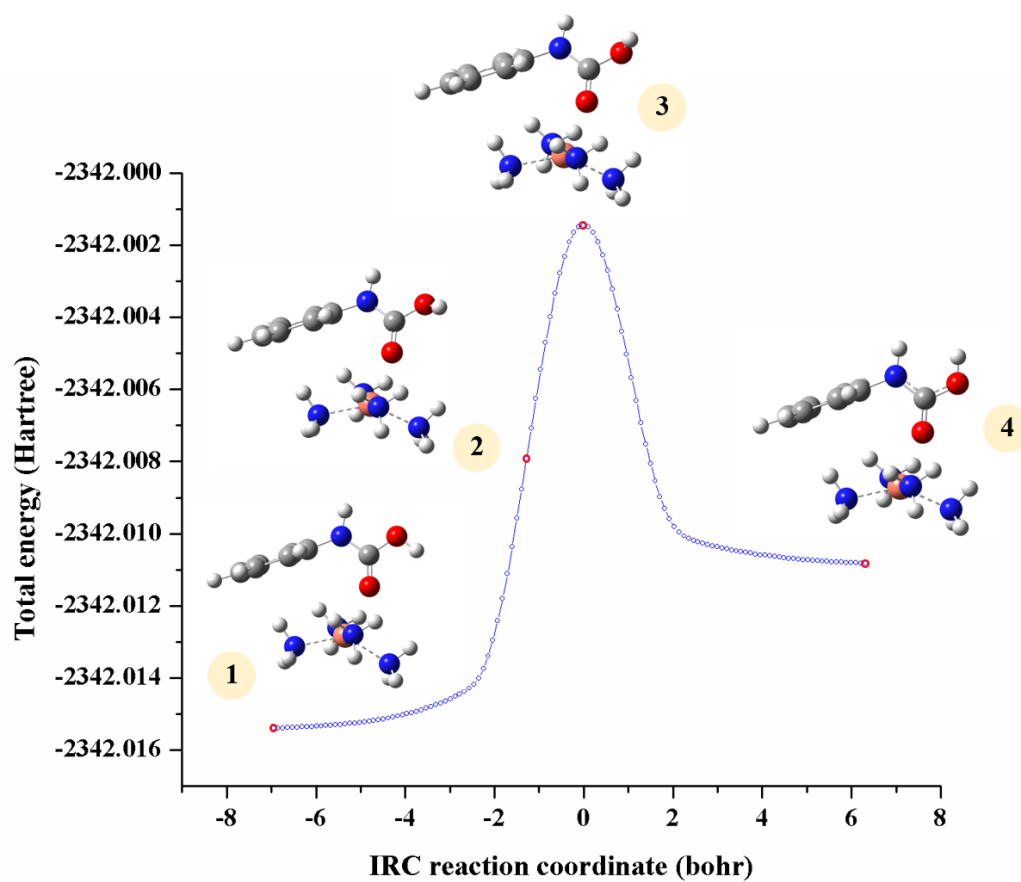
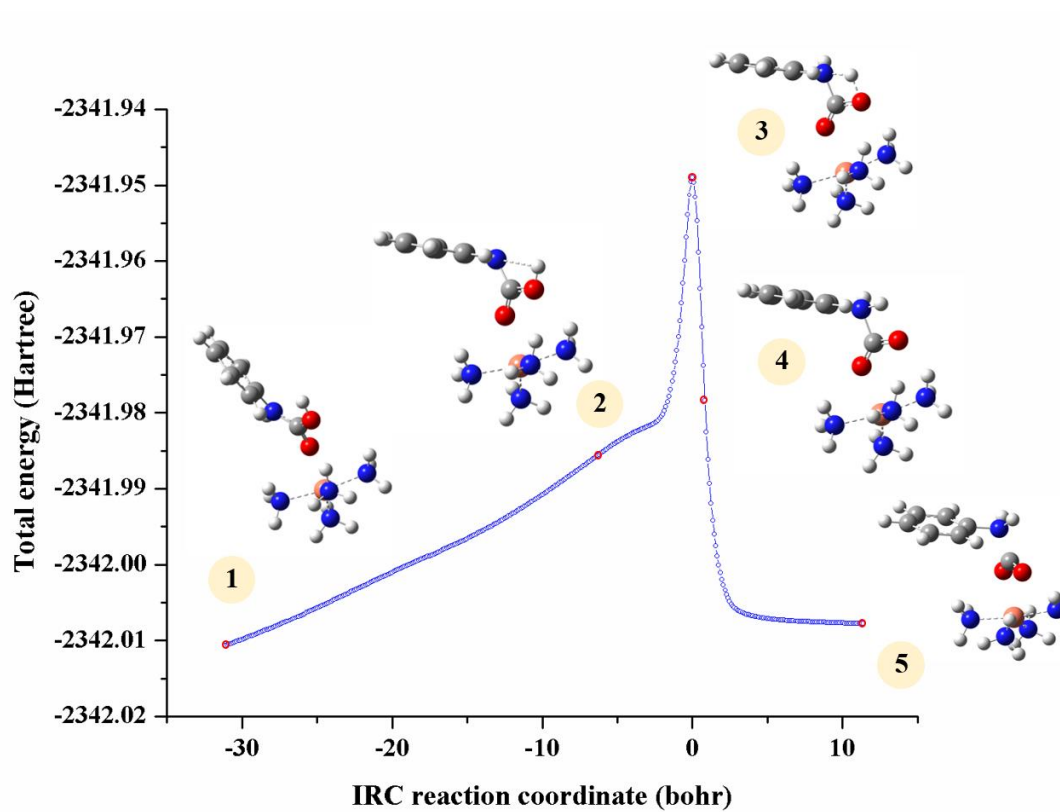**Figure B5** Intrinsic reaction coordinate of TS2(Cu,CO₂) for blowing reaction catalyzed by Cu(NH₃)₄²⁺.

Figure B6 Intrinsic reaction coordinate of TS3(Cu,CO$_2$) for blowing reaction catalyzed by Cu(NH$_3$)$_4{}^{2+}$.

VITA

NAME   Miss Benjatham Sukkaneewat

DATE OF BIRTH 12 November 1987

PLACE OF BIRTH Chumphon, Thailand

INSTITUTIONS   B.Eng. in Petrochemicals and Polymeric Materials,
ATTENDED   Faculty of Engineering, Silpakorn University (2006-2010)

         M.Sc. in Petrochemistry and Polymer Science, Faculty of
         Science, Chulalongkorn University (2010-2012)

         Ph.D. in Petrochemistry and Polymer Science, Faculty of
         Science, Chulalongkorn University (2016-2019)

HOME ADDRESS 37 Pracharat Road, Khan Ngoen, Lang Suan, Chumphon
         86110 Thailand